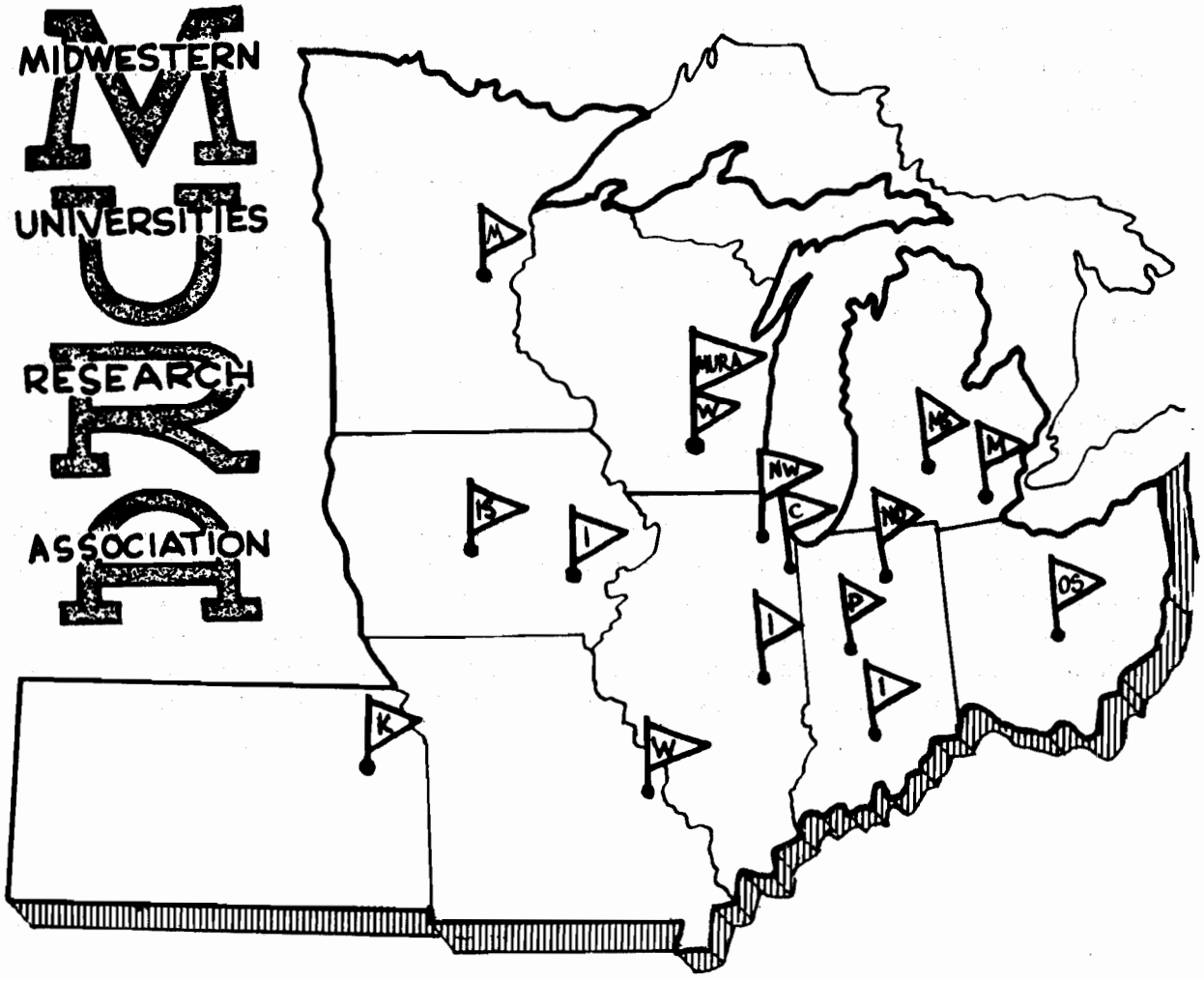

A METHOD OF RADIO-FREQUENCY INFLECTION INTO A PARTICLE ACCELERATOR

DONALD SCOTT ROISELAND

REPORT **NUMBER** 674

A METHOD OF RADIO-FREQUENCY INFLECTION INTO A PARTICLE ACCELERATOR

BY

DONALD SCOTT ROISELAND

A thesis submitted in partial fulfillment of the requirements for the degree of

DOCTOR OF PHILOSOPHY

(Physics)

at the

UNIVERSITY OF WISCONSIN

1963

MURA-674
UC-28: Particle Accelerators and
High Voltage Machines
TID-4500 (20th Edition)

MIDWESTERN UNIVERSITIES RESEARCH ASSOCIATION*

P. O. Box 6, Stoughton, Wisconsin

A METHOD OF RADIO-FREQUENCY INFLECTION INTO A PARTICLE ACCELERATOR

DONALD SCOTT ROISELAND

June 10, 1963

ABSTRACT

A radio-frequency method of inflecting particles (supplied from a given injector) into orbits suitable for subsequent acceleration in a cyclic particle accelerator is studied theoretically and experimentally. The particles circulating in the accelerator are subjected to an "RF bump": a transverse radio-frequency electric field over a small length of the orbit, tuned to the frequency of the radial betatron oscillations. It is shown that, in the absence of nonlinear effects and with no septum (inactive injector extremity), the number of particles made available for acceleration can be as large as the limit set by Liouville 's theorem (100% filling efficiency). In achieving this limit not less than 75% of the injected charge is wasted (25% charge efficiency). Nonlinear effects decrease both the charge and filling efficiencies.

*AEC Research and Development Report. Research supported by the U. S. Atomic Energy Commission, contract no. AT(11-1)-384.

ACKNOWLEDGEMENTS

I wish to thank the many people of the MURA staff whose support has made this research possible. I am particularly grateful to K. R. Symon for suggesting the problem and to both K. R. Symon and C. H. Blanchard for help in preparation of the thesis.

TABLE OF CONTENTS

TABLE OF CONTENTS (Continued)

TABLES

FIGURES

I. INTRODUCTION

Early in 1960, B.C. Cook, working with the MURA FFAG spiral sector electron accelerator[1], studied experimentally a method for extracting beam from a cyclic particle accelerator. This method involved the application of a radio-frequency electric field to a coasting beam.[2,3] Cook found[4,5] among other results, that an RF field of proper frequency could affect the amount of useful beam injected into the machine. Prior to this, other investigators (Ohkawa, Terwilliger) had noted this "RF knock in" injection mechanism. Cook's work is unique in that he measured its efficiency, finding it to be, under proper conditions, about one-half the upper limit set by Liouville's theorem and the known machine parameters. This work was not pursued further until K. R. Symon suggested to the present writer that an analysis of the mechanism be made. The interest in the mechanism stems from its high efficiency and also from the fact that conditions under which Cook made his measurement parallel those that would exist in a large FFAG accelerator employing beam stacking. Here injection would occur at those times when little or no energy is being added to the beam by the various devices normally used to accelerate the beam.

This thesis deals with a particular method for increasing the useful beam injected into a cyclic accelerator in which injection and acceleration occur at separate times. There are several other methods. Kerst has pointed out that space charge and inductance effects can aid injection.[6,7,8,9] That guide field inhomogeneities[10,11] can lead to

"resonant" damping of the radial betatron motion has been considered by Barden[12] and more extensively by Judd[8]. Teng has treated the case of time dependent impulses which (1) are in resonance with the radial oscillation and which (2) depend on the radial coordinate and which (3) act on a bunched beam only at certain accelerator azimuths.[13] A time dependent distortion of the equilibrium orbit aiding injection has been investigated by Kerst, Mills, and Morin.[1,14]

The explanation for Cook's observation rests on properties of the forced harmonic oscillator. This explanation and its implications form the core of the present thesis. The theoretical model of an accelerator used here is rather idealized, the basic assumption being that the radial betatron motion is simple harmonic. Because the angular frequency ω_{RF} of the RF electric field perturbing a particle is set equal to the particle's angular frequency of radial oscillation the mechanism under study will be referred to as Resonant RF Inflection (RRFI). In what follows this RF electric field is called the "RF bump" because it is an irregularity localized around some azimuth in the machine.

An electron's radial oscillation amplitude a_x is usually altered each time the electron traverses the region over which the RF bump acts. The injector and RF are presumably turned off together. At this turn off those electrons with sufficiently small a_x continue to circulate (revolution frequency f_o). They do not collide with the injector. It is such electrons which are available for acceleration. This group is the useful beam injected into the accelerator. It will be shown that, if non-linear effects are sufficiently small and if the injector has a septum of zero thickness, then RRFI makes a number of electrons

available for acceleration equal to the upper limit given by Liouville's theorem. The term filling efficiency denotes the degree to which this limit is realized.

For RRFI to realize 100% filling efficiency more charge must be injected than becomes available for acceleration. Here the ratio of the latter to the former is called charge efficiency. It is shown that RRFI exhibits a charge efficiency $\leq 1/4$. A charge efficiency of about 1/5 usually obtains.

The angular frequency of radial oscillation ω_x and the circulation frequency f_o actually do depend somewhat on the radial oscillation amplitude a_x, and any appreciable dependence of either one decreases the effectiveness of RRFI. The experimental test reported here was conducted in such a way as to minimize these non-linear effects. The experiment for the most part agrees with theory. In any less idealized application of RRFI the inhibitory effects of non-linearity will have to receive closer attention. A step in this direction is taken in Appendix 7. The paragraphs which follow indicate the order in which topics related to the above points will be discussed.

Section II begins by considering differences between the accelerator used in the experiment of Section VI and its idealized representation used in the theory of Sections III, IV, and V. The change in an electron's motion in making a single pass through the RF bump is discussed. An idealized model of this bump is developed. Finally, the injection problem of interest here is stated in terms of these idealizations.

Section III considers those aspects of Resonant RF Inflection which can be treated without recourse to high-speed automatic

computation. The approach used has applicability outside the realm of RRFI. Section IV uses it to illustrate the method of Stochastic Inflection.[15] Section V contains computational results which extend the conclusions of Section III. Three of the computer programs used here, i.e., SHO-16, SHO-18, and SHO-20, are described, respectively, in appendices 4, 5, and 6. Each of the latter begins with a short general description which is followed by a detailed consideration of the actual Fortran program. The program which analyzes the experimental data of Section VI is SHO-14. Its detailed description is given in Appendix 3 but its physical description occurs in Section 6.6. Since higher numbered programs are generally described in terms of how they differ from those of lower number, the reader may find it advantageous to skip consideration of programs used in Section V until after he has met the contents of Section 6.6 and Appendix 3.

The conclusion to the experiment of Section VI appears in Section 6.9. The thesis conclusion, Section VII, enumerates basic properties of RRFI.

II. IDEALIZED MODEL OF ACCELERATOR AND BUMP

The accelerator of Figure 1 is used in the experiment of Section VI. In considering this accelerator, as well as the idealized representation of it met later, it is convenient to introduce cylindrical coordinates (ρ, θ, z). The radial coordinate ρ lies in the plane of the paper. The center of the accelerator corresponds to $\rho = 0$. The azimuth of the electron gun or injector (arrow A) is taken as $\theta = 0$. Since electrons leaving the gun circulate in a clockwise manner, θ is taken to increase in the clockwise direction. The vertical or positive z axis has its origin at $\rho = 0$, is orthogonal to the plane of the paper, and points away from the reader. Specifying the magnetic field $\vec{B}$ on the median plane ($z = 0$) automatically determines $\vec{B}$ for $z \neq 0$. In a conventional cyclotron the median plane field is

$$B_\rho = 0$$
$$B_\theta = 0$$
$$B_z = B_1\left(\frac{\rho}{\rho_1}\right)^n \qquad -1 < n < 0$$

An electron injected under proper conditions into this guide field will not only circulate about the origin but also oscillate about a unique path lying in the median plane. This path, known as an equilibrium orbit, is the one trajectory associated with an electron of energy E_o (speed v_o) which connects smoothly with itself each revolution. In the cyclotron it is just a circle of radius ρ_o.

The oscillation separates into two modes: one radial, the other vertical. Since the guide field is independent of time, $\vec{\nabla} \times \vec{B} = 0$.

Solving for the field $\vec{B}$ off the median plane in linear approximation yields

$$B_\rho = n \frac{z}{\rho} B_1 \left(\frac{\rho}{\rho_1}\right)^n$$
$$B_\theta = 0$$
$$B_z = B_1 \left(\frac{\rho}{\rho_1}\right)^n$$

The equations of motion for an electron of charge $-e$ and relativistic mass m in this field are

$$m(\ddot{\rho} - \rho\dot{\theta}^2) = -e\rho\dot{\theta} B_1 \left(\frac{\rho}{\rho_1}\right)^n$$
$$m(\rho\ddot{\theta} + 2\dot{\rho}\dot{\theta}) = e\dot{\rho} B_1 \left(\frac{\rho}{\rho_1}\right)^n$$
$$m\ddot{z} = e\rho\dot{\theta} n \frac{z}{\rho} B_1 \left(\frac{\rho}{\rho_1}\right)^n$$

The dots denote derivatives with respect to time. For an electron whose trajectory is its equilibrium orbit, $\ddot{\rho} = \dot{\rho} = \ddot{\theta} = 0$. When such is the case the first equation gives $\dot{\theta} = \frac{e}{m} B_1 \left(\frac{\rho_0}{\rho_1}\right)^n = \omega_0 = 2\pi f_0$, where f_0 is the electron revolution frequency. Since electron speed v_0 equals $\omega_0 \rho_0$, electron energy E_0 increases with increasing ρ_0. Upon linearizing the equations of motion about the equilibrium orbit using the substitutions $\rho = \rho_0 + x$ and $\dot{\theta} = \omega_0 + \Delta\dot{\theta}$ one obtains

$$\ddot{x} = -(n+1)\omega_0^2 x$$
$$\Delta\ddot{\theta} = -\frac{\omega_0}{\rho_0}\dot{x}$$
$$\ddot{z} = n\omega_0^2 z$$

The solutions are

$$x = a_x \sin(\omega_x t + \beta_1)$$
$$z = a_z \sin(\omega_z t + \beta_2)$$
$$\omega_x = \sqrt{1+n}\,\omega_0$$
$$\omega_z = \sqrt{-n}\,\omega_0$$
$$\dot{\theta} = \omega_0 \left(1 - \frac{x}{\rho_0}\right)$$

The quantities (1) x and z, (2) a_x and a_z, (3) β_1 and β_2, and (4) ω_x and ω_z are, respectively, (1) the electron's radial and vertical displacements from its equilibrium orbit, (2) the electron's radial and vertical amplitudes of oscillation about this orbit, (3) the phase angles of the radial and vertical oscillations at $t = 0$, and (4) the angular frequencies of the radial and vertical oscillations.

It is sometimes convenient to consider θ as the independent variable rather than the time. If in the original equations of motion $\dot{\rho}$ is replaced by $\left(\frac{d\rho}{d\theta}\right)\dot{\theta}$ and $\ddot{\rho}$ by $\frac{d^2\rho}{d\theta^2}\dot{\theta}^2 + \frac{d\rho}{d\theta}\ddot{\theta}$ etc. then the linearized equations of motion for x and z become

$$\frac{d^2x}{d\theta^2} = -(n+1)x$$

$$\frac{d^2z}{d\theta^2} = -(-n)z$$

It is convenient to introduce the radial and vertical "tunes" ν_x and ν_z where $\nu_x = \sqrt{1+n}$ and where $\nu_z = \sqrt{-n}$. From a practical point of view $\nu_x\,(\nu_z)$ is the $\lim_{N\to\infty} \frac{L}{N}$ where L is the number of complete radial (vertical) oscillations executed by an electron in going around the accelerator N times. The solutions to the preceding equations are

$$x = a_x \sin(\nu_x\theta + \beta_1)$$

$$z = a_z \sin(\nu_z\theta + \beta_2)$$

It is sometimes desirable to express them as

$$x = e^{\pm i\nu_x\theta}$$

$$z = e^{\pm i\nu_z\theta}$$

Two points are worth noting. First, both ν_x and ν_z are independent of ρ_o and hence of electron energy E_o. For certain values of $\nu_x\,(\nu_z)$ unavoidable imperfections in the guide field cause an electron's $a_x\,(a_z)$ to increase until the electron is lost from the beam. The quantity n is chosen such that $\nu_x\,(\nu_z)$ is as far as possible from those values (the "resonant values") which cause trouble.

Unavoidable variation of n over the allowed range of ρ_o also occurs. This variation must never be great enough to shift $\nu_x (\nu_z)$ onto a resonant value. The second point is that electron revolution frequency f_o is independent of oscillation amplitude in linear approximation. The time average of $\dot{\theta} = \omega_o \left(1 - \frac{x}{\rho_o}\right)$, i.e., $\overline{\dot{\theta}}$, is just ω_o since $\overline{x} = 0$. Hence, electrons of the same energy E_o exhibit the same f_o in linear approximation.

To add energy to electrons injected into its guide field, a conventional cyclotron employs a radio-frequency acceleration scheme. The RF voltage is applied across two electrodes between which the circulating electrons pass repetitively. Their direction of motion is parallel to the lines of force between these electrodes. The frequency of the RF voltage is constant in time and is set equal to the revolution frequency of the injected electrons. As long as synchronism between the RF and f_o prevails, some electrons receive energy. As their energy increases so does their ρ_o. At these larger ρ_o two factors operate to destroy synchronism and thereby limit the energy attainable. (1) Consider the expression for ω_o met previously, i.e., $\omega_o = 2\pi f_o = \frac{e}{m} B_1 \left|\frac{\rho_o}{\rho_1}\right|^n$ where m is the relativistic electron mass. Since $-1<n<0$, f_o decreases with increasing ρ_o. This decrease can be minimized by using the largest feasible n. (2) As electron velocity approaches the speed of light, m begins to increase. This also lowers f_o.

The loss of synchronism noted above can be circumvented by varying the RF frequency with time so as to follow the f_o of a single group of nearly monoenergetic electrons all the way from injection out to the largest ρ_o for which the guide field has the proper form. When this group reaches the target the RF frequency is returned to its initial value and the process repeated. The price paid for higher energy is twofold. First, economic difficulties are encountered in constructing

and exciting the larger electromagnet required to contain the higher energy electrons. Second, pulsed operation tends to lower the average number of electrons reaching the target per second.

The economic difficulties noted above can, in some measure, be overcome. In the expression $mv_0 = e B_3 \rho_0$ the electron speed v_0 can be replaced by the speed of light c when dealing with relativistic electrons. Multiplication of the resulting expression by c gives the total electron energy. Once the electron energy an accelerator is to yield has been specified, the maximum value of $B_3 \rho_0$ which must obtain is also known. Choosing the maximum feasible B_3, i.e., B_{max}, fixes the magnet pole radius ρ_{max}. Nothing one can do will decrease this dimension. However, if n were allowed to be greater than zero, say ten or twenty, then it would be possible to cut out the central region of the magnet pole. The field on the remaining annulus would be $B_3 = B_1 \left(\frac{\rho}{\rho_1}\right)^n$. The annulus would extend from ρ_1 to ρ_{max} where $\frac{\rho_{max} - \rho_1}{\rho_{max}} << 1$. Here B_{max} is $B_1 \left(\frac{\rho_{max}}{\rho_1}\right)^n$ and $B_1 << B_{max}$. Electrons would be injected at low energy onto an equilibrium orbit of radius ρ_1 and accelerated out to ρ_{max}. From previous considerations we know, however, that with $n > 0$ $\nu_3 = \sqrt{-n}$ is imaginary and the z motion, $e^{\pm i \nu_3 \theta}$, unstable. It is possible, however, to stabilize it by introducing a suitable azimuthal dependence into the guide field. The spiral sector accelerator of Figure 1 is an example of a machine with $n>0$ which uses azimuthal dependence of a time invariant guide field to stabilize the z motion.[1]

The fact that pulsed operation lowers the average number of electrons reaching the target per second motivates the present thesis. One desires to maximize the number of electrons accelerated per pulse. The properties of the injector, e.g., current emitted by it, etc., enter into the problem but are not of primary concern here. The question here is what can be done to electrons between the time they leave the injector and

the time the injector is turned off such that after injector turn off as many as possible are available for acceleration. For reasons which are not given here, RF acceleration, as it would be used in a full scale version of the accelerator of Figure 1, restricts one to methods of enhancing this number which conserve electron energy. The particular method considered in this thesis (RRFI) was tested experimentally in the accelerator of Figure 1. In developing an idealized representation of this accelerator we begin by noting ways in which the azimuthally dependent guide field makes the electron motion differ from that in the cyclotron previously considered.

The guide field on the median plane in the accelerator of Figure 1 is approximately

$$B_3 = B_1\left(\frac{\rho}{\rho_1}\right)^n \left[1 + \sin(6\theta + \beta_3)\right] \qquad n \cong 0.7$$

The quantity β_3 is a phase angle which depends on $\frac{\rho}{\rho_1}$. An equilibrium orbit in this field is roughly hexagonal. An equilibrium orbit of higher energy is a photographic enlargement of the preceding one coupled with a clockwise rotation sufficient to keep each of its "rounded vertices" at the middle of a magnet. Electron oscillation about the equilibrium orbit is described in terms of new variables θ', x' and z'. These variables, which are never very different from their cognates θ, x, and z, are defined as follows. Let β_4 be the circumference of an equilibrium orbit and β_5, path length along this orbit measured in a clockwise direction from a reference point on the orbit where ρ happens to be orthogonal to the orbit. The quantity θ' equals $2\pi \frac{\beta_5}{\beta_4}$. Next, draw a line between an electron's projection on the median plane and the nearest point on the equilibrium orbit. This projection is assumed close enough to the orbit so that there is only one such nearest point. The length of the line just drawn is $|x'|$ where x' is negative if the projection lies within the

equilibrium orbit and positive if outside. The quantity $\mathfrak{z}'$ equals $\mathfrak{z}$.

The solutions to the linearized equations of motion for the accelerator of Figure 1 are

$$x' \propto e^{\pm i \nu_x \theta'} f(6\theta')$$

$$\mathfrak{z}' \propto e^{\pm i \nu_3 \theta'} g(6\theta')$$

where

$$f(6\theta') = 1 + \sum_{n=1}^{\infty} b_n \sin(n6\theta' + c_n)$$

$$g(6\theta') = 1 + \sum_{n=1}^{\infty} d_n \sin(n6\theta' + h_n)$$

The nature of the guide field fixes the constants b_n, c_n, d_n, and h_n. As in the cyclotron, ν_x and ν_3 are independent of electron energy.

Suppose an observer at θ_1' records the x' and $\mathfrak{z}'$ of an electron as it passes θ_1'. He then jumps ahead to $\theta' = \theta_1' + 2\pi/6$ and waits until he sees the electron pass this point whereupon he again records its x' and $\mathfrak{z}'$. Jumping ahead to $\theta' = \theta_1' + 2\left(\frac{2\pi}{6}\right)$ he repeats the process, etc. Since the observer jumps $\frac{2\pi}{6}$ each time and since $f(6\theta')$ and $g(6\theta')$ are periodic with period $\frac{2\pi}{6}$, the observer finds that the simplest assumption which will allow him to analyze his data is that electron motion is simple harmonic between observation points, i.e., that for all θ'

$$x' \propto e^{\pm i \nu_x \theta'}$$

$$\mathfrak{z}' \propto e^{\pm i \nu_3 \theta'}$$

The idealized representation of the accelerator of Figure 1 which we use throughout this thesis is as follows. We choose θ_1' to be the point on the equilibrium orbit corresponding to the injector azimuth in Figure 1, ..., [illegible] Like the observer above, we assume the x' and $\mathfrak{z}'$ motion to be simple harmonic at all points between the six azimuths $\theta' = \theta = 0, \frac{2\pi}{6}, \frac{4\pi}{6}, \ldots, \frac{10\pi}{6}$. Experimentally (Section VI) this assumption gives no trouble as we, like the observer, restrict ourselves to observing and influencing the beam at azimuths θ which are integral multiples of $\frac{2\pi}{6}$. We also assume the equilibrium orbit to be circular (radius ρ_o), i.e.,

we neglect any discrepancy between x' and x at these six azimuths. Hence, the idealized representation of the accelerator of Figure 1 which we use here is basically the linearized cyclotron model previously considered. We, however, disregard the theoretical predictions for ν_x and ν_3 made on the basis of this cyclotron model and replace them with any values we happen to be interested in.

The dashed circle of Figure 2 represents an equilibrium orbit while the line crossing it a projection onto the median plane of one possible electron orbit. Here $\nu_x = \frac{1}{2}$. The electron orbit originates at $\theta = 0$, the injector being represented by a line segment at $\theta = 0$, extending from the inner vacuum tank wall to some less negative but still negative x. The backside or negative θ side of the injector is a sink. Any electron colliding with it is absorbed. The injector is assumed to be of sufficient vertical extent so that an electron's vertical displacement z is never sufficient to allow it to hop over or under the injector when a projection of its orbit onto the median plane intersects the injector. An electron's z motion is not considered further in the theoretical work of this thesis. It is sufficient to work with the projection of an electron's orbit on the median plane rather than the orbit itself. Nevertheless, it is convenient to talk of electrons so in what follows we assume that all electrons travel in the median plane, i.e., that their vertical oscillation amplitudes are zero.

The positive side of the injector emits electrons only over some small segment near its right hand extremity. Segment $\overline{DE}$ of Figure 3 is known as the septum. It is an unavoidable region of zero emission. To its left is the active segment $\overline{CD}$ each point of which emits electrons over some angular range about the forward direction. An arrow's origin represents the radial displacement of an electron at the instant of its emission while its orientation, the electron's direction

of emission. The angle α measures the inclination of an arrow to the forward direction. It is positive for arrows inclined toward the equilibrium orbit. An electron's radial component of momentum at the time of its emission is $p_x = mv_0 \sin\alpha$. After emission its p_x is given by $p_x = m\dot{x} = m a_x \omega_x \cos(\omega_x t + \beta_1)$.

Instead of working directly with an electron's p_x it is helpful to replace p_x by a number y, proportional to it, having dimension of length.

$$y = \frac{p_x}{m\omega_x}$$

As an electron travels around the accelerator (Figure 2) it is informative to view the motion of its representative point (x,y) in phase space. By phase space we simply mean a plane on which a rectangular coordinate system is inscribed, the horizontal axis of this system measuring x and its vertical axis measuring y. It is convenient to imagine this phase plane as set perpendicular to the equilibrium orbit at the azimuth θ at which the electron happens to be. The equilibrium orbit passes through the point (0,0). We agree to view only that side of the phase plane which faces in the direction of increasing θ. The phase plane's negative x axis coincides with the negative x axis in real space at this same azimuth. We also view the plane in such a way that an electron exhibiting a negative x lies to the left of the vertical line x = 0. The positive y axis points upward. For now we take this phase plane as traveling around the accelerator with angular velocity ω_0 so that the electron under consideration always lies in the plane. Later we shall fix the phase plane at some azimuth θ and simply record the phase points (x,y) of electrons passing through it.

The motion of an electron's representative point (x,y) in phase space is given by

$$x = a_x \sin(\nu_x \theta + \beta_1)$$
$$y = a_x \cos(\nu_x \theta + \beta_1)$$
$$\theta = \omega_0 t$$

The point (x,y) travels around a circle of radius $a_x = \sqrt{x^2 + y^2}$ with angular velocity $\omega_x = \nu_x \omega_0$. Vector notation is helpful in expressing these results. The electron's $\begin{pmatrix} x \\ y \end{pmatrix}$ at $\theta > 0$ is obtained from the $\begin{pmatrix} x \\ y \end{pmatrix}$ it had at $\theta = 0$, [illegible] by rotating the latter clockwise $\nu_x \theta$ radians.

$$\begin{pmatrix} x \\ y \end{pmatrix} = \begin{pmatrix} \cos(\nu_x \theta) & \sin(\nu_x \theta) \\ -\sin(\nu_x \theta) & \cos(\nu_x \theta) \end{pmatrix} \begin{pmatrix} x_0 \\ y_0 \end{pmatrix} = M(\nu_x \theta) \begin{pmatrix} x_0 \\ y_0 \end{pmatrix}$$

The injector is assumed to emit electrons of only one energy E_0. The phase space representation of the current emanating from the injector will prove a useful device. More generally one desires the phase space representation of the beam current at any azimuth θ. Set the phase plane at the desired θ. Let $F(x,y,\theta,t)\,d\theta\,dx\,dy$ be the number of electrons of charge $-e$ between θ and $\theta+d\theta$ having x's between x and x+dx and y's between y and y+dy at time t. Let $i(x,y,\theta,t)dxdy$ be the rate at which charge having x's between x and x+dx and y's between y and y+dy crosses this plane at time t. The increment of charge passing through dxdy in time dt divided by dt is

$$i(x,y,\theta,t)\,dx\,dy = \frac{-e\,F(x,y,\theta,t)\,d\theta\,dx\,dy}{dt}$$

Therefore $\left(\omega_0 = \frac{d\theta}{dt} \; ; \; dt = \frac{d\theta}{\omega_0}\right)$

$$i(x,y,\theta,t)\,dx\,dy = \frac{-e\,F(x,y,\theta,t)\,d\theta\,dx\,dy}{\left(\frac{d\theta}{\omega_0}\right)}$$

$$= -e\,\omega_0\,F(x,y,\theta,t)\,dx\,dy$$

Hence, $i(x,y,\theta,t) = -e\omega_o F(x,y,\theta,t)$. In what follows, $i(x,y,\theta,t)$ will be replaced by the symbol $i(x,y)$. It will sometimes be referred to as the current per unit area of phase space. The particular θ and t associated with $i(x,y)$ will be mentioned in each case. The symbol $i_o(x,y)$ denotes the current per unit area of phase space over the injector. It applies only at $\theta = 0+$ over (x,y) to the left of a vertical line through E in Figures 4 and 5, i.e., for $x < x_E < 0$. Figure 3 shows x_E to be the displacement of the right hand extremity of the injector.

If one draws lines of constant $i_o(x,y)$ on the phase plane at $\theta = 0+$, contours like those of Figure 4 are expected. The current $j_o(x)dx$ emitted by the injector between x and x + dx is

$$j_o(x)\,dx = \left[\int_{-A_x}^{A_x} i_o(x,y)\,dy\right] dx$$

Here A_x is an upper bound on oscillation amplitudes a_x of electrons leaving the injector. The current density $j_o(x)$ associated with the injector has dimensions of current per unit length. One talks of $i_o(x,y)$ and $j_o(x)$ only at $\theta = 0+$ and for $x<x_E$. At $\theta = 0+$, $i(x,y)$ and $j(x)$ include $i_o(x,y)$ and $j_o(x)$, respectively. In much of the theoretical work which follows $i_o(x,y)$ is assumed to be a nonzero constant function of x and y over a region of finite area and to be zero outside this region. When such is the case its nonzero constant value is designated i_o.

Suppose at time t = 0 the injector whose phase plane representation is given by Figure 4 is turned on. In physical space one sees a pencil of charge emanate from the injector and snake around the accelerator. When its head reaches $\theta = 2\pi$ any charge lying to the left of $x = x_E$ collides with the injector. That portion not colliding snakes around again, etc. Eventually equilibrium is achieved, i.e., the current

colliding with the injector equals the current emanating from it.

It is informative to view this approach to equilibrium on a phase plane set at $\theta = 0$. We let ν_x be 1/3. It takes a time $\tau = 1/f_0$ for an electron to travel once around the accelerator. With the injector turned on at $t = 0$, Figure 4 applies at $\theta = 0+$ for $0 < t < \tau$. For $\tau < t < 2\tau$ a second beam manifests itself in phase space at the one o'clock position. A third beam makes its presence felt at the five o'clock position when $2\tau < t < 3\tau$. For $t > 3\tau$ a fourth beam is not realized as electrons associated with it collide with the back side of the injector. (For an electron at $\theta = 0-$ to subsequently collide with the injector its radial displacement x must be $\leq x_\varepsilon$.) Figure 5 gives i(x,y) for $t > 3\tau$ appropriate to θ in the neighborhood of $\theta = 0$. For $t > 3\tau$ the number of electrons circulating is constant. Just as many are being emitted by the injector's forward surface as are colliding with its back side.

Figure 5 also applies when $\nu_x = 4/3, 7/3, 10/3, \ldots$. The transformation $M(\nu_x 2\pi)$ relating the $\begin{pmatrix} x \\ y \end{pmatrix}$ of an electron to its value one revolution later is independent of any integral portion of ν_x . When (1) it is permissible to deal only with the non-integral portion of ν_x and when (2) it is advantageous to consider only rational ν_x then the radial tune will be written as $\nu_x = L/N$ rather than as ν_x . Here L and N are integers and $0 < L < N$. Restricting ν_x to be rational allows one to investigate certain properties of RRFI more easily. When it is advantageous to remove this restriction we shall do so.

Specializing to a ν_x of 1.400, i.e., $\nu_x = L/N = 2/5$, we view a phase plane set at $\theta = 0$. It is assumed that the septum thickness $\overline{DE}$ of Figure 3 is zero and that the gun emits an $i_o(x,y)$ of $i_o > 0$ only over (x,y) lying both within a circle of radius A_x and to the left of $x = x_\varepsilon$. The quantity A_x will be taken several times larger than $|x_\varepsilon|$. The lined portion of Figure 6a corresponds to such an injection region. Supposing

emission to begin at t = 0, Figure 6 gives $i(x,y)$ in the neighborhood of $\theta = 0$ for $t>0$. Since $i(x,y)$ at $\theta = 0+$ is not always the same as $i(x,y)$ at $\theta = 0-$, the following device is used to distinguish differences. An unlined region indicates that an $i(x,y)$ of zero is seen at both $\theta = 0-$ and $\theta = 0+$. A singly shaded region as in Figure 6a indicates an $i(x,y)$ of i_o at $\theta = 0+$ and an $i(x,y)$ of zero at $\theta = 0-$. A region where the vertical lines are twice as dense as those in 6a indicates an $i(x,y)$ of i_o at both $\theta = 0+$ and $\theta = 0-$. Hence, doubly shaded regions as well as white regions indicate continuity in $i(x,y)$ across $\theta = 0$ while singly shaded regions, discontinuity. Discontinuity occurs only over the injector extent and for times t less than or equal to the equilibrium time 5τ.

A ν_x of 1.400 is seen to yield an empty pentagon surrounded by a filled band for $t \geq 5\tau$. If ν_x were 4/3, an empty equilateral triangle would result for $t \geq 3\tau$. With $\nu_x = L/N$ an N-sided equilateral polygon is realized for $t \geq N\tau$ $(N > 2)$. Once such equilibrium has been established a like polygon would also be seen at other azimuths θ except for its being rotated clockwise by $\nu_x\theta$ radians. For simplicity, the phase plane will usually be set in the neighborhood of $\theta = 0$. As N becomes larger the associated polygon looks more and more like the circle it circumscribes. This circle of radius r_o will be called the beam circle. Its interior will be called the area of usable beam. The radius of a general circle in phase space centered at (0,0) will be denoted by r.

In the previous example where $i(x,y)$ is set equal to i_o only two values of $i(x,y)$ are ever realized, i.e., i_o and zero. There can never be doubling up or overlapping of filled regions of phase space. Our present purpose is to illustrate this fact more vividly. Suppose that the injector has been turned on and equilibrium achieved. At some time

t, momentarily stop the beam and break it into a large number of segments each of azimuthal extent $d\theta$. The revolution frequency of each segment is f_0. Each segment maintains the same position with respect to all other segments for all time. Set a single phase plane in the middle of one segment and let it travel around the accelerator with the segment. We plot the representative points (x,y) of all electrons in the segment on this plane. The point density on the plane is $F(x,y,\theta,t)d\theta$ where θ is the azimuth the segment happens to be at time t. Each point on the phase plane rotates clockwise about (0,0) with angular velocity $\omega_x = \nu_x \omega_0$. Rotation does not change the relative positions of representative points so that doubling up or thinning out of the point density can not take place except, perhaps, when the segment passes the injector. However, when the latter occurs all electrons in the segment whose representative points lie to the left of $x = x_E$ collide with the injector. In other words the region of phase plane to the left of $x = x_E$ is completely evacuated just before new points are added to any portion of it. Hence, there can never be a doubling up in the density of the representative points. An observer viewing a phase plane fixed at any azimuth θ can see only one of two values of $i(x,y)$ near any (x,y) at time t, i.e., either i_0 or zero.

The problem with which this thesis deals can now be seen more clearly. As before let $i_0(x,y) = i_0$, $\nu_x = L/N$, and $t > N\tau$. An electron leaving the injector circulates about the accelerator from one to N times depending on the particular $(x,y) = (x_0,y_0)$ it had at its instant of emission. Its oscillation amplitude is always $a_x = \sqrt{x_0^2 + y_0^2}$. If the injector is now turned off, all electrons collide with the injector within $N\tau$ seconds after this turn off. In such a case there is no beam left to accelerate. The general problem then is to apply some kind of energy-conserving perturbation to the circulating electrons while the

injector is on, which leaves, at the time the injector is turned off, as many electrons as possible with α_x's less than γ_0 . The perturbation is presumably turned off at or before injector turn off. Electrons remaining ($\alpha_x < \gamma_0$) continue to circulate without obstruction. It is this beam which is available for acceleration. The particular perturbation considered in this thesis is a "bump" of radial electric field oscillating at an RF frequency f_{RF} . The azimuthal extent of this electric field is much less than 2π . The azimuth θ at which the bump is set turns out to be immaterial. The frequency f_{RF} is usually set at or near the radial oscillation frequency $\nu_x f_0$.

In the experiment of Section VI an eledtrode consisting of a 1" by 1" square plate is set 0.32 " to the left of the equilibrium orbit at $\theta = 2\pi/6$ (Figures 1 and 25). We neglect electrodynamic effects. If the potential on the plate does not change significantly in the time it takes an electron to pass by the plate, then the problem reduces to that of an electron moving through an electrostatic field. An electron initially in a region of zero potential passes through a region of nonzero potential and on into a region of zero potential again. Though the electron's kinetic energy may vary in the neighborhood of the bump it is conserved when the complete pass is considered. Our present purpose is to understand the effect such an electric field bump has on an electron making a single pass of the bump.

It is assumed that all electrons travel in the median plane. They feel no vertical component of electric field. Imagine another 1" by 1" plate set opposite and charged opposite to the one of Figure 25. Consider an electron passing between these plates. Suppose the displacement x of the orbit is negative for $\theta < \frac{2\pi}{6}$, zero for $\theta = \frac{2\pi}{6}$, and positive for $\theta > \frac{2\pi}{6}$. Suppose also that at the time the electron

passes through this condenser the electric field between the plates exerts a force on it in the positive x direction. Since work done by the field on the electron, i.e., $F_x \Delta x$, is positive, the radial field in the neighborhood of $\theta = \frac{2\pi}{6}$ tends to increase the electron's kinetic energy. On the other hand, the electron loses energy as it does work against the azimuthal component of the fringe field at either end of the condenser. In both cases this azimuthal component is such as to slow the electron down. Hence, the electron first experiences a lowering of its kinetic energy, followed by an increase, which in turn is followed by another lowering. The resultant energy change is zero when the overall pass is considered.

We idealize such a bump by replacing it with two delta function kicks: one radial, the other azimuthal. Both are situated at $\theta = 2\pi/6$ and act simultaneously on any electron passing this azimuth. We guess that the azimuthal impulse influences electron motion but little. The only reason for including it is to allow one to simulate the energy conserving property of the actual bump. The radial electron motion is simple harmonic. The radial impulse given to an electron by the bump is $F_x \Delta\tau = m \Delta\dot{\rho}$. Here F_x is the radial electric force acting on an electron for a time $\Delta\tau$. If we view an electron's representative point in phase space as the electron passes the bump, we expect to see its x coordinate remain invariant but its y coordinate jump by an amount $\Delta y = \frac{F_x \Delta\tau}{m\omega_x} = \frac{\Delta\dot{\rho}}{\omega_x}$. Since the square of the electron oscillation amplitude, . . , before application of the bump is $x^2 + y^2$, we expect that afterwards it will be $x^2 + (y + \Delta y)^2$. The change in this quantity across the bump is $\Delta(a_x^2) = 2y\Delta y + \Delta y^2$. It is next shown that this result is nearly correct.

The equations of motion for an electron in our idealized accelerator are

$$m(\ddot{\rho} - \rho\dot{\theta}^2) = -e\rho\dot{\theta} B_1 \left(\frac{\rho}{\rho_1}\right)^n$$

$$m(\rho\ddot{\theta} + 2\dot{\rho}\dot{\theta}) = e\dot{\rho} B_1 \left(\frac{\rho}{\rho_1}\right)^n$$

For an electron whose orbit is its equilibrium orbit, $\ddot{\rho} \equiv \dot{\rho} \equiv \ddot{\theta} \equiv 0$ and $\rho = \rho_0$, $\dot{\theta} = \omega_0 = \frac{e}{m} B_1 \left(\frac{\rho_0}{\rho_1}\right)^n$. Letting α represent $\frac{e}{m} B_1 \frac{1}{\rho_1^n}$, these equations of motion become

$$\ddot{\rho} - \rho\dot{\theta}^2 = -\alpha\rho\dot{\theta}\rho^n$$
$$\rho\ddot{\theta} + 2\dot{\rho}\dot{\theta} = \alpha\dot{\rho}\rho^n$$

The first integrals of these equations are

$$\dot{\rho}^2 + (\rho\dot{\theta})^2 = \text{constant} = v_0^2 = \omega_0^2\rho_0^2 = \alpha^2\rho_0^{2n+2}$$
$$\rho^2\dot{\theta} - \alpha\frac{\rho^{n+2}}{n+2} = \text{constant} = \mathcal{L}$$

The first equation states that electron energy is conserved. That the second is true is seen by differentiating it with respect to time, dividing by $\rho \neq 0$, and comparing the result with the second equation of motion. These two first integrals allow one to find the amplitudes of radial oscillation in terms of the two constants of the motion, ρ_0 and $\mathcal{L}$. When an electron exhibits its maximum or minimum value of ρ, its $\dot{\rho}$ is zero. When such is the case, the first equation yields $\dot{\theta} = \alpha\frac{\rho_0^{n+1}}{\rho}$ which upon substitution into the second gives

$$\rho\alpha\rho_0^{n+1} - \alpha\frac{\rho^{n+2}}{n+2} = \mathcal{L}$$

If one plots the left side of this equation as a function of $\rho > 0$, the positive linear term predominates at small ρ $(n > 0)$. At larger ρ the negative term predominates. The function realizes its maximum at $\rho = \rho_0$. A plot of the right side of this equation is just a horizontal line of ordinate $\mathcal{L}$. The abscissas at which this line intersects the other curve are the maximum and minimum ρ exhibited by an oscillating electron whose constants of the motion are ρ_0 and $\mathcal{L}$.

The left side of this equation resembles a parabola in the neighborhood of its vertex, the resemblance being more perfect the smaller the

interval on either side of ρ_0 one restricts oneself to. When the two values of ρ which satisfy the previous equation lie within such an interval, the electron oscillation is simple harmonic. We replace ρ in the previous equation by $\rho_0 + a_x$ and solve for the lowest power of a_x which occurs.

$$(\rho_0 + a_x)\,\alpha\,\rho_0^{n+1} - \alpha\frac{(\rho_0 + a_x)^{n+2}}{n+2} = \mathcal{L}$$

$$\alpha\rho_0^{n+2}\left[1 + \frac{a_x}{\rho_0} - \frac{1}{n+2}\left(1 + \frac{a_x}{\rho_0}\right)^{n+2}\right] = \mathcal{L}$$

$$\alpha\rho_0^{n+2}\left[1 + \frac{a_x}{\rho_0} - \frac{1}{n+2}\left(1 + (n+2)\frac{a_x}{\rho_0} + \frac{(n+2)(n+1)}{2}\left(\frac{a_x}{\rho_0}\right)^2 + \cdots\right)\right] = \mathcal{L}$$

$$\alpha\rho_0^{n+2}\left[\frac{n+1}{n+2} - \frac{n+1}{2}\left(\frac{a_x}{\rho_0}\right)^2 + \cdots\right] = \mathcal{L}$$

$$a_x^2 = \frac{2}{\alpha}\frac{1}{n+1}\frac{1}{\rho_0^n}\left[\alpha\frac{n+1}{n+2}\rho_0^{n+2} - \mathcal{L}\right]$$

We desire the change in a_x^2 i.e., which occurs when the constants of the motion ρ_0 and $\mathcal{L}$ change slightly because of the bump acting on the electron. Later we shall restrict ourselves to the case of a bump which concerves energy, i.e., one in which $\Delta\rho_0 = 0$.

$$\frac{\partial(a_x^2)}{\partial\rho_0} = \frac{2}{\alpha}\left(\frac{-n}{n+1}\right)\rho_0^{-n-1}\left[\alpha\frac{n+1}{n+2}\rho_0^{n+2} - \mathcal{L}\right]$$

$$+ \frac{2}{\alpha}\frac{1}{n+1}\frac{1}{\rho_0^n}\left[\alpha(n+1)\rho_0^{n+1}\right]$$

$$= -\frac{n}{\rho_0}a_x^2 + 2\rho_0$$

$$\frac{\partial(a_x^2)}{\partial\mathcal{L}} = -\frac{2}{\alpha}\frac{1}{n+1}\frac{1}{\rho_0^n} = \frac{-2}{\omega_0(n+1)}$$

Hence,

$$\Delta(a_x^2) = \left(2\rho_0 - \frac{n}{\rho_0} a_x^2\right)\Delta\rho_0 - \frac{2}{\omega_0}\frac{1}{(n+1)}\Delta\mathcal{L}$$

A bump which increases an electron's energy increases its ρ_0. The ordinate of the parabola vertex becomes greater for greater ρ_0 so that with other things remaining constant one expects a_x^2 to increase. The quantity $2\rho_0\Delta\rho_0$ measures this increase. As ρ_0 increases, however, the parabola becomes more pointed in the neighborhood of its vertex. The damping of the electron oscillation which results is accounted for by the term $-\frac{n}{\rho_0} a_x^2 \Delta\rho_0$. The change in the ordinate $\mathcal{L}$ of the horizontal line intersecting the parabola is $\Delta\mathcal{L}$. The change in a_x^2 due to this shift is $-\frac{1}{\omega_0}\frac{2}{n+1}\Delta\mathcal{L}$. Though $\mathcal{L} = \rho^2\dot{\theta} - \alpha\frac{\rho^{n+2}}{n+2}$ is not proportional to an electron's angular momentum, $\Delta\mathcal{L} = \rho^2\Delta\dot{\theta}$ is proportional to its change in angular momentum due to the bump. The quantity ρ is continuous across the bump while $\dot{\theta}$ is not. In what follows $\Delta\dot{\theta}$ and $\Delta\dot{\rho}$ represent the discontinuous change in an electron's $\dot{\theta}$ and $\dot{\rho}$ due to the bump.

The damping term can be neglected relative to the vertex term. In the experiment of Section VI the ratio of the former to the latter is about 10^{-4}, i.e., $\frac{n a_x^2}{\rho_0} \Big/ 2\rho_0 = \frac{n}{2}\left(\frac{a_x}{\rho_0}\right)^2 \leq \left(\frac{0.7}{2}\right)\left(\frac{0.25''}{12''}\right)^2 = 1.5 \times 10^{-4}$. Restricting ourselves to a bump which conserves energy makes $\Delta\rho_0 = 0$. Hence,

$$\Delta(a_x^2) = -\frac{2}{\omega_0}\frac{1}{n+1}\Delta\mathcal{L}$$

Since electron energy before collision must equal that after, $\dot{\rho}^2 + (\rho\dot{\theta})^2 = (\dot{\rho}+\Delta\dot{\rho})^2 + \rho^2(\dot{\theta}+\Delta\dot{\theta})^2$ or $2\dot{\rho}\Delta\dot{\rho} + \Delta\dot{\rho}^2 + \rho^2(2\dot{\theta}\Delta\dot{\theta} + \Delta\dot{\theta}^2) = 0$. The quantity $\dot{\rho}$ can be small so that it is not valid to neglect $(\Delta\dot{\rho})^2$ relative to $2\dot{\rho}\Delta\dot{\rho}$. We can, however, neglect $\Delta\dot{\theta}^2$ relative to $2\dot{\theta}\Delta\dot{\theta}$. We estimate the error involved. Let $\beta_6 = 2\dot{\rho}\Delta\dot{\rho} + (\Delta\dot{\rho})^2$. Then

$$(\Delta\dot\theta)^2 + 2\dot\theta\,\Delta\dot\theta + \frac{\beta_6}{\rho^2} = 0$$

$$\Delta\dot\theta = -\frac{\beta_6}{2\rho^2\dot\theta}\left[1 + \frac{\beta_6}{4\rho^2\dot\theta^2} + \cdots\right]$$

Since: $\rho = \rho_0\left(1 + \frac{\chi}{\rho_0}\right)$; $\dot\theta = \omega_0\left(1 - \frac{\chi}{\rho_0}\right)$; $\omega_x = \omega_0\sqrt{1+n}$;

$y = \frac{m\dot x}{m\omega_x} = \frac{\dot x}{\omega_x} = \frac{\dot\rho}{\omega_x}$,

we have that

$$\frac{\beta_6}{4\rho^2\dot\theta^2} \cong \frac{2\dot\rho\,\Delta\dot\rho + (\Delta\dot\rho)^2}{4\rho_0^2\omega_0^2} = \frac{\nu_x^2}{4\rho_0^2}\left(2y\,\Delta y + (\Delta y)^2\right)$$

In the experiment of Section VI the maximum y and Δy are, respectively, 0.25" and 0.010". Since $\nu_x \cong 1.36$ and since $\rho_0 \cong 12"$, $\frac{\beta_6}{4\rho^2\dot\theta^2}$ is of the order 10^{-4}. We neglect $\frac{\beta_6}{4\rho^2\dot\theta^2}$ relative to unity in the expression for $\Delta\dot\theta$ above. Hence,

$$\Delta\chi = \rho^2\Delta\dot\theta = \rho^2\left[-\frac{\beta_6}{2\rho^2\dot\theta}\right] = -\frac{\beta_6}{2\dot\theta}$$

$$= \frac{-\left(2\dot\rho\,\Delta\dot\rho + (\Delta\dot\rho)^2\right)}{2\omega_0\left(1 - \frac{\chi}{\rho_0}\right)} \cong \frac{-\left(2\dot\rho\,\Delta\dot\rho + (\Delta\dot\rho)^2\right)}{2\omega_0}\left(1 + \frac{\chi}{\rho_0}\right)$$

so that

$$\Delta(a_x^2) = \frac{-2}{\omega_0(n+1)}\Delta\chi = \frac{2}{\omega_0(n+1)}\,\frac{\left(2\dot\rho\,\Delta\dot\rho + (\Delta\dot\rho)^2\right)}{2\omega_0}\left(1 + \frac{\chi}{\rho_0}\right)$$

$$= \left(2y\,\Delta y + (\Delta y)^2\right)\left(1 + \frac{\chi}{\rho_0}\right)$$

This result differs from the guess made previously by the factor $\left(1+\frac{\chi}{\rho_0}\right)$. This factor comes in because the change $\Delta\chi = \rho^2\Delta\dot\theta$ in an electron's angular momentum produced by a given azimuthal impulse depends on the radius ρ at which the electron happens to be when this impulse is applied to it, i.e.,

$$\Delta x = \rho(\rho\Delta\theta) = \rho\left(\frac{-\beta_6}{2\rho\dot{\theta}}\right) = \rho\left(\frac{-\beta_6}{2\rho_0\omega_0\left[1-\frac{x^2}{\rho_0^2}\right]}\right)$$

$$\cong \rho\left(-\frac{\beta_6}{2\rho_0\omega_0}\right) \qquad \beta_6 = 2\dot{\rho}\Delta\dot{\rho} + (\Delta\dot{\rho})^2$$

In the experiment of Section VI $\left|\frac{x}{\rho_0}\right| \leq \frac{0.25''}{12''} = \frac{1}{48}$. In what follows we neglect the factor $\left(1+\frac{x}{\rho_0}\right)$ so that $\Delta(a_x^2)$ is just equal to $2y\Delta y + (\Delta y)^2$. Hence, the conclusion as regards the effect of an energy conserving bump on an electron is that even though the azimuthal impulse enters into the theoretical picture its presence can be neglected from a practical point of view. An electron's (x,y) gets changed to $(x, y+\Delta y)$ in crossing the bump. It is satisfactory to compute Δy from the radial impulse $F_x\Delta\tau$, i.e., $\Delta y = \frac{F_x\Delta\tau}{m\omega_x}$.

In what follows the radial force exerted by the bump on an electron passing the bump, i.e., $F_x(x)$, is assumed independent of x. This means that all electrons passing the bump at the same time receive the same Δy. In Section VI it is shown that Resonant RF Inflection is relatively insensitive to dependence of F_x on x.

Before considering the properties of Resonant RF Inflection it is of interest to note properties of the accelerator-bump combination which are independent of the particular time dependence exhibited by the bump.

As before choose $i_0(x,y) = i_0$ over the lined region of Figure 6a. We do not require ν_x to be rational nor shall we wait a certain length of time after turning on the injector before viewing the beam. Before turning on the injector divide the "beam" into segments. Each is of azimuthal extent $d\theta$ and each travels around the accelerator once every $\tau = 1/f_0$ seconds. Set a phase plane in the middle of any one of these segments and let it travel with the segment. Though no electrons are in the segment, imagine the entire phase plane to be covered with points, their

density being uniform and equal to the nonzero value of $F(x,y,\theta,t)d\theta$ met previously. These points rotate about (0,0) with angular velocity $\omega_x = \nu_x f_o$. All points receive the same displacement Δy as the segment passes the bump. Neither rotation nor the bump change the relative positions of these points. Also, as the segment passes the injector the positions of these points are not disturbed. After the injector has been turned on each point may or may not have a single electronic charge -e attached to it; if a charge -e is attached, the point is said to be filled; if not, empty. If points covering an area of the phase plane are filled then there are electrons in the segment whose representative points also cover this same area to the same uniform density. If points covering an area are empty, then there are no electrons in the segment whose representative points cover this area. In what follows attention is focused on this hypothetical set of empty and filled points rather than on the actual representative points of electrons in the segment.

(1) Turn on the injector. Consider any one of the segments at the time it makes its initial pass of the injector after the injector has been turned on. At $\theta = 0-$ all points are empty. In crossing $\theta=0$ empty points are converted into filled points provided they lie within the lined region of Figure 6a. Empty points lying outside this region remain empty. Subsequent rotation or displacement Δy does not alter the occupation of any of these points.

(2) Consider any segment making its second pass of the injector after the injector has been turned on. The previous paragraph tells what happens to regions of empty points. Regions of filled points remain filled provided they lie within either the lined region of Figure 6a or to the right of $x = x_E$. In the first instance charge associated with filled points gets replaced with new charge. In the second, the same charge associated with filled points at $\theta = 0-$ is also associated with these

points at $\theta = 0+$. Filled points are converted into empty points provided they lie both to the left of $x = x_E$ and outside the lined region of Figure 6a. The phase space representation of the injector sink extends over the half plane to the left of $x = x_E$.

(3) Consider any segment making its third pass of $\theta = 0$ after the injector has been turned on. At $\theta = 0-$ all points on this segment's phase plane are either empty or filled. Paragraph (1) above tells what happens to empty points. Paragraph (2) above tells what happens to filled points. The net result is that all points are still either singly filled or empty when the segment finds itself at $\theta = 0+$.

(4) Paragraph (3) above is adequate to treat a segment making its fourth or higher pass of $\theta = 0$.

The preceding considerations indicate that no matter what time dependence $\Delta y(t)$ has and no matter how many times the segment passes the bump, the best one can hope to do is to have the interior of the beam circle of the segment under consideration completely covered with singly filled points. When all segments are considered the best one can hope to do is to have the beam circle interior of every segment completely covered with filled points. This limit also corresponds to seeing on a phase plane fixed at any azimuth θ an $i(x,y)$ of i_0 over the complete interior of the beam circle for a period of time τ. If this limit were achieved, the filling efficiency would be 100%; the charge available for acceleration would be $i_0 \pi r_0^2 \tau$. These conclusions also follow from Liouville's theorem.

Since an upper limit on filling is known, the degree to which any bump $\Delta y(t)$ allows filling to approach this ideal can, in principle, be found. We turn our attention to evaluating the filling efficiency for the particular type of bump used by Cook, i.e., $\Delta y(t) = k \sin(\omega_{RF} t + \phi)$. In what follows we refer to the injector as <u>infinite</u> if the region in

phase space at $\theta = 0+$ over which $i_o(x,y) = i_o$ is like that in Figure 6a. Here A_x is several times larger than r_o. When the region over which $i_o(x,y) = i_o$ is as small as possible without decreasing the filling efficiency achieved with an infinite injector, we shall refer to the injector as being finite. With a finite injector the region of (x,y) at $\theta = 0+$ over which $i_o(x,y) = i_o$ will be called the required injection area.

III. RESONANT RF INFLECTION (RRFI)

3.1 INFINITE INJECTOR AND NO SEPTUM

We wish to know how much charge RRFI can trap relative to the theoretical limit set by Liouville's theorem. The terminology used below is defined in the last paragraphs of Section II. We assume an infinite injector having a septum of zero thickness. It turns out to be immaterial at what azimuth the bump is placed. For simplicity we set it at $\theta = 0$. The bump has the form $\Delta y = k \sin(\omega_{RF} t + \phi)$ where the RF frequency f_{RF} is set equal to the electrons' radial oscillation frequency $\nu_x f_0$. In finding the filling efficiency given by such a bump we do a rough treatment of the problem first, following this with a more exact treatment. The latter method is used in Section 3.2 where one works with a finite injector and in Section 3.3 where one estimates the effect of including a septum of nonzero thickness.

Choose $\nu_x = L/N$ with N very large; let $i_o(x,y)$ equal i_o over the lined region of Figure 6a; turn on the injector but not the bump. After waiting at least NT seconds consider a phase plane fixed at any azimuth θ. One finds that Figure 6f illustrates what is seen provided the pentagon in this figure is replaced by an N-sided polygon rotated clockwise $\nu_x \theta$ radians from its orientation at $\theta = 0$. Because N is large, this polygon looks like the beam circle r_0. Next, turn the injector off but imagine at this instant of turn off that the injector somehow becomes transparent to electrons. Figure 6f, as modified above, still applies at all azimuths θ and all times t. Break the beam into segments and set a phase plane in one of them letting it travel around the accelerator with the segment.

Turn on the RF bump. All points on the phase plane, irrespective of whether they are empty or full, rotate clockwise with angular velocity ω_x. Each receives the same displacement Δy when the segment passes the bump. We define the time t to be zero when the segment under consideration makes its first pass of the bump after the RF has been turned on. When other segments are considered, t = 0 will be similarly defined. In each case ϕ will be the RF phase angle existing at a segment's t = 0. This angle varies from one segment to the next.

The segment under consideration passes $\theta = 0$ at $t = 0, \tau, 2\tau, \cdots$. The bump is thought of as being a uniform radial electric field $\mathcal{E}_0 \sin(\omega_{RF} t + \phi)$ v of azimuthal extent $\pm \frac{\Delta\theta}{2}$ about $\theta = 0$. Let $\Delta\tau$ be the time it takes an electron to cross the bump. In terms of time the bump extends $\pm \frac{\Delta\tau}{2}$ seconds to either side of those times when the segment is at $\theta = 0$. The electric force acting on electrons in the segment is the product of $-e\mathcal{E}_0 \sin(\omega_{RF} t + \phi)$ and a periodic square wave of unit height and period τ extending $\pm \frac{\Delta\tau}{2}$ seconds to either side of $t = 0, \tau, 2\tau, \cdots$. Figure 11 illustrates one cycle of this square wave. Expanding it in a Fourier series about t = 0 on the interval $-\frac{\tau}{2} \le t < \frac{\tau}{2}$ yields for the time dependent electrical force felt by points in the segment.

$$-e\mathcal{E}_0 \sin(\omega_{RF} t + \phi) \sum_{n=0}^{\infty} a_n \cos\left(2\pi n \frac{t}{\tau}\right)$$

We neglect all terms but the first. The constant a_0 is just the average height of the square wave over a period τ, i.e., $a_0 = \frac{1 \cdot \Delta\tau}{\tau} = \frac{\Delta\tau}{\tau}$ (This approximation corresponds to, not a bump, but an RF electric field uniformly distributed around the machine. Its interest is that it gives the right answer for the actual problem involving the bump).

The equation of motion for a point on the phase plane is

$$\ddot{x} = -\omega_x^2 x - \frac{e\mathcal{E}_0}{m} \frac{\Delta\tau}{\tau} \sin(\omega_{RF} t + \phi)$$

This is the equation for a forced harmonic oscillator. We set the

forcing frequency ω_{RF} equal to ω_x. It proves convenient to express the constant $-\frac{e\mathcal{E}_0}{m}\frac{\Delta\tau}{\tau}$ in terms of k. The radial impulse $F_x\Delta\tau$ an electron receives in passing the bump is $-e\mathcal{E}_0 \sin(\omega_x t+\phi)\Delta\tau$

Since $\Delta y = k\sin(\omega_x t+\phi) = \frac{F_x\Delta\tau}{m\omega_x}\sin(\omega_x t+\phi)$, we have

$$-\frac{e\mathcal{E}_0}{m\omega_x}\Delta\tau = k$$

$$-\frac{e\mathcal{E}_0}{m}\frac{\Delta\tau}{\tau} = \frac{k\omega_x}{\tau}$$

The equation of motion becomes

$$\ddot{x} + \omega_x^2 x = \frac{k\omega_x}{\tau}\sin(\omega_x t+\phi)$$

The solution for the inhomogeneous portion is

$$x = -\frac{t}{\tau}\frac{k}{2}\cos(\omega_x t+\phi)$$

The complete solution is

$$x = \left\{B - \frac{t}{\tau}\frac{k}{2}\cos\phi\right\}\cos\omega_x t + \left\{A + \frac{t}{\tau}\frac{k}{2}\sin\phi\right\}\sin\omega_x t$$

where A and B are constants. Differentiating x with respect to time and dividing $\dot{x}$ by ω_x yields y.

$$y = -\left\{B - \frac{t}{\tau}\frac{k}{2}\cos\phi\right\}\sin\omega_x t + \left\{A + \frac{t}{\tau}\frac{k}{2}\sin\phi\right\}\cos\omega_x t$$

$$-\frac{1}{\tau\omega_x}\frac{k}{2}\cos(\omega_x t+\phi)$$

We drop the last term realizing this introduces an error into y which is never greater than k/10. It will become apparent that this error is of no practical significance. Here $\nu_x > 1$ and $k \ll r_0$.

We have found that

$$\begin{pmatrix} x \\ y \end{pmatrix} = \begin{pmatrix} \cos\omega_x t & \sin\omega_x t \\ -\sin\omega_x t & \cos\omega_x t \end{pmatrix}\begin{pmatrix} B - \frac{t}{\tau}\frac{k}{2}\cos\phi \\ A + \frac{t}{\tau}\frac{k}{2}\sin\phi \end{pmatrix}$$

To visulaize this result it is helpful to go into a coordinate system rotating with the points on the phase plane. Letting (x', y') represent the coordinates of a point in this new system we have for the transformation between systems

$$\begin{pmatrix} x' \\ y' \end{pmatrix} = \begin{pmatrix} \cos \omega_x t & -\sin \omega_x t \\ \sin \omega_x t & \cos \omega_x t \end{pmatrix}$$

Coupling this with the above result we have

$$\begin{pmatrix} x' \\ y' \end{pmatrix} = \begin{pmatrix} B - \frac{\pm}{\uparrow} \frac{k_2}{2} \cos\phi \\ A + \frac{\pm}{\uparrow} \frac{k_2}{2} \sin\phi \end{pmatrix}$$

Since $\begin{pmatrix} x' \\ y' \end{pmatrix} = \begin{pmatrix} x \\ y \end{pmatrix} = \begin{pmatrix} x_0 \\ y_0 \end{pmatrix}$ at $t = 0$,

$$\begin{pmatrix} x' \\ y' \end{pmatrix} = \begin{pmatrix} x_0 \\ y_0 \end{pmatrix} + \frac{t}{\uparrow} \frac{k_2}{2} \begin{pmatrix} -\cos\phi \\ \sin\phi \end{pmatrix}$$

The orientation of the unit vector $\begin{pmatrix} -\cos\phi \\ \sin\phi \end{pmatrix}$ depends only on the RF phase angle ϕ at t = 0. The scalar $\frac{t}{\uparrow} \frac{k_2}{2}$ multiplies this vector. Every point on the phase plane, therefore, moves away from its original position (x_0, y_0) with constant velocity $\frac{1}{\uparrow} \frac{k_2}{2}$ along a straight line whose orientation is the same for every point. The empty circular region gets pulled away from the beam circle, a region of filled points being pushed into the beam circle. The region of filled points lying inside $r = r_0$ at this stage is crescent-shaped. When $\frac{t}{\uparrow} \frac{k_2}{2}$ equals $2r_0$, the empty region lies outside the beam circle. At this time the interior of the beam circle is completely covered with filled points ($A_x > 3r_0$). We turn off the bump.

Switching from the (x', y') system to the (x, y) system one sees an empty circular region lying outside $r = r_0$ which rotates clockwise about $(0, 0)$ with angular velocity ω_x. The beam circle itself still appears filled. Since covering of the beam circle occurs for any ϕ, we conclude that similar covering would be seen on the phase plane of any segment. If the injector, which is off, is now imagined to switch

from its transparent state to its normal or opaque state, all filled points external to the beam circle become empty points within $N\tau$ seconds after this switch. This result also holds for all segments.

We conclude that Resonant RF Inflection, under the assumptions made above, achieves the Liouville limit; it traps a charge $i_0 \tau r_0^2 \tau$ One questions whether turning off the injector and assuming it to be transparent alters the conclusions from those that would prevail if this had not been done. It does not. With an infinite opaque injector which is continually operating, filled points have no possibility of being converted into empty ones as long as their a_x's are less than A_x. This fact follows from the rules considered near the end of Section II. We note that all filled points occupying the beam circle at the time the RF is turned off have always had amplitudes less than A_x.

The previous example does differ from what takes place with an opaque injector in operation throughout in that no empty circular region lying outside the beam circle is realized. Empty points outside $r = r_0$ but within $r = A_x$ tend to be converted into filled points. Any region of empty points finding itself within the lined region of Figure 6a when the segment passes the injector becomes a filled region. The details of this process are of no interest to us here as once an empty point has been pushed outside the beam circle it remains outside. By choosing $A_x > 3r_0$ and by turning off the RF when $\frac{t}{\tau} \frac{h}{2}$ equals $2r_0$ we have been able to insure that only filled points enter the beam circle.

The ability of RRFI in conjunction with an infinite injector having a septum of zero thickness to realize the Liouville limit will now be illustrated by an alternative method. This approach includes the effect of all terms of the Fourier series met previously rather than just the

first. Exact algebraic transformations are used rather than an approximate differential equation. Nevertheless, basic results given by these two approaches agree. Besides paralleling the actual problem more closely the second approach can answer questions about RRFI other than the one we are presently concerned with.

Choose $\nu_x = L/N$; let $i_o(x,y)$ equal i_o over the lined region of Figure 6a; turn on the injector but not the bump. After waiting N↑ seconds one inserts a phase plane at $\theta = 0$ and finds that Figure 6f applies provided the pentagon in this figure is replaced by an N-sided polygon. Break the beam into segments and set a phase plane in one of them letting it travel around the accelerator with the segment. Previously we allowed ourselves to view this plane at any azimuth. Here we restrict ourselves to viewing points on this plane only when the segment is at $\theta = 0$.

The bump $\Delta y = k \sin(\omega_{RF} t + \phi)$ is set at $\theta = 0+$. Here it is thought of as being produced by a very intense uniform radial electric field $\mathcal{E}_o \sin(\omega_{RF} t + \phi)$ extending over a very small azimuth. Turn on the bump. We define the time t to be zero when the segment makes its first pass of $\theta = 0$ after the bump is on. When other segments are considered, zero time will be similarly defined. In each case ϕ will be the RF phase angle appropriate to a segment's $t = 0$. This angle varies from one segment to the next. When the segment under consideration passes $\theta = 0+$ at time t, every point on its phase plane receives a vertical displacement $\Delta y = k \sin(\omega_{RF} t + \phi)$. We agree not to view the effect of this displacement until the segment appears at $\theta = 0$ one revolution later.

We denote the Δy a point receives at t = 0+ by Δy_0; that at $t = \tau_+$ by Δy_1; etc. Consider a general point (x_0, y_0) on the phase plane at t = 0. At t = 0+ $\begin{pmatrix} 0 \\ \Delta y_0 \end{pmatrix}$ gets added to $\begin{pmatrix} x_0 \\ y_0 \end{pmatrix}$. Since we view the segment only at $\theta = 0$ we do not see the effect of this displacement until t = 0+ at which time the resultant vector $\begin{pmatrix} x_1 \\ y_1 \end{pmatrix}$ is $\begin{pmatrix} x_1 \\ y_1 \end{pmatrix} = M\begin{pmatrix} x_0 \\ y_0 \end{pmatrix} + M\begin{pmatrix} 0 \\ \Delta y_0 \end{pmatrix}$ The vectors $\begin{pmatrix} x_n \\ y_n \end{pmatrix}$ appropriate to $t = n\tau$, n = 0, 1, 2, ..., are given in Table 1. A simpler expression for $\begin{pmatrix} x_n \\ y_n \end{pmatrix}$ obtains if one further restricts viewing times to be integral multiples of $N\tau$, i.e., $t = IN\tau$ where I = 1, 2, 3, ... The details of this simplification are given in Appendix 1. The result is

$$\begin{pmatrix} x_{IN} \\ y_{IN} \end{pmatrix} = \begin{pmatrix} x_0 \\ y_0 \end{pmatrix} + IN\frac{k}{2}\begin{pmatrix} -\cos\phi \\ \sin\phi \end{pmatrix}$$

The first method gave

$$\begin{pmatrix} x' \\ y' \end{pmatrix} = \begin{pmatrix} x_0 \\ y_0 \end{pmatrix} + \frac{t}{\tau}\frac{k}{2}\begin{pmatrix} -\cos\phi \\ \sin\phi \end{pmatrix}$$

Here (x', y') is a point on the segment's phase plane viewed from a coordinate system rotating with the points on this plane. When $IN\tau$ is substituted for t, the result is identical to that found with the second method. One notes that when $t = IN\tau$ the x'-y' axes coincide with x-y axes at $\theta = 0$.

Figure 7 is a plot of $\begin{pmatrix} x_{IN} \\ y_{IN} \end{pmatrix}$ for I = 0, 1, 2, 3, 4, and 5. Here ϕ is $\pi/8$. Arbitrary values have been assigned to x_0, y_0, and $N\frac{k}{2}$. A sequence of evenly spaced points lying on a straight line is realized. A line between two adjacent points directed from the point of lower I to the one of higher I corresponds to $N\frac{k}{2}\begin{pmatrix} -\cos\pi/8 \\ \sin\pi/8 \end{pmatrix}$. The vectors $\begin{pmatrix} x_0 \\ y_0 \end{pmatrix}$ and $\begin{pmatrix} x_{3N} \\ y_{3N} \end{pmatrix}$ also appear in Figure 7. As I increases, the region of filled points $(r_0 < r < A_x$ at $t = 0)$ is displaced across the beam circle eventually covering it $(A_x >> r_0)$. At the time the beam circle interior becomes

covered, the RF is turned off. This covering takes place no matter what orientation the vector $N\frac{k}{2}\begin{pmatrix}-\cos\phi\\ \sin\phi\end{pmatrix}$ has. In what follows $N\frac{k}{2}\begin{pmatrix}-\cos\phi\\ \sin\phi\end{pmatrix}$ is called the N-turn displacement vector. Points initially residing within the beam circle tend to be converted into filled points as they move through the region between $r = r_0$ and $r = A_x$. Filled points moving into the region outside $r = A_x$ eventually become empty points.

From study of the first approach we know that an arbitrary segment which appears filled at one azimuth will appear filled at all azimuths. Hence, upon turning off the injector the charge which remains trapped is $i_0 \pi r_0^2 \tau$.

Though RRFI has been able to realize 100% filling efficiency it is, in another sense, quite inefficient. The ratio of the trapped charge to the charge emitted by the injector is small. When $A_x >> r_0$ the area of the lined region in Figure 6a is approximately $\frac{1}{2}\pi A_x^2$. Multiplying this area by i_0 gives the injector current. In the x'-y' system a point must be displaced $2r_0$ before the beam circle interior is completely covered with filled points. Since its displacement velocity is $\frac{k}{2\tau}$, the minimum time the injector must be on is nearly $\frac{2r_0}{(k/2\tau)} = \frac{4r_0\tau}{k}$. The total charge injected is the product of the injector current and this time, i.e., $i_0\frac{\pi A_x^2}{2}\left(\frac{4r_0\tau}{k}\right)$. The charge efficiency is the ratio of the trapped charge to the injected charge, i.e., $i_0\pi r_0^2\tau / \left(i_0\frac{\pi A_x^2}{2}\frac{4r_0\tau}{k}\right) = \frac{1}{2}\left(\frac{r_0}{A_x}\right)^2\left(\frac{k}{r_0}\right)$. Since $\frac{r_0}{A_x} << 1$ and since $\frac{k}{r_0} << 1$ the charge efficiency here is very low. In Section 3.2 a less pessimistic result is obtained by replacing the area of the lined region in Figure 6a with the required injection area.

3.2. FINITE INJECTOR AND NO SEPTUM

The charge efficiency of RRFI in conjunction with a finite injector having a septum of zero thickness depends on the required

injection area. Study of the case where $\nu_x = 1/3$ leads to an expression for this area applicable to any tune $\nu_x = L/N$ provided k of $\Delta y = k \sin(\omega_x t + \phi)$ is sufficiently small.

When $\nu_x = L/N = 1/3$ the N-turn displacement vector $N\frac{k}{2}\begin{pmatrix} -\cos\phi \\ \sin\phi \end{pmatrix}$ has magnitude $\frac{3}{2}k$. This suggests that an injector of x extent $\frac{3}{2}k(1+\epsilon)$ may be sufficient to maintain 100% filling. Here $0 < \epsilon << 1$. The injector's y extent will be terminated so that on a phase plane fixed at $\theta = 0$ a filled band like that of Figure 8 is realized in the absence of RF. The emitting region of the injector is the shaded area to the left of the dashed vertical line. The back side of the injector ($x < x_0$) continues to act as a sink.

Consider a particular segment of the beam. In the absence of RF it will appear at $\theta = 0$ at some time t which we take here as $t = 0$. It is seen again at $\theta = 0$ τ seconds later. In this time τ, points on the segment's phase plane have rotated clockwise 120°. At $t = 2\tau$ a rotation of 240° is evident. At $t = 3\tau$ all points are back in their original positions. In this three-turn process the charge associated with each point of the band has been replaced at least once. To keep track of which points have their charge replaced at which time the segment, as viewed at $t = 0$, will be subdivided into three overlapping trapezoids as shown in Figure 9. The trapezoid boundaries are thought of as rotating with the points of a segment. In the absence of RF the same filled points occupy a given trapezoid for all time. Points lying in trapezoid $\overline{ABFGA}$ have their charge replaced at $t = \tau, 4\tau, 7\tau, \cdots$, those in $\overline{CDGHC}$ at $t = 2\tau, 5\tau, 8\tau, \cdots$, and those in $\overline{ADEIA}$ at $t = 3\tau, 6\tau, 9\tau, \cdots$.

In the presence of RF the trapezoid boundaries do not suffer displacement; points do. Consequently, empty points can be displaced into a trapezoid, etc. Whenever one of the trapezoids coincides in its

entirety with the injector any empty points within it become filled while filled points in it simply have their charge replaced. Each trapezoid coincides in its entirety with the injector once in every three passes the segment makes of the injector. Only one trapezoid undergoes such coincidence on any given pass. In proving that the chosen injector extent yields 100% filling it is first shown that a point from outside triangle $\overline{ADGA}$ of Figure 9 which gets displaced inside inside of triangle $\overline{JKLJ}$ is seen to reside within the triangular band formed by the overlapping trapezoids on <u>at least three consecutive passes</u> of the injector immediately prior to that pass on which it is first seen to reside within triangle $\overline{JKLJ}$.

The maximum displacement received in one pass of the bump is k; in two passes, $\frac{3}{2}k$; in three passes, $\frac{3}{2}k$. The two-pass value is obtained by maximizing the magnitude of

$$\begin{pmatrix} 0 \\ \Delta y_{t+\tau} \end{pmatrix} + M\left(\tfrac{1}{3}\cdot 2\pi\right)\begin{pmatrix} 0 \\ \Delta y_t \end{pmatrix}$$

as function of t. Since the band formed by the three trapezoids is a minimum of $\frac{3}{2}k(1+\epsilon)$ wide, the conclusion of the previous paragraph is true.

It is next shown that the point lies within one particular trapezoid on the first three of the three or more consecutive passes referred to above. On the pass just prior to that pass on which the point is first seen to reside within the band the point will be associated with that trapezoid, the major portion of which lies between the same pair of dashed lines of Figure 9 as the point itself lies between. If the point happens to be on a dashed line it can be associated with either one of the trapezoids which overlap in its neighborhood. On the next three passes the point resides in the band and is never greater than $\frac{3}{2}k$ away from its original position, i.e., the

position of the point at the time it was associated with a trapezoid. But Figure 9 shows that it must get more than $\frac{3}{2}k$ away to get out of the trapezoid with which it was originally associated. Hence, if the point was originally empty, it is converted into a filled point by the time it reaches the interior of triangle $\overline{JKLJ}$.

The chosen injector extent is therefore sufficient to yield 100% filling of the beam circle for the particular segment considered. Since the preceding arguments are independent of N-turn displacement vector orientation, the same conclusion applies to all segments of the beam. We conclude that when $\nu_x = 1/3$ an injector of x extent $\frac{3}{2}k$ and of y extent about equal to $2\sqrt{3}\,r_o$ is sufficient to maintain the 100% filling property of Resonant RF Inflection. Here $2\sqrt{3}\,r_o$ is the length of a side of the equilateral triangle in which the beam circle r_o is inscribed. If we require that the N-turn displacement, here $\frac{3}{2}k$, be much smaller than $2\sqrt{3}\,r_o$ then the area of the required injection area is just $\frac{3}{2}k(2\sqrt{3}\,r_o)$ or $3\sqrt{3}\,k\,r_o$. It is seen to depend linearly on k, approaching zero as k approaches zero.

One expects that a similar analysis could be carried through for other $\nu_x = L/N$ where $N>3$. We shall assume that such is the case. In what follows the N-turn displacement, $N\frac{k}{2}$, will be kept much less than the length of a side of the N-sided polygon in which the beam circle is inscribed.

The N=3 case has the practical disadvantage for large r_o of requiring a $\pm y$ extent larger than r_o, i.e., $\pm\sqrt{3}\,r_o$. Usually one would like it to be somewhat less than r_o . This can be realized by going to higher N. The circumference of the beam circle is $2\pi r_o$. For high N the length of one side of the N-sided polygon is approximately $\frac{2\pi r_o}{N}$. The $\pm y$ extent of the injector is therefore $\pm\frac{\pi r_o}{N} < r_o$. However, in de-

creasing the y extent, the x extent $N\frac{k}{2}$ has increased. The required injection area is their product, i.e., $N\frac{k}{2}\left(\frac{2\pi r_o}{N}\right) = \pi k r_o$. This result for high N is about 0.6 of that for N = 3.

The charge efficiency appropriate to the case of high N will now be found. The N-turn displacement $N\frac{k}{2}$ shows that $\frac{k}{2}$ can serve as an average displacement per turn. The displacement velocity is $\frac{k}{2\tau}$. For high N, the beam circle will be covered with filled points at the time the displacement equals the diameter of the beam circle $2r_o$. The time required to achieve complete filling is therefore $2r_o$ divided by $\frac{k}{2\tau}$. The charge emitted by the injector in this time is $i_o(\pi k r_o)\frac{2r_o}{(k/2\tau)}$. The trapped charge is $i_o(\pi r_o^2)\tau$. The resulting charge efficiency is 25%.

$$\frac{i_o(\pi r_o^2)\tau}{i_o(\pi k r_o)\left(\frac{2r_o}{k/2\tau}\right)} = \frac{1}{4} = 25\%$$

$N\frac{k}{2} << \frac{2\pi r_o}{N}$

The above result is valid under the conditions of high N, V, and zero septum thickness. Table 2 indicates how the charge efficiency approaches this limit with increasing N. Here the same expression for trapped charge has been used as before. However, in calculating the filling time the diameter of the circle circumscribing the polygon in question has been used instead of the beam circle diameter. This makes the charge efficiencies for low N in Table 2 smaller than they should be. A charge efficiency of about 20% is seen to be applicable for N≥6. In a practical situation the septum thickness is not zero $N\frac{k}{2} << \frac{2\pi r_o}{N}$ and V is violated. For such a case computational study will be relied upon to yield the charge efficiency.

3.3 FINITE INJECTOR AND FINITE SEPTUM

The presence of a septum of nonzero thickness lowers the filling efficiency. In terms of phase space a septum creates a strip of zero $i_o(x,y)$ lying between $x = -(r_o + \overline{DE})$ and $x = -r_o$. The septum thickness is $\overline{DE}$ (Figure 3). An estimate of filling efficiency, FE, can be made by noting that fraction of the required injection area remains uncovered by this strip. For instance, with $N\frac{k_2}{2} << \frac{2\pi r_o}{N}$, FE is zero when $N\frac{k_2}{2} < \overline{DE}$. When $N\frac{k_2}{2} > \overline{DE}$,

$$FE = 100\left[\frac{N\frac{k_2}{2} - \overline{DE}}{N\frac{k_2}{2}}\right]$$

In a practical situation $N\frac{k_2}{2}$ will exceed $\frac{2\pi r_o}{N}$ so that recourse to computation is necessary to determine the shape and size of the required injection area. Nevertheless even when $N\frac{k_2}{2} << \frac{2\pi r_o}{N}$, computational results indicate that the above procedure is at best an approximation, the reason being that not all portions of the required injection area are equally effective in contributing to the current trapped within the beam circle. The physical reason for this behavior is given below.

Let ν_x be 1/3. Break the beam into segments, each segment being viewed at $\theta = 0$ only on every third pass it makes of $\theta = 0$. The RF is turned on at $t = 0$. Viewing the beam at $\theta = 0$ will be limited to times t as follows:

$$0 \leq t < \tau$$
$$3\tau \leq t < 4\tau$$
$$6\tau \leq t < 7\tau$$
$$\cdots \quad \cdots$$

Between consecutive viewings of a segment the displacement vector

increases in length by $\frac{3}{2}k$ but its orientation remains invariant. The orientation appropriate to a segment is given by $\begin{pmatrix} -\cos(\omega_{RF}t_o+\phi) \\ \sin(\omega_{RF}t_o+\phi) \end{pmatrix}$ where $\omega_{RF}t_o+\phi$ is the phase angle of the RF at the time t_o a segment makes its first pass of the RF bump after the RF has been turned on. Choose ϕ to be 120^o. Then only displacement vectors which incline to the right and which lie within an angular range of $\pm 60^o$ about the horizontal are seen. In what follows only displacement vectors lying within $\pm 30^o$ of the horizontal will be considered. We also consider only that charge reaching the beam triangle ($\overline{JKLJ}$; Figure 9) which originates in a small neighborhood about a point (x,y) near $(-r_o,o)$, say $(x,0)$, where $(x,0)$ is to the left of $(-r_o,0)$. One wants to know how the amount of charge residing within the beam triangle which originated from this neighborhood varies with the position $(x,0)$ of this neighborhood.

Redefine $i_o(x,y)$ to be zero for all (x,y) outside a small neighborhood about $(x,0)$ but equal to i_o on this neighborhood. Suppose $(x,0)$ is more than $\frac{3}{2}k$ to the left of $(-r_o,o)$. Charge which becomes attached to points which lie in this neighborhood at time $t=t_o$ is seen at t just less than $t_o+3\tau$ to lie $\frac{3}{2}k$ from $(x,0)$. No matter what orientation the 3-turn displacement vector has, this island of filled points cannot lie within the beam triangle. Because of the way $i(x,y)$ is defined, this island of filled points is converted to a region of empty points at $t=t_o+3\tau$.

When $(x,0)$ is slightly less than $\frac{3}{2}k$ to the left of $(-r_o,0)$ then some of the charge which gets attached to points in the neighborhood of $(x,0)$ reaches the beam triangle. Consider a segment whose 3-turn displacement vector is both perpendicular to the left side of the beam triangle and directed to the right. At $t=t_o$ empty points in the neighborhood of $(x,0)$ become filled. At $t=t_o+3\tau$ an island of filled points

resides $\frac{3}{2}h$ to the right of $(x,0)$ and therefore within the beam triangle. At $t = t_0 + 6\tau$, two such islands are realized. On successive views a straight line chain of islands develops, each island being $\frac{3}{2}h$ from its nearest neighbors. When the first island reaches the other side of the beam triangle, equilibrium obtains. The number of islands trapped is proportional to the length of the chain. The horizontal line of dots in Figure 10 represents this chain for the particular segment under consideration.

Other segments also inject islands along chords of the beam circle. Results for five segments are superimposed in Figure 10. The range of inclinations exhibited by these chords is determined from $(x,0)$. This range is given by the angle between the two vectors of length $\frac{3}{2}h$ in Figure 10 whose origin is $(x,0)$ and which terminate on the beam triangle. As $(x,0)$ is set nearer $(-r_0,0)$, this angle becomes larger. Since angular range measures the number of segments contributing islands to the beam circle, we conclude that when $(x,0)$ is near $(-r_0,0)$, a neighborhood about $(x,0)$ contributes more charge to the beam circle than when $(x,0)$ is further from $(-r_0,0)$. The presence of a septum therefore lowers filling efficiency more than estimated on the basis of area arguments given previously.

The two paragraphs which follow discuss points which will become relevant in Section 5.2. This discussion is based on the example considered above.

A neighborhood of any contributing (x,y) near $(-r_0,0)$ contributes some islands which cross the beam circle on a diameter of this circle. The speed with which an island gets displaced is $\frac{h}{2\tau}$. This result applies not only to islands moving along a diameter but also along shorter chords inclined at some angle to a diameter. Consequently, about the same length of time is required for the small neighborhood about each contributing

(x,y) near $(-r_o,o)$ to achieve its maximum contribution to beam circle filling. This time is about $2r_o/(\frac{k}{2\pi})$

Choose $(x,0)$ to be almost $\frac{3}{2}k$ to the left of $(-r_o,0)$. Then only a few segments have a 3-turn displacement vector with the proper orientation to allow a neighborhood of $(x,0)$ to contribute islands of filled points to the beam circle. Consider a segment which does contribute. Divide the interior of the beam circle into, say, ten concentric annuli of equal area. Since the chord along which islands migrate nearly coincides with $y = 0$ and since the number of islands per unit length of this chord is constant along the chord, the number of islands in an annulus is proportional to the fraction of a beam circle diameter residing in the annulus. This fraction is larger for central annuli than it is for peripheral ones. If one now sets a phase plane at any azimuth and records $i(x,y,\theta,t)$ as a function of time, it is found that $i(x,y,\theta,t)$ for $\sqrt{x^2+y^2} < r_o$ is zero most of the time since most segments exhibit no islands. Nevertheless, when all segments are considered a time average of the quantity

$$\frac{\iint_{\text{Annulus}} i(x,y,\theta,t)\,dx\,dy}{\iint_{\text{Annulus}} dx\,dy},$$

the average being taken over an interval of, say, 100τ seconds after equilibrium prevails, will be nonzero and greater for central annuli than for peripheral ones. Even for central annuli, however, this time average is much less than i_o because of previous restrictions put on the size and position of the region of nonzero $i_o(x,y)$.

3.4 OFF-RESONANCE BEHAVIOR

In an actual accelerator there will be, of course, non-linear

effects. These effects cause the angular frequency of radial oscillation ω_x to depend on the amplitude a_x. This means that it will not be possible for ω_{RF} to be set equal to the ω_x for every electron, since there are electrons of various amplitudes present. The effects produced by this discrepancy are similar to those seen in the linear problem when $\omega_{RF} \neq \omega_x$. For this reason, as well as experimental considerations met later, a treatment of the off-resonance case of the linear problem will be given. In this treatment one starts with an equation of motion, the general solution of which reduces in cases of interest to an expression applicable to a forced harmonic oscillator.

Let $i_o(x,y) = i_o$ over the lined region of Figure 6a $(A_x >> \nu_o)$. The septum thickness is set equal to zero. If ν_x is chosen rational, N of $\nu_x = \frac{L}{N}$ should be large. Break the beam into segments. The bump $\Delta y = k \sin(\omega_{RF} t + \phi)$ is produced by a uniform radial electric field $\mathcal{E}_o \sin(\omega_{RF} t + \phi)$ of azimuthal extent $\pm \frac{\Delta\theta}{2}$ about $\theta = 0$. It takes $\Delta\tau$ seconds for a segment to cross the bump. In considering any particular segment, t is taken to be zero when this segment makes its first pass of $\theta = 0$ after the bump has been turned on. In each case ϕ is the RF phase angle existing at the segment's zero time. The angle ϕ varies from one segment to the next.

Set a phase plane in one of the segments letting it travel with the segment. The electric force acting on a point on this plane can be expressed as the product of $-e\mathcal{E}_o \sin(\omega_{RF} t + \phi)$ and a square wave of period τ and unit height on the interval $\pm \frac{\Delta\tau}{2}$ to either side of $t = 0, \tau, 2\tau \cdots$ Figure 11 illustrates one cycle of this function. If one expands it about t = 0 on the interval $-\frac{\tau}{2} \leq t < \frac{\tau}{2}$ then the equation of motion for a point becomes

$$\ddot{x} = -\omega_x^2 x - \frac{e\mathcal{E}_0}{m} \sin(\omega_{RF} t + \phi) \sum_{n=0}^{\infty} a_n \cos\left(2\pi n \frac{t}{\tau}\right)$$

Here the a_n are the expansion coefficients of the function illustrated in Figure 11.

$$a_0 = \frac{\Delta\tau}{\tau}$$

$$a_n = \frac{2}{\pi n} \sin\left(\pi n \frac{\Delta\tau}{\tau}\right) \qquad n \geq 1$$

The general solution to the equation of motion is

$$x = A \sin(\omega_x t) + B \cos(\omega_x t) - \frac{e\mathcal{E}_0}{2m} \sum_{n=0}^{\infty} a_n \left[\frac{\sin((\omega_{RF} + n\omega_0)t + \phi)}{\omega_x^2 - (\omega_{RF} + n\omega_0)^2} + \frac{\sin((\omega_{RF} - n\omega_0)t + \phi)}{\omega_x^2 - (\omega_{RF} - n\omega_0)^2} \right]$$

The quantities A and B are constants. This solution indicates that there are many resonant values of ω_{RF}. When nearly on resonance, the quantity of interest is the deviation of ω_{RF} from the on-resonance condition. This deviation will be expressed in terms of a quantity δ where

$$\delta + \omega_x = \omega_{RF} \pm n\omega_0 \qquad n \geq 0$$

When an on-resonance condition is nearly realized the general solution yields

$$n \geq 1; \qquad x = A \sin(\omega_x t) + B \cos(\omega_x t) - \frac{e\mathcal{E}_0}{2m} a_n \frac{\sin((\delta + \omega_x)t + \phi)}{\omega_x^2 - (\delta + \omega_x)^2}$$

$$n = 0; \qquad x = A \sin(\omega_x t) + B \cos(\omega_x t) - \frac{e\mathcal{E}_0}{m} a_0 \frac{\sin((\delta + \omega_x)t + \phi)}{\omega_x^2 - (\delta + \omega_x)^2}$$

It is seen that the results of studying the solution for n = 0 can serve for cases where n≥1 through suitable variation of $\mathcal{E}_0$. The case of n = 0 is considered here.

Letting $y = \frac{\dot{x}}{\omega_x}$ and letting $\beta = -\frac{e\mathcal{E}_0 a_0}{m} = -\frac{e\mathcal{E}_0}{m} \frac{\Delta\tau}{\tau}$ one has

$$x = A\sin(\omega_x t) + B\cos(\omega_x t) + \frac{B\sin((\delta+\omega_x)t+\phi)}{(\omega_x^2-(\delta+\omega_x)^2)}$$

$$y = A\cos(\omega_x t) - B\sin(\omega_x t) + \frac{B(\delta+\omega_x)\cos((\delta+\omega_x)t+\phi)}{\omega_x(\omega_x^2-(\delta+\omega_x)^2)}$$

(1) Express $\sin((\delta+\omega_x)t+\phi)$ and $\cos((\delta+\omega_x)t+\phi)$ in terms of sines and cosines of $\omega_x t$ and $\delta t+\phi$. (2) Collect coefficients of $\sin(\omega_x t)$ and $\cos(\omega_x t)$. (3) Neglect δ relative to ω_x in terms like $\delta+\omega_x$ which do not occur as an argument of a trigonometric function. (4) Evaluate the constants A and B in terms of (x,y) at t = 0, i.e., (x_o,y_o). The result is

$$\begin{pmatrix} x \\ y \end{pmatrix} = \begin{pmatrix} \cos(\omega_x t) & \sin(\omega_x t) \\ -\sin(\omega_x t) & \cos(\omega_x t) \end{pmatrix} \begin{pmatrix} x_o + \frac{B}{2\delta\omega_x}(\sin\phi - \sin(\delta t+\phi)) \\ y_o + \frac{B}{2\delta\omega_x}(\cos\phi - \cos(\delta t+\phi)) \end{pmatrix}$$

If the segment's phase plane is viewed from a coordinate system (primed) rotating with points on this plane then the transformation between systems is

$$\begin{pmatrix} x' \\ y' \end{pmatrix} = \begin{pmatrix} \cos(\omega_x t) & -\sin(\omega_x t) \\ \sin(\omega_x t) & \cos(\omega_x t) \end{pmatrix} \begin{pmatrix} x \\ y \end{pmatrix}$$

Hence

$$\begin{pmatrix} x' \\ y' \end{pmatrix} = \begin{pmatrix} x_o + \frac{B}{2\delta\omega_x}(\sin\phi - \sin(\delta t+\phi)) \\ y_o + \frac{B}{2\delta\omega_x}(\cos\phi - \cos(\delta t+\phi)) \end{pmatrix}$$

Collecting terms with no explicit time dependence on the left, squaring the components of the resulting vector, and adding these squared values gives

$$\left(x' - x_o - \frac{B}{2\delta\omega_x}\sin\phi\right)^2 + \left(y' - y_o - \frac{B}{2\delta\omega_x}\cos\phi\right)^2 = \left(\frac{B}{2\delta\omega_x}\right)^2$$

The tip of $\begin{pmatrix} x' \\ y' \end{pmatrix}$ therefore travels around a circle of radius $\left|\frac{\beta}{2\delta\omega_x}\right|$ centered at

$$\begin{pmatrix} x' \\ y' \end{pmatrix} = \begin{pmatrix} x_o + \frac{\beta}{2\delta\omega_x}\sin\phi \\ y_o + \frac{\beta}{2\delta\omega_x}\cos\phi \end{pmatrix}$$

once every $\frac{2\pi}{|\delta|}$ seconds. This circle, of radius $r_r = \left|\frac{\beta}{2\delta\omega_x}\right|$, will be called a resonance circle.

Points on a segment's phase plane between $r = A_x$ and $r = r_o$ will be assumed to be filled at $t = 0$. Points within $r = r_o$ at $t = 0$ are empty. The RF causes each point (x', y') to travel around a circle of radius r_r. A point returns to its original position $\frac{2\pi}{|\delta|}$ seconds later. In this process filled points initially outside the beam circle enter it and then withdraw. Some of the empty points initially within the beam circle move outside it and then return. The number of the latter which do move outside depends on r_r. While outside, these empty points tend to become filled, the probability of this occurring increasing with a point's maximum a_x and with the length of time it spends outside $r = r_o$. Here we assume that every empty point which gets pushed outside $r = r_o$ has become a filled point by the time it returns to the beam circle.

With $r_r > r_o$ all points initially within the beam circle get pushed outside it. Therefore 100% filling efficiency obtains in this case. However, when $r_r < r_o$ not all empty points get outside the beam circle. In this case, the effect of the off-resonance RF is to produce an unfilled circular region of radius $r_o - r_r$ lying within the beam circle. After the RF is turned on one must wait $\frac{2\pi}{|\delta|}$ seconds before this empty region of radius $r_o - r_r$ assumes its circular form. This empty region is not centered at $(0,0)$. Instead, its boundary touches the beam circle at a single point, this point of contact moving around the beam circle once

every $\frac{2\pi}{|\sigma|}$ seconds. The circle appearing at the upper left in Figure 12 is a resonance circle ν_r . Several are also drawn within the beam circle as an aid in visualizing why the empty region of radius $\nu_o - \nu_r$ within the beam circle is circular and why it moves in the manner described above.

In the portion of the experiment of Section VI which deals with off-resonance behavior one sets a vertical wire of thickness dx at $x = 0$ and measures the current collected by this wire (Figure 26). For purposes of illustration it is assumed here that the wire is set at $\theta = 0$, that every electron colliding with it sticks to it, and that there is no secondary emission. Knowing the collected current at time t yields the beam current density $j(x,\theta,t)$ at $x = \theta = 0$, i.e., $j(0,0,t)$ $\frac{\text{amperes}}{\text{meter}}$. The units are not conventional. One is interested in beam current at $\theta = 0$ due to electrons with x's between x and x + dx independent of their z values.

Collected current equals $j(0,0,t)dx$. The device which measures collected current does not respond to fluctuations occurring over a time τ but can to those which occur over a time 100τ. We denote $j(0,0,t)dx$ averaged over an interval extending, say, $\pm 50\tau$ to either side of time t as $\overline{j(0,0,t)dx}$. Experimentally it is found that $\overline{j(0,0,t)dx}$ approaches an equilibrium value shortly after the injector has been turned on. Two such equilibrium values are measured; one with RF on, the other with RF off. Let $\overline{\Delta j(0,0,t)}$ denote the result of subtracting the latter from the former. One measures $\overline{\Delta j(0,0,t)}$ as a function of bump strength k and of the deviation of f_{RF} from the on resonance value $\nu_x f_o$.

It is helpful to introduce the tune ν_{RF} of the RF.

$$\nu_{RF} = \frac{\omega_{RF}}{\omega_o} = \frac{f_{RF}}{f_o}$$

The deviation of ν_{RF} from ν_x will be called $\Delta\nu_{RF}$. In predicting the experimental results mentioned above it is assumed that $\overline{\Delta j(0,0,t)dx}$ is

due only to electrons forced into the beam circle by the RF. In the absence of RF, $i(x,y,\theta,t)$ for $\sqrt{x^2+y^2} < r_0$ is zero. Hence, in the presence of RF one has at $x = \theta = 0$

$$\overline{\Delta j(0,0,t)}\,dx = \left[\int_{-r_0}^{r_0} \overline{i(0,y,0,t)}\,dy\right] dx$$

The bar over i has the same meaning as the one over j. Previous considerations allow $\overline{i(0,y,0,t)}$ to be found.

Suppose that bump strength k and RF frequency f_{RF} have been chosen so that $r_0 > r_v > \frac{r_0}{2}$. Then figure 13 applies when points on a segment's phase plane are viewed from a coordinate system (primed) rotating with these points. The white circle within $r = r_0$ is covered with empty points; the lined region outside, with filled points. If, at the same time one views the phase plane of the particular segment for which Figure 13 happens to apply, one also views phase planes set in other segments, then Figure 13 still applies provided the point where the empty region touches the beam circle is changed appropriately. If at some instant one considers in sequence the segments of a block of segments extending over $\frac{2\pi}{\nu_{RF}}$ radians, one notes that this point of contact moves once around the beam circle.

The average $i(x,y,\theta,t)$ seen on a phase plane fixed at $\theta = 0$ over the time it takes the above block to pass $\theta = 0$ depends on (x,y) only through $r = \sqrt{x^2+y^2}$. This is so as the empty region is seen to revolve once around (0,0) as the block passes $\theta = 0$. This average can be found by considering only one segment of the block. Choose that segment for which Figure 13 applies when the segment passes $\theta = 0$. Choose a circle of radius r about (0,0) on this phase plane. Let the angle subtended by the arc of this circle which lies in the empty region be ψ. The arc lying in the filled region is $2\pi - \psi$. The average $i(x,y,0,t)$ on a narrow

annulus enclosing this circle is $i_o \frac{(2\pi - \Psi)}{2\pi}$. The quantity i_o will be set equal to unity.

The same result, $\frac{2\pi - \Psi}{2\pi}$, obtains if any other segment of the block is considered. Because the center of gravity of the empty portion of the annulus rotates through 2π when all segments of the block are considered, $\frac{2\pi - \Psi}{2\pi}$ also serves as the $\overset{\text{time}}{\vee}$average $i(x,y,0,t)$ exhibited by this block as it passes $\theta = 0$.

Before finding Ψ in terms of r , r_r , and r_o , one question remains. Though $\frac{2\pi - \Psi}{2\pi}$ can serve as the $\overset{\text{time}}{\vee}$average $i(x,y,0,t)$ for a block of segments of azimuthal extent $\frac{2\pi}{\nu_{RF}}$, there is not an integral number of such blocks around the accelerator. That this makes little difference can be seen by viewing any particular segment of the beam as it makes several successive passes of $\theta = 0$. On each pass the empty region appears to have been rotated clockwise nearly $\nu_x 2\pi$ radians from its position on the preceding pass. For practical ν_x the empty region effectively gets averaged over all orientations when enough passes are considered. Hence, $\overline{i(x,y,0,t)} = \frac{2\pi - \Psi}{2\pi}$. It is also true that $\overline{i(x,y,\theta,t)} = \overline{i(x,y,0,t)}$.

The quantity $\overline{i(x,y,\theta,t)}$ will be expressed in terms of r , r_r , and r_o . Figure 12 is applicable when $r_r < \frac{r_o}{2}$. When $r_o > r_r > \frac{r_o}{2}$, Figure 13 applies. Consider the latter case. Since the empty region does not enclose the origin, $\overline{i(x,y,\theta,t)} = 1$ for r going from zero to $2r_r - r_o$. For r lying between $2r_r - r_o$ and r_o , $\overline{i(x,y,\theta,t)} = \frac{2\pi - \Psi}{2\pi}$. The angle Ψ must be found in terms of r , r_r , and r_o . Circle r in Figure 13 intersects the boundary of the empty region at $(x',y') = \left(\pm r \sin\frac{\Psi}{2}, r\cos\frac{\Psi}{2}\right)$. The boundary of the empty region is given by $x'^2 + (y' - r_r)^2 = (r_o - r_r)^2$. Eliminating x' and y' yields

$$\cos\frac{\Psi}{2} = \left[\frac{r^2 - r_o^2 + 2r_o r_r}{2 r r_r}\right]$$

Hence

$$i(x,y,\theta,t) = 1 - \frac{1}{\pi}\cos^{-1}\left[\frac{r^2 - r_o^2 + 2r_o r_r}{2rr_r}\right]$$

$$2r_r - r_o < r < r_o \quad ; \quad r_o > r_r > \frac{r_o}{2}$$

These results, along with those for other ranges of r and r_r, are found in Table 3. A consistency check between these results and those obtained by computation was made. The dot at the tip of each of the four arrows in Figure 22 represent the former while the solid curve nearest these dots represents the latter.

It is of interest to note the difference between $i(x,y,\theta,t)$ and $\overline{i(x,y,\theta,t)}$. Because $i_o(x,y)$ is unity, $i(x,y,\theta,t)$ can have only the one of two values, i.e., one or zero. As time t progresses, x, y, and θ being held constant, $i(x,y,\theta,t)$ may jump discontinuously between these two values. When such change occurs an average over time of $i(x,y,\theta,t)$ will yield an $\overline{i(x,y,\theta,t)}$ intermediate between one and zero. In the example considered above where $r_o > r_r > \frac{r_o}{2}$ (Figure 13) $i(x,y,\theta,t)$ is unity for all t for (x,y) satisfying $\sqrt{x^2+y^2} = r < 2r_r - r_o$. In this case $\overline{i(x,y,\theta,t)}$ is unity. At larger $r = \sqrt{x^2+y^2}$, excluding $r = r_o$, $i(x,y,\theta,t)$ jumps back and forth between one and zero as time progresses. For such (x,y), $\overline{i(x,y,\theta,t)}$ is less than unity. Therefore it is possible for $\overline{i(x,y,\theta,t)}$ to be greater for (x,y) near $(0,0)$ than it is for (x,y) further from $(0,0)$. In all cases $\overline{i(x,y,\theta,t)} \leq 1$.

The quantity

$$\Delta\,\overline{j(0,0,t)}\,dx = \left[\int_{-r_o}^{r_o} \overline{i(0,y,0,t)}\right] dx$$

can now be found. It is convenient to normalize $\Delta\,\overline{j(0,0,t)}dx$ by dividing it by the value of $\Delta\,\overline{j(0,0,t)}dx$ which obtains when the RF frequency is set on resonance, i.e., when $f_{RF} = \nu_x f_o$. Normalization will be indicated

by the subscript N.

$$\Delta \overline{j(0,0,t)}_N = \frac{\int_{-r_0}^{r_0} \overline{i(0,y,0,t)}\, dy}{\int_{-r_0}^{r_0} 1 \cdot dy}$$

Since $\overline{i(0,y,0,t)}$ depends on y only through $r=\sqrt{x^2+y^2}$ where x is zero,

$$\Delta \overline{j(0,0,t)}_N = \int_0^{r_0} \overline{i(0,r,0,t)}\, \frac{dr}{r_0}$$

When reduced variables $r' = \frac{r}{r_0}$ and $r_r' = \frac{r_r}{r_0}$ are introduced,

$$\Delta \overline{j(0,0,t)}_N = \int_0^1 \overline{i(0,r',0,t)}\, dr'$$

The functional form of $\Delta \overline{j(0,0,t)}_N$ appears in Table 4. Because $\Delta \overline{j(0,\theta,t)}_N$ equals $\Delta \overline{j(0,0,t)}_N$ and because $\Delta \overline{j(0,\theta,t)}_N$ is independent of time, $\Delta \overline{j(0,\theta,t)}_N$ will be denoted by $\Delta j(0)_N$. Figure 14 gives $\Delta j(0)_N$ versus r_r'.

Figure 14 is used in predicting experimental results. The quantity r_r' depends on bump strength k and on the amount by which ν_{RF} differs from ν_x, i.e., $\Delta\nu_{RF}$. Since

$$r_r = \left| \frac{\beta}{2\delta\omega} \right|$$

$$\beta = \frac{e\mathcal{E}_0}{m} \frac{\Delta\uparrow}{\uparrow}$$

$$k = \frac{e\mathcal{E}_0}{m} \frac{\Delta\uparrow}{\omega_x}$$

$$\delta = 2\pi f_0 \Delta\nu_{RF}$$

one has

$$r_r = \frac{k}{4\pi |\Delta\nu_{RF}|}$$

$$r_r' = \frac{k/r_0}{4\pi |\Delta\nu_{RF}|}$$

Once $\frac{k}{\gamma_0}$ has been specified, choosing $\Delta\nu_{RF}$ yields γ_r'. One obtains the corresponding $\Delta j(0)$ from Figure 14. Figure 36 gives a plot of $\Delta j(0)_N$ versus $\Delta\nu_{RF}$ for four values of $\frac{k/\gamma_0}{4\pi}$, i.e., 1.0, 2.25, 5.0, and 9.0 each times the quantity 0.493×10^{-3}. The numbers 1.0, 2.25, 5.0, and 9.0 are used to designate these four curves, respectively.

IV. DIGRESSION ON STOCHASTIC INFLECTION

K. R. Symon has suggested the method of Stochastic Inflection.[15] His treatment involves solution of the diffusion equation and allows for a finite injector having a septum. In what follows the second method of Section 3.1 is used to illustrate the 100% filling efficiency property of Stochastic Inflection which prevails when used in conjunction with an infinite injector having no septum.

Set $\nu_x = L/N$; let $i_o(x,y)$ equal i_o over the lined region of Figure 6a ($A_x >> r_o$); turn on the injector; wait $N\tau$ seconds. Inserting a phase plane at $\theta = 0$ one notes that Figure 6f applies provided the empty pentagon is replaced by an N-sided polygon. The bump $\Delta y(t)$ situated at $\theta = 0+$ now has the form $\Delta y = kf(t)$ where f(t) is a random signal of average value zero. Let f(t) be indentically zero for $t<0$. The rms value of Δy for $t>0$ is about k where $k << r_o$. It takes a certain time Δt for this signal to become uncorrelated with a previous value of itself. Here it is assumed that $\frac{\Delta t}{\tau} << 1$. Break the beam into segments, each of azimuthal extent $d\theta = \frac{2\pi}{(\tau/\Delta t)}$. A segment is viewed only at $\theta = 0$ on every N-th pass it makes of this azimuth. Hence, in the absence of a bump points on a segment's phase plane exhibit the same positions on successive viewings. In its presence, all points receive the same displacement so it suffices to focus attention on just one point of the segment, say the one at (0,0) at t = 0. In what follows such a point is called a reference point.

Consider the segment passing $\theta = 0$ at t = 0. As this segment is viewed at $\theta = 0$ at $t = N\tau, 2N\tau, 3N\tau, \ldots$, its reference point will

perform a random walk about (0,0). One can just as well superimpose the results for all segments onto the above segment. One then has at $t = 0$ a distribution function consisting of $\frac{T}{\Delta t}$ reference points set one on top of the other at (0,0). At later viewing times this distribution spreads out around (0,0). When a reference point migrates into the region between $r = 2r_0$ and $r = A_x - r_0$, the beam circle of the segment associated with this reference point is completely covered with filled points If a reference point, after reaching this band, migrates back again inside $r = 2r_0$, the associated beam circle probably is still covered (empty points outside $r = r_0$ and within $r = A_x$ tend to be converted into filled points). Here A_x is made so large that at any viewing time of interest all reference points lie within $r = A_x - r_0$. Eventually most reference points lie outside of $r = 2r_0$. Hence, by waiting long enough the number of segments having unfilled beam circles comprise such a small fraction of the total number that they can be neglected relative to the latter. Therefore 100% filling efficiency prevails.

An advantage of Resonant RF Inflection when used in conjunction with a finite injector appears to lie with its charge efficiency. A disadvantage will be seen to be its sensitivity to non-linearity. The corresponding points relative to Stochastic Inflection are not known by the writer.

V. COMPUTATIONAL RESULTS ON RRFI

5.1 GENERAL CONSIDERATIONS

Computational results presented here extend the conclusions of Section III. Section III shows that RRFI can be described in terms of four parameters: k, r_o, ν_x, and ν_{RF}. The first two are lengths and the latter two dimensionless. Here r_o is taken to be 209 mils and k as varying between about 0.1 and 10 mils. The quantities ν_x and ν_{RF} range between one and two. The bump strength k is not substituted as input data but computed on the basis of other input data and a theoretical model of the experimental RF electrode (Figure 25). This model is described in Section 6.1. The net result is that an electron passing the electrode receives a radial impulse $F_x \Delta\tau = -e\mathcal{E}_o \sin(\omega_{RF} t + \phi)\Delta\tau$ yielding a $\Delta y = \frac{F_x \Delta\tau}{m\omega_x} = k \sin(\omega_{RF} t + \phi)$. The computed k depends on ω_x and hence ν_x. In this sense the computer programs depart from the theory of Section III where k is treated as an independent variable. This independence can be simulated, however, by altering the input data representing the RF voltage on the electrode whenever ν_x is changed.

The programs yield four quantities of interest to us here. (1) The first is the required injection area, its shape and size. (2) The second is the minimum number of revolutions that both the injector and the RF must be on in order to allow RRFI to trap the maximum charge. (3) After equilibrium has been established for a given k, r_o, ν_x, and ν_{RF}, turn the RF bump and the injector off together. On a small neighborhood of (x,y) at some azimuth θ find the time average of $i(x,y,\theta,t)$.

Designate this time average by $\overline{i(x,y,\theta,t)}$. Divide the beam circle into a large number of concentric annuli of equal area. Find the average value of $\overline{i(x,y,\theta,t)}$ over each annulus. Divide this average by i_o. The result is the third item of interest found by computation. It is always less than or equal to one; it is independent of θ and t; it depends on (x,y) only through the variable $r=\sqrt{x^2+y^2}$. Such a quantity was met in the last paragraph of Section 3.3 (except for division by i_o) and again in Section 3.4. When plotting this result it is designated $\overline{i(x,y,\theta,t)}/i_o$. The fact that it has been averaged over an annulus enclosing a circle of radius r will be indicated by marking the abscissa as $r'=r/r_o$.

(4) The time average trapped current is $\iint \overline{i(x,y,\theta,t)}\,dx\,dy$ where the integration is performed over the beam circle interior. Consider that portion of this current which originated from a particular element on the required injection area. Divide this portion by i_o. The result can be thought of as a time average of the beam circle area which could be covered to an i(x,y) of i_o by charge which originated from the element in question. By either Liouville's theorem or Section II the "could be" above can be replaced by "is". Division of this time average area by πr_o^2 yields a time average of the fraction of the beam circle area covered to an i(x,y) of i_o by that portion of the time average current which originated from the element in question. This fraction is proportional to element area.

When one is referred to a plot of any of the four quantities mentioned above the number of the computer program used to obtain the result along with the particular run number appear on the plot. The program and a description of it will be found in an appendix, the table

of contents directing the reader to the appropriate one. The information given there is:

1) the purpose and physical content of the program
2) a description of the Fortran program
3) the output data given and the input data required
4) the input data used on various runs
5) the actual Fortran program

5.2. ON-RESONANCE LINEAR PROBLEM

The programs SHO-16 and SHO-18 are used here to study the on-resonance linear problem. Figure 15 illustrates the shape and size of the required injection area when $k \cong 2.093$, $Y_0 = 209$, and $\nu_x = \nu_{RF} = 1.36$. This figure is not drawn to scale. If it were, its vertical extent would be increased about a factor of six. The number inside a differential element gives a time average of the percentage of the beam circle area covered ($i(x,y) = i_0$) due to charge which originated from the injector element in question. Sixty-nine such elements fill the beam circle to 100.44% of capacity. The discrepancy of 0.449 is caused by the coarseness of various meshes used in the computation. The required injection area is 1.05% of the beam circle area. Its y extent is about 60% of Y_0 and its x extent, about 10%. The trapped current is $1/.0105 = 95$ times that coming from the required injection area. It is common to call this 95 the number of turns injected. One must keep in mind, however, that the injector and the RF must be turned on longer than 95τ seconds to achieve an injected current of 95 turns. The time required in this example is closer to $4(95)\tau$.

One can also speak of the number of turns injected by a particular element on the required injection area. Suppose $i_0(x,y)$ equals $i_0 > 0$ on

that element of Figure 15 which gives a filling efficiency of 1.908%, but that $i_o(x,y)$ is zero outside this element. The number of turns injected is $0.01908\pi r_o^2/(dxdy)$. Since $\pi r_o^2/(69dxdy)$ equals 95, $0.01908\pi r_o^2/(dxdy)$ equals 125 turns.

The charge efficiency is the ratio of the trapped charge to the charge emanating from the required injection area in the time it takes to achieve 100% filling. Here there are 69 contributing elements each of area (8.3)(2.5) square mils. The time required to achieve 100% filling is 432τ. The charge efficiency is $i_o\pi(209)^2\tau / i_o 69(8.3)(2.5)^{432\tau}$ or 22%. When $\frac{Nk}{\lambda} << \frac{2\pi r_o}{N}$, Section 3.2 gives the charge efficiency of RRFI as 25%. This difference between 22% and 25% is due to the condition $\frac{Nk}{\lambda} << \frac{2\pi r_o}{N}$ not being satisfied.

The values of k, r, ν_x, and ν_{RF} used in obtaining Figure 15 are near those values existing in the accelerator of Figure 1 as used in the experiment of Section VI. The septum in this accelerator (5 mils) corresponds to a vertical strip covering the two columns of elements on the right in Figure 15. Contributing elements associated with columns not covered by this strip are 41 in number. The filling efficiency calculated in terms of areas (Section 3.3) is 100(41/69) or 60%. The actual filling efficiency found by adding up the numbers in these 41 elements is 53%.

A septum reduces charge efficiency somewhat. The active region of the required injection area fills the beam circle to 0.53 of capacity. The equilibrium time is the same as before, i.e., 432τ. The resulting charge efficiency is $\frac{(0.53)\, i_o \pi r_o^2 \tau}{i_o(41)(8.3)(2.5)\,432\tau}$ or 19%.

Figures 16 and 17 illustrate required injection areas for ν_x varying between 1.25 and 1.42. These figures are drawn to scale. Here r_o = 209 mils but k, varying here as $1/\nu_x$, has its former value only at

$\nu_x = 1.36$. In discussing Figures 16 and 17 we shall neglect this 7% variation in k about its value at $\nu_x = 1.36$.

The shape, position, and size of these required injection areas depend on ν_x. For N of $\nu_x = L/N$ equal to 3, 4, and 5, the required injection area elongates vertically as expected, its x extent varying roughly as $\frac{3}{2}k$, $\frac{4}{2}k$, and $\frac{5}{2}k$. With a tune shift of $\pm .01$ about these rather impractical values of ν_x a usable shape is realized but its center of gravity is displaced from y = 0. The asymmetry in this displacement about $\nu_x = 1+1/3$ as seen in runs 3 and 5 is expected. For instance, if ν_x were $(1+1/3 + .01)$ and if charge were injected near the bottom of the required injection area existing when $\nu_x = 1\frac{1}{3}$ then this charge would end up 3τ seconds later to the left of its starting point even though the 3-turn displacement vector displaces some of it $\frac{3}{2}k$ to the right. Hence, when $\nu_x = (1+1/3 +0.01)$, less injection area appears below y = 0 than above, etc. Runs 9 and 11 indicate that asymmetry about $\nu_x = 1.4$ disappears by the time a tune shift of ± 0.02 about $\nu_x = 1.4$ is realized.

Previous theory shows that the area of the required injection area decreases by 40% as one shifts from N = 3 to large N provided $\frac{Nk}{2} << \frac{2\pi r_0}{N}$. In Figures 16 and 17 this area is expressed as a percentage of the beam circle area and appears over the figure associated with each run. Runs 3 and 5 in conjunction with Run 4 show this same behavior even though the above condition is violated. If the percentage for Run 4 (N = 3) were taken as unity then the percentage for either Run 3 or Run 5 would be about 0.7.

In Section 3.2 it was found that the size (area) of the required injection area varies linearly with k provided $\frac{Nk}{2} << \frac{2\pi r_0}{N}$.

Figure 18 gives the size of the required injection area versus k when $\nu_x = 1.35674$ $\left(\frac{\nu}{N} = \frac{17837}{50000}\right)$. Since $r_0 = 209$ mils and since k is generally greater than 0.1 mils the previous condition is far from being satisfied. Nevertheless, a linear relation between size and k is seen to exist over the range of k dealt with. As k is varied, the required injection area changes shape. By decreasing k, the number of turns injected (the ratio of the beam circle area to the required injection area) can be made arbitrarily large.

The last paragraph of Section 3.3 considered the manner in which different regions of the required injection area contribute charge to the beam circle. These qualitative results will be illustrated quantitatively by applying SHO-18 to the three elements of Figure 15 having heavier boundaries than the others. Reading from left to right, bottom to top, these rectangles will be designated F, G, and H. Figure 19 gives $\overline{i(x,y,\theta,t)}/i_0$ versus $\nu' = \nu/r_0$ for each of these rectangles. All three are seen to contribute to the central regions of phase space about equally whereas their contributions to the peripheral regions is a strong function of their position on the required injection area. Curve F exhibits a maximum at small ν' in accordance with the prediction made in Section 3.3. As expected, rectangle G contributes more charge than rectangle F. Rectangle G is seen to emphasize the peripheral regions of phase space. Curve H most closely parallels curve F. It is concluded that charge contributed by elements far away from $(-r_0, o)$ acts like charge contributed by F and H whereas elements nearer $(-r_0, o)$ yield behavior paralleling that of G more closely.

Figure 19 in conjunction with Figure 15 indicates that each

portion of the required injection area contributes some charge to the central region of phase space. In Section 3.3 it was seen that such charge gets displaced across the beam circle essentially on a diameter of this circle. Since a diameter is the longest chord it was concluded that all contributing elements near $(-r_0, 0)$ realize their maximum contribution to beam circle filling at nearly the same time. One wonders, however, about the speed with which these various contributions approach equilibrium. Applying the results of Section 3.3 to rectangle F of Figure 15 one concludes that rectangle F realizes its contribution to beam circle filling linearly with time up until maximum filling is achieved. Figure 20 contains computational results from a program written to study such approach to equilibrium. The program itself is not described in this report. Figure 20 gives the ratio of (1) trapped current at time t to (2) the maximum trapped current. Curve F applies to rectangle F of Figure 15. The expected linear dependence is seen. The filling time of G equals that of F as expected, but its time dependence deviates from linearity. Treatment of rectangle H yields a curve like that of G. In a practical situation like that of Figure 15 it is approximately true that all portions of the required injection area realize their contribution to beam circle filling in a manner which depends linearly on the time.

5.3 NON-LINEAR EFFECTS

Non-linearity will certainly be present in the experiment of Section VI. One must be able to decide whether this factor is of importance relative to the experimental data taken there. The program SHO-20 can answer this question. In this program the transformation

relating the $\begin{pmatrix} x \\ y \end{pmatrix}$ of an electron to its $\begin{pmatrix} x \\ y \end{pmatrix}$ one revolution later is kept a pure rotation, i.e.,

$$M(\nu_x 2\pi) = \begin{pmatrix} \cos(\nu_x 2\pi) & \sin(\nu_x 2\pi) \\ -\sin(\nu_x 2\pi) & \cos(\nu_x 2\pi) \end{pmatrix}$$

Non-linearity is introduced by making ν_x depend (quadratically) on electron oscillation amplitude $a_x = \sqrt{x^2 + y^2}$.

Let ν_{xo} be the tune when a_x is near zero, and $\Delta\nu_x$ the change in ν_x when a_x increases from zero to r_o. Then

$$\nu_x = \nu_{xo} + \Delta\nu_x \left(\frac{x^2 + y^2}{r_o^2} \right)$$

We set ν_{RF} equal to the ν_x of an electron whose a_x is r_o, i.e., $\nu_{RF} = \nu_{xo} + \Delta\nu_x$. For an electron residing within the beam circle $|\nu_{RF} - \nu_x| < |\Delta\nu_x|$. Let k $\tilde{=}$ 2.093 mils, r_o = 209 mils, and ν_{RF} = 1.36. Figure 21 gives $\overline{i(x,y,\theta,t)}/i_o$ versus r' for $\Delta\nu_x$'s of 0, 0.00453, 0.01360, and 0.02720. The presence of non-linearity is seen to inhibit filling of the beam circle, the inhibition becoming more pronounced with increasing non-linearity.

It is informative to compare these results with corresponding off-resonance cases of the linear problem (Figure 22). Here ν_x is always 1.36 so that $|\nu_{RF} - \nu_x| = |\Delta\nu_{RF}|$ does not depend on a_x. In the four runs of Figure 22 $|\Delta\nu_{RF}|$ has values of 0, 0.00453, 0.01360, and 0.02720. Comparing runs for which $\Delta\nu_x$ in Figure 21 equals $|\Delta\nu_{RF}|$ in Figure 22 one concludes that an off-resonance case of the linear problem can serve as an upper bound on inhibition to beam circle filling for the corresponding non-linear problem.

In one sense, the above result is expected. The non-linear problem can be viewed as a succession of off-resonance linear problems,

the discrepancy between ν_{RF} and ν_x varying slightly from one problem to the next. In the off-resonance linear problem the greater $|\nu_{RF}-\nu_x|$ is, the more beam circle filling is inhibited. For electrons within the beam circle in the non-linear problem, $|\nu_{RF}-\nu_x|$ is always less than in the corresponding off-resonance linear problem.

In Appendix 7 it is shown that, when ν_{RF} is set at a value intermediate between $\nu_{x0}+\Delta\nu_x$ and ν_{x0}, the inhibition noted in Figure 21 becomes less pronounced. Therefore, if in the off-resonance linear problem $|\Delta\nu_{RF}|$ is such that no inhibition occurs, then in the corresponding non-linear problem where $|\Delta\nu_{RF}|$ above equals $|\Delta\nu_x|$, non-linearity is not expected to be a problem, particularly if ν_{RF} in the non-linear problem is set intermediate between ν_{x0} and $\nu_{x0}+\Delta\nu_x$. Now the curves of Figure 22 can also be obtained via the theory of Section 3.4. From this theory we have

$$r_\nu' = \frac{k/r_0}{4\pi|\Delta\nu_{RF}|}$$

Here inhibition does not occur as long as $r_\nu' \geq 1$. It is concluded that in Section VI where the amount of charge trapped by RRFI is studied experimentally non-linearity should be no problem provided

$$\frac{k/r_0}{4\pi|\Delta\nu_x|} \geq 1$$

VI. EXPERIMENTAL TEST OF RESONANT RF INFLECTION

6.1 PRELIMINARY CONSIDERATIONS

The degree to which experimental conditions are known to fulfill the theoretical requirements of Sections II and III is dealt with here.

(C-1) It is required that the electron beam be observed and affected at azimuths which are integral multiples of $2\pi/6$.

This condition is fulfilled.

(C-2) It is required that electron motion be simple harmonic as far as an observer situated at azimuths allowed by C-1 is concerned (Section II).

The degree to which this requirement is met is not known. The various currents which excite the guide field are set at valves which (1) yield a relatively intense accelerated beam over a range of Q_x substantially greater than that used in the experiment and (2) yield a ν_x allowing one to exploit the capabilities of the experimental measuring apparatus. In the experiment ν_x is near 1.36. The ν_3 which obtains is not measured. From other information it is known to be about 1.2.

(C-3) It is required that an electron's z motion never allow an electron to hop over or under the injector when its displacement x at $\theta = 0-$ is $\leq -r_0$.

It is not known if this condition is fulfilled. We assume that it is. Partial justification of this assumption follows: The vertical oscillation amplitude Q_3 is not restricted except by the vacuum tank.

If the experimental median plane were defined by $z = 0$ then a_z would be ≤ 750 mils. Because $\vec{B}$ is imperfect, the median plane is not flat. Experimentally it is known that the least upper bound on a_z is considerably less than 750 mils. We assume it to be 250 mils. The injector extends $\pm$ 262 mils above and below $z = 0$. If the median plane at the injector is near $z = 0$ then an electron at $\theta = 0-$ with $a_z \leq 250$ will collide with the injector when its x is $\leq -r_o$.

(C-4) It is required that ν_x be independent of a_x and a_z.

This condition is approached closely enough. Experimentally $a_x \leq$ 250 mils. We have assumed $a_z \leq 250$ mils. Does ν_x vary sufficiently with a_x and a_z to inhibit filling efficiency? Figure 23 illustrates the experimental dependences of ν_x on a_x and a_z for ν_x not radically different from 1.36. Experimentally, $\omega_{RF} = \omega_x \neq \omega_z$. An electron's z motion is affected very little by the RF so that its a_z remains essentially what it was at injection. Figure 23 shows that as long as a_x and a_z are ≤ 250 mils, ν_x can vary between any two electrons by at most, say, 0.001. Section 5.3 provides an estimate of whether non-linear effects are important. It is found that they are unimportant when $k \geq 4\pi |\Delta\nu_x| r_o$. In the experiment, $r_o = 209$ mils. Since the required injection area lies to the left of $(-r_o, 0)$, the maximum a_x will be somewhat larger. Here we take it as 250 mils. With $r_o = 250$ mils and with $\Delta\nu_x = 0.001$, it is required that $k \geq 3$ mils. The conditions under which much of the experimental data is taken fulfill this requirement. It turns out that if the experimentally measured RF voltage applied to the RF electrode is three volts then k is a little larger than three mils.

(C-5) It is required that f_o be independent of a_x and a_z.

This condition is approached closely enough.

Does f_o vary sufficiently with a_x to inhibit filling efficiency? In answering this question one begins by showing that a problem in which f_o varies with a_x (ω_{RF} and ν_x constant) is equivalent to one in which ω_{RF} depends on a_x (f_o and ν_x constant). The latter problem is then shown to be equivalent to one in which ν_x depends on a_x (f_o and ω_{RF} constant). Finally, the test $k \geq 4\pi |\Delta\nu_x| r_o$, used in C-4 to insure that the non-linearity considered there does not inhibit filling efficiency, is applied here. A value of $4\pi |\Delta\nu_x| r_o$ about one-third that found in C-4 is obtained. It is concluded that when the non-linearity considered in C-4 is of no consequence experimentally then variation of f_o with a_x is also of no consequence experimentally.

The RF bump causes an electron's a_x to change. We estimate the variation of f_o with a_x when ν_x and electron speed v_o (energy E_o) are held constant. Though ν_x is constant, $\omega_x = 2\pi\nu_x f_o$ varies since f_o varies. Let $x = a_x \sin(\nu_x\theta + \theta_1)$. An increase of 2π in θ corresponds to one revolution. When a_x is zero, the average orbit length per revolution is $2\pi\rho_o$. With $a_x > 0$ this quantity is approximately $2\pi\rho_o\left\{1 + \left(\frac{a_x\nu_x}{2\rho_o}\right)^2\right\}$. The product of revolution frequency $f_o(a_x)$ and average orbit length per revolution is just v_o. Hence

$$f_o(a_x) = \frac{f_o(0)}{\left\{1 + \left(\frac{a_x\nu_x}{2\rho_o}\right)^2\right\}}$$

Set the RF bump, $\Delta y = k \sin(\omega_{RF} t + \phi)$, at $\theta = 0+$. Here k is assumed independent of both ν_x and $f_o(a_x)$. At injection ($t = 0$) an electron has an a_x near r_o. At $t = 0+$ this a_x gets altered to a_{x1}. When making its second pass of the bump its a_x changes from a_{x1} to a_{x2}, etc. The RF phase angle at the time it passes the bump is shown in the following table:

Pass #	$\phi + \omega_{RF} t$
1	ϕ
2	$\phi + \omega_{RF}/f_o(a_{x1})$
3	$\phi + \omega_{RF}/f_o(a_{x2}) + \omega_{RF}/f_o(a_{x2})$
4	$\phi + \omega_{RF}/f_o(a_{x1}) + \omega_{RF}/f_o(a_{x2}) + \omega_{RF}/f_o(a_{x3})$

Call the constant value of ω_{RF} here ω_{RFC}. Upon substitution of $f_o(0)\Big/\left\{1+\left(\frac{a_{xn}\nu_x}{2\rho_o}\right)^2\right\}$ for $f_o(a_{xn})$ in a term like $\omega_{RFC}\Big/f_o(a_{xn})$, one obtains

$$\frac{\omega_{RFC}}{f_o(a_{xn})} = \frac{\omega_{RFC}\left\{1+\left(\frac{a_x\nu_x}{2\rho_o}\right)^2\right\}}{f_o(0)}$$

It is concluded that the same orbit $x(\theta)$ exhibited by the electron in the present problem would also be found in a problem where f_o ($f_o = f_o(0)$) is somehow independent of a_x and where ω_{RF} depends on a_x as

$$\omega_{RF}(a_x) = \omega_{RFC}\left\{1+\left(\frac{a_x\nu_x}{2\rho_o}\right)\right\}$$

Consider then the problem where $\omega_{RF}(a_x) = \omega_{RFC}\left\{1+\left(\frac{a_x\nu_x}{2\rho_o}\right)^2\right\}$ and where f_o and ν_x are held constant. Set ω_{RFC} equal to the ω_x of an electron in the preceding problem whose a_x is r_o, i.e.,

$$\omega_{RFC} = \frac{2\pi\nu_x}{1+\left(\frac{r_o\nu_x}{2\rho_o}\right)^2}\,\frac{f_o(0)}{}$$

Then

$$\omega_{RF}(a_x) = 2\pi\left[\nu_x\,\frac{1+\left(\frac{a_x\nu_x}{2\rho_o}\right)^2}{1+\left(\frac{r_o\nu_x}{2\rho_o}\right)^2}\right] f_o(0)$$

We define the RF tune $\nu_{RF}(a_x)$ to be $\dfrac{\omega_{RF}(a_x)}{2\pi f_o(0)}$.

Then

$$\nu_{RF}(a_x) = \frac{\nu_x}{1+\left(\frac{r_0\nu_x}{2\rho_0}\right)^2} + \frac{\nu_x\left(\frac{r_0\nu_x}{2\rho_0}\right)^2}{1+\left(\frac{r_0\nu_x}{2\rho_0}\right)^2}\left(\frac{a_x}{r_0}\right)^2$$

Let

$$\epsilon = \frac{\nu_x\left(\frac{r_0\nu_x}{2\rho_0}\right)^2}{1+\left(\frac{r_0\nu_x}{2\rho_0}\right)^2}$$

Then $$\nu_{RF}(a_x) = \nu_x - \epsilon + \epsilon\left(\frac{a_x}{r_0}\right)^2$$

The program SHO-20 can treat the case of ν_{RF} varying with a_x. The crosses in Figure 38 give $\overline{i(x,y,\theta,t)}/i_0$ versus r' for k = 2.093 mils, r_0 = 209 mils, ν_x = 1.36, and ϵ = 0.00453. The variation of ν_{RF} with a_x is seen to inhibit filling of the beam circle. The reason why $\overline{i(x,y,\theta,t)}/i_0$ is much less than unity for r' near one is that only a fraction of the required injection area has been used. In this computation

$$\nu_{RF}(a_x) = 1.36 - 0.00453 + 0.00453\left(\frac{a_x}{r_0}\right)^2$$

The dots in Figure 38 are obtained from applying SHO-20 to a case where ν_{RF} is held constant (ν_{RF} = 1.36) and ν_x allowed to vary with a_x. Here

$$\nu_x(a_x) = 1.36 - 0.00453 + 0.00453\left(\frac{a_x}{r_0}\right)^2$$

The results are seen to be nearly the same as those found in the previous problem. Hence, effects observed when ν_{RF} varies with a_x (ν_x and f_0 constant) can be simulated with little error by allowing ν_x to vary with a_x (ν_{RF} and f_0 constant). We have been careful to keep ν_x for $a_x = r_0$ equal to 1.36. If this had not been done, the shape of the required injection area would change between these two problems. This in turn would cause a discrepancy between the two runs of Figure 38.

In the problem above $\Delta\nu_x$ was chosen to be .00453. In general

$$\Delta\nu_x = \epsilon = \frac{\nu_x \left(\frac{r_o\nu_x}{2\rho_o}\right)^2}{1+\left(\frac{r_o\nu_x}{2\rho_o}\right)^2} \cong \nu_x\left(\frac{r_o\nu_x}{2\rho_o}\right)^2$$

For non-linearity to be no problem

$$k \geq 4\pi\,|\Delta\nu_x|\,r_o$$

$$k \geq \frac{\pi}{\rho_o^2}\left(r_o\nu_x\right)^3$$

$r_o = 250$ mils (see C-4)
$\nu_x = 1.36$
$\rho_o \cong 12000$ mils

$$k \geq 0.86$$

In C-4 it is required that $k \geq 3$ mils. Therefore, insuring that the non-linearity considered in C-4 does not inhibit filling efficiency also insures that variation of f_o with a_x (and a_3) does not either.

(C-6) It is required that the injector yield monoenergetic electrons.

This condition is probably fulfilled. The electron gun consists of a filament (-24 kilovolts) and a plate (grounded) with a hole in the latter through which electrons entering the accelerator must pass. The metallic vacuum tank in which electrons circulate is also grounded. Their energy spread ΔE_o is expected to be of the order of kT or about 0.25 ev. The results of C-5 allow one to find whether such a ΔE_o inhibits filling efficiency. Two monoenergetic electrons, one with $a_x = 0$ the other with $a_x = r_o$, exhibit a difference in f_o between them of Δf_o where $\frac{\Delta f_o}{f_o} \cong \left(\frac{r_o\nu_x}{2\rho_o}\right)^2 = 2\times10^{-4}$. We saw above that a $\frac{\Delta f_o}{f_o}$ about three times as large can be tolerated. Now an energy spread ΔE_o also gives rise to a frequency spread $\Delta f_o'$. For the accelerator of Figure 1,

the relationship has the form

$$\frac{\Delta E_o}{E_o} = 4.86\,\frac{\Delta f_o'}{f_o} \qquad (a_x = 0\,;\ a_z = 0)$$

We use the previous limit on $\frac{\Delta f_o}{f_o}$, i.e., 6×10^{-4}, for the value of $\frac{\Delta f_o'}{f_o}$ in the above expression. Since $E_o = 24 \times 10^3$ ev, ΔE_o must be less than 70 ev. The ΔE_o caused by kT satisfies this condition.

If the injector voltage were to vary from pulse to pulse by an amount sufficient to alter filling from pulse to pulse (ω_{RF} constant) the latter could be detected experimentally. Such variation was not seen. High-frequency noise on an individual injector pulse can inhibit filling if of sufficient amplitude. It is known that inhibition caused by noise with quarter period greater than 3-5 microseconds is not present. That noise of higher frequency is not of sufficient amplitude to inhibit filling is an assumption inherent in the experiment.

(C-7) It is required that the RF bump conserve electron energy.

It is thought that this condition is approached closely enough. Though electron energy fluctuates when the electron is in the RF field, electron energy is conserved in the overall pass provided transit time across the bump is short compared to the period of the RF $\frac{1}{\nu_{RF}}$. When this is not true, the energy change caused by the radial impulse is not entirely negated by that due to the azimuthal impulse (Section II). As indicative of the worst that can happen, we assume that none of the energy stored in the radial motion gets transferred to the azimuthal motion as a_x is reduced from 250 mils to zero. When a_x = 250 mils and when $\omega_x = 2\pi\nu_x f_o = 2\pi(1.36)\,42.84 \times 10^6$ then the energy associated with the radial motion is $\frac{1}{2} m \omega_x^2 a_x^2$ = 15 ev. From C-6 we know that an energy spread of 70 ev. can be tolerated.

(C-8) It is required that space charge effects be negligible.

This condition is fulfilled. Electrostatic repulsion between beam electrons tends to lower ν_x ($\nu_o = 0.3c$). When a beam electron ionizes a gas molecule the electron produced is repelled by the beam and collides with the vacuum tank. The trapped ion tends to neutralize the beam and thereby raise ν_x. In the experiment which follows variation of ν_x in time can be detected. The gun current is kept significantly below the value required to produce such variation.

(C-9) It is required that scattering of beam electrons by gas molecules be negligible.

This requirement is fulfilled. In the absence of RF, electrons can be trapped by a space charge mechanism which becomes operative at high injector current. After injector turn off a quantity roughly proportional to the number of circulating electrons is measured at two times, i.e., N_1 at t_1, and N_2 at t_2. We assume that $\frac{N_2}{N_1} = e^{-\frac{(t_2-t_1)}{T}}$ where T is the decay time. The time t_2 is adjusted relative to t_1 so that $\frac{N_2}{N_1}$ is about $\frac{1}{2}$. In this case $t_2 - t_1 = 80$ microseconds (2×10^{-6} mmHg; $\nu_o \doteq 0.3c$).

In the experiment which follows, maximum filling of the beam circle is achieved in about seven microseconds when k equals 3 mils. After achievement of maximum filling, electrons within the beam circle have resided there for various lengths of time ranging from zero up to seven microseconds. The average age is less than 3.5 microseconds. We take (3.5/80) 50% = 3% as indicative of the maximum decrease in trapped current which can arise because of gas scattering when $k \geq 3$ mils. When analyzing the experimental data which follows, no correction for such scattering losses is made.

(C-10) It is required that the RF bump given to an electron be independent of electron displacement x and z.

This condition is not fulfilled. However, in what follows it is shown that RRFI is relatively insensitive to dependence of bump strength k on x, i.e., that the condition above is not the essential thing it appears to be in Sections II and III. Nevertheless, the experiment tests for the unimportance of this condition.

The computer program SHO-20 allows the radial electric field amplitude $\mathcal{E}_o$ to vary as a function of electron displacement x. The three cases of such variation studied are illustrated in Figure 24. Run 5 is a constant field or control case. Run 6 involves a linearly decreasing field while Run 7 uses a step function decrease, the single step occurring at x = 0. Below Figure 24 is listed the average $\overline{i(x,y,\theta,t)}/i_o$ in each of ten concentric annuli of equal area which, taken together, cover the beam circle. In these runs only a fraction of the required injection area is used so that $\overline{i(x,y,\theta,t)}/i_o$ is always less than unity. Runs 6 and 7 deviate little from the control. It is thought that this agreement allows the same conclusion to apply for any monotonic decrease which can be represented as the sum of a constant function of x and an odd function of x. The dashed curve of Figure 24 represents one such possibility. The significant quantity appears to be an average over x of the radial electric field amplitude. In executing successive passes of the bump an electron essentially performs such an average.

Study of decreases which cannot be represented as the sum of a constant function of x and an odd function of x is not pursued. The previous results are taken as justifying the conclusion that Resonant RF Inflection is relatively insensitive to electric field nonuniformity.

The previous result does not discourage the use of a one-sided RF

electrode (Figure 25). A 1" by 1" copper plate terminates the end of a coaxial cable inserted into the vacuum tank at $\theta = 60^{\circ}$. The displacement $x_R < 0$ of this plate can be varied by means of a screw drive. Charged to a voltage $V_0 \sin(\omega_{RF} t + \phi)$ the electric field to the right of the plate both bends away from the median plane and spreads out in azimuth. Let $\mathcal{E}_0(\theta, x, z)\sin(\omega_{RF} t + \phi)$ represent the radial component of this field. The Δy an electron receives in passing the electrode is

$$\Delta y = \frac{-1}{m\omega_x} \int_t^{t+\Delta\tau} e\,\mathcal{E}_0(\theta(t'), x(t'), z(t'))\sin(\omega_{RF} t' + \phi)\,dt'$$

$$\doteq \frac{-e\mathcal{E}_0 \Delta\tau}{m\omega_x} \sin(\omega_{RF} t + \phi) = -k \sin(\omega_{RF} t + \phi)$$

The minus sign will be absorbed in ϕ. We let $k > 0$. Here $\mathcal{E}_0$ in some sense measures the amplitude of the radial component of the RF electric field. In a similar vein, $\Delta\tau$ is the time taken by the electron to cross the region of the bump. The bump strength k above will be thought of as an effective value found by considering many electrons over many successive passes, the various electrons exhibiting all the Q_x, Q_z, β_1, and β_2 present in the experiment. That such an effective k exists will be considered an assumption, the validity of which must be tested experimentally.

An estimate of such an effective value of k will be made. Consider a particle passing the electrode of Figure 25 whose orbit is its equilibrium orbit. Assume that the end plate of this electrode extends from the floor to the ceiling of the vacuum tank as well as an infinite distance out of as well as into the plane of the paper rather than the $\pm\frac{1}{2}$ inch which theoretically prevails. Nevertheless, the electron is

taken to see an electric field $\mathcal{E}_o$ only over the 1" extent noted above. Curvature of the vacuum tank and equilibrium orbit are neglected. Then $\mathcal{E}_o$ on the equilibrium orbit is

$$\mathcal{E}_o = \frac{4V_o}{H}\left[\frac{e^{\frac{\pi x_R}{H}}}{1+e^{\frac{2\pi x_R}{H}}}\right]$$

Here H is the height of the vacuum tank. The voltage V_o is found indirectly. The rms RF voltage V_R on the coaxial line feeding the RF electrode is measured at a point about 2 feet from the electrode. Hence, $V_o = V_R\sqrt{2}\,F_1$ where F_1 (determined in Appendix 2) takes account of standing wave effects on the line which make the voltage on the electrode differ from that at the voltmeter. Hence,

$$k = \left[4\sqrt{2}\,\frac{V_R F_1}{H}\;\frac{e^{\frac{\pi x_R}{H}}}{1+e^{\frac{2\pi x_R}{H}}}\right]\left[\frac{e\,\Delta\tau}{m\omega_x}\right]$$

In Appendix 2 the RF electrode of Figure 25 is investigated using an electrolytic tank. When x_R =-320 mils it is found that the k which obtains is a factor of F_2 = 1.56 larger than that found above. In the experiment which follows two values of x_R are used; -321 mils and -294 mils. It is assumed that F_2 does not charge between these two x_R. The estimate for k becomes

$$k = \left[V_R\,4\sqrt{2}\,\frac{F_1F_2}{H}\;\frac{e^{\frac{\pi x_R}{H}}}{1+e^{\frac{2\pi x_R}{H}}}\right]\left[\frac{e}{m(2\pi)^2}\right]\frac{[2\pi][f_e]}{[\nu_x][f_o]^2}$$

The quantity $\Delta\tau$ has been expressed as $\tau f_e = \frac{f_e}{f_o}$ where f_e is the fraction of 2π over which the 1" electrode extends. The computer program which analyzes the experimental data computes k. The six

numbers in square brackets above are given to the program as A(N) where N is an integer. Which bracket corresponds to which A is evident from the expression

$$k = \frac{[A(4)][A(5)][A(6)][A(7)]}{[A(8)][A(9)]^2}$$

Two independent properties of Resonant RF Inflection are measured which depend on an effective value of k. In predicting these results the expression for k above will be used except for one modification. A factor $F_3 > 0$ will be included where F_3 is to be adjusted in each case so that the theoretical curves look as much as possible like the experimental ones. If the theoretical curves can be made to agree with the experimental curves and if F_3 is unity in both cases, then we take it to mean that (1) it is possible to talk of an effective k as we have assumed, and that (2) the theory of Section III provides an adequate explanation of the observations.

6.2. EXPERIMENTAL APPROACH USED

The beam current density $j(x,\theta,t)$ $\frac{\text{amperes}}{\text{meter}}$ is the basic quantity of experimental interest. A fine wire of thickness dx is set vertically in the beam at some α and θ (Figure 26). The current collected by the wire will be assumed here, for purposes of illustration, to be $j(x,\theta,t)dx$. Knowing this collected current and also dx yields $j(x,\theta,t)$. The device which measures collected current does not respond to fluctuations occurring over a time τ but can to those which occur over a time 100τ. We denote $j(x,\theta,t)$ averaged over, say, 50τ to either side of time t as $\overline{j(x,\theta,t)}$. Experimentally $\overline{j(x,\theta,t)}$ approaches an equilibrium value shortly after the injector has been turned on. This occurs both in the presence and absence of RF.

The injector is pulsed on for about 60 microseconds 15 times per second. Normally, experimental conditions do not vary between pulses so the same $\overline{j(x,\theta,t)}$ is found on successive pulses. The collected current is measured about 40 microseconds after the initiation of each pulse. When measuring $\overline{j(x,\theta,t)}$ in the presence of RF, the RF voltage applied to the electrode of Figure 25 is left on between pulses. In what follows $\overline{j(x,\theta,t)}$ will be denoted as $j(x)_{RF}$ or $j(x)_{NO\ RF}$ depending on whether the RF is on or off.

One experimental quantity involving an effective value of k is $(j(0)_{RF} - j(0)_{NO\ RF})$ as a function of V_R when $\nu_{RF} = \nu_x$. Here V_R is the experimentally measured rms RF voltage applied to the bump electrode. In what follows a quantity like $(j(x)_{RF} - j(x)_{NO\ RF})$ will be called $\Delta j(x)$. Hence, $(j(0)_{RF} - j(0)_{NO\ RF})$ above becomes $\Delta j(0)$. A second quantity involving k is the family of resonance curves consisting of $\Delta j(0)$ as a function of ν_{RF} for ν_{RF} in the neighborhood of ν_x at various V_R. In predicting the first quantity it is necessary to measure $i_o(x,y)$. As regards the resonance curves, however, $i_o(x,y)$ will be assumed constant and the septum as being of zero thickness. Such resonance curve predictions have previously been met in Section 3.4.

In what follows the method of measuring a current density $j(x)$ is dealt with first (Section 6.3). Then the determination of $\Delta j(0)$ and certain other quantities is considered (Section 6.4). The measurement of $i_o(x,y)$ is considered next (Section 6.5) followed by a rather physical description of the computer program which uses this $i_o(x,y)$ to predict $\Delta j(0)$ (Section 6.6). The value of F_3 which gives the best correlation between the computational prediction and the experimental result is noted (Section 6.7). Section 6.8 deals with (1) the

determination of the experimental resonance curves and (2) their correlation with the theoretical curves of Section 3.4.

6.3. METHOD OF MEASURING A CURRENT DENSITY

A probe supporting a 0.5 mil vertical tungsten wire is positioned along the inner wall of the vacuum tank at $\theta = 300^{o}$ (Figures 1 and 26). A screw drive and turn indicator allow the fine wire to intercept the electron beam at desired x. Not all the 24 kilovolt electrons striking the wire stick to it. The fraction which sticks is denoted by s. The energy dependence of s need not concern us as essentially monoenergetic electrons are dealt with in any particular run. The quantity s will be seen to drop out of the calculation. Charge collected by the fine wire (diameter D_F) is fed through about three feet of 100-ohm coaxial cable to a grid resistor R_g of a preamplifier (Figure 27). The voltage gain of the preamplifier is μ. Its output voltage V is fed to an oscilloscope. Consequently, a voltage V proportional to j(x) can theoretically be measured.

$$V = \mu R_g \Delta D_F j(x)$$

The electron gun is pulsed 15 times per second, the pulse length being kept at about 60 microseconds. Because the electron revolution frequency is 43 megacycles a constant circulating current is achieved at about the same time. The quantity j(x) is usually sampled at about 40 microseconds, its value being constant from 20 to 60 microseconds. One desires the rise time of the grid resistor coaxial cable combination to be appreciably less than 40 microseconds. The largest R_g consistent with this condition is desired for two reasons.

First, relatively weak beams must be used so that space charge effects are unimportant. Second, the input signal should exceed the equivalent grid noise of the first tube by a fair amount. The R_g chosen is 39,000 ohms. Rise times associated with other sections of the preamplifier are shorter than the resulting input rise time. The first tube rather than R_g is the dominant noise source.

The grid of the first tube is biased negative by a 1.5 volt penlight cell. Normally this would mean that the fine wire would give rise to significant changes in electron momenta. Consequently, a second cell is inserted into the coaxial line so as to neutralize the fine wire. Prior to a run these two batteries are allowed to buck one another for several minutes to insure their proper cancellation later.

The preamplifier gain μ drops out of the calculation provided it is constant during a run. This is checked before and after each run through the use of a ten microsecond square wave pulse generator and the voltage divider of Figure 27. The oscilloscope has two input jacks. The test pulse as well as the preamplifier output are connected to the oscilloscope at all times during a gain measurement. No impedence changes occur as one shifts from viewing the input pulse to viewing the output pulse. The gain of the preamplifier is about 250. The preamplifier is linear up to an output voltage of 0.4 volt. Usually output signals under 0.4 volt are used. Useful readings can be made even when the desired output signal is of the order of the noise level. The pulse rate of 15 cycles per second essentially averages the noise as viewed on the oscilloscope. Systematic displacement of the center of the symmetrical fuzz is easy to see. Sixty cycle pickup is not bothersome since each of the 15 pulses occurring per second is initiated on the same portion of every fourth cycle of the 60 cycle

line voltage.

The purpose of this fine wire probe will become clear as we consider a measurement of $\Delta j(0)$ and $i_o(x,y)$.

6.4. MEASUREMENT OF $\Delta j(0)$

An RF oscillator, voltmeter, and frequency meter are connected together at a common point. This point in turn is connected to the RF electrode via two feet of 200 ohm coaxial cable. The voltmeter reading is V_R. The beam circle radius r_o is fixed by the injector voltage. The latter is quite reproducible from pulse to pulse and can be adjusted to give an r_o in the range desired. The exact value of r_o which obtains must be found from other information. In Section 6.5 one estimates r_o from the plot of $i_o(x,y)$.

The position of the fine wire (Figure 25) is adjusted until the oscilloscope trace indicates that the wire intercepts beam. This adjustment is made by a screw drive mechanism attached to the fine wire probe. A turn indicator allows one to keep track of the fine wire position. The reading on this indicator will be called the fine wire turn number. An increase of one turn corresponds to the fine wire being displaced 50 mils in the positive x direction.

The pulse on the oscilloscope is 60 microseconds long, about 20 microseconds being required for it to reach an equilibrium value V. The 20 microsecond rise time is a property of the injector, not of the beam. Since the revolution time τ is 1/43 microsecond, circulating charge reaches an equilibrium value shortly after the injector voltage has achieved its equilibrium value. This is also true in the

presence of RF. With $r_o = 209$ mils and with $k \geq 3$ mils filling of the beam circle is achieved in less than or equal to $\frac{2r_o}{k\beta/2} \tau \hat{=} 7$ microseconds. Since V is measured about 40 microseconds after initiation of the pulse, the circulating charge is in equilibrium at this time both in the absence of RF and in its presence. In equilibrium the rate at which electrons leave the injector equals the rate at which they are lost from the beam. Electrons are lost from the beam by collisions with the vacuum tank, with the injector, and with the fine wire.

The RF is turned on and the frequency scanned until an increase in collected current is seen, i.e., until $j(x)_{RF}$ exceeds $j(x)_{No\ RF}$. One chooses the RF case or the NO RF case by switching the plate supply of the oscillator either on or off. In the RF case the RF voltage is not pulsed, but remains on between injector pulses. Generally, $j(x)_{RF}$ is at most only two or three times as large as $j(x)_{No\ RF}$ so that one does not have to switch oscilloscope scales between the RF case and the NO RF case. The oscilloscope reticle has 20 division (here .02 volt per division). The voltages V corresponding to $j(x)_{RF}$ and $j(x)_{No\ RF}$, respectively, will be measured and plotted in these reticle units.

Having maximized $j(x)_{RF}$ as a function of f_{RF}, $\Delta j(x)$ is then maximized in a rough manner as a function of x. It is maximized once more, this time as a function of an injection parameter known as inflector voltage. Once decided upon, the various injection parameters are held fixed throughout a run.

The RF electrode is next given a positive displacement until a decrease in $j(x)_{RF}$ is noted. It is then withdrawn one turn (71 mils). Along with other data this allows one to estimate how far the face of the RF electrode is from the equilibrium orbit. Normally such a fact would be superfluous. Here it is useful when comparison is made between

results of the present run and those of the run in which the resonance curves are determined. Unfortunately r_o differed between these two runs. In comparing results a correction of the order of 3% is made.

In order to fix the origin in the plot of $i_o(x,y)$ of Section 6.5 the fine wire turn number corresponding to x = 0 must be known. With $\nu_{RF} = \nu_x$ and with a given V_R we expect to be able to obtain this quantity from a plot of $\Delta j(x)$ versus fine wire turn number (x). The latter ought to be symmetrical about x = 0 because nonzero $\Delta j(x)$ is due mainly to charge forced inside the beam circle by the RF. Assuming that the beam circle is uniformly covered, $\Delta j(x)$ should vary roughly as $\sqrt{r_o^2 - x^2}$. Figure 28 is a plot of $j(x)_{NO\ RF}$ and $\Delta j(x)$ versus fine wire turn number. Here V_R is 3 volts. The symmetry of the latter curve, in conjunction with that exhibited by another curve taken at 6 volts, allows one to estimate the fine wire turn number corresponding to x = 0. The value settled on is 9.75 turns.

The arrows in Figure 28 indicate a relationship between the bumpiness of the two curves. The quantity $\Delta j(x)$ is not entirely the result of circulating charge residing within the beam circle since in the presence of RF, charge outside this circle is expected to be modified somewhat relative to charge outside this circle in the NO RF case. The mountains and valleys produced by such outside charge in the absence of RF presumably tend to flatten out and fill in, respectively, in its presence yielding the indicated result. Now the highest mountains of the NO RF case occur at the edges of the beam. Consequently, negative $\Delta j(x)$ might be expected in such regions. Experimentally such negative values are found but for different ν_x than presently considered. Here this effect is masked by an erratic

behavior from pulse to pulse in the values of $j(x)_{RF}$ and $j(x)_{NO\ RF}$ at the beam extremities (Figure 28). The jumpiness is due to beam electrons which arise from field emission. Presumably they have large α_x and therefore circulate only a few times. Their erratic behavior is associated with small variations in gun voltage from pulse to pulse. An erratic beam is seen when the injector filament is turned off.

The data necessary to determine ν_x and f_o is found next. It consists of two or more RF frequencies at which $\Delta j(x)$ exhibits a maximum. In the run here being described four of them are

$\nu_{RF_1} f_o$	$= \nu_x f_o$	58.123	Mc.
$\nu_{RF_2} f_o$	$= (\nu_x - 1) f_o$	15.300	Mc.
$\nu_{RF_3} f_o$	$= (2 - \nu_x) f_o$	27.549	Mc.
$\nu_{RF_4} f_o$	$= (3 - \nu_x) f_o$	70.389	Mc.

The correspondence between relations of the above type and the measured frequencies is a matter of trial and error, a consistent assignment being necessary. Here f_o is 42.84 Mc. while $\nu_x = 1.357$.

The curve drawn through the encircled points in Figure 34 is the experimental result for $\Delta j(0)$ versus V_R. This data was taken several months prior to the resonance curve data of Section 6.8. At some point between these two experiments the writer caught himself reading V_R off the DC scale of the RF voltmeter rather than off the AC scale. Subsequent readings were made correctly. At the time, however, the taking of readings off the AC scale felt line an unfamiliar procedure. There is a definite possibility that all V_R up to this time had been read off the wrong scale. The DC scale is linear; the AC scale, non-linear. Figure 40 is a plot of the correction factor for going from an incorrect value of V_R on the DC scale to

a correct value on the AC scale. In Figure 34 V_R was scanned from low values to high values. Presumably the 3.0 volt scale was used for $V_R \leq 3.0$ volts and the 10 volt scale for $V_R > 3.0$ volts. The second curve of Figure 34 is the experimental $\Delta j(0)$ versus V_R curve noted above corrected for such an error in reading the voltmeter. The two curves are not radically different. In what follows no decision will be made as to which is the correct one. The next two sections, 6.5 and 6.6, are concerned with the prediction of $\Delta j(0)$ versus V_R via (1) a measurement of $i_o(x,y)$ followed by (2) a computational study using this $i_o(x,y)$ as input data.

6.5. MEASUREMENT OF $i_o(x,y)$

A second probe, identical to the fine wire probe except for a thicker wire (10 mils rather than 0.5 mil), is positioned at $\theta = 240^o$ (Figures 1 and 26). The phase space at $\theta = 0$ covered by current leaving the injector is indicated by the rectangle in the 1 position of Figure 30. Here ν_x is 1.36. Four sectors later ($\theta = 240^o$) this rectangle is rotated clockwise $4\left(\frac{2\pi}{6}\right)1.36$ radians and appears in the 2 position. The radial position x of the thick wire is set to intercept a portion of the passing current. It leaves a shadow in the phase space representation of this current which manifests itself one sector later ($\theta = 300^o$) at the 3 position. At $\theta = 300^o$ the radial position of the fine wire is also set to intercept beam and cuts out a strip as illustrated. A metal plate collects the beam between $\theta = 300^o$ and $\theta = 360^o$ thereby insuring that only single turn beam is being dealt with experimentally.

At $\theta = 300^{\circ}$ or the 3 state of Figure 30, the fine wire collects a certain current. If the thick wire were withdrawn to more negative x so as to miss the beam, the current collected by the fine wire would increase. This increase is associated solely with the phase area comprising the intersection of the fine wire with the shadow of the thick wire. Dividing this increase by the intersection area yields an average i(x,y) over this small parallelogram whose center is at (x,y). Varying the displacement of the thick wire and fine wire probes allows one to determine i(x,y) at $\theta = 300^{\circ}$. To realize good detail the fine wire should cross the shadow of the thick wire approximately at right angles and the diameters of both wires should be significantly less than the shortest "diameter" of the phase space representation of the single turn beam. Letting D_F and D_T represent the diameter of the fine wire and thick wire, respectively, the intersection of the fine wire with the shadow of the thick wire is seen from Figure 30 to be of area $D_F D_T / \cos\bar{\beta}$. Here $\bar{\beta}$ equals $\left(\frac{\pi}{2} - \frac{2\pi}{6}\nu_x\right)$. The voltage increase recorded by the oscilloscope upon removal of the thick wire from the beam is $\Delta V = \mu R_g \Delta i(x,y) D_F D_T / \cos\bar{\beta}$

To obtain a plot of i(x,y) appropriate to $\theta = 0$, i.e., $i_o(x,y)$, one proceeds as follows. The thick wire is set so as to miss the beam. The fine wire is advanced in increments across the beam, the trace displacement j(x) being recorded. Figure 31 gives two such plots of j(x) versus fine wire turn number from the same experimental run. A time lag of about four hours separates curve II from curve I. The voltage corresponding to j(x) is expressed in reticle divisions. Here one reticle division equals 0.004 volt. (The mismatch of curves I and II indicates unwanted variation. In this period, μ increased

nine percent. This does not explain the relative displacement of these curves nor does the change in μ appear definitively in this control data).

The 9.75_T curve of Figure 31 represents what is measured when the beam is scanned by the fine wire as before but with the thick wire set so as to intercept a portion of the beam. The thick wire turn number appropriate to this curve is 9.75. Ten such T curves are found, each at a different thick wire displacement. The first seven mesh fairly well with control curve I while the tenth goes with control curve II. The relative displacement of the two control curves apparently took place sometime during the measurement of the eighth and ninth T curves. These two curves, corresponding to thick wire turn numbers of 9.5 and 9.75, respectively, mesh with control curve II at their right-hand extremity. At their left-hand extremity, it is ambiguous with which control curve 9.5_T should be associated, while 9.75_T meshes with control I. The 9.5_T and 9.75_T curves will be associated with control curve II.

The 9.75_{Td} curve of Figure 31 gives the result of subtracting 9.75_T from curve II. The nine other Td curves are obtained in a similar fashion. Before one can use the Td curves to build up a contour map of $i_o(x,y)$, the fine wire and thick wire turn numbers corresponding to $x = 0$ must be determined. Section 6.4 yields 9.75 as the turn number appropriate to the fine wire. (It is an accident that this number equals the thick wire turn number associated with the 9.75_T curve of Figure 31). The thick wire turn number corresponding to $x = 0$ is found as follows. The fine wire is set near $x = 0$. Then $\Delta j(0)$ is recorded as a function of thick wire turn number. A plot of the results yields

a rectangular curve the symmetry of which allows one to estimate the thick wire turn number corresponding to x = 0. The result for the present run is 13.4.

Consider the 9.75_{Td} curve of Figure 31. Its maximum value of 5.5 reticle units occurs at a fine wire turn number of 6.8. Adjusting these turn numbers so they represent wire positions relative to x = 0, one has -3.65 turns for the thick wire, i.e., (9.75 - 13.4) and -2.95 turns for the fine wire, i.e., (6.8 - 9.75). In terms of Figure 30 these two displacements define an intersection of the fine wire with the shadow of the thick wire. This intersection is solved for graphically. One draws a perpendicular to the x axis of Figure 30 at x = -2.95 turns. The x axis which serves to measure the thick wire displacement at $\theta = 240^{o}$, i.e., the 2 axis of Figure 30, is rotated clockwise by $\frac{2\pi}{6} \nu_x$ radians when viewed at $\theta = 300^{o}$. Its negative portion as seen at this fine wire azimuth is represented in Figure 30 by the line extending upward from the origin and inclined at an angle $\overline{\beta}$ to the vertical. One marks off 3.65 turns on this axis and draws a perpendicular to it through this point. The intersection of these two constructed perpendiculars is a point (x,y) where an i(x,y) of 5.5 exists.

After a sufficient number of such i(x,y) values are plotted, contours of equal i(x,y) can be drawn. The result is given in Figure 32. The method of plotting has essentially rotated the i(x,y) at the 3 position of Figure 30 to the 1 position so that the $\dot{\imath}$(x,y) of Figure 32 should be designated i_o(x,y). The x axis of Figure 32 is a portion of the 3 axis of Figure 30. The diagonals slanted to the left in Figure 32 represent perpendiculars to the x axis of Figure 30, while those slanted to the right perpendiculars to the axis inclinded at an angle $\overline{\beta}$ to the

vertical. The original or unadjusted turn numbers are used to designate these diagonals. The subscript T stands for thick wire turn numbers while F serves for fine ones. The 13.4_T diagonal intersects the 9.75_F diagonal at (0,0).

At the beginning of a run current injected by Resonant RF Inflection is maximized as a function of an injection parameter known as inflector voltage. In terms of Figure 32, the main effect of varying this voltage is to displace $i_o(x,y)$ up or down. Figure 32 indicates that this maximization process places the region of high $i_o(x,y)$ in the neighborhood of y = 0. This is expected on the basis of Section 5.2 which shows that for most tunes ν_x and relatively low RF voltages the region most effective in producing usable beam lies in the neighborhood of $(-r_o, 0)$.

The beam circle radius r_o is estimated from Figure 32. The septum thickness is five mils. One expects $i_o(x,y)$ to exhibit an abrupt rise at $x = -(r_o + 5)$. Figure 32 gives some indication of such an effect. The thick wire diameter limits the spatial resolution of $i_o(x,y)$. An r_o of 209 mils is chosen. For such a case the septum extends from x = -214 mils to x = -209 mils. The line x = -214 mils skims, for the most part, the right hand side of the high intensity plateau. A region of high intensity (seven units) lies below the base line of Figure 32. The injection parameters and tune selected here do not allow it to contribute charge to the beam circle. This region is probably the origin of the field emission component of the beam noticed in Section 6.4.

6.6. PHYSICAL BASIS OF COMPUTER PROGRAM USING $i_o(x,y)$ TO PREDICT $\Delta j(0)$

The computer program SHO-14 takes $i_o(x,y)$ of Figure 32 and finds $\Delta j(0)$ as a function of bump strength k. In making this prediction the program allows for fine wire absorption effects. A detailed description of this program as well as other somewhat similar ones will be found in the appendices. Here a more physical description of the approach used in SHO-14 will be given.

A rectangle enclosing the required injection area is divided into rectangular elements each of area dxdy. The current emitted by one such element is $i_o(x,y)dxdy$. The relation between $j(x)$ and $i_o(x,y)$ is built up by summing over the individual contributions of these various elements. Consider $j(x)_{NO\ RF}$ first. The gun is turned on at $t = 0$. A pencil of charge from a particular element snakes around the accelerator several times before its head collides with the injector. At the time of this collision the circulating current due to this element reaches equilibrium. To evaluate its contribution to $j(x)_{NO\ RF}$ at some observation azimuth θ the following procedure is employed. Beginning at $t = 0$ the successive displacements x of the pencil head are recorded as it makes successive passes of the observation azimuth. An additional steady current of $i_o(x,y)dxdy$ comes into being with each new pass. The x axis at the observation azimuth is divided into cells. Each of the above increases is assigned to the cell in which its associated displacement lies. When equilibrium is reached the program moves to a consideration of the next injector element. After all such elements have been considered, $j(x)_{NO\ RF}$ is found by dividing the current associated

with each cell by the cell width.

The quantity $j(x)_{RF}$ is found next. Here the gun and RF are considered to be on at a time defined to be t = 0. For clarity, we shall assume that both the gun and the RF are turned on at this time though this is not essential. Again consider the pencil of charge emitted by a particular injector element. Break this pencil into units of equal azimuthal extent corresponding to equal durations of emission. This duration is taken as one period of the RF. The first unit is emitted from t = 0 to t = $\frac{\tau}{\nu_{RF}}$. Its azimuthal extent is $\frac{2\pi}{\nu_{RF}}$ radians. The second unit is emitted from t = $\frac{\tau}{\nu_{RF}}$ to t = $\frac{2\tau}{\nu_{RF}}$, etc. Break each unit into subunits. The azimuthal extent $d\theta$ of all subunits is the same. Theoretically, the RF electrode is considered to be of zero azimuthal extent. In such a case each $d\theta$ subunit of the first unit of charge has a unique relationship to the phase of the RF as it passes this electrode. Computationally, this condition is approximated by dividing a unit into JB subunits each of azimuthal extent $2\pi/\nu_{RF}\,JB$ radians. JB is any integer greater than zero. In what follows any particular subunit of the first unit will be called a <u>first subunit.</u>

For a particular first subunit there is a corresponding subunit in each of the following units in the sense that each of these latter subunits has the same relationship to the phase of the RF upon its initial traversal of the bump as did the first subunit. Because of this relationship the dynamical history of each of these latter subunits is identical to that of the first except for a time lag which is some integral multiple of $\frac{\tau}{\nu_{RF}}$. Therefore, if one observes some event involving the first subunit, say at t = t_1, a repeat performance

of this event will be given by the second subunit at $t = t_1 + \frac{\tau}{\nu_{RF}}$ The third subunit does the same at $t = t_1 + \frac{2\tau}{\nu_{RF}}$, etc. Now the first subunit travels about the machine anywhere from several to several hundred times before colliding with the injector. A particular event associated with this first subunit could be, say, the observation of its passing $\theta = 300^{\circ}$ for its tenth time. One would observe a burst of current of magnitude $i_o(x,y)dxdy$, and duration $\frac{\tau}{\nu_{RF}} \cdot \frac{1}{JB}$ seconds. A certain displacement x would also be associated with this burst. From previous considerations we know that this burst will be followed by an evenly spaced sequence of similar bursts $\frac{\tau}{\nu_{RF}}$ seconds apart. We also know that these latter bursts are caused by subunits executing their tenth pass of $\theta = 300^{\circ}$ and that their displacement is the same as that of the first subunit on its tenth pass of this azimuth. The average current due to such a sequence of bursts is the charge per burst, $i_o(x,y)dxdy \frac{\tau}{\nu_{RF}} \frac{1}{JB}$, multiplied by the bursts per second, $\nu_{RF} f_o$.

The result is

$$\frac{i_o(x,y)\,dx\,dy}{JB}$$

To compute the contribution to $j(x)_{RF}$ from subunits having the same relationship to the phase of the RF on their initial pass of the bump we therefore need only evaluate the displacement of one of these subunits, say the one from the first unit, i.e., a particular <u>first subunit</u>, as it makes successive passes of $\theta = 300^{\circ}$. Each pass can be considered an origin of a sequence of charge bursts of identical displacement yielding from this time onward an average current of $i_o(x,y)dxdy/JB$. Therefore $i_o(x,y)dxdy/JB$ is added to the appropriate cell on each subsequent pass of this first subunit. After all passes

of the first subunit have been treated in this manner, the program shifts to a consideration of the next first subunit. After all JB first subunits have been scanned, the program shifts to the next injector element. At the end of the calculation the contents of each cell are divided by the cell width to yield $j(x)_{RF}$.

Given $i_o(x,y)$ from Figure 32, k, r_o, ν_x, and ν_{RF} (here $\nu_x = \nu_{RF}$) the program SHO-14 yields $j(x)_{RF}$, $j(x)_{NO\ RF}$ and $\Delta j(x)$. Two sets of these quantities are obtained; one uncorrected for fine wire absorption, the other corrected for it. In the case of the latter, the results are strictly valid only in the neighborhood of the specific value of x at which the fine wire is set. Figure 29 gives computational results which correspond roughly to $\Delta j(x)$ of Figure 28 in the sense that the value of k used in the computation is comparable to the k which is thought to be appropriate to Figure 28. Curve A of Figure 29 does not take fine wire absorption effects into account while Curve B does, but only for the case of a 0.5 mil wire placed at x = 0. The bumpiness of curves A and B is mainly statistical rather than physical as indicated by curve C. Curve C is the central portion of Curve A recomputed under the condition that one of the meshes used inthe program be twice as fine as before. Curve A shows the negative values of $\Delta j(0)$ expected at the beam extremities.

6.7 COMPARISON OF COMPUTED AND EXPERIMENTAL VALUES OF $\Delta j(0)$.

From the end of Section 6. 1

$$k = F_3 \left[V_R\, 4\sqrt{2}\, \frac{F_1 F_2}{H} \right] \left[\frac{e^{\frac{\pi r_B}{H}}}{1 + e^{\frac{2\pi r_B}{H}}} \right] \left[\frac{e}{m(2\pi)^2} \right] \frac{[2\pi][f_e]}{[\nu_x][f_o]^2}$$

In the experimental determination of $\Delta j(0)$ versus V_R of Section 6.4 the RF electrode is pulled back 71 mils from that point where it first decreases $j(0)_{RF}$. From Figure 32 it is seen that this point of interference will be near x = -250 mils. Hence, an χ_R of about -321 mils prevails. Values of the other parameters in the expression for k above are:

F_1 = 2.0 (Appendix 2-1)

F_2 = 1.56 (Appendix 2-2)

H = 0.0381 meters (1500 mils)

$e/(m(2\pi)^2)$ = 0.4255×10^{10} coulombs/Kg. (24 KV. electron)

fe = 0.013

ν_x = 1.357

f_o = 42.84 Mc.

Hence,

$k = F_3 V_R \; 0.261 \times 10^{-4}$ meters

$= F_3 V_R \; 1.03$ mils

Figure 33 gives computational results for $\Delta j(0)$ versus V_R for three values of Y_o ; 205 mils, 209 mils, and 214 mils. In all cases (1) F_3 equals 0.340 and (2) the septum thickness is 5 mils. The required injection area exceeds the region over which $i_o(x,y)$ is known for V_R equal to 20 and 25 volts. Extrapolated values of $i_o(x,y)$ are used when computing $\Delta j(0)$ at these two V_R.

The experimental $\Delta j(0)$ versus V_R appears in Figure 34 (Section 6.4, last paragraph). In Figure 35 comparison is made between the computational result for an Y_o of 209 mils (dashed curves) and the experimental result (solid curves). The three dashed curves are the same computational result for three different values of F_3; 1.02, 1.46, and 2.55.

An F_3 of 1.46 gives best agreement.

6.8. EXPERIMENTAL RESONANCE CURVES AND THEIR COMPARISON WITH THEORY

The experimental resonance curves were found in a separate run. Instead of measuring ν_x and f_o the currents which excite the guide field were set near values existing in the run which determined $\Delta j(0)$ versus V_R of Section 6.4 and $i_o(x,y)$ of Section 6.5. To measure a resonance curve one first selects a V_R . Then $\Delta j(0)$ is recorded as a function of RF frequency $f_{RF} = \nu_{RF} f_o$ for ν_{RF} lying in the neighborhood of ν_x . Off-resonance values of $\Delta j(0)$ are divided by the on-resonance or maximum value of this quantity. Hence, each experimental curve of Figure 37 exhibits a maximum of unity. The abscissa of Figure 37 measures $\Delta\nu_{RF}$ in units of 0.002. The curves are designated by the V_R appropriate to each. Here

$$\Delta\nu_{RF} = (\nu_{RF} f_o - \nu_x f_o)/f_o$$

$$\nu_x \cong 1.357$$

$$f_o \cong 42.84 \text{ Mc.}$$

$$r_o = 182 \text{ mils}$$

The corresponding theoretical curves appear in Figure 36. They were met previously in Section 3.4. There it was found that each curve is generated by a specific value of the dimensionless number $\frac{ke/r_o}{4\pi}$ The four values are 1.0, 2.25, 5.0, and 9.0 each times 0.493×10^{-3}. The associated curves are designated by the numbers 1.0, 2.25, 5.0, and 9.0, respectively.

From Section 6.1

$$k = F_3 \left[V_R \, 4\sqrt{2} \, \frac{F_1 F_2}{H} \, \frac{e^{\frac{\pi x_R}{H}}}{1 + e^{\frac{2\pi x_R}{H}}} \right] \left[\frac{e}{m(2\pi)^2} \right] \frac{[2\pi][f_e]}{[V_x][f_o]^2}$$

The parameters whose values differ from their values in Section 6.7 are x_R and F_3. Here x_R = .294 mils so that $e^{\frac{\pi x_R}{H}} \Big/ \left(1 + e^{\frac{2\pi x_R}{H}}\right)$ = 0.418. Previously $e^{\frac{\pi x_R}{H}} \Big/ \left(1 + e^{\frac{2\pi x_R}{H}}\right)$ was 0.404 with k being equal to $F_3 V_R$ 1.029 mils. In the present section, therefore,

$$k = F_3 V_R \; 1.029 \left(\frac{0.418}{0.404}\right) = F_3 V_R \; 1.06 \text{ mils}$$

Multiplying this expression by $1/(r_o 4\pi)$ yields

$$\frac{k/r_o}{4\pi} = F_3 V_R \frac{1.06}{r_o 4\pi}$$

Consider the V_R = 1.0 volt curve of Figure 37. The values of $\frac{k/r_o}{4\pi}$ and V_R associated with its theoretical cognate of Figure 36 are, respectively, 1.0 (0.493×10^{-3}) and 1.0. Substituting these values in the expression above gives

$$1.0 \left(0.493 \times 10^{-3}\right) = F_3 (1.0) \frac{1.06}{182\, 4\pi}$$

Hence, F_3 = 1.06. This value of F_3 makes the theoretical curves of Figure 36 look as much as possible like the experimental ones.

6.9 DISCUSSION OF RESULTS

The results of Section 6.7 (Figure 35) indicate that fair agreement between the experimental and computational curves for $\Delta j(0)$ versus V_R can be had provided F_3 in the expression for k of Section 6.1 is set equal to 1.46. The same conclusion applies to the resonance curves of Section 6.8.(Figures 36 and 37) except that there the factor

F_3 is 1.06. The reason for the discrepancy between these two factors has not been isolated. The discussion which follows reviews two points which were considered in attempting to account for this discrepancy.

Inherent in the theoretical resonance curves of Figure 36 is the assumption of an injector which has no septum and which exhibits a constant $i_o(x,y)$. One questions what effect the introduction of variable $i_o(x,y)$ has on the width (shape) of these resonance curves. Once the answer to this question is known, the effect of introducing a septum will also be known since the latter is just a special case of the former. Applying the program SHO-14 to specific elements (Figure 15) on the required injection area, one finds that the shape of the resonance curves obtained varies with the position of the element. For an element near $(-r_o,0)$, resonance curves like those of Figure 36 are obtained except that the flat top is modified. A dip appears in the center, the curve rising to a maximum value where a curve of Figure 36 breaks. When an element as far as possible to the left of $(-r_o,0)$ is considered, its resonance curve has a maximum at $\Delta\nu_{RF} = 0$ and decreases monotonically with increasing $|\Delta\nu_{RF}|$. An element between the above two gives resonance curves much like those of Figure 36. When all elements on the required injection area are considered, the two complementary types of behavior noted above cancel leaving the flat-topped curves of Figure 36. Experimentally, flat-topped curves are observed at the higher V_R (Figure 37). It appears that taking injector properties into account will not significantly alter the value of F_3 associated with the resonance curve experiment.

The resonance curve data (Figure 37) does not depend strongly on injection parameters; the experimental and theoretical curves for Δ j(0)

versus k of Figure 35 do. The main consideration in choosing an F_3 which makes the latter look alike is that their leading edges mesh. The experimental V_R at which nonzero $\Delta j(0)$ begins is sensitive to assumption C-3 of Section 6.1, i.e., that an electron's vertical displacement is never sufficient to allow it to hop over or under the injector when its radial displacement would otherwise lead to collision with the injector. We indicate how violation of this condition would be expected to affect the experimental results.

Assume an infinite injector having no septum. Let $V_x = L/N$ and let $i_o(x,y) = i_o$. Turn on the injector. Assume that when an electron <u>first</u> finds itself with a radial displacement $x \leq -r_o$ at $\theta = 0-$ that the injector appears transparent to this electron but that when this electron finds itself in a similar situation the second time, the injector appears opaque. After waiting $2N\tau$ seconds, Figure 6f applies except for (1) the pentagon being replaced by an N-sided polygon and (2) $i(x,y)$ over the shaded region being $2i_o$ rather than i_o. Break the beam into segments, viewing any particular one only as it passes $\theta = 0$. on every N-th pass it makes of $\theta = 0$. Turn on the RF bump ($\theta = 0+$). Choose k so that $\frac{Nk}{2} << \frac{2\pi r_o}{N}$. Consider a segment whose N-turn displacement vector is directed in the positive x direction.

Charge which originates to the left of $x = -r_o - 2\left(\frac{Nk}{2}\right)$ never reaches the beam circle. To see this, consider points which at $t = 0$ lie between $x = -r_o - 3\left(\frac{Nk}{2}\right)$ and $x = -r_o - 2\left(\frac{Nk}{2}\right)$. At $t = N\tau$ they appear displaced $\frac{Nk}{2}$ to the right. At $t = N\tau-$ all charge attached to this group of points still originated to the left of $x = -r_o - 2\left(\frac{Nk}{2}\right)$. The points are doubly filled. One half the charge on each point has age $N\tau$; the other half, $2N\tau$. That half of age $2N\tau$ collides with the injector at

$t = N\tau$. Its place is taken by new charge of age zero. The injector appears transparent to that half of the charge which is of age $N\tau$. This half subsequently collides with the injector at $t = 2N\tau$ between $x = -r_o - N\frac{h}{2}$ and $x = -r_o$. Hence, charge which originates to the left of $x = -r_o - 2(N\frac{h}{2})$ never reaches the beam circle.

The required injection area is seen from the above example to be of x extent $2(N\frac{h}{2})$. Introduce a septum of thickness $\overline{DE}$. As long as $N\frac{h}{2} < \frac{\overline{DE}}{2}$, no charge reaches the beam circle. When $\overline{DE} > N\frac{h}{2} > \frac{\overline{DE}}{2}$, charge reaches the beam circle. The $i(x,y)$ associated with this charge is i_o. When $N\frac{h}{2} > \overline{DE}$, the $i(x,y)$ associated with filled regions pushed into the beam circle can have two possible values, i_o or $2i_o$. By increasing $N\frac{h}{2}$ sufficiently, regions of $2i_o$ can be made to predominate over regions of i_o.

It is concluded that if in the experiment of Section VI the assumption of an opaque injector is violated in some degree then (1) charge will begin to reach the beam circle at lower RF voltages than with an opaque injector and (2) the amount of charge trapped at any RF voltage (k) will be greater than or equal to that trapped with an opaque injector, other things remaining the same. In other words, injector transparency would make F_3 larger in the $\Delta j(0)$ versus V_R experiment than in the resonance curve experiment and would also make the experimental curve of Figure 35 lie above the computational one. The former is seen; the latter is not. No conclusion is possible. One notes, however, that even with a perfectly opaque injector, the experimental curve will lie below the computational one if the vacuum tank has not eliminated all electrons with large a_3--which it eliminates anyway because of their large a_3--before such electrons have reached $\theta = 300^o$.

In such a case the experimental $i_o(x,y)$ used in finding the computational curve of Figure 35 would be greater than it should be.

We conclude that the theory of Section III provides an adequate zero-th order explanation of the experimental results. Beyond this it is not possible to say too much as reasons for discrepancies of the order of 40% have not been isolated.

VII. CONCLUSION

Section III considers properties of RRFI which can be investigated analytically. The computational results of Section V extend these results. Section VI is an attempt to test the predictions of Sections III and V experimentally. To accomplish the latter it is necessary to restrict α_x so that non-linearity is effectively absent. In a less idealized application, non-linearity will inhibit the effectiveness of RRFI (Section 5.3; Appendix 7). In what follows we simply review basic properties of the on-resonance linear problem.

(1) In the absence of a septum RRFI achieves the Liouville limit: it exhibits 100% filling efficiency. The size or area of the required injection area depends linearly on bump strength k. The number of turns injected is given by the ratio of the beam circle area πr_o^2 to the required injection area. Making k arbitrarily small makes the number of turns injected arbitrarily large.

(2) Charge efficiency is the ratio of (a) the charge trapped to (b) the charge emanating from the required injection area in the minimum time required to trap the above charge. When 100% filling obtains, an upper limit on charge efficiency is 25% $\left(\nu_x = \frac{L}{N} \; ; \; N\frac{k\ell}{2} << 2\pi r_o \right)$. Raising k lowers charge efficiency somewhat. In a situation like that of Figure 15 it is about 20%.

(3) The shape of the required injection area depends strongly on ν_x ; less strongly on k. The size of this region is relatively insensitive to ν_x but, as noted above, varies linearly with k. When the

required injection area is broken into differential elements one notes (Figure 15) that each element contributes roughly the same amount of charge to the beam circle. Because of this, the filling efficiency in the presence of a septum is given roughly by the fraction of the required injection area not covered by the septum. Introducing a septum does not alter the charge efficiency appreciably.

(4) Resonant RF Inflection is relatively insensitive to dependence of k on x, at least when $k(x) > 0$ is the sum of an odd function of x and a constant function of x.

APPENDIX 1

DETERMINATION OF THE N-TURN DISPLACEMENT VECTOR USING ALGEBRAIC TRANSFORMATIONS

Table 1 gives

$$\begin{pmatrix} x_n \\ y_n \end{pmatrix} = M^n \begin{pmatrix} x_0 \\ y_0 \end{pmatrix} + \sum_{p=0}^{n-1} M^{n-p} \begin{pmatrix} 0 \\ \Delta y_p \end{pmatrix}$$

where

$$M = \begin{pmatrix} \cos(2\pi\nu_x) & \sin(2\pi\nu_x) \\ -\sin(2\pi\nu_x) & \cos(2\pi\nu_x) \end{pmatrix}$$

and where $\Delta y_p = k \sin(\omega_x p\tau + \phi) = k\sin(2\pi\nu_x p + \phi)$ A simple expression for $\begin{pmatrix} x_n \\ y_n \end{pmatrix}$ is desired when $\nu_x = \frac{L}{N}$ with n = IN; I = 1, 2, 3, ...

Upon substitution of IN for n in $\begin{pmatrix} x_n \\ y_n \end{pmatrix}$ one obtains

$$\begin{pmatrix} x_{IN} \\ y_{IN} \end{pmatrix} = M^{IN} \begin{pmatrix} x_0 \\ y_0 \end{pmatrix} + \sum_{p=0}^{IN-1} M^{IN-p} \begin{pmatrix} 0 \\ \Delta y_p \end{pmatrix}$$

Since

$$M = \begin{pmatrix} \cos(2\pi\frac{L}{N}) & \sin(2\pi\frac{L}{N}) \\ -\sin(2\pi\frac{L}{N}) & \cos(2\pi\frac{L}{N}) \end{pmatrix}$$

it is true that $1 = M^N = M^{2N} = \cdots = M^{IN}$. Hence,

$$\begin{pmatrix} x_{IN} \\ y_{IN} \end{pmatrix} = \begin{pmatrix} x_0 \\ y_0 \end{pmatrix} + \sum_{p=0}^{IN-1} M^{-p} \begin{pmatrix} 0 \\ \Delta y_p \end{pmatrix}$$

Break this sum into I units of N terms each. The first N terms of the sum belong to the first unit, etc. Now all units have the same value. This fact is shown below.

The bump Δy_p has the form $\Delta y_p = k \sin(2\pi\frac{L}{N}p + \phi)$. Because of

this, $\Delta y_p = \Delta y_{p+N} = \Delta y_{p+2N} = \cdots$. One can therefore write

$$M^{-p}\begin{pmatrix} 0 \\ \Delta y_p \end{pmatrix} = M^{-(p+N)}\begin{pmatrix} 0 \\ \Delta y_{p+N} \end{pmatrix} = M^{-(p+2N)}\begin{pmatrix} 0 \\ \Delta y_{p+2N} \end{pmatrix} = \cdots$$

If the first expression here is summed over P from P = 0 to P = N - 1, one obtains just the first unit mentioned above. Treating the second expression in a like manner yields the second unit mentioned above, etc. Hence, all units have the same value.

The previous result allows one to write

$$\begin{pmatrix} x_{IN} \\ y_{IN} \end{pmatrix} = \begin{pmatrix} x_0 \\ y_0 \end{pmatrix} + I \sum_{p=0}^{N-1} M^{-p}\begin{pmatrix} 0 \\ \Delta y_p \end{pmatrix}$$

Express the term $\Delta y_p = k \sin(2\pi \frac{I}{N} P + \phi)$ as

$$\Delta y_p = k \sin(2\pi \tfrac{I}{N} P)\cos\phi + k\cos(2\pi \tfrac{I}{N} P)\sin\phi$$

Now

$$M^{-p} = \begin{pmatrix} \cos(2\pi \frac{I}{N} P) & -\sin(2\pi \frac{I}{N} P) \\ \sin(2\pi \frac{I}{N} P) & \cos(2\pi \frac{I}{N} P) \end{pmatrix}$$

so that

$$M^{-p}\begin{pmatrix} 0 \\ \Delta y_p \end{pmatrix} = k\begin{pmatrix} -\sin^2(2\pi \frac{I}{N} P)\cos(\phi) & -\sin(2\pi \frac{I}{N} P)\cos(2\pi \frac{I}{N} P)\sin(\phi) \\ \sin(2\pi \frac{I}{N} P)\cos(2\pi \frac{I}{N} P)\cos(\phi) + \cos^2(2\pi \frac{I}{N} P)\sin(\phi) \end{pmatrix}$$

Substituting this result in $\begin{pmatrix} x_{IN} \\ y_{IN} \end{pmatrix}$ gives

$$\begin{pmatrix} x_{IN} \\ y_{IN} \end{pmatrix} = \begin{pmatrix} x_0 \\ y_0 \end{pmatrix} + Ik\cos\phi \sum_{p=0}^{N-1}\begin{pmatrix} -\sin^2(2\pi \frac{I}{N} P) \\ \sin(2\pi \frac{I}{N} P)\cos(2\pi \frac{I}{N} P) \end{pmatrix} + Ik\sin\phi \sum_{p=0}^{N-1}\begin{pmatrix} -\sin(2\pi \frac{I}{N} P)\cos(2\pi \frac{I}{N} P) \\ \cos^2(2\pi \frac{I}{N} P) \end{pmatrix}$$

It is seen that only two basic quantities need be found, i.e., $\sum_{p=0}^{N-1}\sin(4\pi \frac{I}{N} P)$ and $\sum_{p=0}^{N-1}\cos^2(2\pi \frac{I}{N} P)$. This is so because $\sum_{p=0}^{N-1}\sin(2\pi \frac{I}{N} P)\cos(2\pi \frac{I}{N} P)$ can be expressed in terms of the first quantity above, i.e.,

$$\sum_{P=0}^{N-1} \sin\left(2\pi \frac{L}{N} P\right) \cos\left(2\pi \frac{L}{N} P\right) = \frac{1}{2} \sum_{P=0}^{N-1} \sin\left(4\pi \frac{L}{N} P\right)$$

and because $\sum_{P=0}^{N-1} \sin^2\left(2\pi \frac{L}{N} P\right)$ can be expressed in terms of the second quantity above, i.e.,

$$\sum_{P=0}^{N-1} \sin^2\left(2\pi \frac{L}{N} P\right) = \sum_{P=0}^{N-1} \left(1 - \cos^2\left(2\pi \frac{L}{N} P\right)\right) = N - \sum_{P=0}^{N-1} \cos^2\left(2\pi \frac{L}{N} P\right)$$

The sums $\sum_{P=0}^{N-1} \sin\left(4\pi \frac{L}{N} P\right)$ and $\sum_{P=0}^{N-1} \cos^2\left(2\pi \frac{L}{N} P\right)$ are evaluated.

Now

$$\sin\left(4\pi \frac{L}{N} P\right) = \left[\frac{e^{i 4\pi \frac{L}{N} P} - e^{-i 4\pi \frac{L}{N} P}}{2i}\right]$$

and

$$\cos^2\left(2\pi \frac{L}{N} P\right) = \left[\frac{e^{i 4\pi \frac{L}{N} P} + 2 + e^{-i 4\pi \frac{L}{N} P}}{4}\right]$$

Summing either of the above over P from P = 0 to P = N - 1 yields sums like $\sum_{P=0}^{N-1} e^{\pm i 4\pi \frac{L}{N} P}$. Such a sum is a geometric series. The ratio R of any term to the preceding one is $e^{\pm i 4\pi \frac{L}{N}}$. The sum S of this geometric series is $S = \frac{1 - R^{\ell+1}}{1 - R}$ where $\ell = N-1$. Hence,

$$\sum_{P=0}^{N-1} e^{\pm i 4\pi \frac{L}{N} P} = \frac{1 - e^{\pm i 4\pi L}}{1 - e^{\pm i 4\pi \frac{L}{N}}} = \frac{1 - 1}{1 - e^{\pm i 4\pi \frac{L}{N}}}$$

$$= 0 \quad \text{since} \quad 0 < \frac{L}{N} < 1$$

Consequently, $\sum_{P=0}^{N-1} \sin\left(4\pi \frac{L}{N} P\right) = 0$ and $\sum_{P=0}^{N-1} \cos^2\left(2\pi \frac{L}{N} P\right) = \frac{N}{2}$. It is concluded that $\sum_{P=0}^{N-1} \sin\left(2\pi \frac{L}{N} P\right) \cos\left(2\pi \frac{L}{N} P\right) = 0$ and that $\sum_{P=0}^{N-1} \cos^2\left(2\pi \frac{L}{N} P\right) = \sum_{P=0}^{N-1} \sin^2\left(2\pi \frac{L}{N} P\right) = \frac{N}{2}$. Upon substitution of these results into the expression for $\begin{pmatrix} x_{IN} \\ y_{IN} \end{pmatrix}$ above one obtains

$$\begin{pmatrix} x_{IN} \\ y_{IN} \end{pmatrix} = \begin{pmatrix} x_0 \\ y_0 \end{pmatrix} + Ik \cos\phi \begin{pmatrix} -\frac{N}{2} \\ 0 \end{pmatrix} + Ik \sin\phi \begin{pmatrix} 0 \\ \frac{N}{2} \end{pmatrix}$$

This is equivalent to

$$\begin{pmatrix} x_{zN} \\ y_{zN} \end{pmatrix} = \begin{pmatrix} x_0 \\ y_0 \end{pmatrix} + I N \frac{k}{2} \begin{pmatrix} -\cos\phi \\ \sin\phi \end{pmatrix}$$

Here $N\frac{k}{2}\begin{pmatrix} -\cos\phi \\ \sin\phi \end{pmatrix}$ is the N-turn displacement vector.

APPENDIX 2

EVALUATION OF THE FACTORS F_1 AND F_2 USED IN THE ESTIMATE FOR k OF SECTION 6.1

(1) The RF oscillator, voltmeter, and frequency meter are connected together at a common point. This point in turn is connected to the RF electrode (Figure 25) via about two feet of 200 ohm coaxial cable (Hewlett Packard 46A-16A). A sinusoidal wave traveling toward the electrode is reflected at the electrode. A standing wave results. Consider the electrode to be at x = 0. Take the cable as extending from $x = -\infty$ to x = 0. Let C(0) be the capacitance terminating the cable, i.e., at x = 0. With $C(0) \approx 0$, the rightmost node occurs at $x = -\frac{\lambda}{4}$. An antinode occurs at x = 0. Here λ is the wavelength of the RF wave on the coaxial line. In what follows λ_{vac} is the wavelength in free space or, synonomously, on a coaxial line whose dielectric is free space.

Experimentally, the RF voltmeter is at $x = -\lambda' \approx -\frac{\lambda_{vac}}{8}$. With C(0) = 0 and with $\lambda = \lambda_{vac}$, $\frac{V_R(0)}{V_R(-\lambda')} = \frac{1}{\cos 45^\circ} = 1.4$. Nonzero C(0) shifts the node closer to x = 0. In such a case both $V_R(0)$ and $V_R(-\lambda')$ decrease but the latter decreases faster than the former so that their ratio increases. When $\lambda < \lambda_{vac}$, the node moves still further to the right.[16] An expression is found for $\frac{V_R(0)}{V_R(-\lambda')}$ which takes these two factors into account. The treatment which follows is based on one given by J. C. Slater.[17]

The current at x at time t due to a wave traveling to the right is $A e^{i(\omega_{RF} t - \beta x)}$. The line is considered loss free so β is real and equals $\frac{2\pi}{\lambda}$. The current due to a wave traveling to the left is $B e^{i(\omega_{RF} t + \beta x)}$. The total current is $I(x,t) = A e^{i(\omega_{RF} t - \beta x)} + B e^{i(\omega_{RF} t + \beta x)}$ The impedence Z_o of the line is assumed purely resistive. It is positive for a wave traveling to the right and negative for one traveling to the left. The voltage at x at time t is $V_o(x,t) = Z_o \left[A e^{i(\omega_{RF} t - \beta x)} - B e^{i(\omega_{RF} t + \beta x)} \right]$. The impedence of the line at x, i.e., $Z(x)$, when waves of both types are considered is

$$Z(x) = \frac{V_o(x,t)}{I(x,t)} = Z_o \frac{\left[A e^{-i\beta x} - B e^{i\beta x} \right]}{\left[A e^{-i\beta x} + B e^{i\beta x} \right]}$$

The impedence $Z(0)$ terminating the line is $\frac{-i}{\omega_{RF} C(0)}$. Here $\omega_{RF} = 2\pi f_{RF}$ where f_{RF} is the frequency of the RF. This capacitative reactance will be represented by iX where X is real and equals $\frac{-1}{\omega_{RF} C(0)}$. At x = 0 one has

$$Z(0) = Z_o \frac{(A - B)}{(A + B)} = Z_o \frac{(1 - B/A)}{(1 + B/A)}$$

Solving this boundary condition for B/A yields

$$B/A = \frac{Z_o - Z(0)}{Z_o + Z(0)} = \frac{Z_o - iX}{Z_o + iX} = \frac{Z_o^2 - X^2 - 2iXZ_o}{Z_o^2 + X^2}$$

Letting $\sin\eta = \frac{X}{\sqrt{Z_o^2 + X^2}}$ and letting $\cos\eta = \frac{Z_o}{\sqrt{Z_o^2 + X^2}}$ one finds that B/A equals $e^{-i2\eta}$. Substituting for B/A in $V_o(x,t)$ and multiplying the result by $\frac{e^{i\eta}}{e^{i\eta}}$ yields

$$V_o(x,t) = Z_o \frac{A}{e^{i\eta}} \left[e^{i(\omega_{RF} t - \beta x + \eta)} - e^{i(\omega_{RF} t + \beta x - \eta)} \right]$$

Since A is arbitrary, let $A/e^{i\eta}$ equal A′ where A′ is real. The real portion of V (x,t) is $Z_o A' \left[\cos(\omega_{RF} t - \beta x + \eta) - \cos(\omega_{RF} t + \beta x - \eta) \right]$

or just $-2Z_o A' \sin(-\beta x + \pi)\sin(\omega_{RF} t)$. The rms value of this quantity is $\sqrt{2}\, Z_o A' |\sin(-\beta x + \pi)|$. Hence

$$\frac{V_R(0)}{V_R(x)} = \frac{|\sin(\pi)|}{|\sin(-\beta x + \pi)|} = \frac{1}{|\cos(-\beta x) + \cot\pi \sin(-\beta x)|}$$

Since $\cot(\pi) = Z_o/X = -Z_o \omega_{RF} C(0)$,

$$\frac{V_R(0)}{V_R(x)} = \frac{1}{|\cos(-\beta x) - Z_o \omega_{RF} C(0) \sin(-\beta x)|}$$

To compute $-\beta x = -\frac{2\pi x}{\lambda}$, λ must be known. If L_x and C_x represent, respectively, the cable's inductance and capacitance per unit length then the propagation velocity of a wave down the cable is $1/\sqrt{L_x C_x}$. Hence, $\lambda = \frac{1}{\sqrt{L_x C_x}\, f_{RF}}$. Now $L_x = \frac{\mu_o}{2\pi} \ln\left(\frac{D_o}{D_i}\right)$; $C_x = \frac{2\pi \epsilon \epsilon_o}{\ln\left(\frac{D_o}{D_i}\right)}$; D_o and D_i are, respectively, the diameters of the outside and inside conductors; ϵ is the dielectric constant of the material (beads) separating the conductors; $\mu_o \epsilon_o = \frac{1}{c^2}$ where c is the speed of light; $\epsilon_o = 8.85 \times 10^{-12}$ farads per meter. Hence, $\lambda = \frac{c}{\sqrt{\epsilon}\, f_{RF}}$. The characteristic impedence of the line Z_o is 200 ohms where $Z_o = \sqrt{\frac{L_x}{C_x}} = \frac{1}{\sqrt{\epsilon}} \frac{\ln\left(\frac{D_o}{D_i}\right)}{2\pi \epsilon_o c}$ The quantities D_o and D_i are, respectively, 0.480" and 0.0092". Hence, $\sqrt{\epsilon} = 1.18$ and $\lambda = \frac{c}{1.18\, f_{RF}}$. Here $f_{RF} = \nu_x f_o = 58.1 \times 10^6$ 1/sec. When x =-2', $-\beta x = -\frac{2\pi x}{\lambda}$ is 0.876 radians or 50.4°. Hence, $\cos(-\beta x) = 0.637$ and $\sin(-\beta x) = 0.770$.

Express C(0) in units of 10^{-12} farads. Then $Z_o \omega_{RF} C(0)$ becomes $(200)(2\pi)(58.1 \times 10^6)10^{-12} C(0)$ or $0.073\, C(0)$. The quantity

$$\frac{V_R(0)}{V_R(x)} = \frac{1}{|\cos(-\beta x) - Z_o \omega_{RF} C(0) \sin(-\beta x)|}$$

becomes for x =-2'

$$\frac{V_R(0)}{V_R(-2')} = \frac{1}{|0.637 - 0.0562\, C(0)|}$$

Substituting values of C(0) one obtains

C(0) $\mu\mu$fd.	$\frac{V_R(0)}{V_R(-2')}$
0	1.57
1	1.72
2	1.91
3	2.14
4	2.43
5	2.81

A measurement of $V_R(0)/V_R(-2')$ was made. A second RF electrode-coaxial cable combination like that of Figure 25 in conjunction with a shield to simulate the electrical effects of the vacuum tank was made. Differences between the two systems follow.

The stem protruding from the brass draw tube in Figure 25 is soldered to a 1" by 1" copper plate. The other end of this stem sets in a socket which in turn is held in place by a plastic spacer. The 1" by 1" plate in conjunction with the stem, which we call the RF electrode, can be removed from the socket. The brass draw tube and socket, less the RF electrode, is simulated with a General Radio #874 50-ohm coaxial connector. The plastic spacer in the 874 is thinner than in the brass draw tube. The socket is larger. It is assumed that the termination capacitance presented by the socket and spacer is the same in both cases. This capacitance is denoted by C_i. No attempt is made to simulate the 9/8" by 9/8" grounded plate situated at the end of the draw tube (Figure 25).

The first step in determining $\frac{V_R(0)}{V_R(-2')}$ is to find the input capacitance of the RF voltmeter (HP-410B) used in the measurement. A second

RF voltmeter (HP-411) is placed at x = -2'. The RF electrode and the shield simulating the vacuum tank are removed from the 874. The HP-410B is attached to the central terminal of the 874, the ground lead of the HP-410B being attached to the outside conductor of the 874. The voltage at x = -2' is recorded. The HP-410B is disconnected and various capacitances shunted across the 874 until one is found which gives the same voltage at x = -2' as noted above. The best compromise proved to be a 3.3±.5 $\mu\mu$fd. capacitor. This capacitor is taken to be electrically equivalent to the RF voltmeter. The exact value of this capacitance is noted by C_m.

The HP-411 at x = -2' is disconnected. It is not used in any of the subsequent measurements. The above capacitor is shunted across the line at x = -2' and the RF voltage at the 874, as measured by the HP-410B, adjusted to 2.8 volts. Five different capacitors are then shunted across the 874 and the $V_R(0)$ associated with each recorded. The HP-410B at x = 0 and the 3.3 uufd. capacitor at x = -2' are interchanged. The $V_R(-2')$ are recorded as this same sequence of capacitors is shunted across the 874. In addition, the 3.3±.5 uufd. capacitor simulating the HP-410B at x = 0 is removed along with any of the previous shunts and $V_R(-2')$ recorded. The 1" by 1" electrode and the shield simulating the vacuum tank are attached to the 874 and $V_R(-2')$ recorded.

The above data appears in the table below. Here C_a denotes that portion of the capacitance terminating the coaxial cable due to the RF electrode and shield. The last column on the right contains predictions of the total capacitance terminating the cable, i.e., $C(0)'$. These predictions are made via information contained in the previous table coupled with the measured values of $\frac{V_R(0)}{V_R(-2')}$ found in the next to the

last column below.

#	C(-2')	C(0) μμfd.	$V_R(0)$ volts		$V_R(-2')$ volts	$\frac{V_R(0)}{V_R(-2')}$	C(0)' μμfd.
			measured	estimated			
1	C_m	$C_i + C_m$	2.8		1.16	2.4	4.0
2	C_m	$C_i + C_m + 3.3$	2.75		.51(5)	5.3	8.0
3	C_m	$C_i + C_m + 5.0$	2.67		.33	8.1	9.1
4	C_m	$C_i + C_m + 7.5$	2.57		.66(5)	3.9	16.0
5	C_m	$C_i + C_m + 10$	2.42		1.0	2.4	18.7
6	C_m	C_i		2.82	1.76	1.6	.2-.3
7	C_m	$C_i + C_a$		2.82	1.38	2.0	2.6

Comparing C(0) and C(0)' in lines 1, 2, and 3 leaves one with the feeling that the measurements are consistent. Consideration of lines 1 through 5, however, leaves one with the opposite feeling. This discrepancy is not pursued. It is concluded from lines 1, 2, and 3 that $C_i + C_m$ is about 4 uufd. This result in conjunction with line 6 says that C_m is $3.7 - 3.8 \frac{\mu\mu fd.}{v}$ This is consistent with the known value of C_m, i.e., $3.3 \pm .5$ uufd. Line 7 indicates that the total capacity terminating the cable is about 2.6 uufd. Since $C_i \cong 0.2 - 0.3 \ll 2.6 \frac{\mu\mu fd}{v}$, the assumption that C_i is the same in the original arrangement of Figure 25 as it is in the present one is not critical. One concludes that it is not unreasonable to associate a $\frac{V_R(0)}{V_R(-2')}$ of about two with the arrangement of Figure 25. Hence, $F_1 = 2.0$.

(2) The effectiveness of the RF electrode of Figure 25 was investigated using an electrolytic tank.[18] If this electrode is held at a potential V_0 and if the vacuum tank is filled to one-half its height with slightly acidified water then the electric field throughout the vacuum tank is the same after filling as before. The reason for this follows: A small current $\vec{j} = \sigma \vec{E}$ $\frac{\text{amperes}}{\text{meter}^2}$ flows in the water. Here

$\vec{E}$ is the electric field at a point and σ, the conductivity of the water. Since no current flows across the interface between water and air, the component of $\vec{E}$ normal to the interface at the interface must be zero. In the absence of water the component of $\vec{E}$ normal to the median plane on the median plane is also zero. The potentials on all metallic surfaces serving as boundaries for either the region occupied by air or the region occupied by water are the same after filling as before filling. It is known that a unique solution to the electrostatic problem exists within a charge free region when either (1) the potential or (2) the normal component of $\vec{E}$ is specified at each point on a surface enclosing the region. Hence, $\vec{E}$ within either the region occupied by water or the one occupied by air is the same as it was before filling occurred.

If any of the metallic surfaces above the water are now altered, $\vec{E}$ within the water does not change. This is so because (1) the component of $\vec{E}$ normal to the interface at the interface is still zero and because (2) potentials on other surfaces bounding the water remain constant. Figure 39 shows how the problem is set up in an electrolytic tank. We shall, however, continue to speak of the vacuum tank of Figure 25 as being half filled with water.

The quantity of interest is the radial impulse an electron traveling in the median plane receives as it passes the RF electrode. Hence, only the potential gradient in the x direction on the surface of the water need be found and then only along the electron orbit. As in Section 6.1 curvature of the electron orbit as well as that of the inside wall of the vacuum tank is neglected. The electron is taken to pass 0.32" from the RF electrode. A sliding carriage above the water in

conjunction with suitable measuring devices allows the tip of a fine wire touching the surface of the water to be set reproducibly at any desired point on this surface.

The tip of the wire is set on the assumed electron orbit and moved along it in 0.1" steps past the RF electrode. At each step the setting of the voltage divider giving a null in the voltmeter reading is recorded for two radial positions of the wire, i.e., x = -0.02" and x = 0.02". The voltage divider is a linear 40 turn Helipot. We let P_n^- and P_n^+ be, respectively, the number of turns on the Helipot dial which gives a voltmeter null when the wire is at x = -0.02" and x = 0.02". Here $P_n^- \geq P_n^+$. If the wire were to touch the RF electrode, P_n would be 40. The radial electric field at x = 0 for the n-th step is

$$\mathcal{E}_n = \frac{V_0 \left[\frac{P_n^-}{40} - \frac{P_n^+}{40} \right]}{0.04"}$$

The time a particle spends in the neighborhood of the n-th step is $\frac{0.1"}{v_0}$. Here v_0 is the electron speed. The impulse an electron receives on passing the electrode is

$$\sum_n -e\,\mathcal{E}_n \left(\frac{0.1"}{v_0} \right) = -\frac{eV_0}{v_0} \frac{1}{16} \sum_n \left(P_n^- - P_n^+ \right)$$

The P_n are recorded over a range extending about ± 1.5" to either side of the center of the RF electrode. In the first trial, however, only one side of this range is traversed. The first trial gives $-1.64 \left(\frac{eV_0}{v_0} \right)$ for this impulse; the second, $-1.73 \left(\frac{eV_0}{v_0} \right)$.

The expression for the radial electric field on the equilibrium orbit found in Section 6.1 is

$$\mathcal{E}_0 = \frac{4V_0}{H} \frac{e^{\frac{\pi x_B}{H}}}{1 + e^{\frac{2\pi x_B}{H}}}$$

Since H is 1.5" and since x_R is -0.32", the impulse an electron receives in a time $\Delta\tau = \frac{1''}{v_0}$ is

$$-e\mathcal{E}_0\Delta\tau = -\frac{eV_0}{v_0}\left(\frac{4}{1.5}\right)\left[\frac{e^{-\frac{\pi(0.32)}{1.5}}}{1+e^{-\frac{2\pi(0.32)}{1.5}}}\right]$$

$$= -1.08\left(\frac{eV_0}{v_0}\right)$$

Upon comparing this result with the two trials above one concludes that the kick given an electron by the electrode of Figure 25 is about $\left[\frac{1.64+1.73}{2(1.08)}\right] = 1.56$ times stronger than estimated in Section 6.1. Hence, $F_2 = 1.56$.

(3) It was investigated whether the time varying magnetic field associated with the electric field in the neighborhood of the RF Electrode of Figure 25 is of sufficient strength to contribute appreciably to the Δy given an electron passing the bump. Such influence was found to be negligible.

APPENDIX 3

DESCRIPTION OF COMPUTER PROGRAM SHO-14

Given $i_o(x,y)$ SHO-14 predicts, via the theory of Sections II and III, $j(x)_{RF}$, $j(x)_{NO\ RF}$, and $\Delta j(x)$. Two sets of these quantities are given; one includes the effects of fine wire absorption, the other does not. The physical content of SHO-14 is discussed in Section 6.6. This appendix considers the actual Fortran program. The program, as it appears at the end of this appendix, is divided into consecutive blocks designated 14-1, 14-2, etc. These blocks are described in the order in which they are met. In what follows the term "electron" denotes either (1) the head of a pencil of charge in the NO RF case or (2) a sub-unit in the RF case.

The Fortran program SHO-14 is intended 14-1
for use with an IBM-704 computer having a 32-K core.
The CC's specify the experimental $i_o(x,y)$ at mesh points of a rectangular grid (Figure 43). CALL MURCB2 ( ) is a subroutine peculiar to the MURA Fortran Library.[19] It specifies the manner in which input data is punched on cards and read into the core.

Input data other than $i_o(x,y)$ is entered 14-2
in terms of the A's.

The subroutines SIN4F( ) and COS4F( ) 14-3
of 14-3 and 14-7, respectively, are peculiar to the MURA Fortran Library.[19] If the number g is used as the argument of the first then the associated subroutine computes sin(2πg). In 14-3 sin(2πg) is

computed and stored as B(I) for JA values of g ranging from zero to (JA-1)/JA in increments of 1/JA. Later the B(I) are selected as needed to simulate the RF bump

When a series of runs is submitted, the 14-4
program returns to statement 110 at the completion of each run. Hence, the A's can be changed between runs but the CC's as well as the value of A(1) actually used in a run remain invariant from one run to the next. A(1) is used prior to statement 110.

The experimental $i_o(x,y)$ as contained in 14-5
the singly subscripted CC's is expressed in terms of the doubly subscripted G1(I,J) after the manner of Figure 43.

The rectangle of Figure 43, defined by A(16) 14-6
through A(19) is divided into cells. The width and height of a cell are, respectively, APC and ARC.

In the absence of external influences the 14-7
transformation M relating the $\begin{pmatrix} x \\ y \end{pmatrix}$ of an electron to its $\begin{pmatrix} x \\ y \end{pmatrix}$ one revolution later is

$$M(2\pi\nu_x) = \begin{pmatrix} \cos(2\pi\nu_x) & \sin(2\pi\nu_x) \\ -\sin(2\pi\nu_x) & \cos(2\pi\nu_x) \end{pmatrix} = \begin{pmatrix} DH & DG \\ -DG & DH \end{pmatrix}$$

Experimentally, the observation azimuth is 14-8
at $\theta = -\frac{2\pi}{6}$ while the RF electrode is at $\theta = \frac{2\pi}{6}$.
Computing time can be decreased by taking the observation azimuth as the point of reference rather than $\theta = 0$. The quantity $A(25) \geq 0$ is the fraction of a turn the observation azimuth is behind the injector. The fraction of a turn the RF bump is ahead of the injector is given by $A(23) \geq 0$. The counterclockwise transformation from $\theta = 0$ to the observation azimuth is

$$M(-\nu_x 2\pi A(25)) = \begin{pmatrix} DD & -DC \\ DC & DD \end{pmatrix}$$

The counterclockwise transformation from the RF bump to the observation azimuth is

$$M(-\nu_x 2\pi (A(25) + A(23))) = \begin{pmatrix} AF & -AE \\ AE & AF \end{pmatrix}$$

When an electron passes the observation azimuth it is of interest to know whether it will collide with the injector on its next attempt to cross $\theta = 0$. This test can be made at the observation azimuth by transforming the phase space representation of the injector sink at $\theta = 0$ back to the observation azimuth. One then notes whether the (x,y) of the particle lies inside or outside the half plane representing this sink; if inside, collision will result. The transformed sink is shown in Figure 45. It is the half plane lying below the solid diagonal line. Here $\gamma = \nu_x 2\pi A(25)$. It will be required that $0 < \gamma < \pi$. The y intercept of the solid diagonal is b_1. The parallel dashed line drawn through (x,y) has a y intercept of b_2. If $(b_2 - b_1) > 0$ then no collision will take place.

14-9

$$b_1 = \frac{-r_0}{\sin\gamma} = \frac{-A(24)}{DC} = -DV$$

$$b_2 = y + \frac{\cos\gamma}{\sin\gamma} x = y + \frac{DD}{DC} x = y + DT\,x$$

The resulting collision test, as it appears in 14-20, 14-23, 14-34, and 14-37, is: IF (Y+X*DT+DV)>0, then no collision. The program also allows the observation azimuth to be placed at $\theta = 0$. In such a case A(25) = 0 and the collision test becomes : IF (X+A(24))>0, then no collision.

14-10

The portion of the x axis at the observation azimuth defined by $A(27) \leq x \leq -A(27)$ where $A(27)<0$ is divided into cells of width equal to the fine wire diameter A(28). It is required that A(27) be an integral multiple of A(28) thereby yielding $2|A(27)|/A(28)$ cells in all. The leftmost cell is number one. When an electron passes the observation azimuth its displacement x is noted and an appropriate $i_o(x,y)dxdy$ added to the storage location corresponding to the cell in which this displacement lies. The relevant cell number JG is the integral portion of (((-A(27) + x) / A(28)) + 1.0). The actual test is JG = (DPP+x) / A(28). It is equivalent to

$$JG = \frac{-A(27) + x}{A(28)} + 1.0000004$$

The .0000004 is superfluous. It is required that electron displacement x always satisfy $A(27)<x<-A(27)$.

The number of the cell corresponding most nearly to the position of the fine wire is JJH = A(33).

14-11

These instructions allow the addition of a Kx^2 bump $\begin{pmatrix} 0 \\ \Delta y \end{pmatrix}$ to the $\begin{pmatrix} x \\ y \end{pmatrix}$ of an electron passing the observation azimuth.

$$\begin{pmatrix} 0 \\ \Delta y \end{pmatrix} = \begin{pmatrix} 0 \\ A(30)\frac{x^2}{r_o^2} \end{pmatrix} = \begin{pmatrix} 0 \\ x**2*BEEP \end{pmatrix}$$

The bump strength when $|x| = r_o$ is A(30). The Δy is computed at the center of each of the cells of 14-10 and stored as GGBU(I). Here I represents the number of a cell. The total number of cells is INT2.

14-12

The program finds $j(x)_{NO\ RF}$ and $j(x)_{RF}$ both in the presence and absence of fine wire absorption effects. The various "GG" storage locations of 14-12 are associated with these four current densities. The code used to distinguish them is:

WNR	Wire; No RF
NWNR	No Wire; No RF
W R	Wire; RF
NW R	No Wire; RF

The experimental $i_o(x,y)$ is specified at 14-13

points lying on or within the rectangle of Figure 43 defined by A(16) through A(19). It is convenient to introduce a second rectangle (Figure 44) lying on or within the previous one over which the program extracts information in any particular run. The latter is broken into rectangular cells corresponding to the differential elements dxdy of Section 6.6. In 14-13 dxdy = AREA = AP*AR/A(26) provided A(26) is unity. A(26) is a scale factor which allows the experimental $i_o(x,y)$ to be punched in the most convenient units and which yields j(x) expressed in oscilloscope reticle units.

The dxdy elements of the rectangle of 14-14

Figure 44 are scanned from left to right, bottom to top. The value of $i_o(x,y)$ at the center of the particular dxdy element the program happens to be considering is G2. Linear interpolation is used.

The observation azimuth rather than $\theta = 0$ 14-15

is the reference azimuth. When the program considers a new dxdy element, the $\begin{pmatrix} x \\ y \end{pmatrix}$ associated with it is first transformed back to the observation azimuth (14-8). This nonphysical operation is negated in 14-16.

Given the $\begin{pmatrix} x \\ y \end{pmatrix}$ of the head of a pencil of charge 14-16

14-16 finds its $\begin{pmatrix} x \\ y \end{pmatrix}$ one revolution later (14-7).

The number of the cell in which this head 14-17

lies is JG (14-10).

The current $i_o(x,y)dxdy$ = G2*AREA 14-18

(14-13), 14-14) should be added to GGWNR(JG) (14-12); instead only G2 is added. The multiplication omitted here is performed in 14-24.

The Kx^2 bump is added in (14-11). 14-19

Division 14-20 tests whether the pencil 14-20
head collides with the injector on its next attempt to pass $\Theta = 0$ (14-9). If it will collide, the program shifts to a consideration of the next dxdy; if it will not, the program proceeds to 14-21.

Statement 210 tests whether the pencil head 14-21
collides with the fine wire. If it does not, control passes back to statement 180 of block 14-16. This loop is repeated until the pencil head either collides with the injector or with the fine wire. Because one may be interested in obtaining $j(x)_{NWNR}$, control shifts to statement 14-22 when the collision is of the latter type.

Since $j(x)_{NWR}$ and $j(x)_{NWNR}$ are not 14-22
observed experimentally, it may be of interest to skip computation of these quantities in order to decrease computing time. Division 14-22 tests whether $j(x)_{NWNR}$ is to be computed. If it is not to be found, the program jumps to a consideration of the next dxdy; otherwise, the program goes to 14-23.

This loop parallels 14-15 through 14-20. 14-23

In 14-24 G2 is added to GGWNR(JG) is added to GGNWNR(JG) so that the latter is associated with $j(x)_{NWNR}$ as it is supposed to be rather than with $(j(x)_{NWNR} - j(x)_{WNR})$ as it is in 14-23.

When the pencil head collides with the injector the program jumps to a consideration of the next differential element dxdy. After all dxdy elements have been treated control passes to 14-24.

The multiplication of $i_o(x,y)$ by dxdy 14-24
neglected in 14-18 and 14-23 is performed here as well as

the addition omitted in 14-23. The resulting GGWNR(I) and GGNWNR(I) need only be divided by the cell width A(28) to yield $j(x)_{WNR}$ and $j(x)_{NWNR}$ This division is performed in 14-40.

Division 14-25 begins the determination of $j(x)_{WR}$ and $j(x)_{NWR}$. Here AD equals k of $\Delta y = k \sin(\omega_{RF} t + \phi)$ The expression for k is derived in Section 6.1. 14-25

The straightforward way of taking into account the RF bump $\Delta y = k \sin(\omega_{RF} t + \phi)$ is to add the bump vector $\begin{pmatrix} 0 \\ \Delta y \end{pmatrix}$ to the $\begin{pmatrix} x \\ y \end{pmatrix}$ exhibited by a subunit as it passes the azimuth of the RF bump. Here, however, an equivalent procedure is employed which allows computing time to be saved. The bump vector is transformed back to the observation azimuth and this transformed bump $\begin{pmatrix} \Delta x' \\ \Delta y' \end{pmatrix}$ added to the $\begin{pmatrix} x \\ y \end{pmatrix}$ exhibited by the above subunit as it passes the observation azimuth. By 14-8 one has 14-26

$$\begin{pmatrix} \Delta x' \\ \Delta y' \end{pmatrix} = \begin{pmatrix} AF & -AE \\ AE & AF \end{pmatrix} \begin{pmatrix} 0 \\ \Delta y \end{pmatrix} = \begin{pmatrix} -AE \\ AF \end{pmatrix} \Delta y$$

$$\begin{pmatrix} \Delta x' \\ \Delta y' \end{pmatrix} = \begin{pmatrix} AG \\ AH \end{pmatrix} \sin(\omega_{RF} t + \phi)$$

Division 14-26 computes AG and AH.

The transformed RF bump vector $\begin{pmatrix} \Delta x' \\ \Delta y' \end{pmatrix}$ of 14-26 is evaluated for JA values of $(\omega_{RF} t + \phi)$ running from zero to $\frac{2\pi(JA-1)}{JA}$ in increments of $\frac{2\pi}{JA}$ (14-3). When an RF bump is to be added to a subunit an appropriate bump vector $\begin{pmatrix} G(I) \\ F(I) \end{pmatrix}$ is selected from this reservoir. 14-27

The number of subunits in the first unit is JB. The definition of AAJA in QRST is given in 14-3. The program makes use of JB, AG, and QRST when selecting the appropriate transformed bump vector $\begin{pmatrix} G(I) \\ F(I) \end{pmatrix}$ of 14-27 to add to the $\begin{pmatrix} x \\ y \end{pmatrix}$ of a 14-28

subunit. See 14-33.

The rectangle of Figure 44 defined by A(12) through A(15) is considered in 14-13 in connection with the NO RF case. This same rectangle also serves in the presence of RF. Statistical considerations, however, allow the dxdy elements into which this rectangle is broken to be larger than in 14-13. Both dx and dy are usually increased by a factor of $\sqrt{JB}$ (14-28). These larger dxdy must still be fine enough to represent variation in $i_o(x,y)$ over this rectangle (Figure 32) as well as variation in the relative effectiveness of different portions of this rectangle to contribute charge to the beam circle (Figure 15). 14-29

The statement, AREA = AP*AR*AB/A(26), parallels the AREA statement of 14-13 except for the factor AB = 1/JB. See Section 6.6.

See 14-14. 14-30

See 14-15. 14-31

This statement controls scanning of the JB subunits into which the first unit is divided. 14-32

Division 14-33 selects the appropriate transformed RF bump vector $\begin{pmatrix} G(I) \\ F(I) \end{pmatrix}$ of 14-27 and adds it to the $\begin{pmatrix} x \\ y \end{pmatrix}$ of the subunit passing the observation azimuth. 14-33

When the L-th subunit of the first unit makes its first pass of the RF electrode the phase angle of the RF, $\omega_{RF} t + \phi$, is assigned the value $2\pi\left(\frac{L}{JB} + A(2)\right)$. See 14-28 and 14-32. Here $A(2) = \nu_{RF}$. Any constant besides A(2) would serve just as well. In 14-33, as in the rest of SHO-14, the factor 2π does not appear in the argument of a trigonometric function. The subroutines used to generate values of the sine and cosine add this factor of 2π implicitly (14-3). In describing 14-33, however, the 2π will be included. The RF phase angle mentioned above

resides at line three of 14-33. If the L-th subunit makes a second pass of the RF bump, statement 390 of 14-37 increases the above phase angle by $2\pi\nu_{RF}$. On the L-th subunit's Q-th pass, $\omega_{RF}t+\phi$ equals $2\pi\left(\frac{L}{JB}+Q\,A(2)\right)$.

When the L-th subunit makes its Q-th pass of the observation azimuth, the transformed RF bump vector which should be added to the subunit's $\begin{pmatrix}x\\y\end{pmatrix}$ is $\begin{pmatrix}AG\\AH\end{pmatrix}\sin(\omega_{RF}t+\phi)$. Here $(\omega_{RF}t+\phi)$ equals $2\pi\left(\frac{L}{JB}+Q\,A(2)\right)$. The particular $\begin{pmatrix}G(I)\\F(I)\end{pmatrix}=\begin{pmatrix}AG\\AH\end{pmatrix}\sin\left(\frac{2\pi(I-1)}{JA}\right)$ of 14-27 which nearly corresponds to the above bump vector is selected as follows: (1) Any integral multiple of 2π is temporarily dropped from $(\omega_{RF}t+\phi)$.; (2) The fraction left is divided by $2\pi/JA$; (3) The fractional portion of the preceding result is discarded. The integer remaining can range from zero to JA-1; (4) Unity is added to the preceding integer. The resulting integer ranges from one to JA. It is this integer which is used for I in $\begin{pmatrix}G(I)\\F(I)\end{pmatrix}$.

Statement 310 and the one following it perform the four operations listed above. The latter statement is equivalent to

$$NN = \frac{(AAA - (\text{Integral Portion of } AAA))}{(1/JA)} + 1.0000004$$

If the .0000004 were missing and if AAA were zero or nearly zero then NN = 1.0000000. When the program converts 1.0000000 to an integer without the decimal point, it is not certain whether one or zero results. To insure that unity obtains the .0000004 has been included above.

Since AAA increases by A(2) = ν_{RF} every time a subunit makes a revolution, N of statement 310 may become quite large. Fortran sets an upper limit on integers of 32768. Hence, ν_{RF} multiplied by the number of revolutions necessary to achieve equilibrium, i.e., $\frac{2\nu_0}{k/2}$ (Section 3.2) must always be less than, say, 32,000.

Division 14-34 parallels 14-16 through 14-20

14-34

except as follows: (1) The quantity G2 is added to GGWR(JG) rather than to GGWNR(JG). G2 is $i_o(x,y)$ whereas it should be $i_o(x,y)dxdy/JB$. The omitted multiplication is performed in 14-39 (14-29). (2) The last statement of 14-34 increases the RF phase angle AAA by A(2) = ν_{RF} in preparation for the addition of the next RF bump to the subunit. This addition occurs, however, only if the previous collision test indicates that the subunit makes another pass of the RF bump.

The fine wire collision test of 14-35 parallels that of 14-21. If no collision occurs, control switches back to 14-33 which adds in the next RF bump. This loop is repeated until the subunit either collides with the injector or with the fine wire. If the collision is with the injector, the program jumps to a consideration of the next subunit of the first unit; if with the fine wire, control passes to 14-36. 14-35

Division 14-36, paralleling 14-22, tests whether $j(x)_{NWR}$ is to be found; if it is not, the program shifts to a consideration of the next subunit of the first unit; if it is, control passes to 14-37. 14-36

Division 14-37 is required to compute $j(x)_{NWR}$. This block parallels that beginning with statement 310 of 14-33 and extending through 14-34. One difference is that G2 in 14-37 is added to GGNWR(JG) rather than to GGWR(JG). In 14-39 GGWR(JG) are added to GGNWR(JG) so that the latter becomes associated with $j(x)_{NWR}$ as it is supposed to be rather than with $\left(j(x)_{NWR} - j(x)_{WR}\right)$ as it is in 14-37. 14-37

After all JB subunits of the first unit have been scanned the program considers the next differential element dxdy (14-14). After all dxdy elements have been scanned control passes to 14-39. 14-38

Division 14-39 performs the multiplication 14-39

of $i_o(x,y) = G2$ by dxdy/JB which was omitted in 14-34 and 14-37. Here the addition of the GGWR(I) to the GGNWR(I) omitted in 14-37 is also performed. The resulting GGWR(I) and GGNWR(I) need only be divided by the cell width A(28) to yield $j(x)_{WR}$ and $j(x)_{NWR}$. This division is performed in 14-40.

In 14-40 the contents of each cell of the 14-40

four groups mentioned in 14-24 and 14-39 are effectively divided by the cell width A(28) to yield the four current densities, $j(x)_{WNR}$, $j(x)_{NWNR}$, $j(x)_{WR}$, and $j(x)_{NWR}$. Before this division is performed, however, the following device is introduced. Since it is usually impractical to call for the contents of all cells associated with a particular j(x), the cells are grouped into boxes, each box containing NDIVPB consecutive cells. The contents of each such box is divided by the box width to yield a current density j(x). It is required that the total number of cells INT2 into which the allowed portion of the x axis is broken be an integral multiple of NDIVPB.

Division 14-41 subtracts the j(x) found 14-41

in the absence of RF from that found in its presence to yield $(j(x)_{NWR} - j(x)_{NWNR})$ and $(j(x)_{WR} - j(x)_{WNR})$. The output given by SHO-14 is:

1) A(1) through A(35).
2) $j(x)_{NWR}$, $j(x)_{NWNR}$, $(j(x)_{NWR} - j(x)_{NWNR})$
3) $j(x)_{WR}$, $j(x)_{WNR}$, $(j(x)_{WR} - j(x)_{WNR})$
4) k of $\Delta y = k \sin(\omega_{RF} t + \phi)$

The output is read from left to right, top to bottom. The j(x)'s are

printed out as a function of box number beginning with box one (14-40). The contents of the first and last box for each of the six j(x)'s should be zero; if they are not, this run as well as all succeeding runs may be invalid. These runs should be resubmitted using a larger |A(27)| (14-10). In addition, any single run is invalid if $\nu_{RF}\left(\frac{2r_0}{k/2}\right) = A(2)^{*}4.0^{*}A(24)/k$ exceeds 32000 (14-33).

The input data required by SHO-14 follows. 14-42

(1) The CC's. The CC's of 14-1 correspond to values of $i_o(x,y)$ found, for instance, at the mesh points on and within the rectangle of Figure 43, when this rectangle is laid over the experimental $i_o(x,y)$ of Figure 32. The rectangle referred to here is defined by A(16) through A(19). Figure 43 illustrates how one associates a particular CC with a particular mesh point.

(2) The A's. When an A represents an integer I it will be punched as I.1. If it were punched as I.0, it is not certain whether the program converts it to I or to I-1. In what follows "I.1" denotes an A which is an integer.

A(1) I.1. 1.1≤A(1)≤4000. Division 14-3 evaluates $\sin(\omega_{RF}t+\phi)$ for JA = A(1) values of $(\omega_{RF}t+\phi)$ ranging from zero to 2π (JA-1)/JA in increments of 2π/JA.

(2)>0. A(2) = $\nu_{RF} = \omega_{RF}/2\pi f_o = f_{RF}/f_o$

A(3) 1. A(3)≥1.1. The first unit is broken into JB = A(3) subunits. (Section 6.6, 14-28, 14-32, 14-33).

A(4) The amplitude of the radial RF electric field over the azimuthal extent of the bump is A(4) = $\mathcal{E}_o$ (Section 6.1).

A(5) The quantity A(5) equals e/(m(2π)²) where e is the absolute value of the particle charge and m its relativistic mass (Section 6.1).

A(6) 2π

A(7) The fraction of the accelerator azimuth over which the RF bump extends is A(7) = f_e (Sections 621)

A(8) A(8)>0. A(8) = $\nu_x = \omega_x / 2\pi f_o$

A(9) The particle revolution frequency is A(9) = f_o (Section 621).

A(10) I.1. A(10)≥1.1. See A(15).

A(11) I.1. A(11)≥1.1. See A(15).

A(12) A(12)<0. A(12)<A(13). See A(15).

A(13) A(13)<0. A(13)>A(12). See A(15).

A(14) A(14)<A(15). See A(15).

A(15) A(15)>A(14). The quantities A(12) through A(15) define the rectangle of Figure 44. All portions of the rectangle boundary must lie on or within the rectangle of Figure 43. The latter is defined by A(16) through A(19). The rectangle of Figure 44 is surveyed into differential elements dxdy. In the RF case the number of such elements per row and per column is A(10) and A(11), respectively (14-29).

A(16) A(16)<0. A(16)<A(17). See A(21).

A(17) A(17)<0. A(17)>A(16). See A(21).

A(18) A(18)<A(19). See A(21).

A(19) A(19)>A(18). See A(21).

A(20) I.1. 2.1≤A(20)≤30.1. See A(21).

A(21) I.1. 2.1≤A(21)≤20.1. Mesh points at which $i_o(x,y)$ is defined extend over a rectangular region bounded by A(16) through A(19) (14-5, Figure 43). Some of the points lie on the rectangle boundary. The number of points per column and per row is given by A(20) and A(21), respectively.

A(22) Not used

A(23) A(23)≥0. 0≤A(23) + A(25)<1.

The fraction of a turn the RF bump is ahead of the injector is A(23). The second condition above requires that a particle leaving the injector encounter the RF bump before reaching the observation azimuth.

A(24) The beam circle radius is A(24) = r_o.

A(25) $0 \leq A(25)\, 2\pi\nu_x < \pi$. The fraction of a revolution the observation azimuth is behind the injector is A(25)≥0 (14-8,14-9).

A(26) A(26)>0. Theoretically, A(26) is unity; practically, A(26) is a scale factor which facilitates comparison of computational results with experimental ones (14-13, 14-29).

A(27) A(27)<0. It is required that |A(27)|/A(28) be an integer <1000 (14-10). The negative x value at which one begins to divide the x axis into cells is A(27).

A(28) A(28)>0. It is required that |A(27)|/A(28) be an integer <1000 (14-10). The fine wire diameter is A(28).

A(29) Not used.

A(30) The strength of the Kx^2 bump when $|x| = r_o$ is A(30). A(30) has dimension of length (14-11, 14-19).

A(31) I.1. 1.1≤A(31). See A(32).

A(32) I.1 1.1≤A(32). The quantities A(31) and A(32) do in the absence of RF what A(10) and A(11) do, respectively, in its presence. Usually $A(31) \cong \sqrt{A(3)}\, A(10)$ and $A(32) \cong \sqrt{A(3)}^{*} A(11)$ (14-13, 14-29).

A(33) I.1. 1.1≤A(33)≤2000.1. The number of the cell whose position corresponds to the fine wire displacement is A(33) (14-10).

A(34) I.1 1.1≤A(34)≤2000.1. The number of cells per box is A(34), ie., NDIVPB of 14-40. The total number of cells, INT2 = 2.0|A(27)|/A(28), must be an integral multiple of NDIVPB. A(35) is not used.

RUN	CARD	DATA
	1	.32 + 2
	2	.31 + 2
	.	
	.	FROM FIG. 32
	.	X10
	.	
	493	
	494	
		END DATA
	1	.40001 + 4
		END DATA
R-1	2	.135674 + 1
	3	.251 + 2
	4	.236 + 8
	5	.452 +10
	6	.62832 + 1
	7	.13 - 1
	8	.135674 + 1
	9	.4284 + 8
	10	.51 + 1
	11	.91 + 1
	12	.235 + 3
	13	-.214 + 3
	14	-.5 + 2
	15	.75 + 2
	16	-.235 + 3
	17	-.205 + 3
	18	-.5 + 2
	19	.75 + 2
	20	.261 + 2
	21	.191 + 2
	23	.16666666
	24	.209 + 3
	25	.16666666
	26	.50568 + 3
	27	-.3 + 3
	28	.5
	31	.211 + 2
	32	.501 + 2
	33	.6011 + 3
	34	.201 + 2
		END DATA
R-2	3	.501 + 2
		END DATA
		END DATA
		END DATA

FORTRAN PROGRAM SHO-14

```
C     SHO-14                                                        14- 1
      DIMENSION CC(600), A(35), B(4000),
     1G1(20,30), GGBU(2000), GGWNR(2000),
     2GGNWNR(2000), GGWR(2000), GGNWR(2000),
     3F(4000), G(4000)
      PRINT 520
      CALL MURCD2(CC)
      CALL MURCD2(A)                                                14- 2
      JA = A(1)                                                     14- 3
      AAJA = 1./FLOATF(JA)
      DO 100 I = 1, JA
  100 B(I) = SIN4F (FLOATF(I-1)/ FLOATF(JA))
  110 CALL MURCD2(A)                                                14- 4
      PRINT 500, (A(I), I = 1, 35)
      JCNX = A(21)                                                  14- 5
      JCNY = A(20)
      NN = 0
      DO 120 J = 1, JCNY
      DO 120 I = 1, JCNX
      NN = NN+1
  120 G1(I,J) = CC(NN)
      FPNX = JCNX-1                                                 14- 6
      FPNY = JCNY-1
      APC = (A(17) -A(16)) / FPNX
      ARC = (A(19) -A(18)) / FPNY
      DG = SIN4F (A(8))                                             14- 7
      DH = COS4F (A(8))
      DC = SIN4F (A(8) * A(25))                                     14- 8
      DD = COS4F (A(8) * A(25))
      AE = SIN4F (A(8) *(A(23)+ A(25)))
      AF = COS4F (A(8) *(A(23)+ A(25)))
      IF (A(25)) 130, 140, 130                                      14- 9
  130 DT = DD/DC
      DV = A(24)/DC
  140 DPP = 1.0000004 *A(28)-A(27)                                  14-10
      JJH = A(33)
      BEEP = A(30)/ A(24) **2                                       14-11
      XBEG = A(28) / 2.0
      INT = -A(27) / A(28) +0.1
      INT2 = 2* INT
      DO 150 I = 1, INT
      N = INT+I
      GGBU(N) = XBEG **2 + BEEP
      NN = INT-I+1
      GGBU(NN) = GGBU(N)
  150 XBEG = XBEG+A(28)
      DO 160 I = 1, 2000                                            14-12
      GGWNR(I) = 0.0
      GGNWNR(I) = 0.0
      GGWR(I) = 0.0
  160 GGNWR(I) = 0.0
```

```
290   DE = X*DD-Y*DC                                          14-31
      DF = X*DC+Y*DD
300   DO 400 L = 1, JB                                        14-32
      X = DE                                                  14-33
      Y = DF
      AAA = A(2) + FLOATF(L) *A3
310   N = AAA
      NN = (QRST+AAA-FLOATF(N)) / AAJA
      X = X+G(NN)
      Y = Y+F(NN)
      DD = X*DH+Y*DG                                          14-34
      Y = -X*DG+Y*DH
      X = DD
      JG = (DPP+X) / A(28)
      GGWR(JG) = GGWR(JG) + G2
      Y = Y + GGBU(JG)
      IF (A(25)) 330, 320, 330
320   IF (X+A(24)) 400, 400, 340
330   IF (Y+X*DT+DV) 400, 400, 340
340   AAA = AAA+A(2)
      IF (JG-JJH) 310, 350, 310                               14-35
350   IF (SENSE SWITCH 2) 400, 360                            14-36
360   N = AAA                                                 14-37
      NN = (QRST+AAA-FLOATF(N)) / AAJA
      X = X+G(NN)
      Y = Y+F(NN)
      DD = X*DH+Y*DG
      Y  =-X*DG+Y*DH
      X = DD
      JG = (DPP+X) / A(28)
      GGNWR(JG) = GGNWR(JG) + G
      Y = Y + GGBU(JG)
      IF (A(25)) 380, 370, 380
370   IF (X+A(24)) 400, 400, 390
380   IF (Y+X*DT+DV) 400, 400, 390
390   AAA = AAA+A(2)
      GO TO 360                                               14-38
400   CONTINUE
410   CONTINUE
```

```
      JC = A(31)                                                    14-13
      AO = JC
      AP = (A(13) -A(12)) / AO
      JD = A(32)
      AQ = JD
      AR = (A(15) -A(14)) / AQ
      EB = A(12) -AP/2.0
      EA = A(14) -AR/2.0
      AREA = AP*AR/A(26)
      DO 260 J = 1, JD                                              14-14
      AT = J
      Y = EA+AT* AR
      CAT = Y
      DO 260 I = 1, JC
      AS = I
      X = EB+AS*AP
      Y = CAT
      M = (X-A(16)) / APC+1.0
      N = (Y-A(18)) / ARC+1.0
      FPM = M-1
      FPN = N-1
      PAT = (X-FPM*APC-A(16)) / APC
      RAT = (Y-FPN*ARC-A(18)) / ARC
      M1 = M+1
      N1 = N+1
      G2      =G1(M,N)+PAT*(G1(M1,N)
     1-G1(M,N))+RAT*(G1(M,N1)-G1(M,N))
     2+PAT*RAT*(G1(M1,N1)-G1(M,N1)-
     3G1(M1,N)+G1(M,N))
      IF (G2) 260, 260, 170
170   DE = X*DD-Y*DC                                                14-15
      Y  = X*DC+Y*DD
      X = DE
180   DO = X*DH+Y*DG                                                14-16
      Y  =-X*DG+Y*DH
      X = DO
      JG = (DPP+X) / A(28)                                          14-17
      GGWNR(JG) = GGWNR(JG) + G2                                    14-18
      Y = Y + GGBU(JG)                                              14-19
      IF (A(25)) 200, 190, 200                                      14-20
190   IF (X+A(24)) 260, 260, 210
200   IF (Y+X*DT+DV) 260, 260, 210
210   IF (JG-JJH) 180, 220, 180                                     14-21
220   IF (SENSE SWITCH 2) 260, 230                                  14-22
230   DO = X*DH+Y*DG                                                14-23
      Y  =-X*DG+Y*DH
      X = DO
      JG = (DPP+X) / A(26)
      GGNWNR(JG) = GGNWNR(JG) + G2
      Y = Y + GGBU(JG)
      IF (A(25)) 250, 240, 250
240   IF (X+A(24)) 260, 260, 230
250   IF (Y+X*DT+DV) 260, 260, 230
260   CONTINUE
```

```
      DO 270 I = 1, INT2                                          14-24
      GGWNR(I) = GGWNR(I) * AREA
      GGNWNR(I) = GGNWNR(I) * AREA
270   GGNWNR(I) = GGWNR(I) +GGNWNR(I)
      AD = A(4)*A(5)*A(6)*A(7)/(A(8)*A(9)**2)                     14-25
      AG = -AE*AD                                                 14-26
      AH =  AF*AD
      DO 280 I = 1, JA                                            14-27
      G(I) = AG * B(I)
280   F(I) = AH * B(I)
      JB = A(3)                                                   14-28
      AB = 1.0/ FLOATF(JB)
      QRST = 1.0000004*AAJA
      JC = A(10)                                                  14-29
      AO = JC
      AP = (A(13) -A(12)) / AO
      JD = A(11)
      AQ = JD
      AR = (A(15) - A(14)) / AQ
      EB = A(12) - AP/2.0
      EA = A(14) - AR/ 2.0
      AREA=AP*AR*AB/A(26)
      DO 410 J = 1, JD                                            14-30
      AT = J
      Y = EA+AT*AR
      CAT = Y
      DO 410 I = 1, JC
      AS = I
      X = EB+AS*AP
      Y = CAT
      M = (X-A(16))/APC +1.0
      N = (Y-A(18))/ARC +1.0
      FPM = M-1
      FPN = N-1
      PAT = (X-FPM*APC-A(16)) / APC
      RAT = (Y-FPN*ARC-A(18)) / ARC
      M1 = M+1
      N1 = N+1
      G2      =G1(M,N)+PAT*(G1(M1,N)
     1-G1(M,N))+RAT*(G1(M,N1)-G1(M,N))
     2+PAT*RAT*(G1(M1,N1)-G1(M,N1)-
     3G1(M1,N)+G1(M,N))
      IF (G2) 410, 410, 290
```

```
      DO 420 I = 1, INT2                                          14-39
      GGWR(I) = GGWR(I) * AREA
      GGNWR(I) = GGNWR(I) * AREA
420   GGNWR(I) = GGWR(I) +GGNWR(I)
      NDIVPB = A(34)                                              14-40
      NBOX = INT2/NDIVPB
      L = 0
      DO 440 I=1,NBOX
      VGWNR = 0.0
      VGNWNR = 0.0
      VGWR = 0.0
      VGNWR = 0.0
      DO 430 J = 1, NDIVPB
      L = L+1
      VGWNR = VGWNR + GGWNR(L)
      VGNWNR = VGNWNR + GGNWNR(L)
      VGWR = VGWR+GGWR(L)
430   VGNWR = VGNWR+GGNWR(L)
      GGWNR(I) = VGWNR
      GGNWNR(I) = VGNWNR
      GGWR(I) = VGWR
440   GGNWR(I) = VGNWR
      BBBB = NDIVPB
      DP = BBBB* A(28)
      DO 450 I = 1, NBOX
      GGWNR(I) = GGWNR(I) / DP
      GGNWNR(I) = GGNWNR(I) / DP
      GGWR(I) = GGWR(I) / DP
450   GGNWR(I) = GGNWR(I) /DP
```

APPENDIX 4

DESCRIPTION OF COMPUTER PROGRAM SHO-16

The program SHO-16 tells which differential elements dxdy of the rectangle defined by A(12) through A(15) in Figure 44 contribute charge to the interior of the beam circle. To minimize computing time it is assumed that if a dxdy element in any row contributes no charge to the beam circle then all dxdy in the same row and to the left of this one do not contribute either. See Figure 15. The program allows the addition of a Kx^2 bump to electrons passing the observation azimuth. In the experimental work of Section VI, SHO-16 is used in conjunction with SHO-14 to test whether the experimental $i_o(x,y)$ fed into SHO-14 is defined over a region sufficiently large to allow SHO-14 to yield a valid prediction for $\Delta j(x)$.

Division 16-1 differs from 14-1 in not calling for the CC's. In SHO-16 $i_o(x,y)$ is not required. 16-1

See 14-2. 16-2

See 14-3. 16-3

See 14-4. 16-4

See 14-7. 16-5.

See 14-8. 16-6

See 14-9. 16-7

In 16-20 the square of the beam circle radius $r_o^2 = FA$ is compared with the $r^2 = x^2 + y^2$ associated with a subunit to see whether the latter lies indide or outside the beam circle. 16-8

Like SHO-14, SHO-16 allows the addition of a 16-9

```
      IF (SENSE SWITCH 2) 480, 460                                    14-41
460   PRINT 530
      PRINT 510, (GGNWR(I), I = 1, NBOX)
      PRINT 540
      PRINT 510, (GGNWNR(I), I = 1, NBOX)
      DO 470 I = 1, NBOX
470   GGNWR(I) = GGNWR(I) -GGNWNR(I)
      PRINT 550
      PRINT 510, (GGNWR(I), I = 1, NBOX)
480   PRINT 560
      PRINT 510, (GGWR(I), I = 1, NBOX)
      PRINT 570
      PRINT 510, (GGWNR(I), I = 1, NBOX)
      DO 490 I = 1, NBOX
490   GGWR(I) = GGWR(I) -GGWNR(I)
      PRINT 580
      PRINT 510, (GGWR(I), I = 1, NBOX)
      PRINT 590
      PRINT 500, (AD)
500   FORMAT (1H0(5E18.8)/1H0)
510   FORMAT (2X,10E11.4)
520   FORMAT (7H1SHO-14//)
530   FORMAT (28H  CURRENT DENSITY-NO WIRE-RF//)
540   FORMAT (31H  CURRENT DENSITY-NO WIRE-NO RF//)
550   FORMAT
     1(36H  CURRENT DENSITY-NO WIRE-DIFFERENCE//)
560   FORMAT (25H  CURRENT DENSITY-WIRE-RF//)
570   FORMAT (28H  CURRENT DENSITY-WIRE-NO RF//)
580   FORMAT (33H  CURRENT DENSITY-WIRE-DIFFERENCE//)
590   FORMAT (7H       K)
600   FORMAT (1H1)
      PRINT 600
      GO TO 110
      END (0, 1, 1, 1, 1)
```

14-42

INPUT DATA REQUIRED BY SHO-14

14-43

INPUT DATA EXAMPLES

Kx^2 bump to a subunit passing the observation azimuth. In SHO-15, however, the strength of the bump is computed each time it is applied rather than selecting an appropriate value from a reservoir of stored values. In SHO-16

$$\begin{pmatrix} \Delta x \\ \Delta y \end{pmatrix} = \begin{pmatrix} 0 \\ A(30)\,\frac{x^2}{r_0^2} \end{pmatrix}$$

$$BEEP = A(30)/r_0^2 = A(30)/A(24)**2$$

$$SUB = x^2 = X**2$$

Instruction 312 of 16-20 alters the y of a subunit appropriately, i.e., Y = Y + SUB*BEEP.

The quantity LMN(I,KKK) is associated with 16-10
the (I,KKK)-th differential element dxdy of the rectangle defined by A(12) through A(15) in Figure 44. At the end of a run each LMN(I,KKK) is either zero or one; if zero, the associated dxdy contributes no charge to the interior of the beam circle; if one, the dxdy does contribute some charge.

See 14-25. 16-11

See 14-26 16-12

See 14-27 16-13

See 14-28. 16-14

Division 16-15 would be identical to 14-29 15
if the statement, AREA = AP*AR*AB/A(26), were deleted from the latter.

This block scans a row of differential 16
elements dxdy from right to left. Figure 15 is more informative in this regard than Figure 44. In the former, I starts with eight each time the program considers a new row J.

See 14-31. 16-17

See 14-32. 16-18

See 14-33. 16-19

(1) Given the $\begin{pmatrix} x \\ y \end{pmatrix}$ of a subunit, its $\begin{pmatrix} x \\ y \end{pmatrix}$ one 16-20
revolution later is computed. (2) The $r^2 = x^2 + y^2$ associated with the subunit is found and compared with the square of the beam circle radius $r_0^2 = FA$ (16-8). If the subunit lies within the beam circle then LMN(K,J) is set equal to one (16-10) and the program shifts to a consideration of the next differential element dxdy. If the subunit does not lie within the beam circle, the Kx^2 bump is added in. (3) The program tests whether the subunit will collide with the injector on its next attempt to cross $\theta = 0$; if it will, the program shifts to a consideration of the next subunit; if it will not, $A(2) = \nu_{RF}$ is added to the RF phase angle in preparation for the application of the next RF bump to the subunit.

If none of the JB subunits associated with the (I,J)-th 16-21
dxdy element ever has an $r = \sqrt{x^2 + y^2} < r_0$ then the LMN(I,J) associated with this element is zero. In such a case the computation reaches the statement between 400 and 401. Control then passes to statement 410, bypassing consideration of all differential elements dxdy in the same row as the previous one and to the left of it. Hence, it is assumed that such bypassed elements contribute no charge to the beam circle.

The print out given by SHO-16 consists of three 16-22
items; (1) the input data A(1) through A(35), (2) an arrow designating the direction of the positive y axis as regards the data which follows, and (3) the LMN(I,J) of 16-10. In viewing the block of LMN(I,J)'s, the output sheet should be rotated clockwise 90° from the normal viewing position. The (I,J)-th element of this block is now associated with the (I,J)-th differential element dxdy of Figure 44 or Figure 15.

All input data required by SHO-16 can be fed in in terms of the A's, i.e., A(1) through A(15), A(23), A(24), A(25), and A(30). The description of these quantities as given in 14-42 is adequate except for:

A(10)	I.1	1.1≤A(10)≤40.1
A(11)	I.1	1.1≤A(11)≤100.1

RUN	CARD	DATA
	1	.40001 + 4
		END DATA
R-1	2	.125 + 1
	3	.251 + 2
	4	.1416 + 8
	5	.452 +10
	6	.62832 + 1
	7	.13 - 1
	8	.125 + 1
	9	.4284 + 8
	10	.61 + 1
	11	.501 + 2
	12	-.215 + 3
	13	-.209 + 3
	14	-.3 + 3
	15	.3 + 3
	23	.16666666
	24	.209 + 3
	25	.16666666
		END DATA
R-2	2	.13 + 1
	8	.13 + 1
	10	.81 + 1
	11	.241 + 2
	12	-.229 + 3
	14	-.1 + 3
	15	.1 + 3
		END DATA
R-3	2	.132 + 1
	8	.132 + 1
	11	.221 + 2
	14	-.13333333+ 1
	15	.5 + 2
		END DATA
R-4	2	.13333333+ 1
	8	.13333333+ 1
	11	.481 + 2
	12	-.213 + 3
	14	-.4 + 3
	15	.4 + 3
		END DATA
R-5	2	.134 + 1
	8	.134 + 1
	11	.271 + 2
	12	-.229 + 3
	14	-.50 + 2
	15	.175 + 3
		END DATA
R-6	2	.135946 + 1
	8	.135946 + 1
	11	.241 + 2
	14	-.1 + 3
	15	.1 + 3
		END DATA
R-7	2	.136 + 1
	8	.136 + 1
		END DATA
R-8	2	.136762 + 1
	8	.136762 + 1
		END DATA
R-9	2	.138 + 1
	8	.138 + 1
		END DATA
R-10	2	.14 + 1
	8	.14 + 1
	10	.61 + 1
	11	.481 + 2
	12	-.215 + 3
	14	-.2 + 3
	15	.2 + 3
		END DATA
R-11	2	.142 + 1
	8	.142 + 1
	10	.81 + 1
	11	.201 + 2
	12	-.229 + 3
	14	-.83333333+ 2
	15	.83333333+ 2
		END DATA
R-12	2	.135674 + 1
	4	.236 + 7
	8	.135674 + 1
	10	.201 + 2
	11	.361 + 2
	12	-.219 + 3
	14	-.75 + 2
	15	.75 + 2
		END DATA
R-13	4	.472 + 7
		END DATA
R-14	4	.708 + 7
	10	.151 + 2
	12	-.224 + 3
		END DATA
R-15	4	.944 + 7
		END DATA
R-16	4	.1416 + 8
	10	.101 + 2

RUN	CARD	DATA	
	11	.241	+ 2
	12	-.234	+ 3
	14	-.1	+ 3
	15	.1	+ 3
		END DATA	
R-17	4	.1888	+ 8
		END DATA	
R-16	4	.236	+ 8
		END DATA	
		END DATA	
		END DATA	

FORTRAN PROGRAM SHO-16

```
C       SHO-16                                                          6
        DIMENSION A(35), B(4000), F(4000),
       1G(4000), LMN(40, 100), KLMN(100)
        PRINT 630
        CALL MURCD2(A)                                                  16- 2
        JA = A(1)                                                       16- 3
        AAJA=1./FLOATF(JA)
        DO 100 I=1,JA
  100   B(I)=SIN4F(FLOATF(I-1)/FLOATF(JA))
  110   CALL MURCD2(A)                                                  16- 4
        PRINT 640, (A(I), I = 1, 35)
        DG = SIN4F (A(8))                                               16- 5
        DH = COS4F (A(8))
        DC = SIN4F (A(8)*A(25))                                         16- 6
        DD = COS4F (A(8)*A(25))
        AE = SIN4F (A(8)*(A(23)+A(25)))
        AF = COS4F (A(8)*(A(23)+A(25)))
        IF (A(25)) 130, 141, 130                                        16- 7
  130   DT = DD/DC
        DV = A(24)/DC
  141   FA = A(24)**2                                                   16- 8
        BEEP = A(30) / A(24) **2                                        16- 9
        DO 161 I = 1, 40                                                16-10
        DO 161 KKK = 1, 100
  161   LMN(I, KKK) = 0
        AD=A(4)*A(5)*A(6)*A(7)/(A(8)*A(9)**2)                           16-11
        AG=-AE*AD                                                       16-12
        AH= AF*AD
        DO 280 I=1,JA                                                   16-13
        G(I) = AG* B(I)
  280   F(I) = AH* B(I)
        JB=A(3)                                                         16-14
        AB=1.0/FLOATF(JB)
        QRST = 1.0000004 * AAJA
        JC=A(10)                                                        16-15
        AO=JC
        AP=(A(13)-A(12))/AO
        JD=A(11)
        AQ=JD
        AR=(A(15)-A(14))/AQ
        EB=A(12)-AP/2.0
        EA=A(14)-AR/2.0
```

```
      DO 410 J = 1, JD                                          16-16
      AT=J
      Y=EA+AT*AR
      CAT=Y
      DO 401 INI = 1, JC
      I = JC+1-INI
      AS=I
      X=EB+AS*AP
      Y=CAT
      DE = X*DD - Y*DC                                          16-17
      DF = X*DC + Y*DD
300   DO 400 L = 1, JB                                          16-18
      X = DE                                                    16-19
      Y = DF
      AAA=A(2)+FLOATF(L)*Ad
310   N = AAA
      NN = (QRST+AAA-FLOATF(N))/AAJA
      X = X+G(NN)
      Y = Y+F(NN)
      DD = X*DH+Y*DG                                            16-20
      Y  =-X*DG+Y*DH
      X = DD
      SUB = X**2
      IF (SUB+Y**2-FA) 311, 312, 312
311   LMN(I, J) = 1
      GO TO 401
312   Y = Y +SUB*BEEP
      IF (A(25)) 330, 320, 330
320   IF (X+A(24)) 400, 400, 340
330   IF (Y+X*DT+DV) 400, 400, 340
340   AAA = AAA+A(2)
      GO TO 310                                                 16-21
400   CONTINUE
      IF (LMN(I, J)) 410, 410, 401
401   CONTINUE
410   CONTINUE
```

16-22

```
      PRINT 670
      DO 620 L = 1, JC
      I = JC+1-L
      DO 610 K = 1, JD
      MM = JD+1-K
610   KLMN(K) = LMN(I, MM)
620   PRINT 650, (KLMN(KK), KK = 1, JD)
630   FORMAT (1H1SHO-16////)
640   FORMAT ((2X,5E18.8//))
650   FORMAT (10X,100I1)
670   FORMAT (18H      C--- --- Y ----C///)
700   FORMAT (1H1)
      PRINT 700
      GO TO 110
      END (0, 1, 1, 1, 1)
```

16-23

INPUT DATA RECORD READ BY SHO-16

16-24

INPUT DATA EXAMPLES

APPENDIX 5

DESCRIPTION OF COMPUTER PROGRAM SHO-18

The program SHO-18 requires that $i_o(x,y)$ be specified via input data at each point of a rectangular array (Figure 43). All these points lie on or within the rectangle defined by A(16) through A(19). In a run, information is extracted from this array over a second rectangle (Figure 44) lying on or within the one above. The second rectangle, defined by A(12) through A(15), is broken into differential elements dxdy. The program SHO-18 averages $i_o(x,y)$ over just those dxdy which contribute charge to the beam circle. (1) Designating this average as $\langle i_o(x,y) \rangle$, SHO-18 divides $i_o(x,y)$ at the center of each contributing dxdy by $\langle i_o(x,y) \rangle$. (2) SHO-18 finds, at the observation azimuth, the time average of the fraction of the beam circle area covered by charge originating from each dxdy. (3) The program computes $\overline{i(x,y,\theta,t)}/\langle i_o(x,y) \rangle$ as a function of $r' = r/r_o$, i.e., it averages $\overline{i(x,y,\theta,t)}/\langle i_o(x,y) \rangle$ over an area enclosing a circle of radius r. Usually $i_o(x,y) = i_o$ so that the above result becomes $\overline{i(x,y,\theta,t)}/i_o$ versus r'. The quantity $\overline{i(x,y,\theta,t)}/i_o$ versus r' does not depend on θ or t, i.e., it applies at any azimuth after maximum filling of the beam circle has been achieved. See Section 5.[illegible]) Other quantities computed by SHO-18 are described in 18-24 through 18-32.

The program SHO-18 can serve as an inefficient substitute for SHO-16 (R-1 of Figure 15 corresponds to R-7 of Figure 17). Like SHO-16 it assumes that if a dxdy element in a row of such elements contributes no

charge to the beam circle then all dxdy elements in the same row and to the left of this one do not contribute either. SHO-18 allows the application of a Kx^2 bump to a subunit passing the observation azimuth.

See 14-1. 18-1

See 14-2. 18-2

See 14-3. 18-3

See 14-4. 18-4

See 14-5. 18-5

See 14-6. 18-6

See 14-7. 18-7

See 14-8. 18-8

See 14-9. 18-9

The interior of the beam circle at the 18-10
observation azimuth is divided into JH = A(22) concentric annuli of equal area centered at (0,0) which, taken together, completely cover this interior. There are 400 annuli in all, (400 - JH) of them lying outside the beam circle. The central annulus, a circle, is number one. The storage location P(JG) is associated with the JG-th annulus. The P(JG) eventually become synomonous with $\overline{i(x,y,\theta,t)}/i_o$. The latter quantity is defined two paragraphs prior to 18-1. The quantity JJH = A(29) is the number of annuli beginning with number one whose associated P's are printed out.

The program, in considering a specific subunit passing the observation azimuth, must determine which P(JG) is to receive the $i_o(x,y)dxdy/JB$ associated with this subunit (Section 6.6). Since all annuli have the same area $\pi r_o^2/JH$, JG is given by

$$JG = \frac{x^2 + y^2}{r_0^2/JH} + 1.0$$

If $x^2 + y^2$ happens to be zero, JG = 1.0. When the program converts 1.0 to an integer without the decimal point, it is not certain whether one or zero results. To insure that one obtains, .0000004 is added to 1.0 above. The resulting test as it appears in 18-22 is JG = (DPP + SUB + Y**2)/DP.

See 16-9. 18-11

The P(I) are the 400 storage locations which 18-12

eventually contain $\overline{i(x,y,\theta,t)}/\langle i_o(x,y)\rangle$ versus r′ (18-10).

(2) Initially, G2(I,J) is the value of $i_o(x,y)$ at the center of the (I,J)-th differential element dxdy of the rectangle defined by A(12) through A(15) in Figure 44. Later G2(I,J) corresponds to this $i_o(x,y)$ divided by $\langle i_o(x,y)\rangle$. (3) The effectiveness with which the (I,J)-th differential element dxdy contributes charge to the beam circle is measured by GGLMN(I,J). See 18-30. (4) The quantities NEQUT1 and NEQUT2 are used in determining how many revolutions are needed for Resonant RF Inflection to achieve maximum filling of the beam circle. See 18-21.

See 14-25. 18-13

See 14-26. 18-14

See 14-27. 18-15

See 14-28. 18-16

If the statement AREA = AP*AR*AB/A(26) were 18-17

deleted from 14-29 then 18-17 would be identical to 14-29.

Division 18-18 parallels 14-30 except for (1) 18-18

scanning a row of differential elements dxdy from right

to left rather than left to right and (2) the replacement of G2 by G2(I,J). The reason for the first change is dealt with in 16-21. The G2(I,J) are used in computing $\langle i_o(x,y) \rangle$.

See 14-31. 18-19

See 14-32. 18-20

Division 18-21 would be identical to 14-33 18-21

if statements invelving NEQUT1 and NEQUT2 were deleted from the former. As SHO-18 considers a subunit from a particular differential element dxdy, NEQUT1 counts the number of revolutions this subunit makes up until it collides with the injector. The quantity NEQUT2 is the maximum NEQUT1 exhibited when all subunits from all differential elements are considered. Hence, NEQUT2 is the computational analog of the expression $2r_o/(k/2)$ found in Section 3.2.

(1) Given a subunit's $\binom{x}{y}$ its $\binom{x}{y}$ one 18-22

revolution later is found. (2) The program tests in which annulus JG the subunit lies and adds $i_o(x,y)$ = G2(I,J) to P(JG) (18-10). The program should have added $i_o(x,y)dxdy/JB$. The multiplication by dxdy/JB is taken care of in 18-27 and 18-31 (4) If JG corresponds to an annulus lying inside the beam circle then 1.0 is added to GGLMN(I,J) (18-12, 18-30). (5) The Kx^2 bump is added in. (6) The program tests whether the subunit will collide with the injector on its next attempt to cross $\theta = 0$; if it will, the program shifts to a consideration of the next subunit; if not, the RF phase angle is increased by A(2) = ν_{RF} in preparation for the addition of the next RF bump to the subunit.

The use made of GGLMN(I,J) in 18-23 parallels 18-23

the use made of LMN(I,J) in 16-21. SHO-18 sets the G2(I,J) associated with the (I,J)-th dxdy element to zero if this element

makes no contribution to the beam circle filling. When the G2(I,J) are printed out, the previous step allows one to distinguish between those dxdy which contribute charge to the beam circle and those which do not.

18-24 The trouble number TRNUMB is the number I of the largest annulus whose associated storage location P(I) exhibits nonzero occupation at the end of a run. For this run as well as all succeeding runs of the series to be valid, TRNUMB must be less than or equal to 399; if it is not, the uncertain runs should be re-submitted using (1) a smaller number of annuli within the beam circle (18-10), (2) a smaller rectangle of the type defined by A(12) through A(15) set nearer (0,0), and (3) a smaller RF bump strength k (18-13).

18-25 Division 18-25 tests which differential elements dxdy of the rectangle defined by A(12) through A(15) in Figure 44 contribute charge to the beam circle. The total area of these contributing elements is found (REIA) as well as the average value of $i_o(x,y)$ over these contributing elements. This average, $\langle i_o(x,y) \rangle$, is AVIOI.

18-26 The beam circle area BEGA is computed.

18-27 The time average value of i(x,y) over the beam circle, i.e., AVIOBC, is found by computing the time average trapped current and dividing this result by the beam circle area BEGA. The factor dxdy/JB = AB*AP*AR omitted in 18-22 is taken into account here.

18-28 The quantity BUMPK is set equal to k of $\Delta y = k \sin(\omega_{RF} t + \phi)$ (18-13).

18-29 See 18-21.

Up to now $i_o(x,y)$ has been stored as G2(I,J). 18-30

From a physical point of view it is of interest to have $i_o(x,y)$ divided by $\langle i_o(x,y)\rangle$. Accordingly, G2(I,J) is divided by AVIOI (18-25).

When the program reaches 18-24, GGLMN(I,J) is the ratio of (1) the time average trapped current at equilibrium due to charge originating from the (I,J)-th differential element to (2) the current emanating from this (I,J)-th element. In 18-30 these GGLMN(I,J) are multiplied by the factor $\left[\frac{1.0\,dx\,dy}{JB}\right]\left[\frac{1}{1.0\,\pi r_o^2}\right]$. This multiplication is interpreted as follows. The $\left[\frac{1.0\,dx\,dy}{JB}\right]$ gives the time average trapped current at equilibrium due to the (I,J)-th dxdy under the assumption that $i_o(x,y) = 1.0$. Section 6.6 deals with the origin of the factor $i_o(x,y)dxdy/JB$ which is here 1.0dxdy/JB. The time average of the fraction of the beam circle area covered to unit $i(x,y)$ by such a time average current is found by dividing this current by $1.0\,\pi r_o^2$. Summing these modified GGLMN(I,J) over all (I,J) gives the time average of the fraction (PCBCCV) of the beam circle area covered to unit $i(x,y)$ by the total time average trapped current stemming from an $i_o(x,y)$ of unity.

Division 18-31 finds the average $\overline{i(x,y,\theta,t)}$ over 18-31

an annulus and divides this result by $\langle i_o(x,y)\rangle$. The factor AB*AP*AR = dxdy/JB omitted in 18-22 is included here. Unity divided by the area of an annulus equals FLOATF(JH)/BECA. The quantity AVIOI is $\langle i_o(x,y)\rangle$.

The area ratio, ARRAT, is the ratio of the 18-32

beam circle area (BECA: 18-26) to the area of that portion of the injection region treated by the program which contributes charge to the interior of the beam circle (REIA: 18-25). The filling efficiency, FEFF, is the average $\overline{i(x,y,\theta,t)}$ over the beam circle

(AVIOBC: 18-27) divided by $\langle i_o(x,y)\rangle$ (AVIOI; 18-25). The current ratio, CURAT, is the ratio of the time average trapped current to the current emanating from REIA (18-25).

$$\text{CURAT} = \frac{(\text{AVIOBC})(\text{BECA})}{(\text{AVIOI})(\text{REIA})} = (\text{FEFF})(\text{ARRAT})$$

The charge efficiency, CEFF, is the ratio of the trapped charge at equilibrium to the total charge emitted from REIA in the time it takes the system to achieve equilibrium.

$$\text{CEFF} = \frac{(\text{AVIOBC})(\text{BECA})\hat{\tau}}{(\text{AVIOI})(\text{REIA})(\text{EQUT2})\hat{\tau}} = \frac{\text{CURAT}}{\text{EQUT2}}$$

The print out given by SHO-18 follows: 18-33

(1) A(1) through A(35) 18-34

(2) $G2(I,J) = i_o(x,y)/\langle i_o(x,y)\rangle$ 18-12, 18-23, 18-30

(3) GGLMN(I,J) 18-12, 18-30

(4) $P(I) = \overline{i(\alpha,y,\theta,t)}/\langle i_o(\alpha,y)\rangle$ 18-10, 18-12, 18-31

(5)

[illegible]AT	18-32
[illegible]AT	18-32
FEFF	18-32
CEFF	18-32
PCBCCV	18-30
AVIOBC	18-27
AVIOI	18-25
BECA	18-26
REIA	18-25
EQUT2	18-29
BUMPK	18-28
TRNUM	18-24

In (2) and (4) above the numbers G2(I,J) and GGLMN(I,J) occupy a position in their respective blocks equivalent to that held by the (I,J)-th differential element dxdy (Figure 44) with respect to its

neighbors provided I does not exceed ten. When I exceeds ten all numbers associated with any row J are printed out at ten numbers per line for as many lines as needed. The printer then skips two spaces and begins printing out numbers associated with row (J-1). In (4) above the P(I) are printed out at ten numbers per row for as many rows as needed. The first number of the first row is P(1). Here I runs from 1 to JJH = A(29). The twelve numbers in (5) above are printed out in the same order as they appear there at five numbers per row for as many rows as needed.

If EQUT2 of (5) above multiplied by ν_{RF} = A(2) is greater than 32,000 (14-41) or if TRNUMB is greater than 399 (18-24) then this run as well as all succeeding runs of the series may be invalid. To remedy the first defect either the integral portion of ν_{RF} or the revolutions required to achieve equilibrium, i.e., $\frac{2r_o}{k/2}$, should be decreased. To remedy the latter defect (1) the number of annuli lying within the beam circle, JH = A(22), should be decreased, (2) the rectangle defined by A(12) through A(15) in Figure 44 should be made smaller and should be set closer to $(-r_o, 0)$, and (3) the bump strength k should be made smaller.

The input data required by SHO-18 follows. 18-34

(1) The CC's: See 14-42.

(2) The A's. A(1) through A(25), A(29), and A(30).

The description of these A's as given in 14-42 is adequate except for the following changes and additions.

A(10) I.1. $1.1 \leq A(10) \leq 40.1$.

A(11) I.1. $1.1 \leq A(11) \leq 40.1$.

A(22) I.1. $1.1 \leq A(22) < 400.1$. The integral portion of A(22)

is the number of annuli residing within the beam circle (18-10; 18-12; 18-31).

A(29) I.1. $1.1 \leq A(29) \leq 400.1$. The integral portion of A(29) is the number of annuli whose contents P(I) one desires to have printed out beginning with annulus number one, (18-10, 18-12; 18-31).

RUN	CARD	DATA
	1	.1 + 1
	2	.1 + 1
	3	.1 + 1
	4	.1 + 1
		END DATA
	1	.40001 + 4
		END DATA
R-1	2	.136 + 1
	3	.251 + 2
	4	.1416 + 8
	5	.452 +10
	6	.62832 + 1
	7	.13 - 1
	8	.136 + 1
	9	.4264 + 8
	10	.81 + 1
	11	.151 + 2
	12	-.229 + 3
	13	-.209 + 3
	14	-.58333333+ 2
	15	.66666666+ 2
	16	.235 + 3
	17	.205 + 3
	18	-.1 + 3
	19	.1 + 3
	20	.21 + 1
	21	.21 + 1
	22	.101 + 2
	23	.16666666
	24	.209 + 3
	25	.16666666
	29	.201 + 2
		END DATA
R-2	10	.11 + 1
	11	.11 + 1
	12	-.229 + 3
	13	-.2265 + 3
	14	-.83333333+ 1
	15	
		END DATA
R-3	12	-.2115 + 3
	13	-.209 + 3
	14	-.83333333+ 1
	15	
		END DATA
R-4	12	-.2115 + 3
	13	-.209 + 3
	14	.58333333+ 2
	15	.66666666+ 2

RUN	CARD	DATA
		END DATA
R-5	10	.61 + 1
	11	.101 + 2
	12	-.233 + 3
	13	-.209 + 3
	14	-.73958333+ 2
	15	.82291666+ 2
	22	.201 + 2
	29	.401 + 2
		END DATA
R-6	2	.13577333+ 1
		END DATA
R-7	2	.13554667+ 1
		END DATA
R-8	2	.13464 + 1
		END DATA
		END DATA
		END DATA

FORTRAN PROGRAM SHO-18

```
C       SHO-18                                                          18-  1
        DIMENSION CC(600), A(35), B(4000),
       1G1(20, 30), F(4000), C(4000), P(400),
       2G2(40, 40), GGLMN(40, 40)
        PRINT 810
        CALL MURCD2(CC)
        CALL MURCD2(A)                                                  18-  2
        JA = A(1)                                                       18-  3
        AA=A=1./FLOATF(JA)
        DO 100 I=1,JA
  100   B(I)=SIN4F(FLOATF(I-1)/FLOATF(JA))
  110   CALL MURCD2(A                                                   18-  4
        PRINT 820, (A(I), I = 1, 35)
        JCNX=A(21)                                                      18-  5
        JCNY=A(20)
        NN=0
        DO 120 J=1, JCNY
        DO 120 I=1, JCNX
        NN=NN+1
  120   G1(I, J) = CC(NN)
        FPNX=JCNX-1                                                     18-  6
        FPNY=JCNY-1
        APC=(A(17)-A(16))/FPNX
        ARC=(A(19)-A(18))/FPNY
        DC = SIN4F (A(8))                                               18-  7
        DH = COS4F (A(8))
        DC = SIN4F (A(8)*A(25))                                         18-  8
        DD = COS4F (A(8)*A(25))
        AE = SIN4F (A( ) (A(23)+A(25)
        AF = COS4F (A(8 *(A(23)+A(25))
        IF (A(25)) 130, 14 , 130                                        18-  9
  130   D1 = DD/DC
        DV=A(24)/DC
```

```
142   JH = A(22)                                              18-10
      JJH = A(29)
      DP = A(24)**2/FLOATF(JH)
      DPP = 1.0000004*DP
      BEEP = A(30) / A(24) **2                                18-11
      DO 162 I = 1, 400                                       18-12
162   P(I) = 0.0
      DO 163 I = 1, 40
      DO 163 J = 1, 40
      G2(I, J) = 0.0
163   GGLMN(I, J) = 0.0
      NEQUT1 = 0
      NEQUT2 = 0
      AD=A(4)*A(5)*A(6)*A(7)/(A(8)*A(9)**2)                   18-13
      AG=-AE*AD                                               18-14
      AH= AF*AD
      DO 280 I=1,JA                                           18-15
      G(I) = AG* B(I)
280   F(I) = AH* B(I)
      JB=A(3)                                                 18-16
      AB=1.0/FLOATF(JB)
      QRST = 1.0000004 * AAJA
      JC=A(10)                                                18-17
      AO=JC
      AP=(A(13)-A(12))/AO
      JD=A(11)
      AQ=JD
      AR=(A(15)-A(14))/AQ
      EB=A(12)-AP/2.0
      EA=A(14)-AR/2.0
```

```
      DO 410 J = 1, JD                                              18-18
      AT=J
      Y=EA+AT*AR
      CAT=Y
      DO 401 INI = 1, JC
      I = JC+1-INI
      AS=I
      X=EB+AS*AP
      Y=CAT
      M=(X-A(16))/APC+1.0
      N=(Y-A(18))/APC+1.0
      FPM=M-1
      FPN=N-1
      PAT=(X-FPM*APC-A(16))/APC
      RAT=(Y-FPN*APC-A(18))/ARC
      M1=M+1
      N1=N+1
      G2(I,J)=G1(M,N)+PAT*(G1(M1,N)
     1-G1(M,N))+RAT*(G1(M,N1)-G1(M,N))
     2+PAT*RAT*(G1(M1,N1)-G1(M,N1)-
     3G1(M1,N)+G1(M,N))
290   DE = X*DD - Y*DC                                              18-19
      DF = X*DC + Y*DD
300   DO 400 L = 1, JB                                              18-20
      IF (NEQUT1 - NEQUT2) 305, 305, 304                            18-21
304   NEQUT2 = NEQUT1
305   NEQUT1 = 0
      X = DE
      Y = DF
      AAA=A(2)+FLOATF(L)*AB
310   N = AAA
      NN = (QRS1+AAA-FLOATF(N))/AAJA
      X = X+G(NN)
      Y = Y+F(NN)
      DD = X*DH+Y*DG                                                18-22
      Y  =-X*DG+Y*DH
      X = DD
      NEQUT1 = NEQUT1 + 1
      SUB = X**2
      JG = (DPP+SUB+Y**2)/DP
      P (JG) = P(JG)+G2(I,J)
      IF (JG-JH) 313, 313, 314
313   GGLMN(I, J) = GGLMN(I, J)+1.0
314   Y = Y+SUB*BEEP
      IF (A(25)) 330, 320, 330
320   IF (X+A(24)) 400, 400, 340
330   IF (Y+X*DI+DV) 400, 400, 340
340   AAA = AAA+A(2)
      GO TO 310                                                     18-23
400   CONTINUE
      IF (GGLMN(I, J)) 402, 402, 401
402   G2(I,J) = 0.0
      GO TO 410
401   CONTINUE
410   CONTINUE
```

```
      DO 710 I=1,400                                                  18-24
      J= 401-I
      IF (P(J)) 710, 710, 720
710   CONTINUE
720   TRNUMB= J
      AVIOI = 0.0                                                     18-25
      REIA = 0.0
      DO 740 J = 1, JD
      DO 740 I = 1, JC
      IF (GGLMN(I, J)) 740, 740, 730
730   AVIOI = AVIOI+G2(I, J)
      REIA = REIA+1.0
740   CONTINUE
      AVIOI= AVIOI/REIA
      REIA = REIA* AP*AR
      BECA = A(5)* A(24)**2/3.0                                       18-26
      AVIOBC = 0.0                                                    18-27
      DO 750 I = 1, JH
750   AVIOBC = AVIOBC+P(I)
      AVIOBC = AVIOBC*AB*AP*AR/BECA
      BUMPK = AD                                                      18-28
      EQUT2 = NEQUT2                                                  18-29
      DO 760 J = 1, JD                                                18-30
      DO 760 I = 1, JC
      G2(I, J) = G2(I, J)/AVIOI
760   GGLMN(I, J) = GGLMN(I, J)* AB* AP*AR/BECA
      PCBCCV = 0.0
      DO 770 J=1,JD
      DO 770 I=1,JC
770   PCBCCV = PCBCCV + GGLMN(I,J)
      DO 780 I = 1, 400                                               18-31
780   P(I) = P(I)*AB*AP*AR*FLOATF(JH)/
     1(BECA* AVIOI)
      ARRAT = BECA/REIA                                               18-32
      FEFF = AVIOBC/AVIOI
      CURAT = FEFF*ARRAT
      CEFF = CURAT/EQUT2
```

```
      PRINT 860                                                    18-33
      PRINT 850
      DO 790 J = 1, JD
      K = JD+1-J
      PRINT 830, (G2(I, K), I = 1, JC)
790   PRINT 860
      PRINT 860
      PRINT 850
      DO 800 J = 1, JD
      K = JD+1-J
      PRINT 830, (GGLMN(I, K), I = 1, JC)
800   PRINT 860
      PRINT 860
      PRINT 850
      PRINT 840, (P(I), I = 1, JJH)
      PRINT 860
      PRINT 850
      PRINT 820, (ARRAT, CURAT, FEFF, CEFF,
     1PCBCCV, AVIOBC, AVIOI, BECA, RETA,
     2EQUT2 , BUMPK, TRNUMB)
810   FORMAT (7H1SHO-18/////)
820   FORMAT (2X,5E18.8//)
830   FORMAT (5X,10F11.5)
840   FORMAT (2X,10E11.4//)
850   FORMAT (21H0**********)
860   FORMAT (1H0)
900   FORMAT (1H1)
      PRINT 900
      GO TO 110
      END (0, 1, 1, 1, 1)
```

18-34

INPUT DATA REQUIRED BY SHO-18

18-35

INPUT DATA EXAMPLES

APPENDIX 6

DESCRIPTION OF COMPUTER PROGRAM SHO-20

The program SHO-20 is more general than SHO-18 in that it allows (1) the RF bump strength k to depend on x, (2) ν_x to vary with a_x, and (3) ν_{RF} to vary with a_x. The variation of ν_{RF} with a_x is a nonphysical device utilized in C-5 of Section 6.1 to simulate the variation of f_o with a_x. Even when ν_x depends on a_x, SHO-20 still uses a rotational transformation M to relate the $\begin{pmatrix} x \\ y \end{pmatrix}$ of a subunit to its $\begin{pmatrix} x \\ y \end{pmatrix}$ one revolution later. The amount of rotation, however, depends on a_x, i.e., $M = M(2\pi\nu_x(a_x))$. The program SHO-20 is less general than SHO-18 in that (1) $i_o(x,y) = 1.0$, (2) both the azimuth of the RF bump and the observation azimuth are fixed at $\theta = 0$, and (3) no provision is made for the addition of a Kx^2 bump to a subunit. The program SHO-16 is not intended for use with SHO-20.

Division 20-1 differs from 14-1 in not calling for the CC's. **20-1**

See 14-2. **20-2**

See 14-3. **20-3**

Division 20-4 reads in any input data differing from that used in the previous run; it prints out all input data used in the present run, i.e., the A's and the nonzero DIVAR's. The DIVAR's in conjunction with the interpolation procedure of 20-15 define how the bump strength $k(x)>0$ of the radial RF bump $\Delta y = k \sin(\omega_{RF} t+\phi)$ varies with x. The range of x over which this variation is **20-4**

defined is $|x| \leq$ A(36). The integral portion of A(37), i.e., KKEND, gives the number of cells into which either the negative or positive half of this line segment is divided. The quantity KEND = 2* KKEND is the total number of such cells. The leftmost cell is number one; the rightmost, KEND.

Instead of computing and storing a k(x) appropriate to each cell, SHO-20 associates with each cell I a dimensionless factor D2VAR(I). When the program is ready to add $\Delta y = k \sin(\omega_{RF} t + \phi)$ to the y of a subunit's $\binom{x}{y}$, it first determines in which cell I the subunit displacement x lies and then (indirectly) multiplies k as computed in 20-12 by D2VAR(I) to yield k(x). It will be required that the D2VAR(I) be positive for all allowed x, i.e., D2VAR(I)>0 for $1 \leq I \leq$ KEND. This condition is met by requiring (1) D1VAR(I)$\geq$0, (2) D1VAR(1)>0, and (3) D1VAR(KEND)>0. Since the D2VAR(I) are not evaluated until 20-5, one uses the empty locations D2VAR(I) in 20-4 to aid in printing out (1) the values of I at which D1VAR(I)>0 and (2) the nonzero D1VAR's associated with these I.

Division 20-5 computes the D2VAR(I) for $1 \leq I \leq$KEND. 20-5

Statement 118 of 20-5 sets D2VAR(I) equal to D1VAR(I). No further consideration is given the D1VAR(I) during the course of the run. The program interpolates linearly between neighboring nonzero D2VAR's to obtain nonzero positive values for those D2VAR(I) ($1 \leq I \leq$KEND) which are still zero after the execution of statement 118.

The x axis at θ = 0+ ($|x| \leq$ A(36)) is divided 20-6

into KEND cells each of width DELK. The integral portion of (((x + A(36))/DELK) + 1.0) is the number of the cell in which a subunit exhibiting a displacement x at θ = 0+ resides. In 20-18 this

integer is given by IVAR = (X + BABO)/DELK. This expression is equivalent to IVAR = (((x + A(36))/DELK + 1.0000004). It is required that a subunit's displacement x always satisfy the condition $|x| < A(36)$ The .0000004 above is superfluous.

Non-linearity in the x motion is simulated 20-7 by keeping $M(2\pi\nu_x)$ a pure rotation and allowing ν_x to vary quadratically with a subunit's $a_x = \sqrt{x^2+y^2}$. Division 20-7 evaluates the elements of $M(2\pi\nu_x)$, i.e., RRG(I) and RRH(I), for discrete ν_x arising as a_x is varied from zero to A(36) in small steps.

Letting ν_{xo} be the ν_x of an electron having an a_x near zero and $\Delta\nu_x$ the change in an electron's ν_x as its a_x is increased from near zero to A(36) one has

$$\begin{array}{ccccc} \nu_x & = & \nu_{xo} & + & \Delta\nu_x \dfrac{[x^2+y^2]}{A(36)^2} \\ \downarrow & & \downarrow & & \downarrow \\ XXNU & = & A(8) & + & A(39)\dfrac{[x^2+y^2]}{A(36)^2} \end{array}$$

Consider a circle in phase space centered at (0,0) and of radius A(36). Its interior is broken into KCIR = A(40) concentric annuli of equal area which, taken together, completely cover this interior. The smallest annulus, a circle, is number one; the largest, KCIR. The $x^2 + y^2$ associated with an annulus will be that of its inside boundary. Since the annuli are of equal area, the $x^2 + y^2$ of the I-th annulus is $(I-1)A(36)^2/KCIR$. Hence, the ν_x associated with the I-th annulus, i.e., with an electron or subunit whose a_x lies in the I-th annulus, is

$$XXNU = A(8) + A(39)\frac{[I-1]}{KCIR}$$

It is required that a subunit's $a_x = r = \sqrt{x^2 + y^2}$ always be less than A(36).

The program SHO-20 allows V_{RF} to vary quadratically with a_x. In the spirit of 20-7, 20-8

$$V_{RF} = V_{RF_0} + \Delta V_{RF} \frac{[x^2 + y^2]}{A(36)^2}$$

$$RFNUST(I) = A(2) + A(38) \frac{[I - 1]}{KCIR}$$

When a subunit passes $\Theta = 0$ the program must evaluate in which of the KCIR annuli defined in 20-7 the subunit's $a_x = r = \sqrt{x^2+y^2}$ lies. Since all annuli have the same area, the appropriate annulus number is given by the integral portion of 20-9

$$\frac{\pi [x^2 + y^2]}{\left[\frac{\pi A(36)^2}{KCIR}\right]} + 1.0$$

In 20-19 this integer is given by IAMP = (RRO + RRPT)/RRP. This expression is equivalent to

$$IAMP = \frac{[x^2 + y^2]}{\left[\frac{A(36)^2}{KCIR}\right]} + 1.0000004$$

The .0000004 insures that IAMP = 1 when $x^2 + y^2 = 0$. If it were missing, it is not certain whether one or zero results when the program converts 1.0 to an integer without the decimal point. To insure that IAMP≤KCIR it is required that a subunit's a_x always be less than A(36).

See 18-10. 20-10

Division 20-11 is identical to 18-12 20-11 when the statement involving G2(I,J) is deleted from the latter.

20-12 See 14-25.

20-13 When the RF bump does not depend on subunit displacement x it has the form $\Delta y = k \sin(\omega_{RF} t + \phi)$ Division 20-13 stores this Δy for JA values of $(\omega_{RF} t + \phi)$ varying from zero to $2\pi(JA-1)/JA$. in increments of $2\pi/JA$.

20-14 See 14-28.

20-15 See 18-17.

20-16 Division 20-16 would parallel 18-18 if the interpolation process used to find G2(I,J) in 18-18 were omitted.

20-17 See 14-32.

20-18 The program SHO-20 allows for variation of bump streng k with subunit displacement x. It restricts the bump and observation azimuths to $\vartheta = 0$. Since the nonphysical backward rotation of 18-19 does not appear in SHO-20, only 1 of $\begin{pmatrix} x \\ y \end{pmatrix}$ in 20-18 is altered by the bump $\Delta y = k(x) \sin(\omega_{RF} t + \phi)$. (See 20-4, 20-5, 20-6. 20-12, 20-13, and 20-14).

20-19 (1) After the addition of the RF bump he integer IAMP is found which selects appropriate elements for the rotation matrix $M(2\pi\nu_x(a_x))$ (20-7; 20-9). (2) Given the $\begin{pmatrix} x \\ y \end{pmatrix}$ of a subunit its $\begin{pmatrix} x \\ y \end{pmatrix}$ one revolution later is computed. (3) The subunit revolution number is increased by one. (18-21). (4) The program tests in which annulus JG the subunit's a_x lies and adds 1.0 to the associated storage location P(JG). The number $\int_0(x,y)dxdy/JB = 1.0dxdy/JB$ rather than 1.0 should have been added (Section 6.6). The multiplication by dxdy/JB is taken care of in 20-24 and 20-28. The JG-th annulus referred to above is one of the 400 used in determining

$\overline{i(x,y,\theta,t)}/i_o$ (18-10). It is not related to the set of annuli used in connection with the variation of ν_x and ν_{RF} with a_x (20-7). (5) If JG corresponds to an annulus lying within the beam circle then unity is added to GGLMN(I,J) (18-12; 18-30). (6) The test as to whether the subunit collides with the injector is made. If no collision takes place, the RF phase angle is brought up to date by adding $\nu_{RF}(a_x)$ = RFNUST(IAMP) to it (20-8).

20-20 Division 20-20 would be identical to 16-21 if in the latter LMN(I,J) were replaced by GGLMN(I,J). The purpose of the GGLMN(I,J) is given in 18-12 and 18-30. The assumption inherent in 16-21 is also present in 20-20.

20-21 See 18-24.

20-22 If G2(I,J) in statement 730 of 18-25 were replaced by 1.0 then 20-22 would be identical to 18-25. In SHO-20 $i_o(x,y) = 1.0$.

20-23 See 18-26.

20-24 See 18-27.

20-25 See 18-28. (20-12)

20-26 See 18-21.

20-27 If the statement involving G2(I,J) in 18-30 were omitted then 20-27 would be identical to 18-30.

20-28 See 18-31.

20-29 See 18-32.

20-30 The print out given by SHO-20 parallels that given by SHO-18 except that the block of numbers appearing immediately after the A's in SHO-18, i.e., the G2(I,J)'s, is replaced in SHO-20 by (1) the values of I for which DIVAR(I)≠0 followed

by (2) the nonzero DlVAR(I) themselves. The I's are printed out at ten numbers per row for as many rows as needed. The block of nonzero DlVAR's follows. The position of an I in the first block corresponds to the position of the associated DlVAR(I) in the second.

In addition to the requirements for a valid run stipulated in 18-33, i.e., A(2)*EQUT2<32,000 and TRNUMB<399, SHO-20 requires that a subunit's $a_x = r = \sqrt{x^2+y^2}$ always be less than A(36). Whether or not this latter condition has been fulfilled throughout a run is determined as follows: The radius of the outside boundary of the TRNUMB-th annulus of the set of annuli defined in 18-10 serves as a least upper bound on a_x above. If the radius of this boundary is less than A(36), all is well. Since the annuli are of equal area and since JH = A(22) of them reside within the beam circle r_0 = A(24), the third condition for a valid run can be expressed as

$$\frac{TRNUMB}{JH} < \frac{A(36)^2}{A(24)^2}$$

If the output data shows that any of the above conditions is violated in a run then this run as well as all succeeding runs of the series may be invalid. In addition to applying the corrections mentioned in 18-33 it may be necessary to increase A(36).

In terms of input data, SHO-20 differs from SHO-18 in (1) not requiring the CC's which in SHO-18 define $i_o(x,y)$ and (2) in requiring the DlVAR's which in SHO-20 specify how the bump strength k(x) of $\Delta y = k(x)\sin(\omega_{RF}t+\phi)$ varies with x. Specific input data required by SHO-20 follows. 20-31

(1) <u>The A's</u>: A(1) through A(15), A(22), A(24), A(29), and A(36) through A(40). The description of these A's as found

in 18-34 is adequate except as follows:

A(2) The quantity A(2) is the ν_{RF} associated with an electron exhibiting nearly zero radial oscillation amplitude a_x (20-8).

A(8) The quantity A(8) is the ν_x of an electron exhibiting nearly zero radial oscillation amplitude (20-7).

A(36) A(36)>0. The quantity A(36) should be larger than the maximum a_x exhibited by any electron in the computation. It is the radius of a circle in phase space centered at (0,0) the interior of which is divided into concentric annuli which are used in simulating the variation of ν_x and ν_{RF} with a_x (20-7).

A(37) I.1. 1.1≤A(37)≤1500.1. The portion of the x axis serving as a diameter of the circle defined by A(36) is divided into cells of equal width. The integral portion of A(37) is the number of such cells along either the negative or the positive half of this diameter. These cells are used in simulating the variation of bump strength k(x) with x (20-4; 20-5; 20-6).

A(38) The quantity A(38) is the change in the ν_{RF} associated with an electron when its radial oscillation amplitude is increased from near zero to A(36) (20-8).

A(39) The quantity A(39) is the change in an electron's ν_x when its radial oscillation amplitude a_x is increased from near zero to A(36) (20-7).

A(40) I.1. 1.1≤A(40)≤3000.1. The integral portion of A(40) is the number of concentric annuli of equal area into

which the interior of the circle defined by A(36) is divided. These annuli are used in simulating the variation of ν_x and ν_{RF} with an electron's radial oscillation amplitude a_x (20-7; 20-8).

(2) The D1VAR's: The D1VAR's in conjunction with an interpolation procedure in 20-5 specify how k(x) of the radial RF bump $\Delta y = k(x)\sin(\omega_{RF}t+\phi)$ varies with electron displacement x (20-4; 20-5). It is required that

D1VAR(I)≥0 (1≤I≤KEND)

D1VAR(1)>0

D1VAR(KEND)>0

where

2≤KEND≤3000

KEND = 2*KKEND

KKEND = A(37)

1.1≤A(37)≤1500.1

RUN	CARD	DATA
	1	.40001 + 4
		END DATA
R-1	2	.136 + 1
	3	.251 + 2
	4	.1416 + 8
	5	.452 +10
	6	.62832 + 1
	7	.13 - 1
	8	.136 + 1
	9	.4284 + 8
	10	.61 + 1
	11	.201 + 2
	12	-.233 + 3
	13	-.209 + 3
	14	-.10714286+ 3
	15	.10714286+ 3
	22	.401 + 2
	24	.209 + 3
	29	.601 + 2
	36	.3 + 3
	37	.11 + 1
	38	
	39	
	40	.30001 + 4
		END DATA
	1	.1 + 1
	2	.1 + 1
		END DATA
R-2	39	.46702226- 2
		END DATA
	1	.1 + 1
	2	.1 + 1
		END DATA
R-3	39	.9340344 - 2
		END DATA
	1	.1 + 1
	2	.1 + 1
		END DATA
R-4	39	.28021336- 1
		END DATA
	1	.1 + 1
	2	.1 + 1
		END DATA
R-5	3	.501 + 2
	10	.21 + 1
	11	.61 + 1
	12	-.219 + 3
	13	-.214 + 3
	14	-.25 + 2

RUN	CARD	DATA
	15	.25 + 2
	37	.9601 + 3
	38	
	39	
	40	.11 + 1
		END DATA
	2	
	1	.1 + 1
	1920	.1 + 1
		END DATA
R-6	1	.40001 + 4
		END DATA
	1	.19 + 1
	160	.19 + 1
	1761	.1
	1920	.1
		END DATA
R-7	1	.40001 + 4
		END DATA
	160	
	1761	
	960	.19 + 1
	961	.1
		END DATA
R-8	2	.13554667+ 1
	37	.11 + 1
	38	.9340344 - 2
	39	
	40	.30001 + 4
		END DATA
	960	
	961	
	1920	
	1	.1 + 1
	2	.1 + 1
		END DATA
R-9	2	.136 + 1
	8	.13554667+ 1
	38	
	39	.9340344 - 2
		END DATA
	1	.1 + 1
	2	.1 + 1
		END DATA
R-10	2	.13622665+ 1
	3	.251 + 2
	8	.136 + 1
	10	.61 + 1
	11	.141 + 2

RUN	CARD	DATA
	12	-.233 + 3
	13	-.209 + 3
	14	-.75 + 2
	15	.75 + 2
	38	
	39	.9340344 - 2
		END DATA
	1	.1 + 1
	2	.1 + 1
		END DATA
R-11	2	.13645332+ 1
		END DATA
	1	.1 + 1
	2	.1 + 1
		END DATA
R-12	2	.13668 + 1
		END DATA
	1	.1 + 1
	2	.1 + 1
		END DATA
R-13	2	.13532 + 1
	8	.13464 + 1
	10	.81 + 1
	11	.101 + 2
	12	-.241 + 3
	13	-.209 + 3
	14	-.75 + 2
	15	.75 + 2
	38	
	39	.28021336- 1
		END DATA
	1	.1 + 1
	2	.1 + 1
		END DATA
R-14	2	.13566 + 1
		END DATA
	1	.1 + 1
	2	.1 + 1
		END DATA
R-15	2	.136 + 1
		END DATA
	1	.1 + 1
	2	.1 + 1
		END DATA
		END DATA
		END DATA

FORTRAN PROGRAM SHO-20

```
C     SHO-20                                                    20- 1
      DIMENSION A(40), B(40000), F(4000),
     1P(400), GGLMN(40, 40), D1VAR(3000),
     2D2VAR(3000), RRG(3000), RRH(3000),
     3RFNUST(3000)
      PRINT 810
      CALL MURCD2(A)                                            20- 2
      JA = A(1)                                                 20- 3
      AAJA=1./FLOATF(JA)
      DO 100 I=1,JA
100   B(I)=SIN4F(FLOATF(I-1)/FLOATF(JA))
110   CALL MURCD2(A)                                            20- 4
      CALL MURCD2(D1VAR)
      PRINT 820, (A(I), I = 1, 40)
      KKEND = A(37)
      KEND = 2*KKEND
      DO 111 I = 1, 3000
111   D2VAR(I) = 0.0
      L = 0
      DO 113 I = 1, KEND
      IF (D1VAR(I)) 113, 113, 112
112   L = L+1
      D2VAR(L) = FLOATF(I)
113   CONTINUE
      PRINT 870, (D2VAR(I), I = 1, L)
      DO 114 I = 1, L
114   D2VAR(I) = 0.0
      L = 0
      DO 116 I = 1, KEND
      IF (D1VAR(I)) 116, 116, 115
115   L = L+1
      D2VAR(L) = D1VAR(I)
116   CONTINUE
      PRINT 880, (D2VAR(I), I = 1, L)
      DO 117 I = 1, L
117   D2VAR(I) = 0.0
```

```
      DO 118 I = 1, KEND                                          20- 5
118   D2VAR(I) = D1VAR(I)
      I = 1
119   JBEG = I
      BEG = D2VAR(I)
121   I = I+1
      IF (I-KEND) 122, 126, 126
122   IF (D2VAR(I)) 121, 121, 123
123   JEND = I
      END = D2VAR(I)
      IF (JEND-JBEG-1) 119, 119, 124
124   K = JBEG+1
      L = JEND-1
      DO 125 J = K,L
125   D2VAR(J) = (END-BEG)*FLOATF (J-JBEG)/
     1FLOATF(JEND-JBEG) +BEG
      GO TO 119
126   JEND = I
      END = D2VAR(I)
      IF (JEND-JBEG-1) 129, 129, 127
127   K = JBEG+1
      L = JEND-1
      DO 128 J = K, L
128   D2VAR(J) = (END-BEG)*FLOATF(J-JBEG)/
     1FLOATF (JEND-JBEG)+BEG
129   DELK = A(36)/FLOATF(KKEND)                                  20- 6
      DDELK = 1.0000004*DELK
      BABO = A(36) +DDELK
      KCIR = A(40)                                                20- 7
      PARX = A(39) /FLOATF(KCIR)
      DO 131 I = 1, KCIR
      XXNU = A(8) +PARX* FLOATF(I-1)
      RRG(I) = SIN4F(XXNU)
131   RRH(I) = COS4F(XXNU)
      PARRF = A(38)/FLOATF(KCIR)                                  20- 8
      DO 132 I = 1, KCIR
132   RFNUST(I) = A(2)+PARRF* FLOATF(I-1)
      RRP = A(36)**2/ FLOATF(KCIR)                                20- 9
      RRPT = 1.0000004* RRP
142   JH = A(22)                                                  20-10
      JJH = A(29)
      DP = A(24)**2/FLOATF(JH)
      DPP = 1.0000004*DP
      DO 162 I = 1, 400                                           20-11
162   P(I) = 0.0
      DO 163 I = 1, 40
      DO 163 J = 1, 40
163   GGLMN(I, J) = 0.0
      NEQUT1 = 0
      NEQUT2 = 0
```

```
      AD=A(4)*A(5)*A(6)*A(7)/(A(8)*A(9)**2)                    20-12
      DO 280 I=1,JA                                            20-13
280   F(I) = AD*B(I)
      JB=A(3)                                                  20-14
      AB=1.0/FLOATF(JB)
      QRST = 1.0000004 * AAJA
      JC=A(10)                                                 20-15
      AO=JC
      AP=(A(13)-A(12))/AO
      JD=A(11)
      AQ=JD
      AR=(A(15)-A(14))/AQ
      EB=A(12)-AP/2.0
      EA=A(14)-AR/2.0
      DO 410 J = 1, JD                                         20-16
      AT=J
      Y=EA+AT*AR
      CAT=Y
      DO 401 INI = 1, JC
      I = JC+1-INI
      AS=I
      DE = EB+AS*AP
      DF = CAT
300   DO 400 L = 1, JB                                         20-17
      IF (NEQUT1 - NEQUT2) 305, 305, 304                       20-18
304   NEQUT2 = NEQUT1
305   NEQUT1 = 0
      X = DE
      Y = DF
      AAA=A(2)+FLOATF(L)*AB
310   N = AAA
      NN = (QRST+AAA-FLOATF(N))/AAJA
      IVAR = (X+BABO)/DELK
      Y = Y+D2VAR(IVAR)* F(NN)
      RRO = X**2+Y**2                                          20-19
      IAMP = (RRO+RRPT)/RRP
      DO = X*RRH(IAMP)+ Y*RRG(IAMP)
      Y  =-X*RRG(IAMP)+ Y*RRH(IAMP)
      X = DO
      NEQUT1 = NEQUT1 + 1
      JG = (DPP+RRO) /DP
      P(JG) = P(JG) +1.0
      IF (JG-JH) 313, 313, 320
313   GGLMN(I, J) = GGLMN(I, J)+1.0
320   IF (X+A(24)) 400, 400, 340
340   AAA = AAA+ RENUST(IAMP)
      GO TO 310                                                20-20
400   CONTINUE
      IF (GGLMN(I, J)) 410, 410, 401
401   CONTINUE
410   CONTINUE
```

```
      DO 710 I=1,400                                              20-21
      J= 401-I
      IF (P(J)) 710, 710, 720
710   CONTINUE
720   TRNUMB= J
      AVIOI = 0.0                                                 20-22
      REIA = 0.0
      DO 740 J = 1, JD
      DO 740 I = 1, JC
      IF (GGLMN(I, J)) 740, 740, 730
730   AVIOI = AVIOI+1.0
      REIA = REIA+1.0
740   CONTINUE
      AVIOI= AVIOI/REIA
      REIA = REIA* AP*AR
      BECA = A(6)* A(24)**2/2.0                                   20-23
      AVIOBC = 0.0                                                20-24
      DO 750 I = 1, JH
750   AVIOBC = AVIOBC+P(I)
      AVIOBC = AVIOBC*AB*AP*AR/BECA
      BUMPK = AD                                                  20-25
      EQUT2 = NEQUT2                                              20-26
      DO 760 J = 1, JD                                            20-27
      DO 760 I = 1, JC
760   GGLMN(I,J) = GGLMN(I,J)*AB*AP*AR/BECA
      PCBCCV = 0.0
      DO 770 J=1,JD
      DO 770 I=1,JC
770   PCBCCV = PCBCCV + GGLMN(I,J)
      DO 780 I = 1, 400                                           20-28
780   P(I) = P(I)*AB*AP*AR*FLOATF(JH)/
     1(BECA* AVIOI)
      ARRAT = BECA/REIA                                           20-29
      FEFF = AVIOBC/AVIOI
      CURAT = FEFF*ARRAT
      CEFF = CURAT/EQUT2
```

```
      PRINT 860                                                    20-30
      PRINT 850
      DO 800 J = 1, JD
      K = JD+1-J
      PRINT 830, (GGLMN(I, K), I = 1, JC)
800   PRINT 860
      PRINT 860
      PRINT 850
      PRINT 840, (P(I), I = 1, JJH)
      PRINT 860
      PRINT 850
      PRINT 820, (ARRAT, CURAT, FEFF, CEFF,
     1PCBCCV, AVIOBC, AVIOI, BECA, REIA,
     2EQUT2 , BUMPK, TRNUMB)
810   FORMAT (7H1SHO-20/////)
820   FORMAT (2X,KE18.8//)
830   FORMAT (5X,10F11.5)
840   FORMAT (2X,10E11.4//)
850   FORMAT (21H0********************)
860   FORMAT (1H0)
870   FORMAT (10F10.1)
880   FORMAT (10F10.4)
900   FORMAT (1H1)
      PRINT 900
      GO TO 110
      END (0, 1, 1, 1, 1)
```

20-31

INPUT DATA REQUIRED BY SHO-20

20-32

INPUT DATA EXAMPLES

APPENDIX 7

EFFECTS OF NON-LINEARITY ON RRFI

Figure 21 of Section 5.3 shows how non-linearity can decrease filling efficiency. Here $k = 2.095 \frac{\text{mils}}{\text{r}}$, $r = 209 \frac{\text{mils}}{\text{r}}$ and $\nu_x(0) = \nu_{RF} = 1.36$. As $\nu_x(a_x)$ is made a successively stronger function of $\left(\frac{a_x^2}{r_o^2}\right)$, filling efficiency (FE) drops.

Run	$\nu_x(a_x)$	FE %
R-1	$1.36 + 0.0 \left(\frac{a_x}{r_o}\right)^2$	100
R-2	$1.36 + 0.00227 \left(\frac{a_x}{r_o}\right)^2$	78
R-3	$1.36 + 0.00453 \left(\frac{a_x}{r_o}\right)^2$	41
R-4	$1.36 + 0.01360 \left(\frac{a_x}{r_o}\right)^2$	11

Filling efficiency can be increased by making a better choice of ν_{RF}. Figure 41 illustrates runs paralleling R-3 above except for ν_{RF} being changed slightly.

Run	ν_{RF}	FE %
R-3	1.36	41
R-10	1.36 + 0.00227	89
R-11	1.36 + 0.00453	71
R-12	1.36 + 0.00680	41

Here filling efficiency has been increased from 41% to 89% by setting ν_{RF} half-way between $\nu_x(0)$ and $\nu_x(r_o)$. Figure 42 illustrates a similar sequence modeled after R-4. In R-13, R-14, and R-15 $\nu_x(a_x) = 1.36 - .0136 + .0136 \left(\frac{a_x}{r_o}\right)^2$. This change over R-4 is of little physical consequence.

Run	ν_{RF}	FE o/o
R-4	1.36	11
R-13	1.36 − .0136 + .0068	49
R-14	1.36 − .0136 + .0102	61
R-15	1.36 − .0136 + .0136	42

Here maximum filling ($\tilde{=}$ 61%) is achieved when ν_{RF} is set 3/4 of the way between $\nu_x(0)$ and $\nu_x(r_o)$. This fraction gets nearer to unity and the filling efficiency drops below 61% when $(\nu_x(r_o) - \nu_x(0))$ is made larger than 0.0136.

Consider R-14. Raise k until filling efficiency has increased from 61% to 100%. Adjust ν_{RF} so that the k which gives 100% filling is a minimum. The size of the required injection area has increased in this process. A practical injector, even if its septum thickness were zero, would probably be able to cover only a fraction of this area to an $i_o(x,y)$ of i_o. From study of the on-resonance linear problem one might expect the filling efficiency which prevails to be slightly greater than the fraction of the required injection area so covered. (Presumably $i_o(x,y)$ equals i_o near $(-r_o, 0)$ but is zero further from $(-r_o, 0)$. Figure 15 indicates that dxdy near $(-r_o, 0)$ are slightly more effective in filling the beam circle than dxdy further from $(-r_o, 0)$). What actually prevails is thought to deviate from the on-resonance linear problem in two basic respects. (1) It takes longer than $\frac{2r_o}{k/2}\tau$ to achieve maximum filling and (2) dxdy near $(-r_o, 0)$ contribute more charge to the beam circle; dxdy further from $(-r_o, 0)$ contribute less than in the on-resonance linear problem. Point (1) means that the charge efficiency will be less than in the on-resonance linear problem. Point (2) means

that with a practical injector covering only that portion of the required injection area near $(-r_0, 0)$, filling efficiency will be somewhat higher than anticipated on the basis of the on-resonance linear problem.

Statements (1) and (2) above are inferred from behavior of the off-resonance linear problem in the special case of $r_r = r_0$, i.e., where k is just sufficient to achieve 100% filling in the absence of a septum. The rest of this appendix considers those aspects of the off-resonance linear problem which support statements (1) and (2) above.

(1) In the off-resonance linear problem maximum filling occurs in a time $\frac{2\pi}{|\sigma|} = \frac{\tau}{|\Delta\nu_{RF}|}$ provided $r_r \leq r_0$. One assumes here that every empty point initially within the beam circle which gets pushed outside the beam circle has become a filled point by the time it returns to the beam circle. When $r_r = r_0$, maximum filling corresponds to 100% filling. Consider the case where $r_r = r_0$. Substituting for $|\Delta\nu_{RF}|$ in the expression above its value as obtained from the relation $r_r = \frac{k}{4\pi|\Delta\nu_{RF}|}$ one obtains

$$\frac{\tau}{|\Delta\nu_{RF}|} = \frac{4\pi r_0}{k}\tau = \frac{2\pi r_0}{(k/2)}\tau$$

This result can be understood by viewing points on a segment's phase plane from a coordinate septum rotating with these points. One notes that each point must be displaced once around a resonance circle of circumference $2\pi r_0$ before complete filling obtains. The average displacement per revolution along this curved path is the same as along the straight line path in the on-resonance linear problem, i.e., k/2. Hence, filling time is $\frac{2\pi r_0}{k/2}\tau$ as noted above. This filling time is a factor of π larger than in the on-resonance linear problem.

Consequently, charge efficiency is reduced by a factor of $\frac{1}{\pi}$ over this case. This reduction is the worst that can happen, however, as either increasing or decreasing ν_r makes the charge efficiency greater. In the latter case 100% filling no longer prevails.

When ν_{RF} deviates from ν_x by the amounts considered above, the shape and size of the required injection area do not differ radically from what they are when $\Delta\nu_{RF} = 0$.

The above results suggest that in the presence of non-linearity a decrease in charge efficiency over the on-resonance linear problem is to be expected when non-linearity is on the verge of destroying the 100% filling efficiency property of RRFI.

(2) Let $\nu_x = L/N$. Choose N large so that the N-sided polygon looks like the beam circle. Let $N\frac{\lambda_\beta}{2} << \frac{2\pi r_0}{N}$. Break the beam into segments, viewing any particular segment only at $\theta = 0$ on every N-th pass it makes of $\theta = 0$. Define the time t to be zero when the RF is turned on. Viewing times t will be limited to:

$$0 < t < \tau$$
$$N\tau < t < N\tau + \tau$$
$$2N\tau < t < 2N\tau + \tau$$
$$\vdots \qquad \vdots \qquad \vdots$$

When viewing segments in any one of these intervals one notes that the N-turn displacement vector exhibits all orientations ($\nu_x > 1$). There will be degeneracy in the sense that a given N-turn displacement vector orientation can be exhibited by more than one segment. Even though ν_x is not an integer it will be assumed that the number of segments which exhibit N-turn displacement vectors lying within a given angular range is proportional to this range. Only charge injected into the beam circle which crosses the leftmost side of the beam polygon as viewed

at $\theta = 0$ during the allowed viewing times will be considered. This restriction is not essential to the arguments which follow. One could just as well consider charge entering across any other side of the beam polygon by shifting to a different set of viewing intervals.

Pick a point on the required injection area, say, $(x,0)$ where $x \leq -r_o$. Consider a small circular neighborhood about this point. Take $i_o(x,y) = i_o > 0$ on this neighborhood. Outside this neighborhood $i_o(x,y) = 0$. Let $v_{RE} = v_x$. If this point is less than $N\frac{\lambda_e}{2}$ to the left of $(-r_o,0)$ then for that segment whose N-turn displacement vector is directed parallel to the x axis and to the right one sees a string of filled islands move across the beam circle on the line $y = 0$. Each island is separated from its nearest neighbors by a distance $N\frac{\lambda_e}{2}$. When equilibrium is achieved the number of islands in this string is $\frac{2r_o}{N\lambda_e/2}$, i.e., the length of the trajectory across the beam circle is proportional to the amount of charge injected from a neighborhood about the point. Henceforth, the term "point" will be used to mean the neighborhood about the point.

The results for all segments will be superimposed onto the above segment (Figure 10). When the point on the required injection area is less than $N\frac{\lambda_e}{2}$ to the left of $(-r_o,0)$ strings of islands are seen along chords lying in an angular range of $\pm \xi_1$ about the orientation considered above. This angle ξ_1 is zero when the point is $N\frac{\lambda_e}{2}$ to the left of $(-r_o,0)$. It approaches $\pm \frac{\pi}{2}$ as this point nears $(-r_o,0)$. The angle ξ_1 will be taken positive for chords lying below the x axis and as negative for those lying above. As a measure of the charge injected into the beam circle by the point one finds the integral of chord length over an angular range $\pm \xi_1$ about the chord $y = 0$. To facilitate this it

will be assumed that when the point is to the left of $(-r_o,0)$ all chords nevertheless pass through $(-r_o,0)$, i.e., $(-r_o,0)$ serves as the origin of these chords.

It proves convenient to define a new coordinate system (x'',y'') which has its origin at $(x,y) = (-r_o,0)$. The equation of the beam circle in this system is $(x''-r_o)^2 + y''^2 = r_o^2$ or $x''^2 - 2x''r_o + y''^2 = 0$. A chord inclined at an angle ξ to the horizontal has the equation $y'' = -\tan(\xi)x''$. This chord intersects the beam circle at $(x'',y'') = (0,0)$ and at a second point which is found from these two equations. Substituting y'' from the second for y'' in the first gives

$$x''^2 - 2x''r_o + x''^2\tan^2\xi = 0$$

$$x'' = \frac{2r_o}{1+\tan^2\xi}$$

Hence the second intersection is at

$$(x'', y'') = \left(\frac{2r_o}{1+\tan^2\xi} , \frac{-2r_o\tan\xi}{1+\tan^2\xi} \right)$$

The length of the chord between intersections is

$$\sqrt{(x''-0)^2+(y''-0)^2} = \frac{2r_o}{\sqrt{1+\tan^2\xi}} = 2r_o\cos\xi$$

The charge injected by the point over an angular range of $\pm\xi_1$ about $y = 0$ is proportional to

$$\int_{-\xi_1}^{\xi_1} 2r_o\cos\xi\, d\xi = 2r_o\, 2\sin\xi_1$$

Next, an expression analogous to the one above for the off-resonance linear problem will be found. The special case of $r_r = r_o$ is worked with. Here islands do not move across the beam circle on chords as before but on arcs of circles (r_o). A specific example will be considered first.

Islands moving into the beam circle along the x axis at $(x,y) = (-r_o,0)$ have their direction of motion subsequently altered so that they leave the beam circle at $(x,y) = (0,\pm r_o)$. The sign depends on the sign of $\nu_{RF} - \nu_x$. The path length within the beam circle for these islands is $\frac{2\pi r_o}{4}$. In the on-resonance linear case islands similarly injected have path length $2r_o$. It is concluded that when the injection point is near $(x,y) = \left(-r_o - N\frac{\lambda}{2}, 0\right)$, a factor of $\frac{\pi}{4}$ less charge gets into the beam circle from this point in the off-resonance linear problem ($r_\nu = r_o$) than in the on-resonance one.

The particular trajectory which is inclined at an angle ξ to $y = 0$ at $(x,y) = (-r_o, 0)$ is the portion of the circle $(x''-r_o\sin\xi)^2 + (y''-r_o\cos\xi)^2 = r_o^2$ which lies within the beam circle. The length of this trajectory will be found. The trajectory subtends an angle γ on itself, i.e., on the trajectory circle, where $\sin\frac{\gamma}{2}$ equals one-half the distance between the intersections of the trajectory circle with the beam circle all divided by r_o.

The equation for the beam circle is $(x''-r_o)^2 + y''^2 = r_o^2$ or $x''^2 - 2r_o x'' + y''^2 = 0$. The previous equation gives

$$x''^2 - 2x''r_o\sin\xi + y''^2 - 2y''r_o\cos\xi = 0$$

One intersection occurs at $(x'',y'') = (0,0)$. Upon eliminating the quantity $x''^2 + y''^2$ from the above two equations one obtains

$$y'' = x''\left(\frac{1-\sin\xi}{\cos\xi}\right)$$

Substituting this result into the beam circle equation gives

$$x''^2 - 2r_o x'' + x''^2\left(\frac{1-\sin\xi}{\cos\xi}\right)^2 = 0$$

or

$$x'' = \frac{2r_o}{1+\left(\frac{1-\sin\xi}{\cos\xi}\right)^2}$$

The second point of intersection is

$$(x'', y'') = \left(\frac{2r_0}{1 + \left(\frac{1 - \sin\xi}{\cos\xi}\right)^2} \, , \, \frac{2r_0 \left(\frac{1 - \sin\xi}{\cos\xi}\right)}{1 + \left(\frac{1 - \sin\xi}{\cos\xi}\right)^2} \right)$$

The distance between the two points of intersection is

$$\sqrt{(x''-0)^2 + (y''-0)^2} = \frac{2r_0}{\sqrt{1 + \left(\frac{1 - \sin\xi}{\cos\xi}\right)^2}}$$

Hence,

$$\gamma = 2 \sin^{-1} \frac{1}{\sqrt{1 + \left(\frac{1 - \sin\xi}{\cos\xi}\right)^2}}$$

The length of the trajectory under consideration is $r_0\gamma$.

$$r_0\gamma = 2r_0 \sin^{-1} \frac{1}{\sqrt{1 + \left(\frac{1 - \sin\xi}{\cos\xi}\right)^2}} = 2r_0 \cot^{-1}\left(\frac{1 - \sin\xi}{\cos\xi}\right)$$

The charge injected along trajectories inclined within $\pm\xi_1$ of $y = 0$ at $(x,y) = (-r_0, 0)$ is proportional to

$$\int_{-\xi_1}^{\xi_1} 2r_0 \cot^{-1}\left(\frac{1 - \sin\xi}{\cos\xi}\right) d\xi$$

The integrand equals $2r_0\left(\frac{\xi}{2} + \frac{\pi}{4}\right)$. The integral becomes

$$2r_0 \int_{-\xi_1}^{\xi_1} \left(\frac{\xi}{2} + \frac{\pi}{4}\right) d\xi = 2r_0 \, \frac{\pi}{4} \, 2\xi_1$$

The result from the on-resonance linear problem which corresponds to the above result is $2r_0 \, 2\sin\xi$. The ratio of the former to the latter is

$$\frac{2r_0 \, \frac{\pi}{4} \, 2\xi_1}{2r_0 \, 2\sin\xi_1} = \frac{\pi}{4} \, \frac{\xi_1}{\sin\xi_1}$$

When $\xi_1 \to 0$, $\frac{\pi}{4}$ obtains. Hence an injection point near $(x,y) = (-r_0 - N\frac{\lambda}{2}, 0)$ in the off-resonance linear problem ($r_r = r_0$) contributes

a factor of $\frac{\pi}{4}$ less charge to the beam circle than in the on-resonance linear problem. When considering injection points nearer $(x,y) = (-r_o,0)$ one is reached where equivalence between the two problems obtains. Here $\frac{\pi}{4}\frac{\xi_1}{\sin\xi_1} = 1$. An ξ_1 of 67^o applies. Points still closer to $(-r_o,0)$ inject change over a still larger range. Such points contribute more charge to the beam circle in the off-resonance linear problem than they do in the on-resonance one. When $\xi_1 = \frac{\pi}{2}$, $\frac{\pi}{4}\frac{\xi_1}{\sin\xi_1}$ becomes $\frac{\pi^2}{8}$ or 1.23.

When using an injector which provides an $i_o(x,y)$ of i_o only over a small neighborhood near $(-r_o,0)$, the above results suggest that with non-linearity present a slightly larger filling efficiency than found in the corresponding on-resonance linear problem should obtain when the non-linearity is on the verge of destroying the 100% filling property of RRFI. On the other hand, introduction of a septum is expected to inhibit filling efficiency more in this non-linear problem than it does in the corresponding on-resonance linear one.

REFERENCES

1. Kerst, D. W., et al., Rev. Sci. Instr. 31, 1076 (1960).

2. Hammer, C. L., R. W. Pidd, and K. M. Terwilliger, Rev. Sci. Instr., 26, 555 (1955).

3. Cole, F. T., R. O. Haxby, L. W. Jones, C. H. Pruett, and K. M. Terwilliger, Rev. Sci. Instru., 28, 403 (1957).

4. Cook, B. C., Minutes of MURA Staff Meeting No. 111,2(April 5,1960).

5. Cook, B. C., Bulletin of the American Physical Society 5, series II, 226 (1960).

6. Kerst, D. W., Physical Review 74, 503 (1948).

7. Kerst, D. W., Rev. Sci. Instr., 21, 462 (1950).

8. Judd, D. L. A Study of the Injection Process in Betatrons and Synchrotons. Unpublished Doctoral dissertation, California Institute of Technology (1950).

9. Kovrizhnykh, L. M. and A. N. Lebedev, Soviet Physics JETP 34(7), 679 (1958).

10. Davis, Leverett, Jr. and R. V. Langmuir, Physical Review 75, 1457 (1949).

11. Jones, W. B., H. R. Kratz, J. L. Lawson, G. L. Ragan and H. G. Voorhies, Physical Review 78, 60 (1950).

12. Barden, S. E., Proceedings of the Physical Society (London) 64B, 85 and 579 (1951).

13. Teng, L. C., Argonne National Laboratory Report ANLAD-49 (1958).

14. Mills, F. E. and D. C. Morin, Proceedings of the 1961 International Conference on High Energy Accelerators, 395, (1961).

15. Symon, K. R., Minutes of MURA Staff Meeting No. 111,1 (April 5,1960).

16. Rowe, E. M. A conversation.

17. Slater, J. C. Microwave Transmission. New York: Dover Publications, Inc., 1959, pp. 23-26.

18. Curtis, C. D. and R. E. Rothe, MURA Report No. 531 (1959).

19. Westlund, G. A., MURA Reports No. 536 and No. 550 (1959).

Table 1

t	Resultant Vector
0τ	$\begin{pmatrix} x_0 \\ y_0 \end{pmatrix} = \begin{pmatrix} x_0 \\ y_0 \end{pmatrix}$
1τ	$\begin{pmatrix} x_1 \\ y_1 \end{pmatrix} = M\begin{pmatrix} x_0 \\ y_0 \end{pmatrix} + M\begin{pmatrix} 0 \\ \Delta y_0 \end{pmatrix}$
2τ	$\begin{pmatrix} x_2 \\ y_2 \end{pmatrix} = M^2\begin{pmatrix} x_0 \\ y_0 \end{pmatrix} + M^2\begin{pmatrix} 0 \\ \Delta y_0 \end{pmatrix} + M\begin{pmatrix} 0 \\ \Delta y_1 \end{pmatrix}$
...	. ....
$n\tau$	$\begin{pmatrix} x_n \\ y_n \end{pmatrix} = M^n\begin{pmatrix} x_0 \\ y_0 \end{pmatrix} + \sum_{p=0}^{n-1} M^{n-p}\begin{pmatrix} 0 \\ \Delta y_p \end{pmatrix}$

Table 2

N	Charge Efficiency %
3	7.6
4	13.8
5	17.4
6	19.6
7	21.0
8	21.8
9	22.4
10	23.0
11	23.4
12	23.8
∞	25.0

Table 3

Range of r_r	Range of r	$\overline{i(x,y,\theta,t)}/i_o$
$0 \le r_r \le r_o/2$	$0 \le r \le r_o - 2r_r$	0
	$r_o - 2r_r \le r \le r_o$	$1 - \frac{1}{\pi}\cos^{-1}\left[\frac{r^2 - r_o^2 + 2r_o r_r}{2 r r_r}\right]$
$r_o/2 \le r_r \le r_o$	$0 \le r \le 2r_r - r_o$	1
	$2r_r - r_o \le r \le r_o$	$1 - \frac{1}{\pi}\cos^{-1}\left[\frac{r^2 - r_o^2 + 2r_o r_r}{2 r r_r}\right]$
$r_o \le r_r < \infty$	$0 \le r \le r_o$	1

Table 4

Range of r_r'	$\Delta\overline{j(0,\theta,t)}_N = \Delta j(0)_N$
$0 \le r_r' \le 1/2$	$2r_r' - \frac{1}{\pi}\int_{1-2r_r'}^{1}\cos^{-1}\left[\frac{r'^2 - 1 + 2r_r'}{2r'r_r'}\right]dr'$
$1/2 \le r_r' \le 1$	$1 - \frac{1}{\pi}\int_{2r_r'-1}^{1}\cos^{-1}\left[\frac{r'^2 - 1 + 2r_r'}{2r'r_r'}\right]dr'$
$1 \le r_r' < \infty$	1

Fig. 1

SPIRAL SECTOR MODEL [1]

A	Injector	$\theta = 0°$
B	RF Electrode	$\theta = 60°$
C	Thick Wire Probe	$\theta = 240°$
D	Fine Wire Probe	$\theta = 300°$
E	Vacuum Tank Wall	
F	One Possible Equilibrium Orbit	
G	Magnet Edge	
H	Magnet Edge	
I	Magnet Backleg	
J	Vacuum Tank Wall	

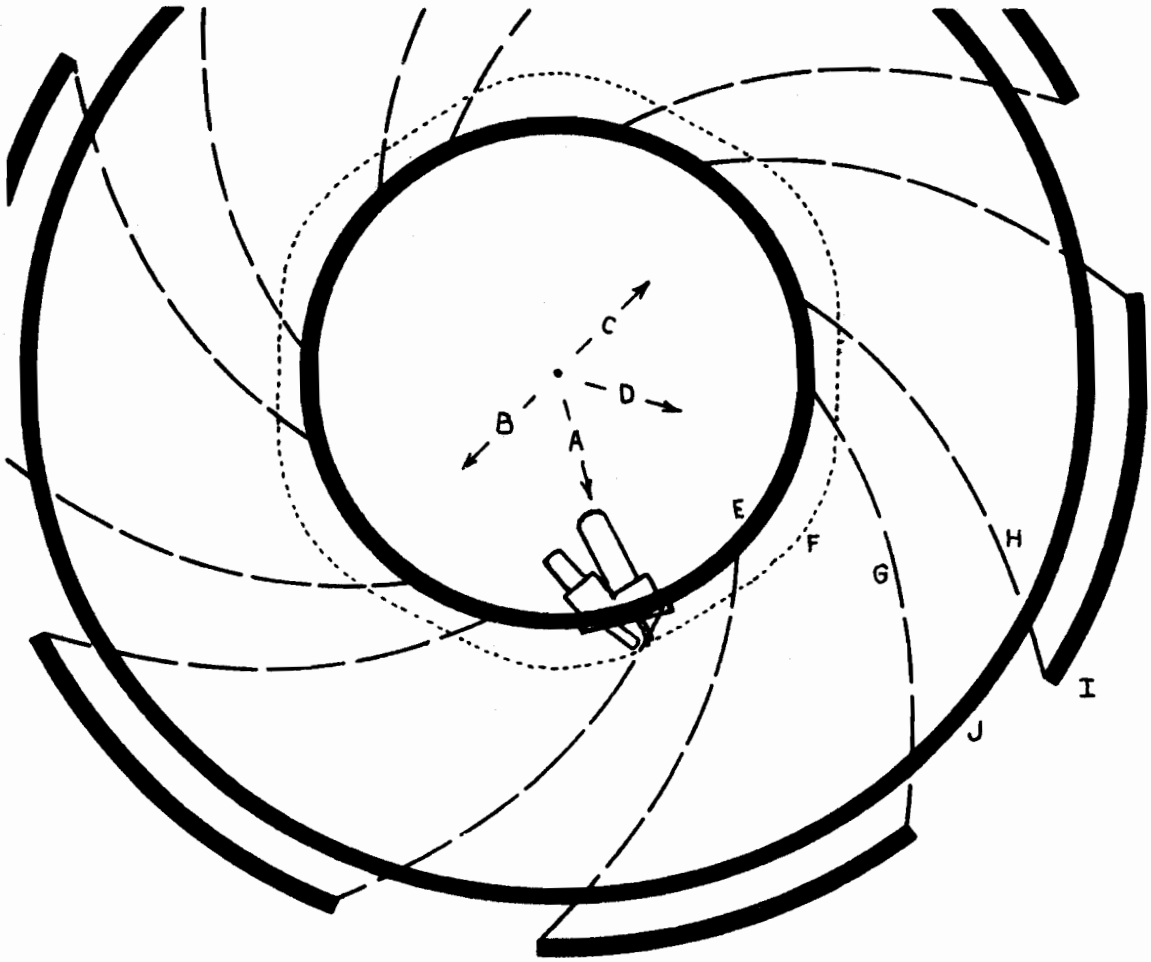

G Equilibrium Orbit
B Vacuum Tank
A Vacuum Tank

Fig. 2

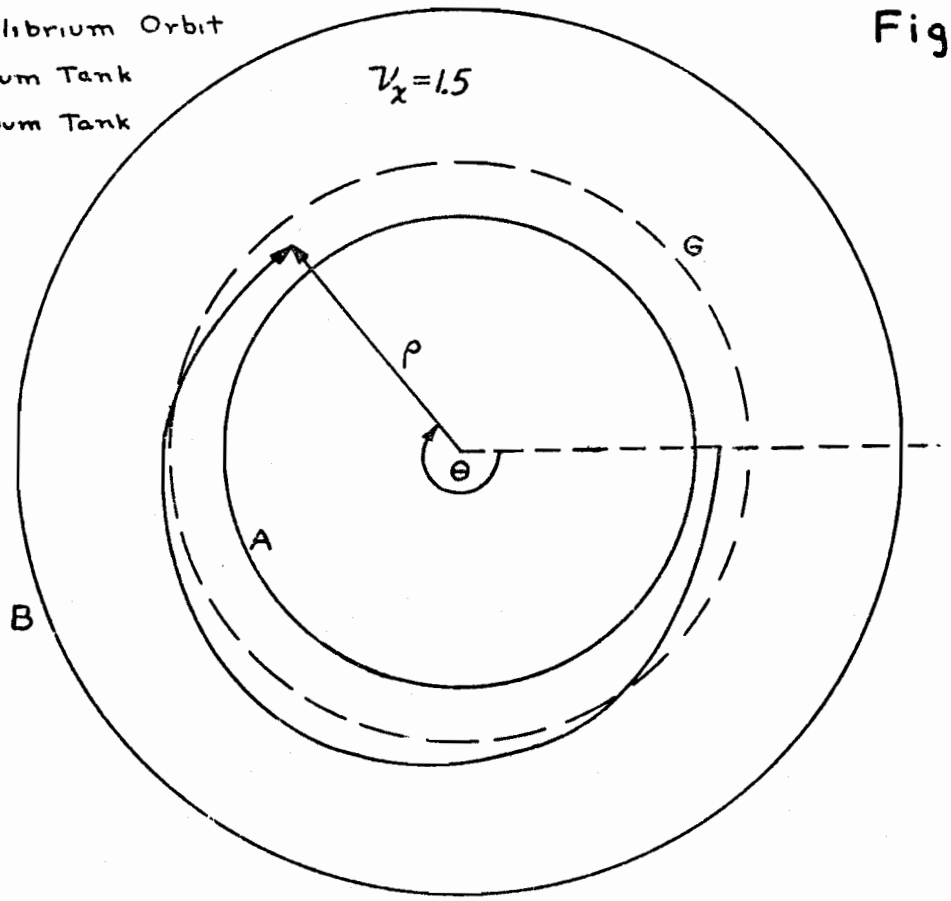

Fig. 3

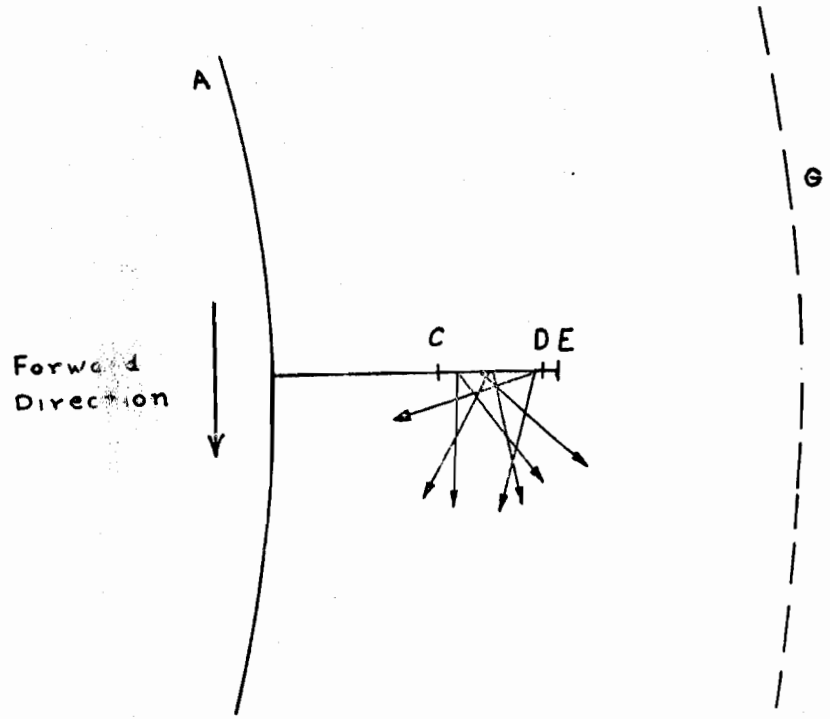

Fig. 4

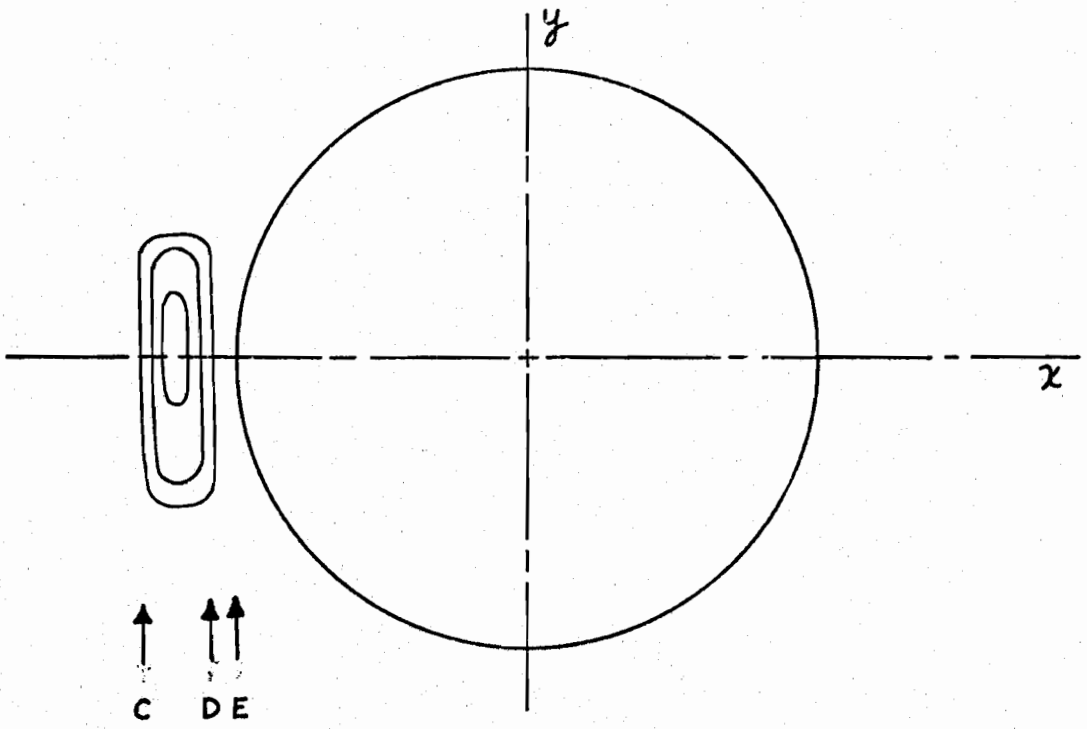

Fig. 5

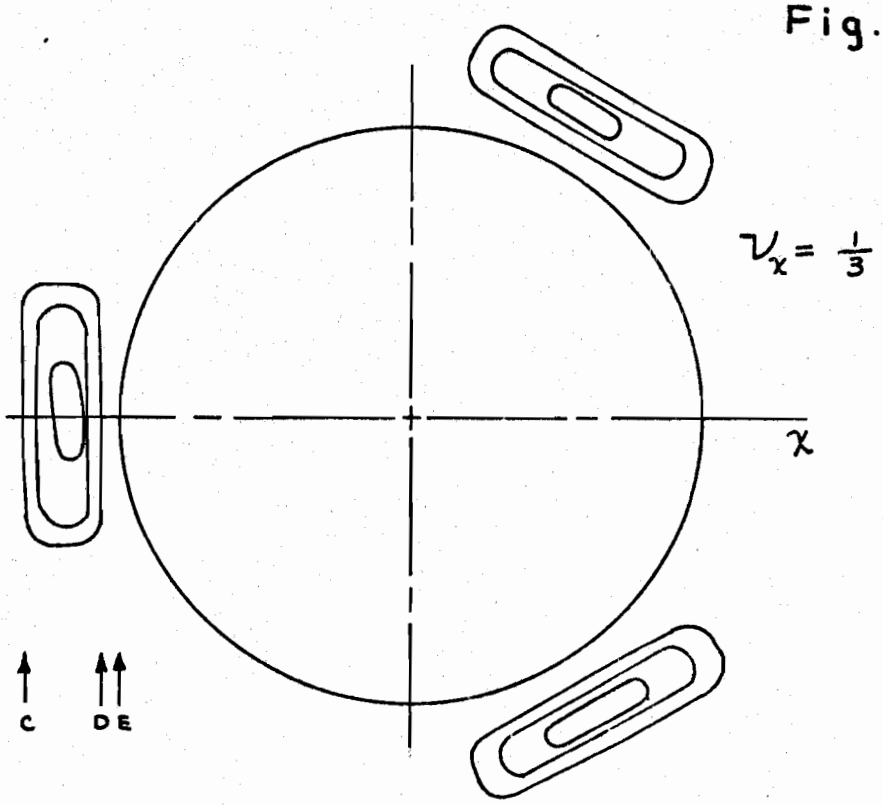

Fig. 6

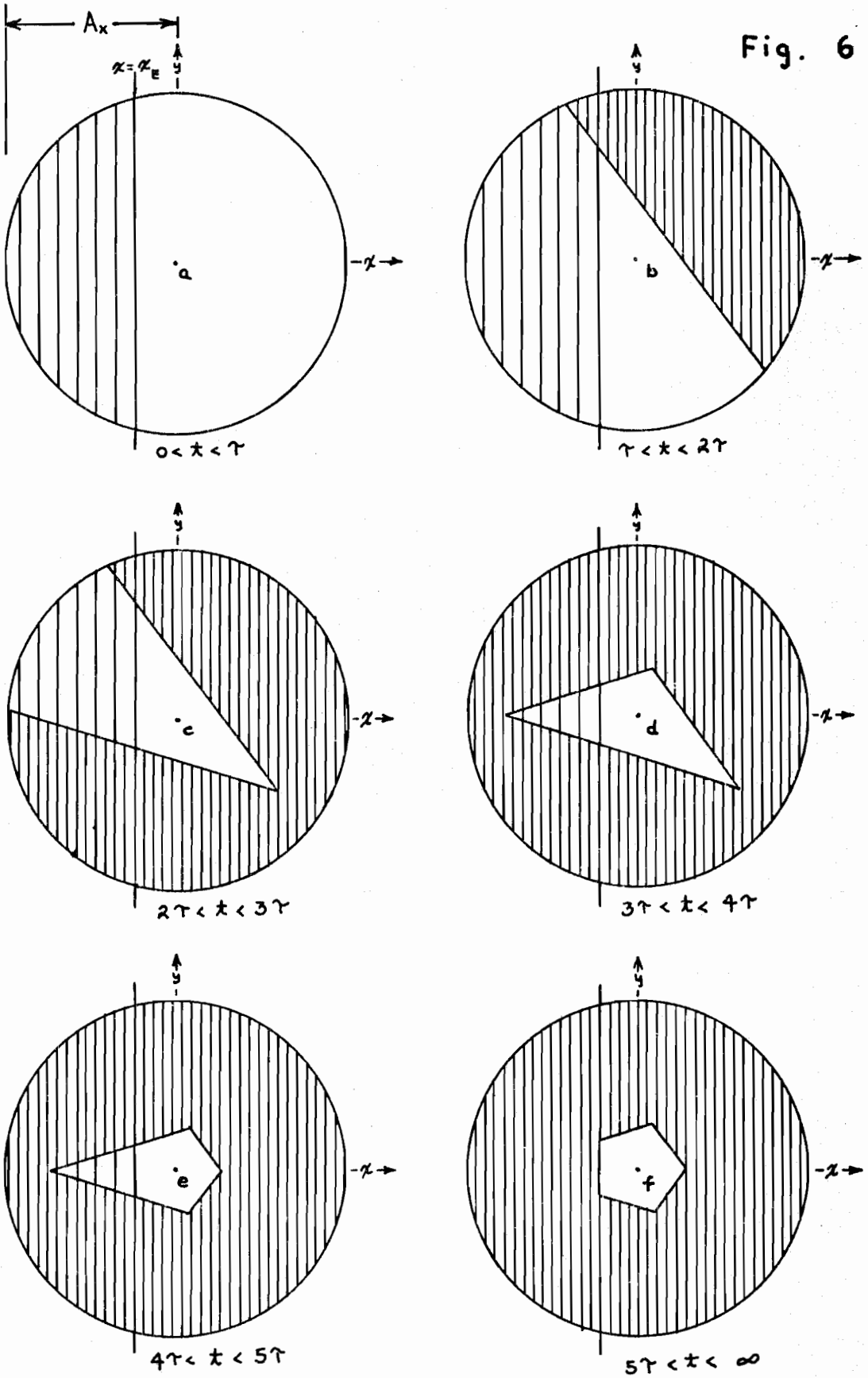
A_x
$x = x_E$
y
x
a
$0 < t < \tau$
b
$\tau < t < 2\tau$
c
$2\tau < t < 3\tau$
d
$3\tau < t < 4\tau$
e
$4\tau < t < 5\tau$
f
$5\tau < t < \infty$

Fig. 7

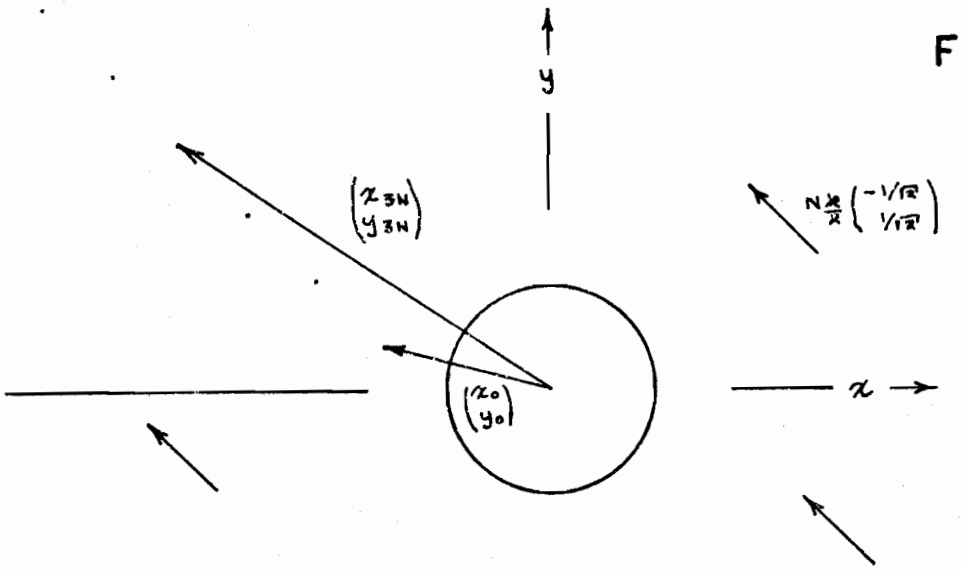

Fig. 8

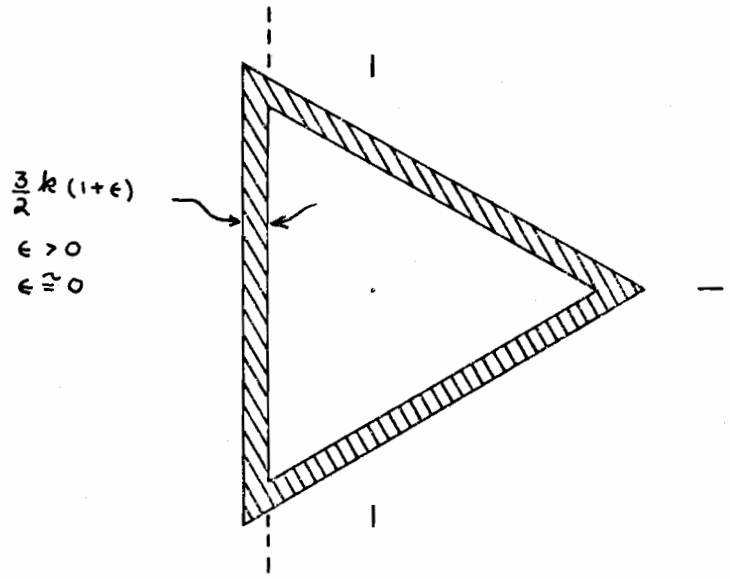

Fig. 9

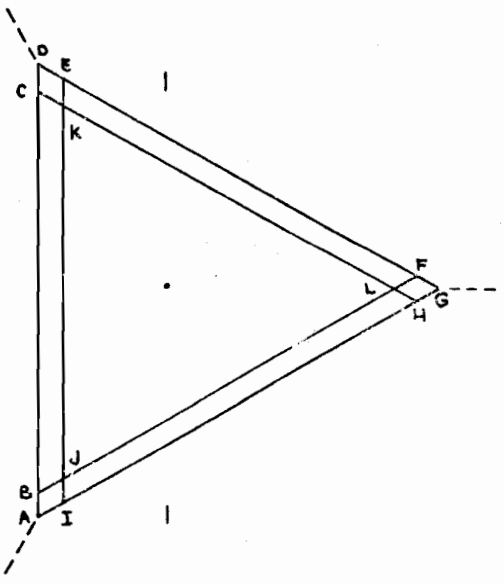

Fig. 10

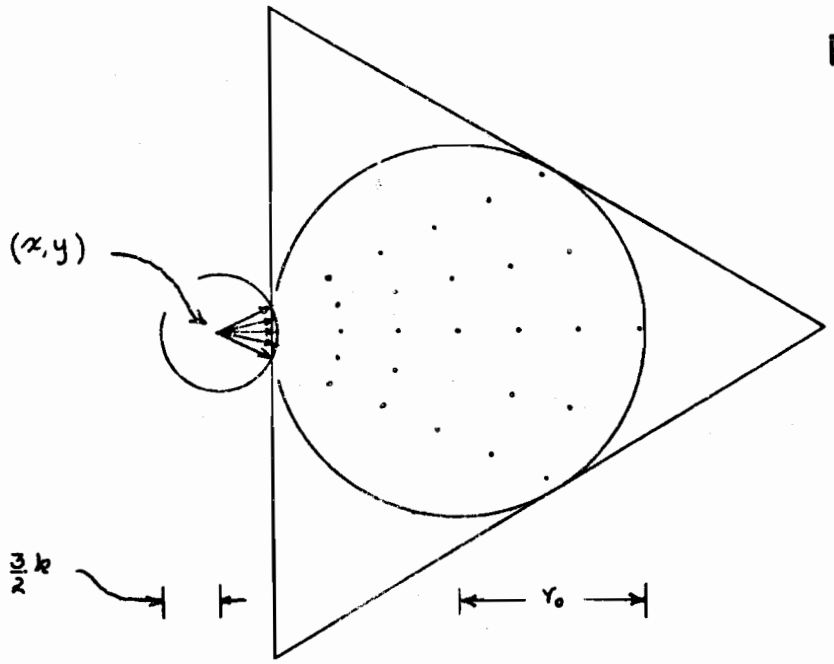

Fig. 11

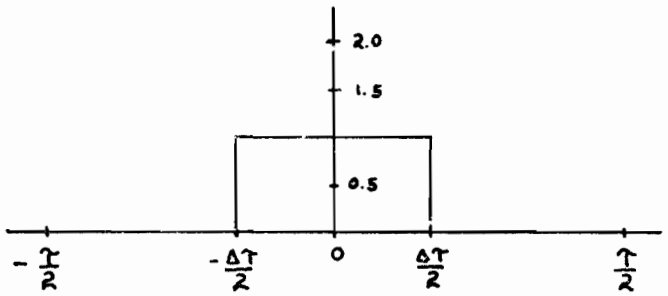

Fig. 12

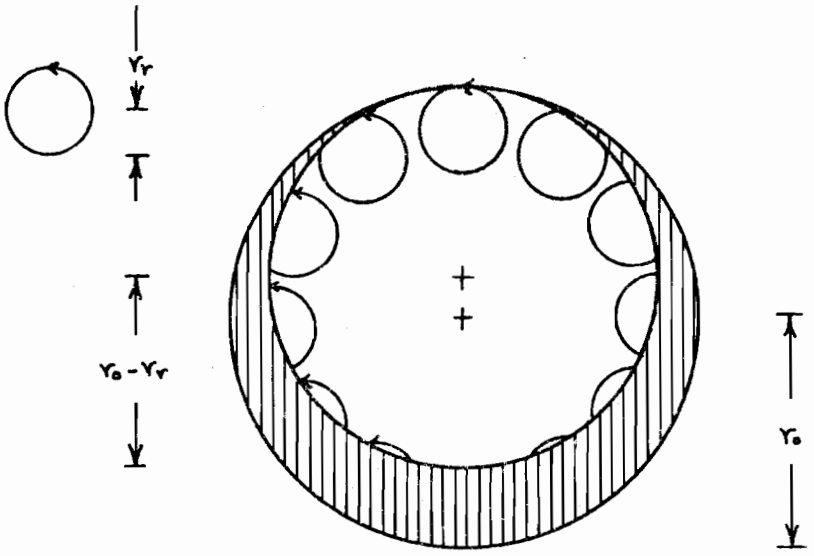

Fig. 13

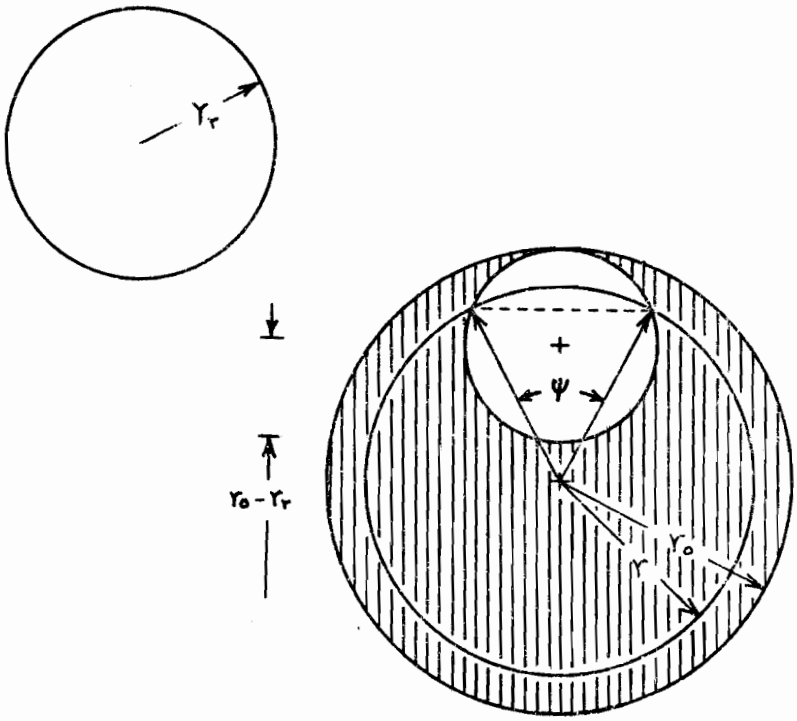
r_r
$r_o - r_r$
ψ
r
r_o

Fig. 14

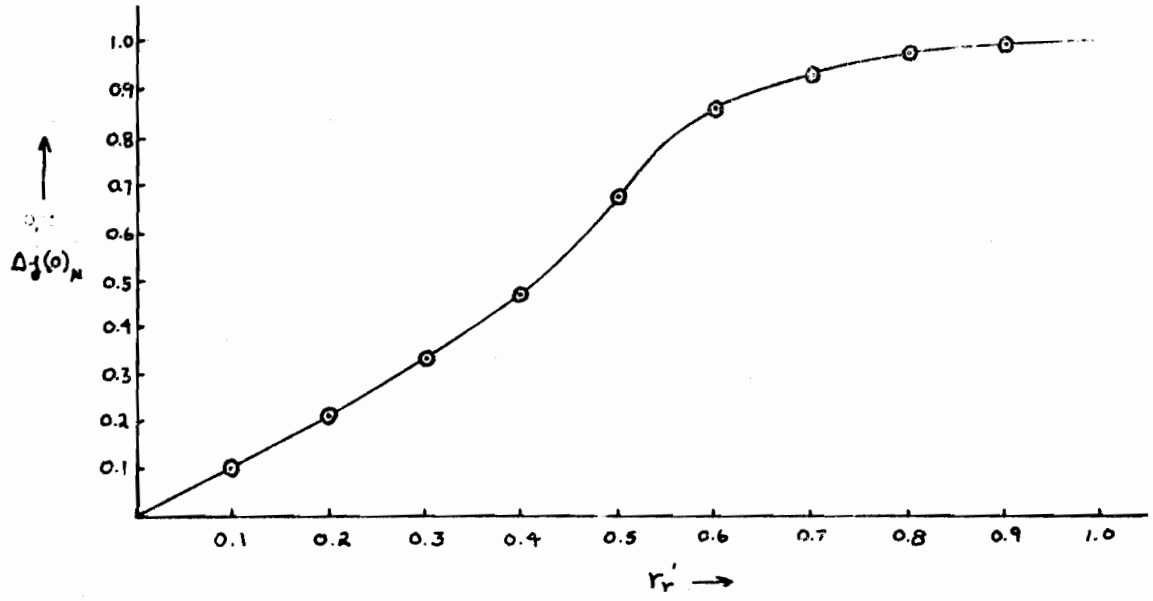
$\Delta_J(0)_N$
1.0
0.9
0.8
0.7
0.6
0.5
0.4
0.3
0.2
0.1
0.1
0.2
0.3
0.4
0.5
0.6
0.7
0.8
0.9
1.0
r_r' →

Fig. 15

SHO - 18 , RUN - 1

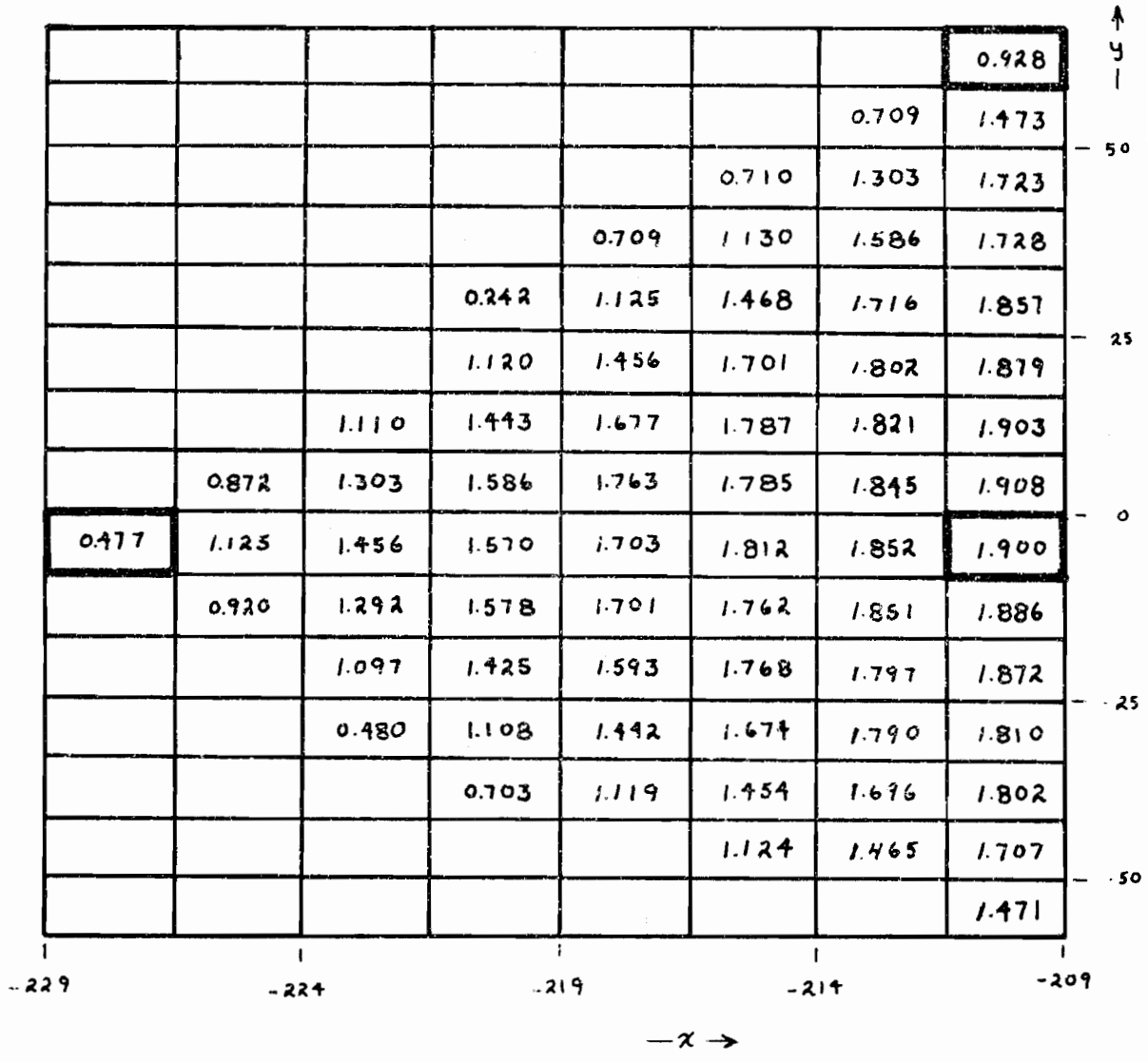

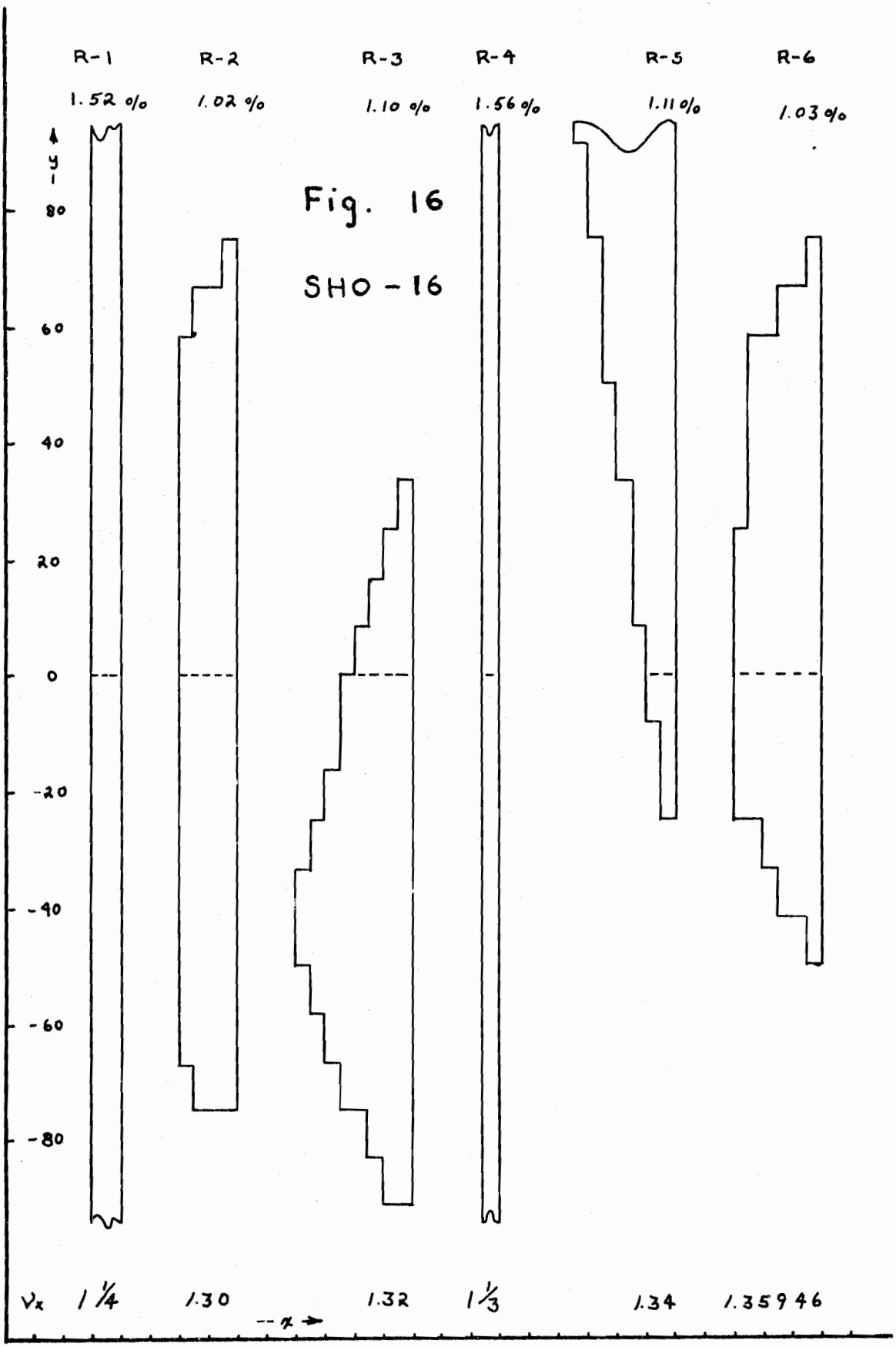
R-1
1.52 %
R-2
1.02 %
R-3
1.10 %
R-4
1.56 %
R-5
1.11 %
R-6
1.03 %
y
80
60
40
20
0
-20
-40
-60
-80
ν_x
1 1/4
1.30
1.32
1 1/3
1.34
1.35946
x

Fig. 16

SHO - 16

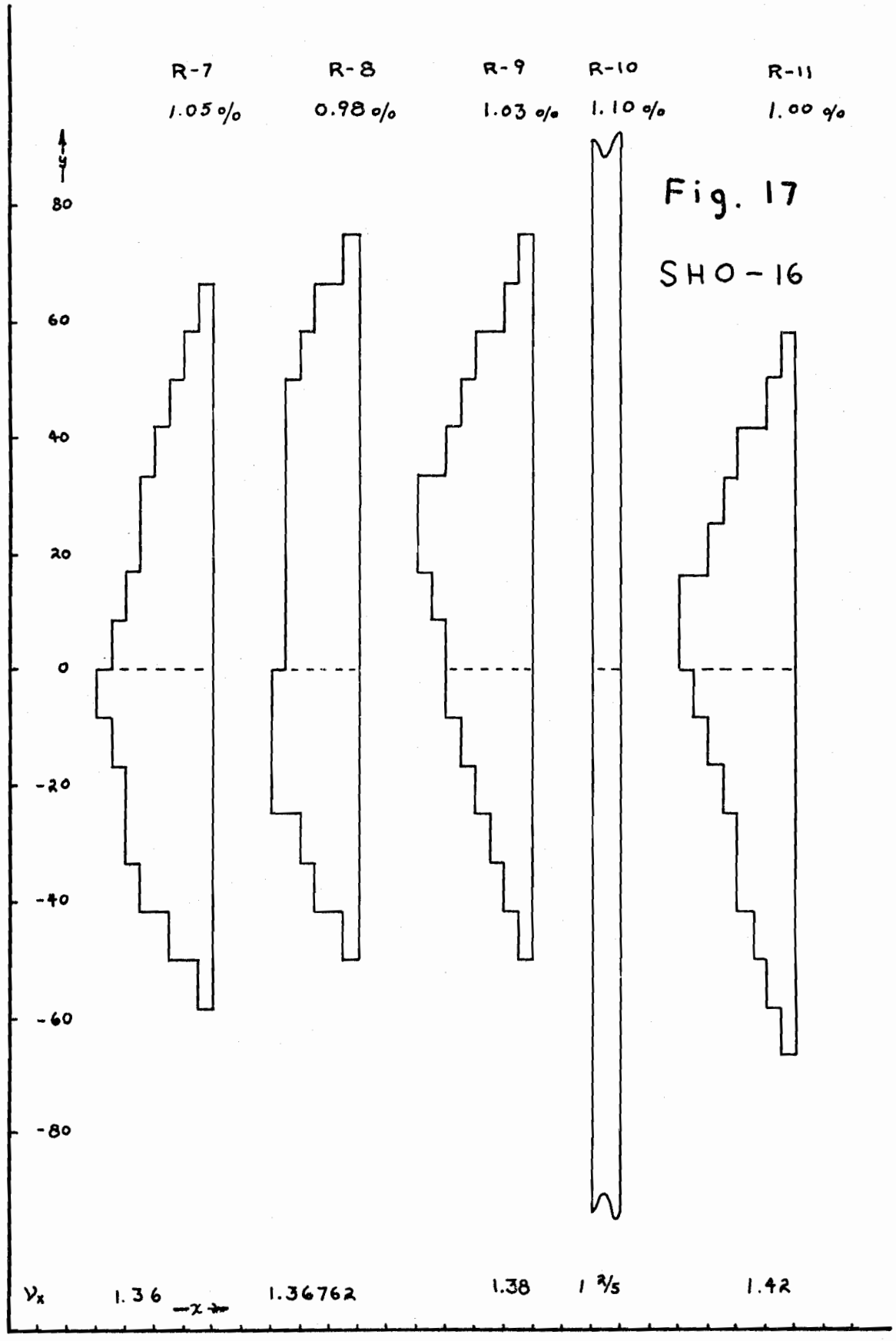
R-7
1.05 %
R-8
0.98 %
R-9
1.03 %
R-10
1.10 %
R-11
1.00 %
y
80
60
40
20
0
-20
-40
-60
-80
ν_x
1.36
x
1.36762
1.38
1 3/5
1.42

Fig. 17

SHO-16

Fig. 18

SHO - 16

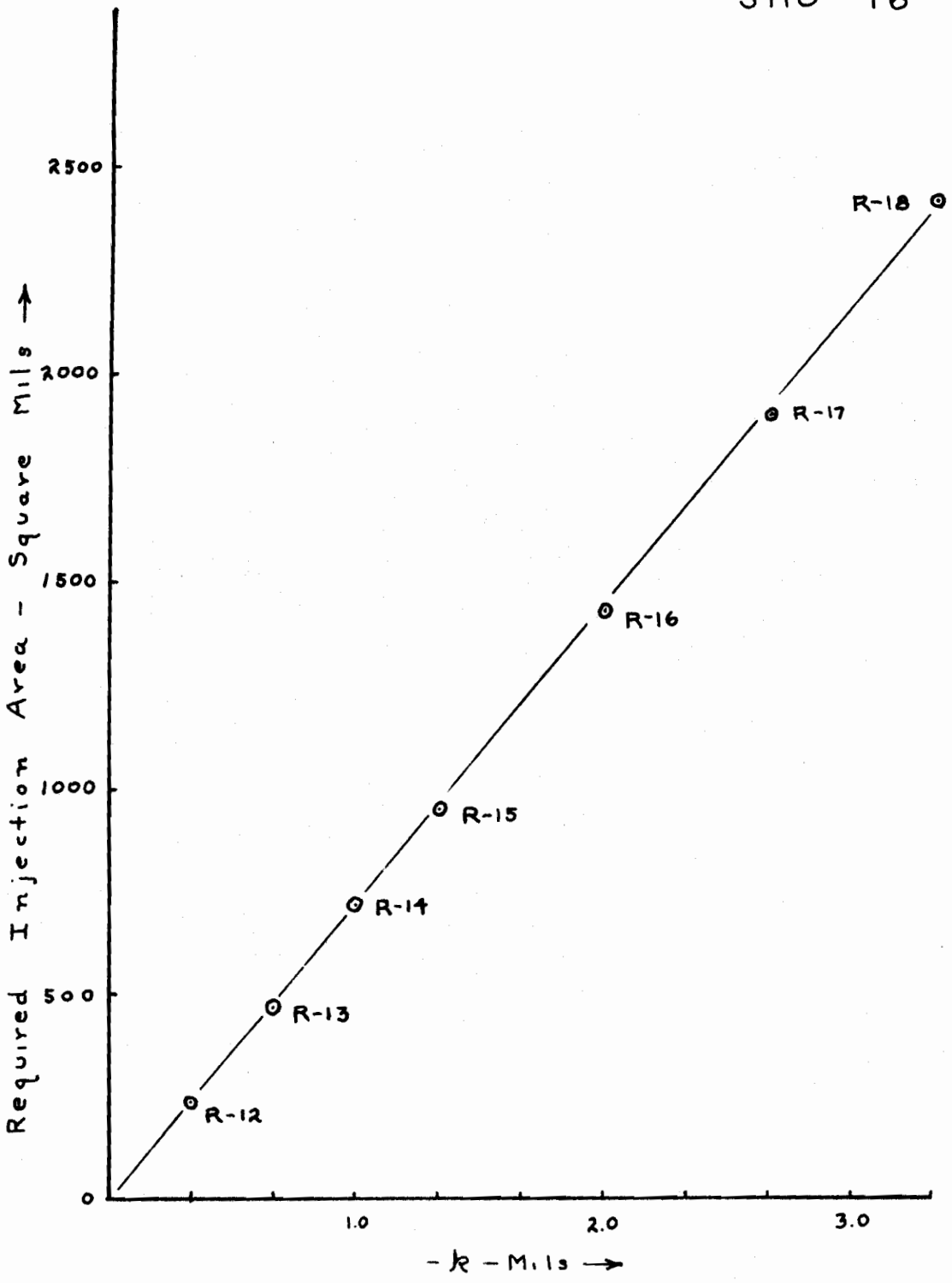
Required Injection Area - Square Mils →
2500
2000
1500
1000
500
0
R-18
R-17
R-16
R-15
R-14
R-13
R-12
1.0
2.0
3.0
- R - Mils →

Fig. 21

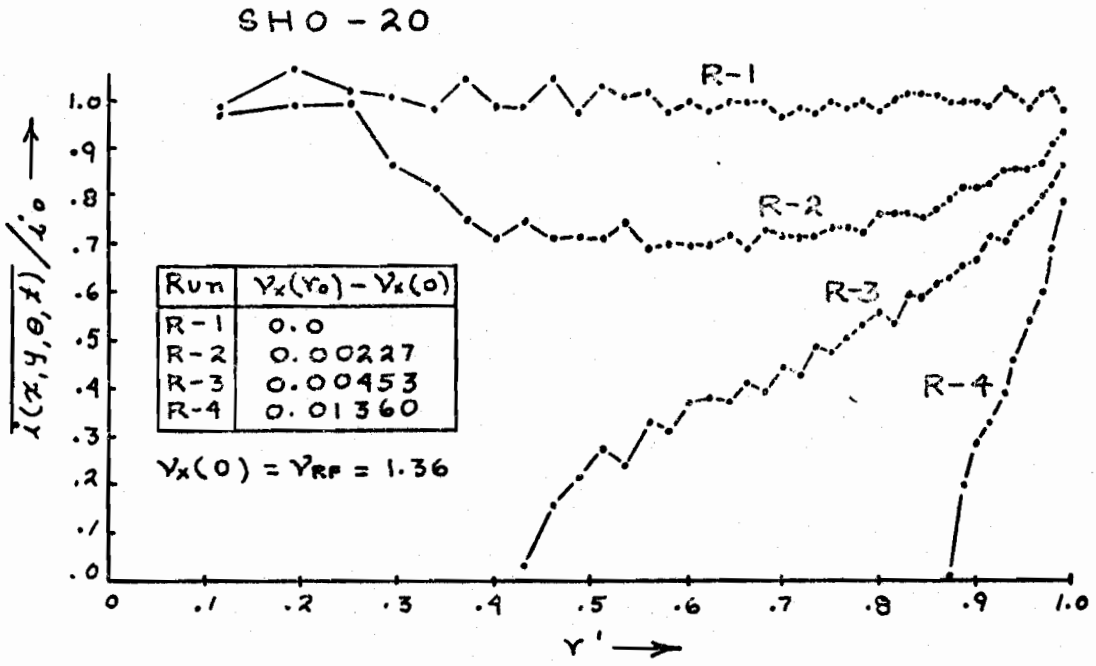
SHO - 20
R-1
R-2
R-3
R-4
Run | $V_x(r_0) - V_x(0)$
R-1 | 0.0
R-2 | 0.00227
R-3 | 0.00453
R-4 | 0.01360
$V_x(0) = V_{RF} = 1.36$
$\overline{i(x,y,\theta,t)}/i_0$
r'

Fig. 22

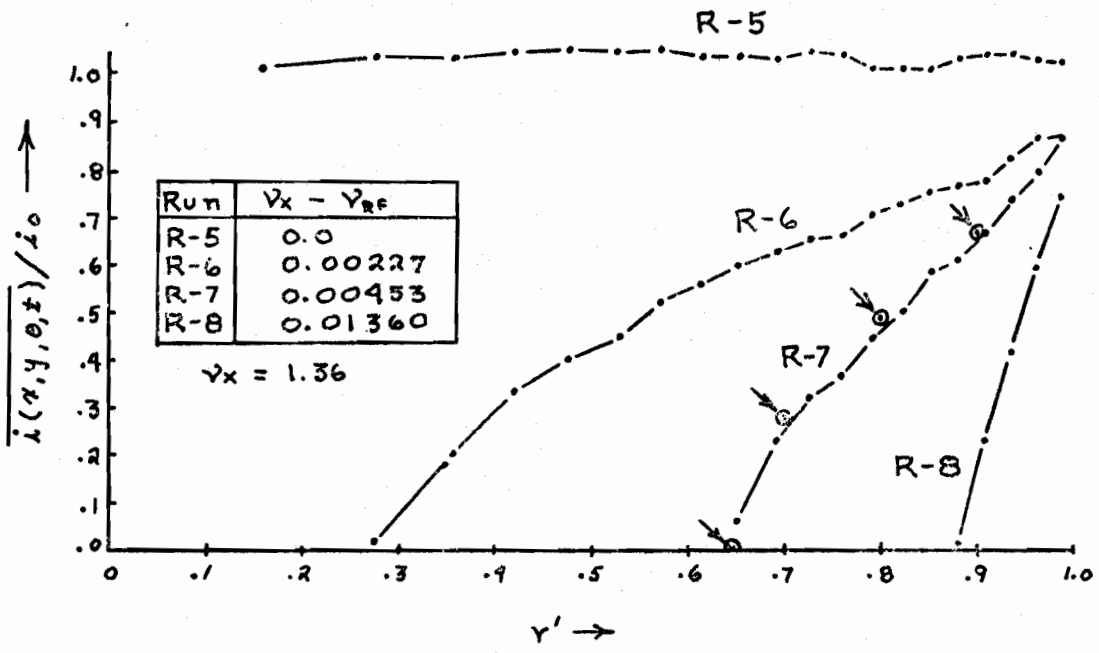
SHO - 18
R-5
R-6
R-7
R-8
Run | $V_x - V_{RF}$
R-5 | 0.0
R-6 | 0.00227
R-7 | 0.00453
R-8 | 0.01360
$V_x = 1.36$
$\overline{i(x,y,\theta,t)}/i_0$
r'

Fig. 19

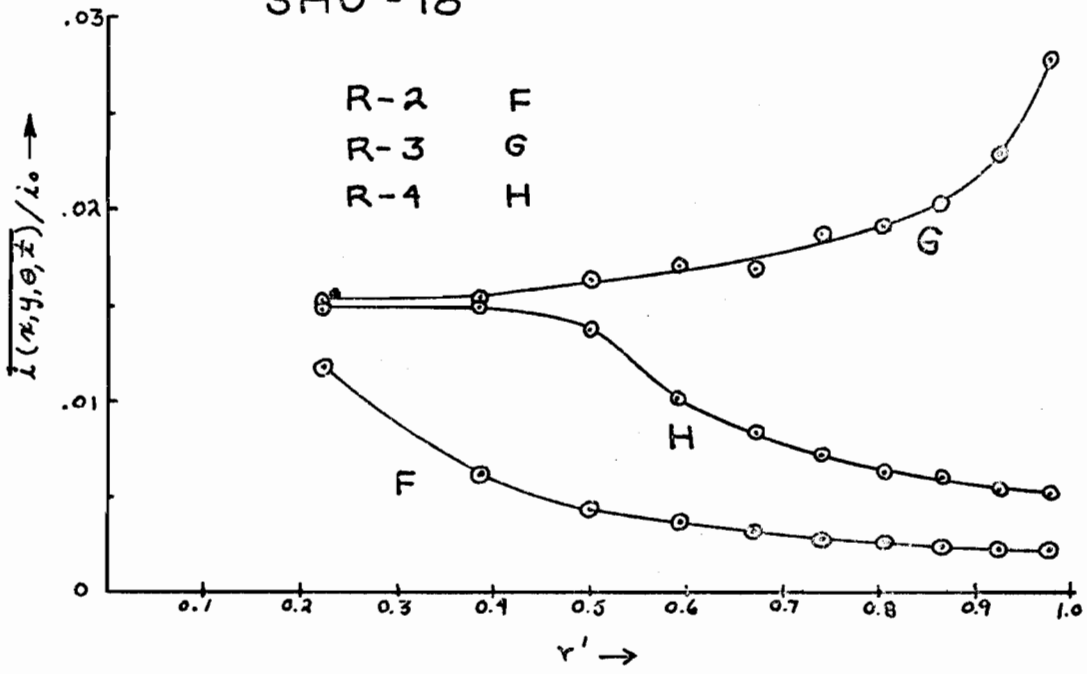
SHO - 18
R-2 F
R-3 G
R-4 H
$\overline{i(x,y,\theta,t)}/i_0 \rightarrow$
.03
.02
.01
0
0.1
0.2
0.3
0.4
0.5
0.6
0.7
0.8
0.9
1.0
r' →
F
G
H

Fig. 20

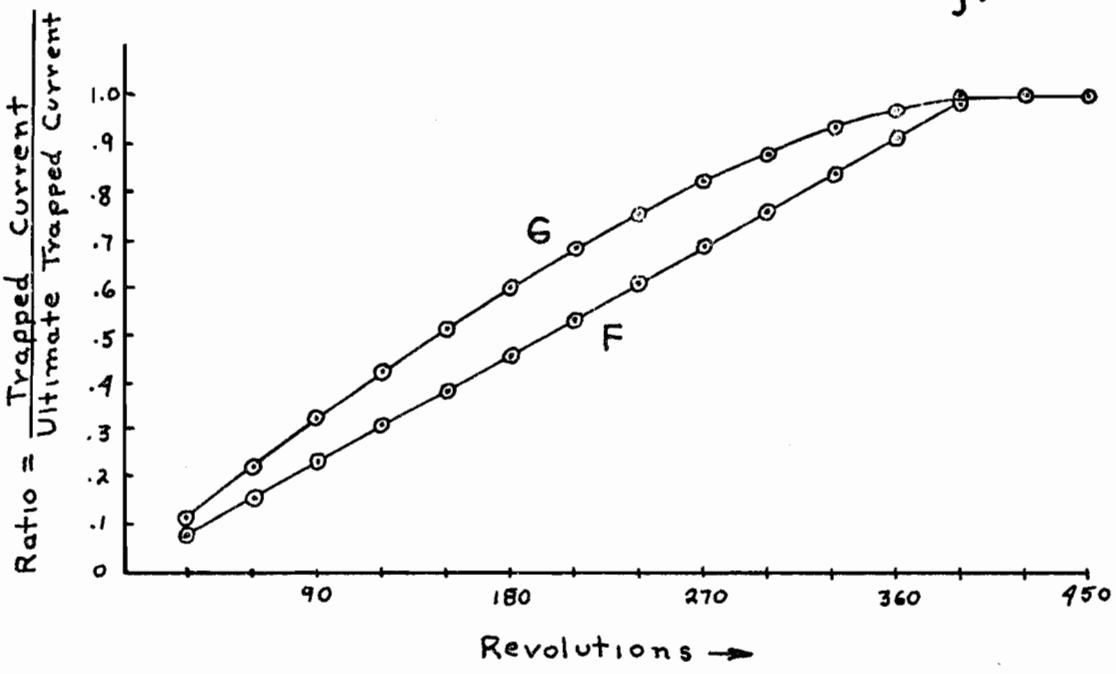
Ratio = Trapped Current / Ultimate Trapped Current
0
.1
.2
.3
.4
.5
.6
.7
.8
.9
1.0
90
180
270
360
450
Revolutions →
G
F

Fig. 23[1]

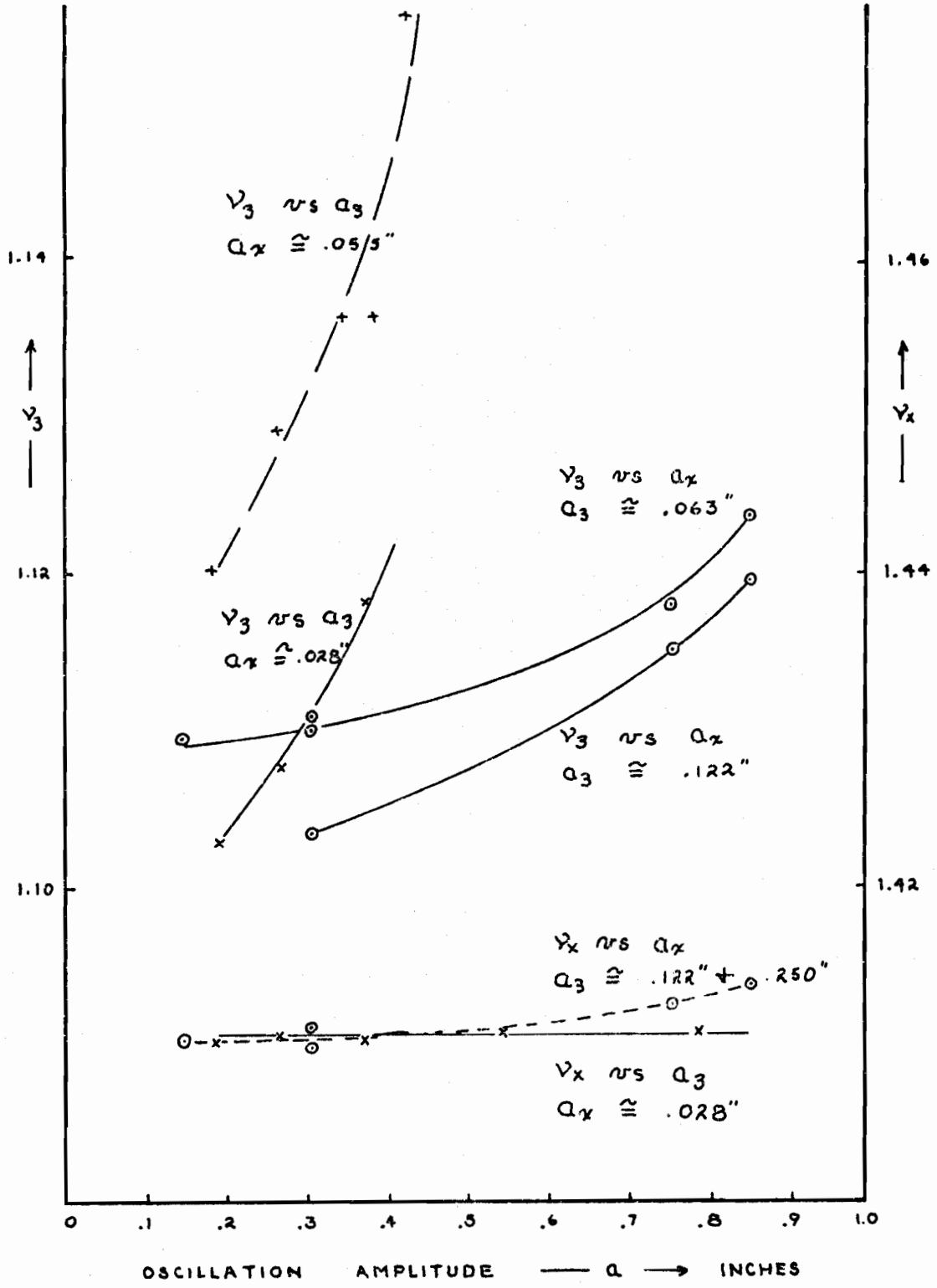
1.14
1.12
1.10
ν_3
1.46
1.44
1.42
ν_x
ν_3 vs a_3
$a_x \cong .055"$
ν_3 vs a_x
$a_3 \cong .063"$
ν_3 vs a_3
$a_x \cong .028"$
ν_3 vs a_x
$a_3 \cong .122"$
ν_x vs a_x
$a_3 \cong .122" + .250"$
ν_x vs a_3
$a_x \cong .028"$
0 .1 .2 .3 .4 .5 .6 .7 .8 .9 1.0
OSCILLATION AMPLITUDE —— a ——→ INCHES

Fig. 24

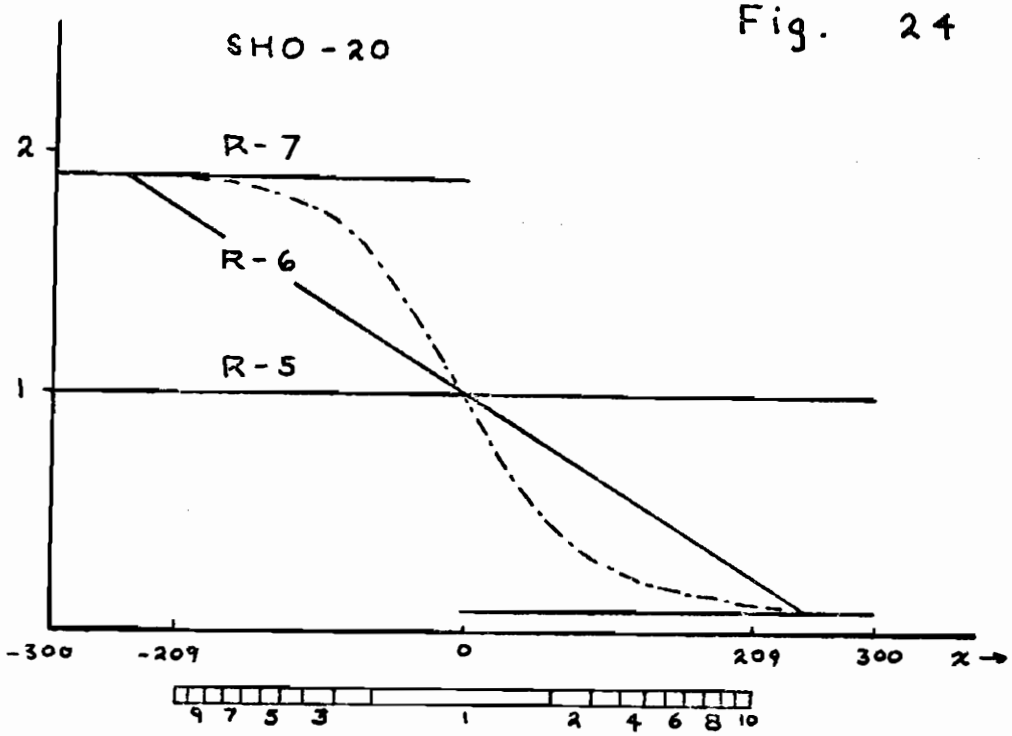

Phase Space Annulus Number	R-5 $\frac{\overline{i(x,y,\theta,t)}}{i_0}$	R-6 $\frac{\overline{i(x,y,\theta,t)}}{i_0}$	Deviation from R-5 %	R-7 $\frac{\overline{i(x,y,\theta,t)}}{i_0}$	Deviation from R-5 %
1	1751	.1742	- 0.49	.1740	- 0.60
2	1820	.1810	- 0.55	.1830	0.55
3	.1848	.1854	0.32	.1831	- 0.92
4	.1927	.1909	- 0 96	.1911	- 0.86
5	.2006	.2012	0.30	.1964	- 2.06
6	2021	.2043	1.11	.1981	- 1.98
7	.2107	.2108	0.05	.2066	- 1.92
8	.2162	.2210	2.22	.2121	- 1.87
9	.2237	.2276	1.77	.2190	-2.08
10	.2111	.2095	- 0.76	. 1999	-5.31
Avg.	.1999	.2006	0.35	.1964	- 1.75

Fig. 24

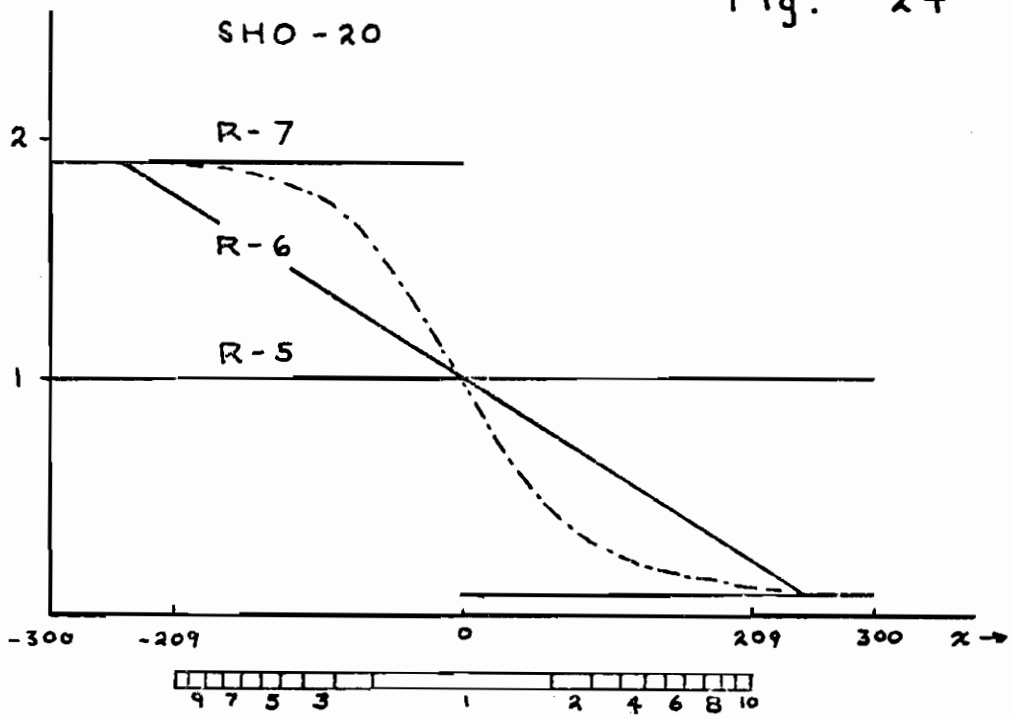

Phase Space Annulus Number	R - 5 $\frac{\bar{I}(x,y,\theta,t)}{I_0}$	R - 6 $\frac{\bar{I}(x,y,\theta,t)}{I_0}$	Deviation from R - 5 %	R - 7 $\frac{\bar{I}(x,y,\theta,t)}{I_0}$	Deviation from R - 5 %
1	.1751	.1742	- 0.49	.1740	- 0.60
2	.1820	.1810	- 0.55	.1830	0.55
3	.1848	.1854	0.32	.1831	- 0.92
4	.1927	.1909	- 0 96	.1911	- 0.86
5	.2006	.2012	0.30	.1964	- 2.06
6	.2021	.2043	1.11	.1981	- 1.98
7	.2107	.2108	0.05	.2066	- 1.92
8	.2162	.2210	2.22	.2121	- 1.87
9	.2237	.2276	1.77	.2190	- 2.08
10	.2111	.2095	- 0.76	.1999	- 5.31
Avg.	.1999	.2006	0.35	.1964	- 1.75

Fig. 25

RF Electrode, Beam, + Vacuum Tank

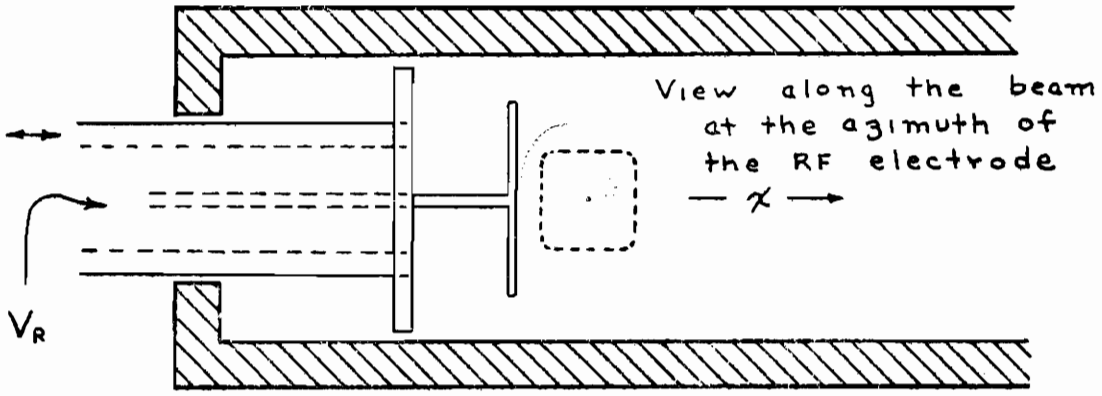

Fig. 26

Wire Probe

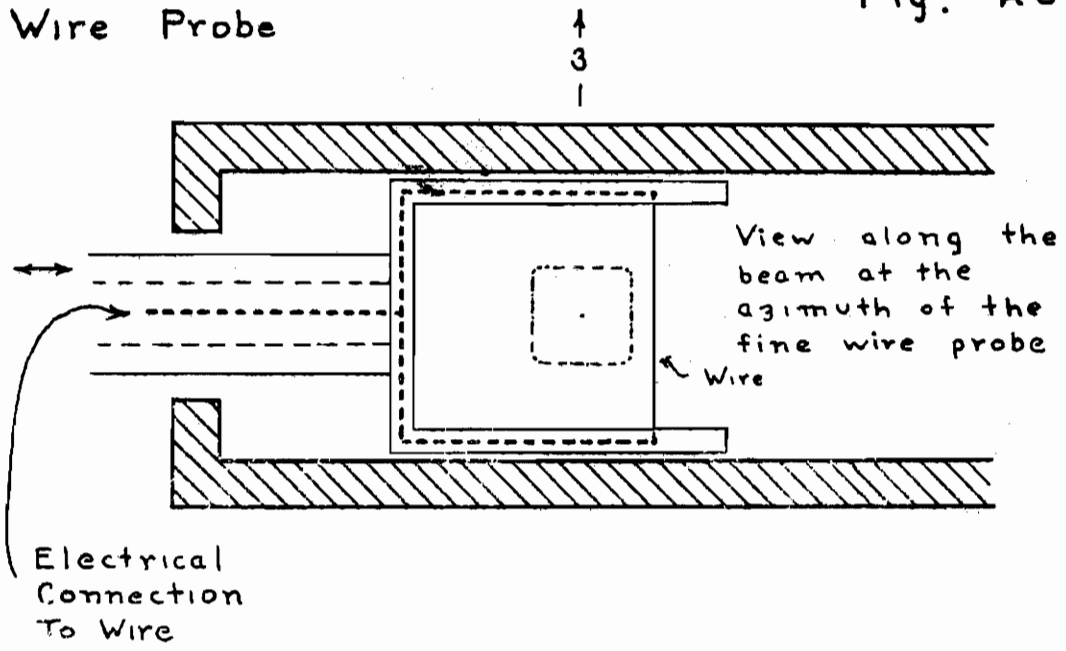

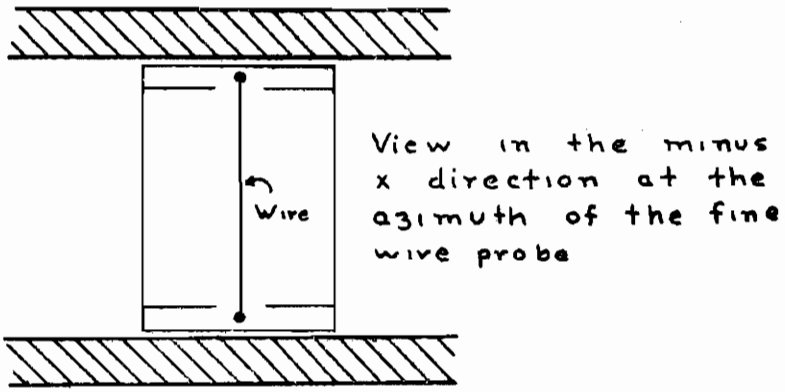

Preamplifier + Accessories

Fig. 27

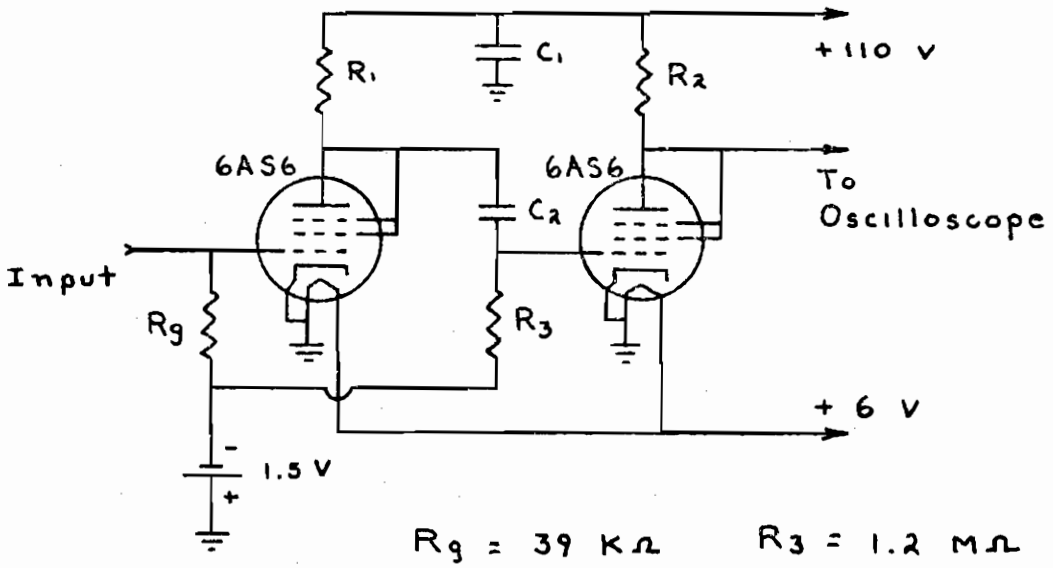

R_g = 39 KΩ R_3 = 1.2 MΩ

R_1 = 10 KΩ C_1 = 100 μfd.

R_2 = 10 KΩ C_2 = .01 μfd.

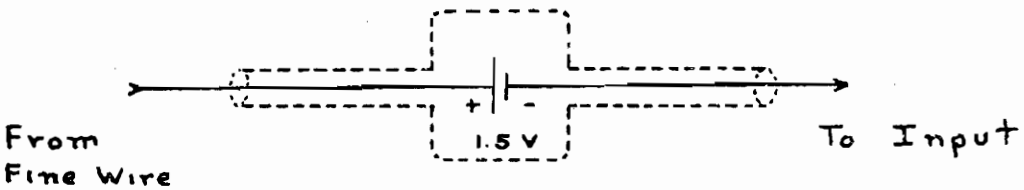

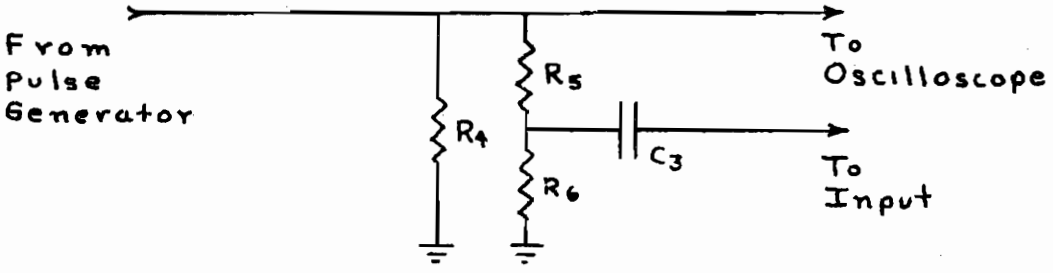

R_4 = 39 Ω R_6 = 10 Ω

R_5 = 1000 Ω C_3 = 0.1 μfd.

Fig. 28

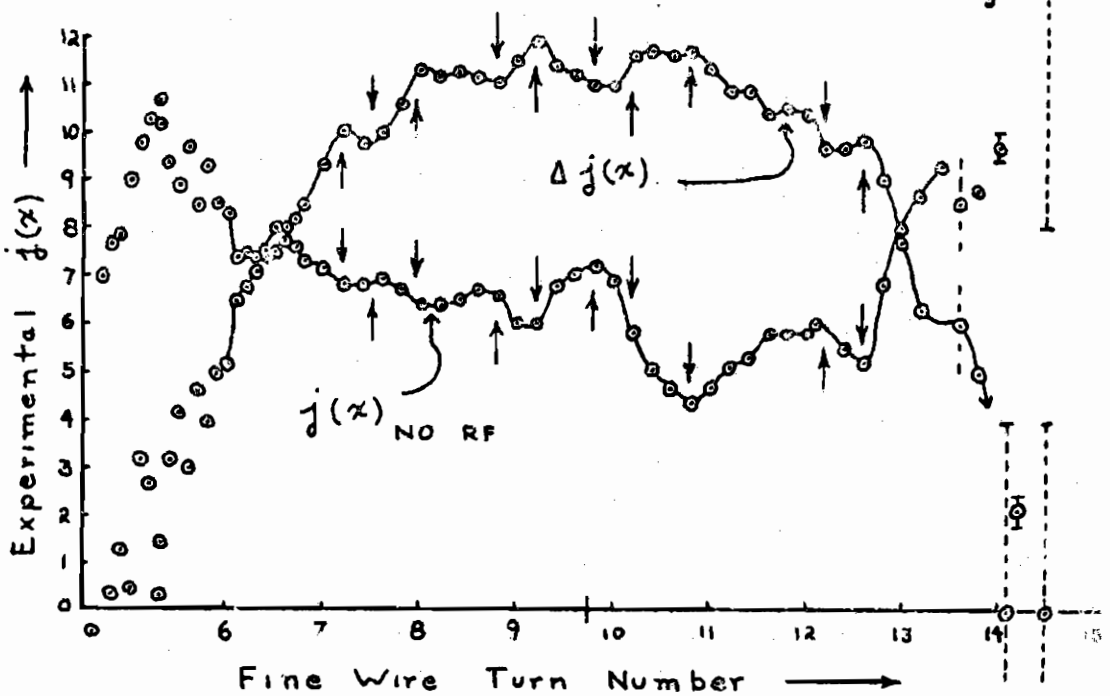
Experimental j(x)
Δ j(x)
j(x) NO RF
Fine Wire Turn Number

Fig. 29

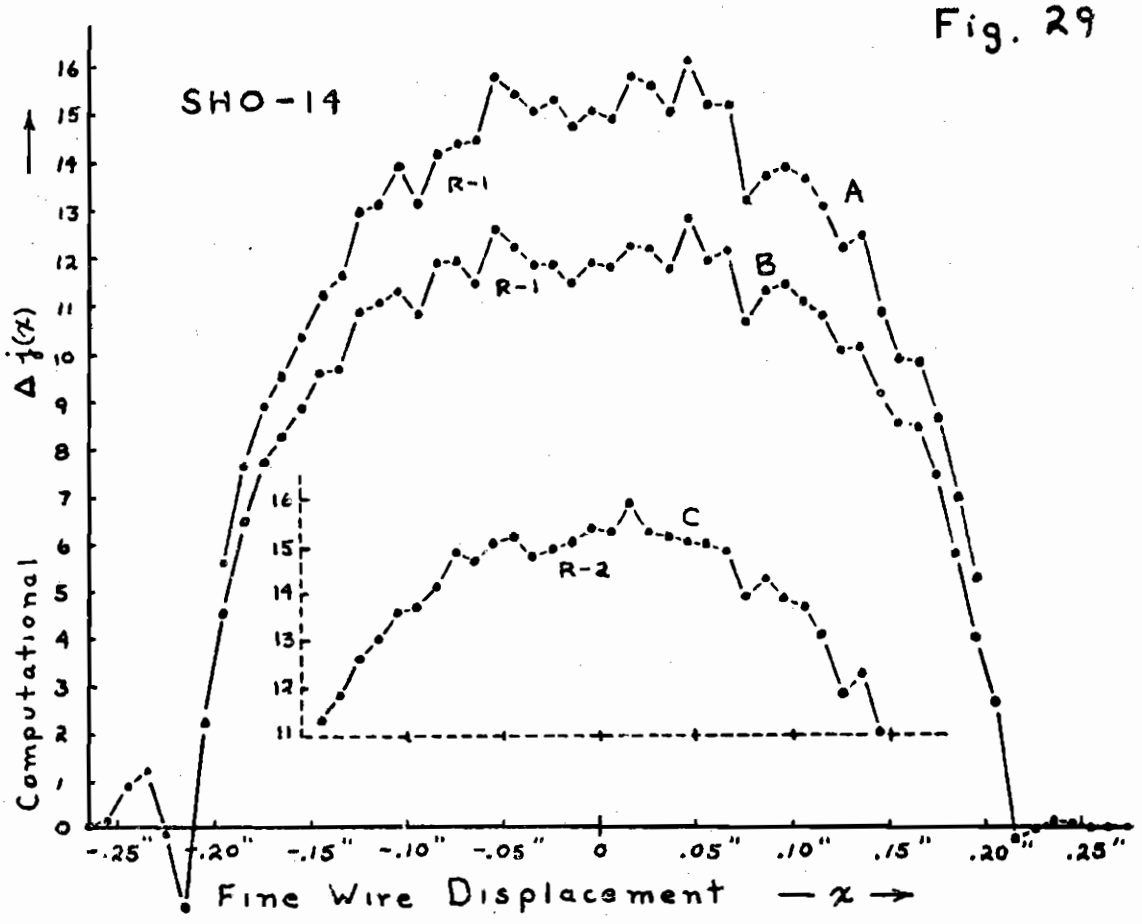
SHO-14
R-1
A
R-1
B
R-2
C
Δ j(x)
Computational
-.25" -.20" -.15" -.10" -.05" 0 .05" .10" .15" .20" .25"
Fine Wire Displacement — x →

Fig. 30

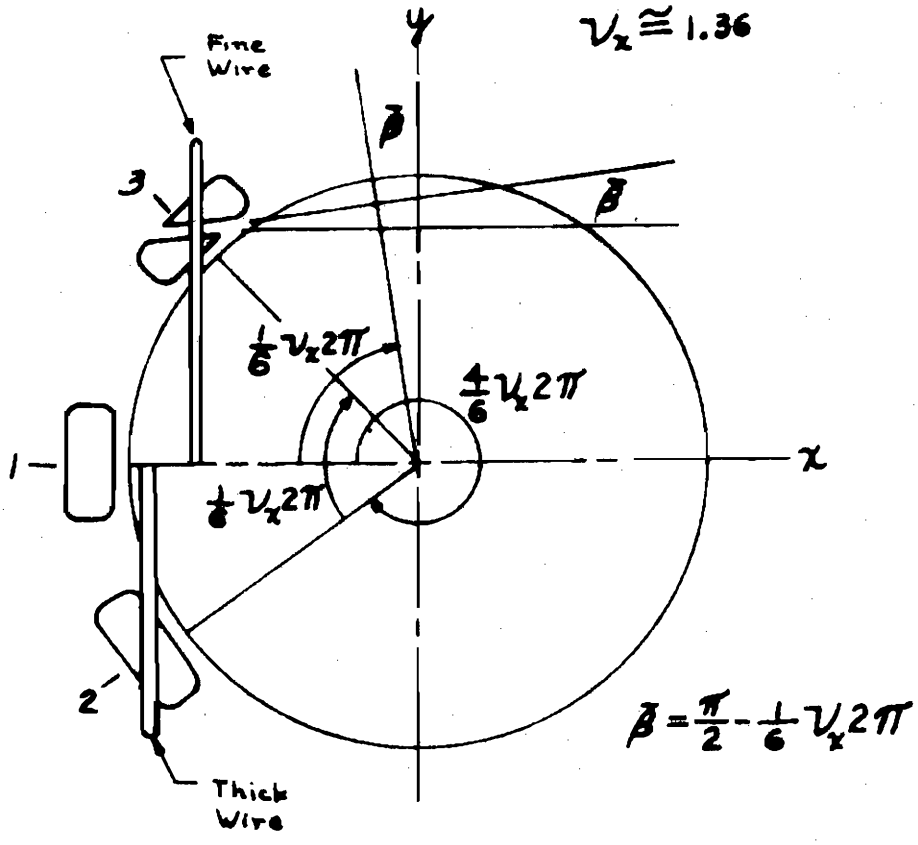
Fine Wire
3
1
2
Thick Wire
ψ
x
$\nu_x \cong 1.36$
β
β
$\frac{1}{6}\nu_x 2\pi$
$\frac{4}{6}\nu_x 2\pi$
$\frac{1}{6}\nu_x 2\pi$
$\beta = \frac{\pi}{2} - \frac{1}{6}\nu_x 2\pi$

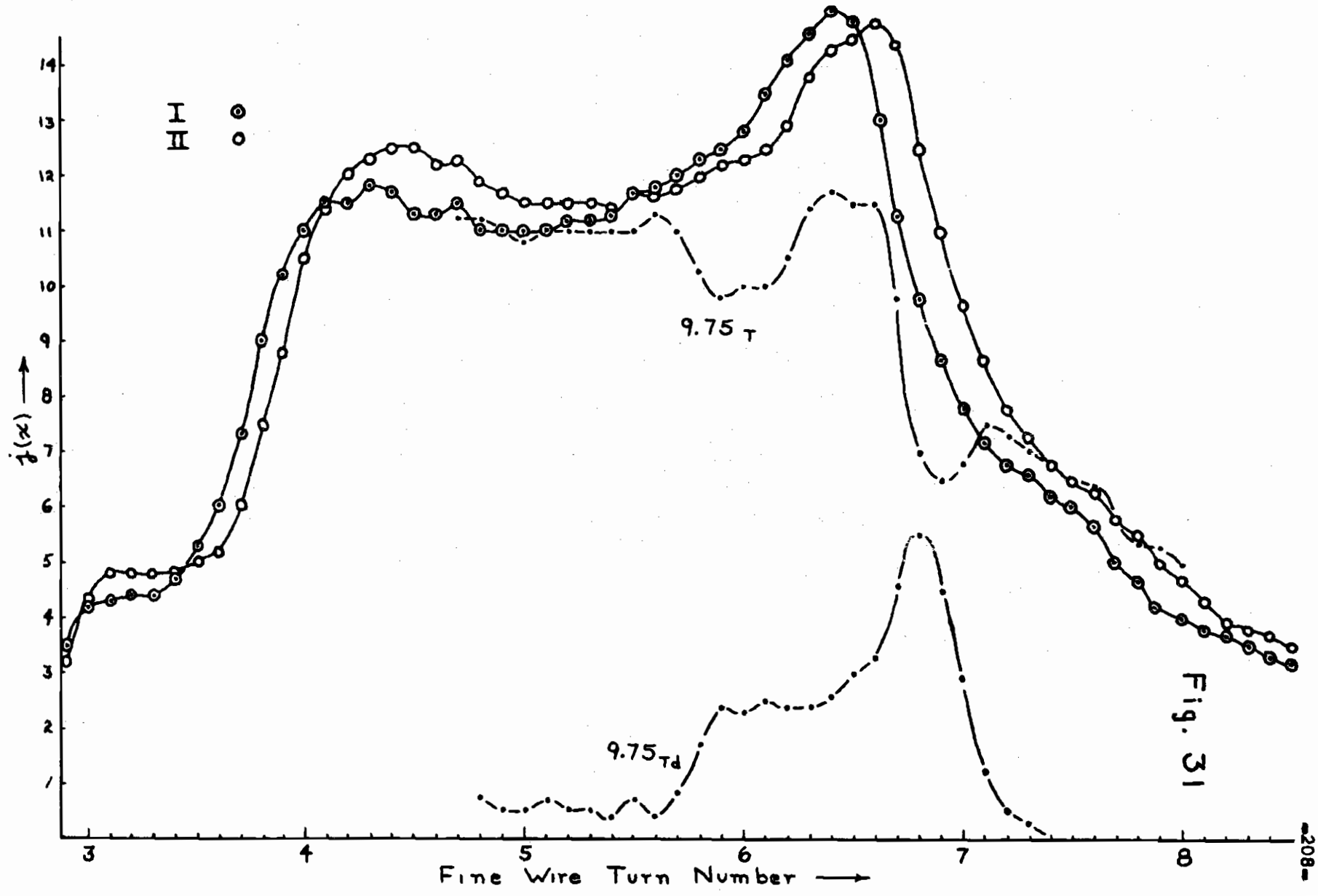
I ⊙
II o
9.75 T
9.75 Td
i(x) ⟶
Fine Wire Turn Number ⟶
1
2
3
4
5
6
7
8
9
10
11
12
13
14

Fig. 31

Fig. 32

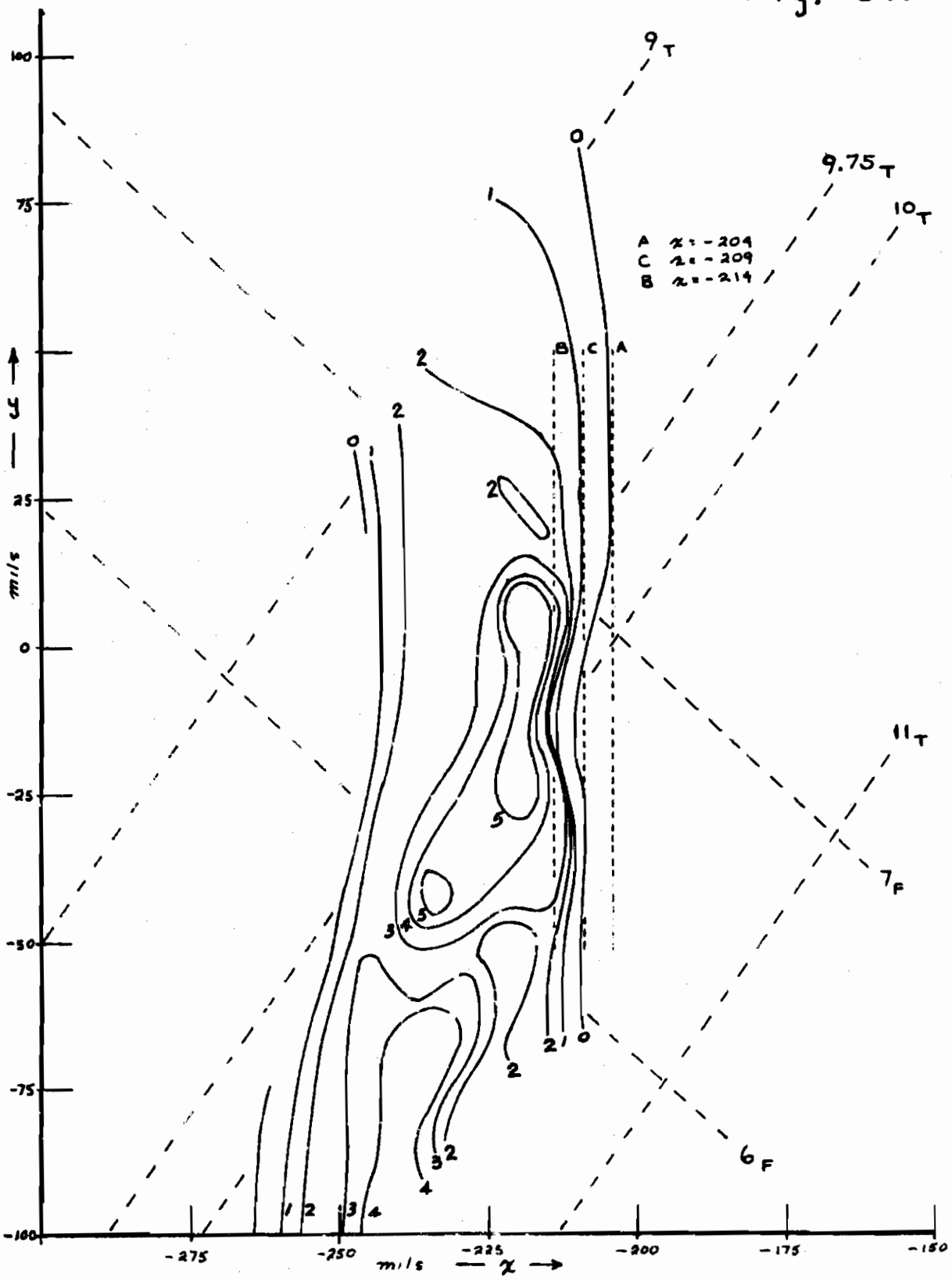
9T
9.75T
10T
11T
7F
6F
A x = -209
C x = -209
B x = -214
A
B
C
100
75
25
0
-25
-50
-75
-100
y
mils
-275
-250
-225
-200
-175
-150
mils
x

Fig. 33

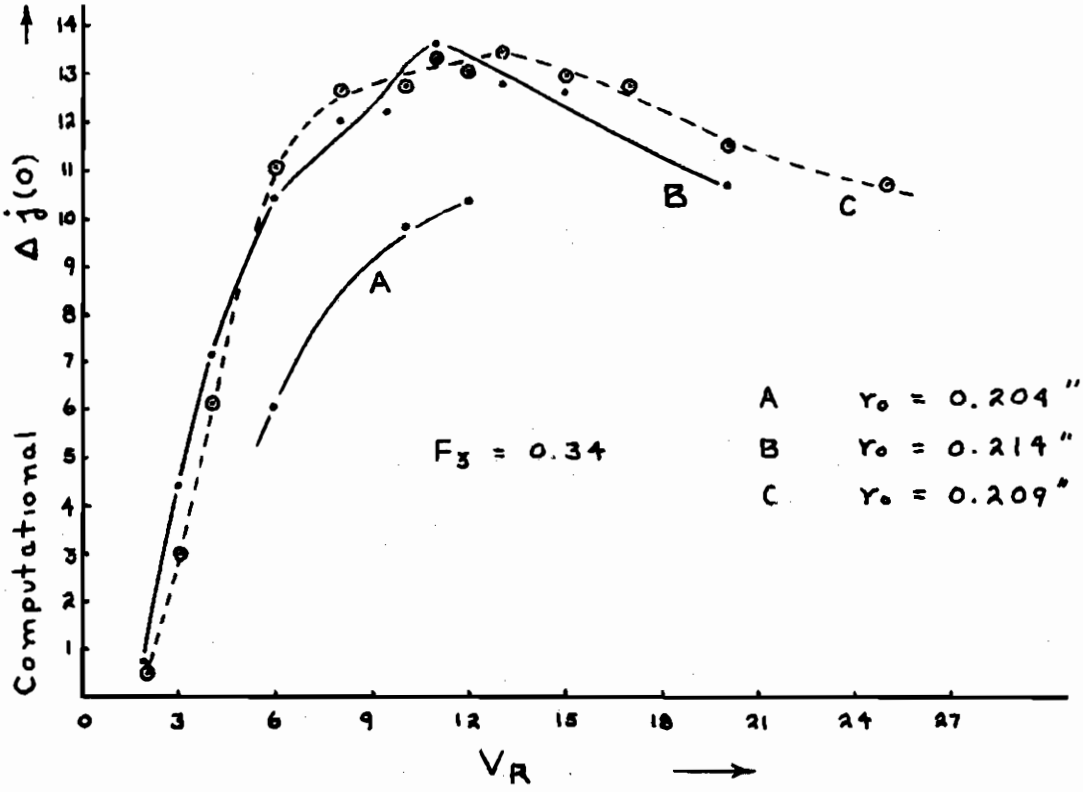
Computational
Δ j(0)
A
B
C
F_3 = 0.34
A r_0 = 0.204"
B r_0 = 0.214"
C r_0 = 0.209"
V_R

Fig. 34

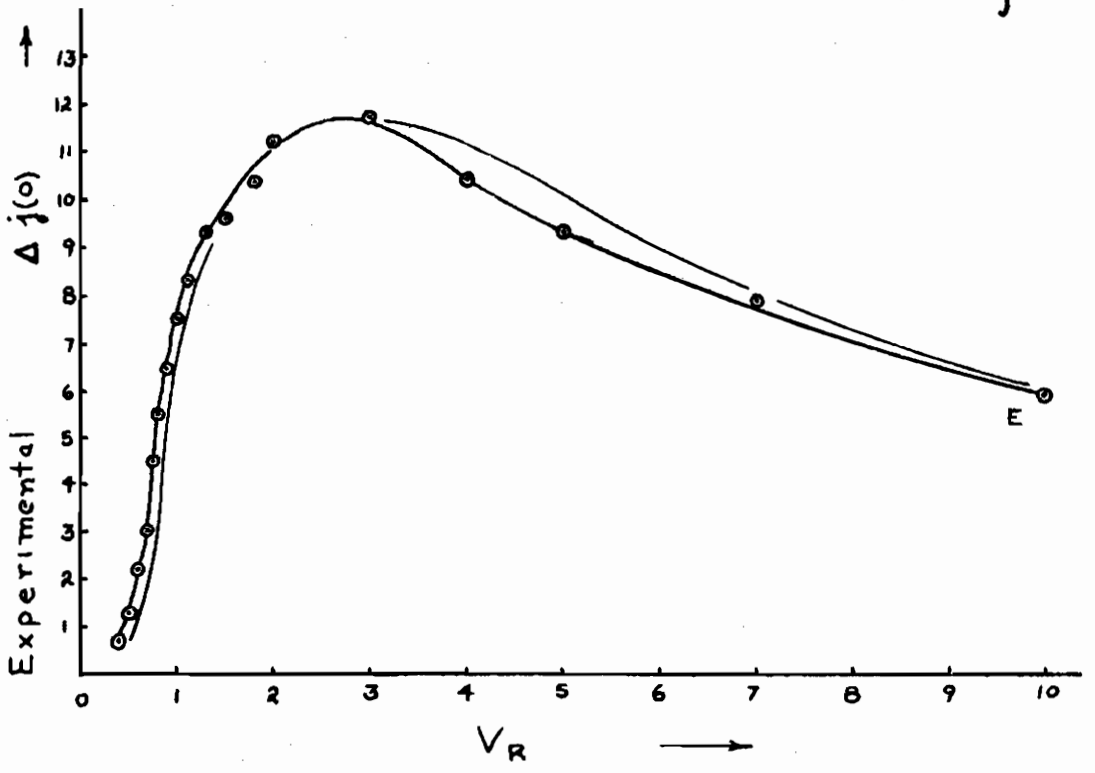
Experimental
Δ j(0)
E
V_R

Fig. 35

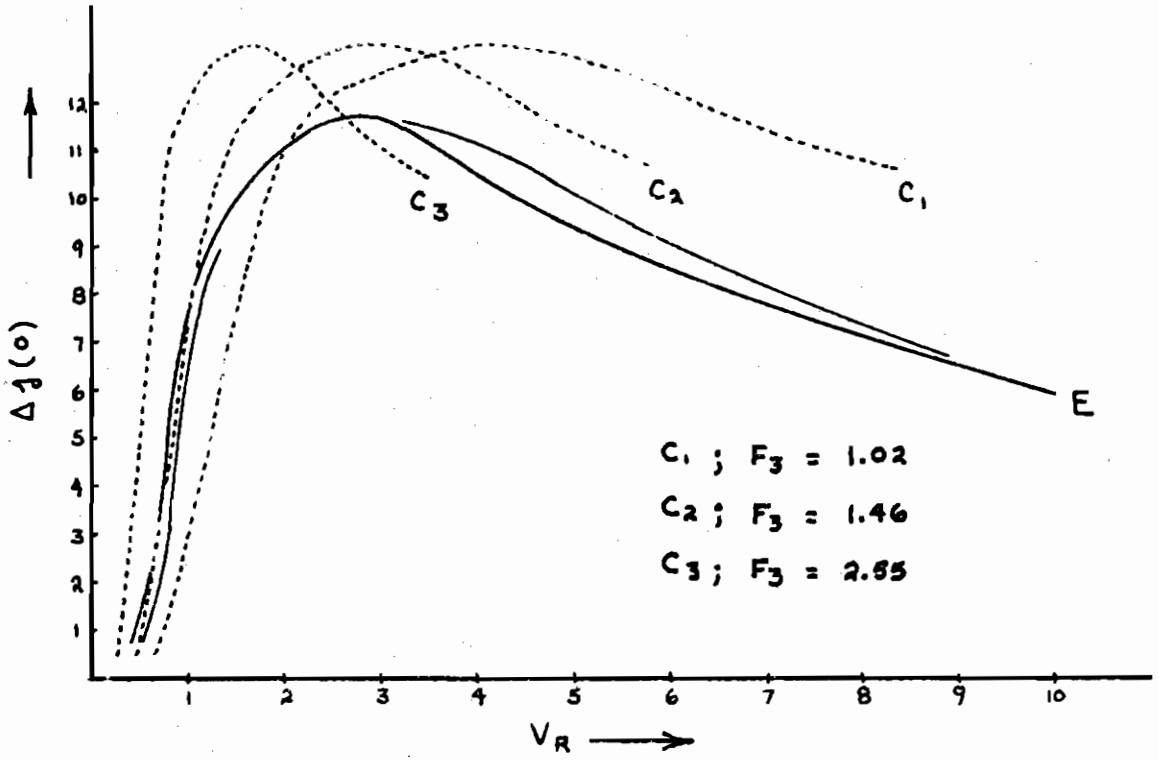

Fig. 36

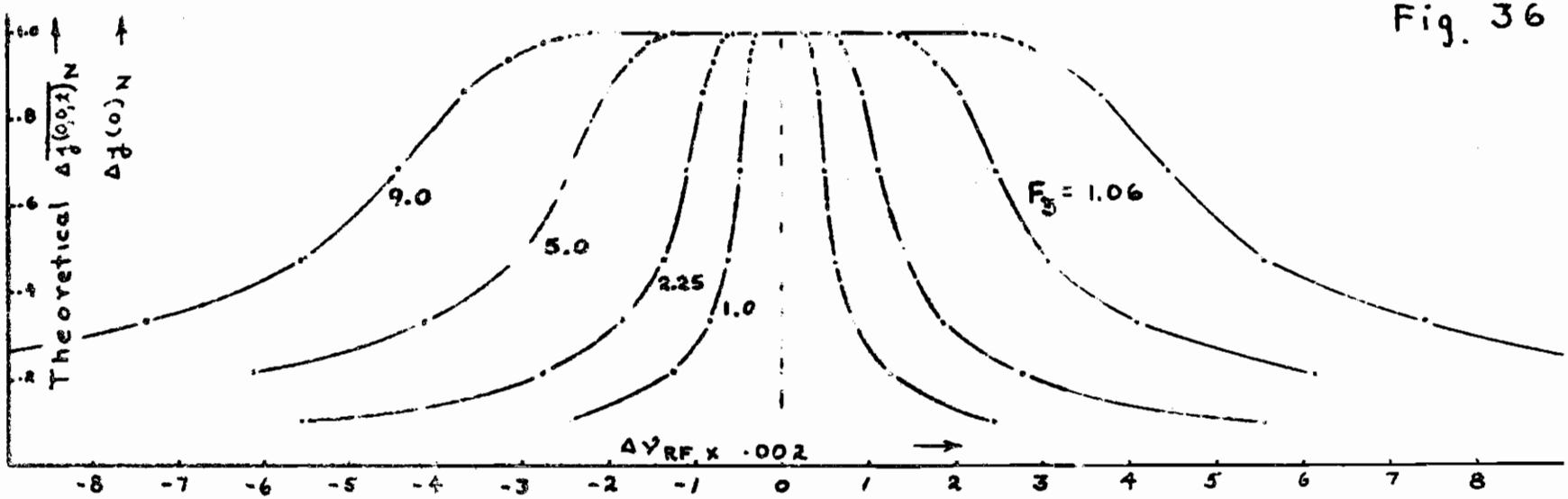
Theoretical $\Delta\overline{j(0,t)}_N$
$\Delta j(0)_N$
9.0
5.0
2.25
1.0
$F_s = 1.06$
$\Delta V_{RF} \times .002$
-8 -7 -6 -5 -4 -3 -2 -1 0 1 2 3 4 5 6 7 8

Fig. 37

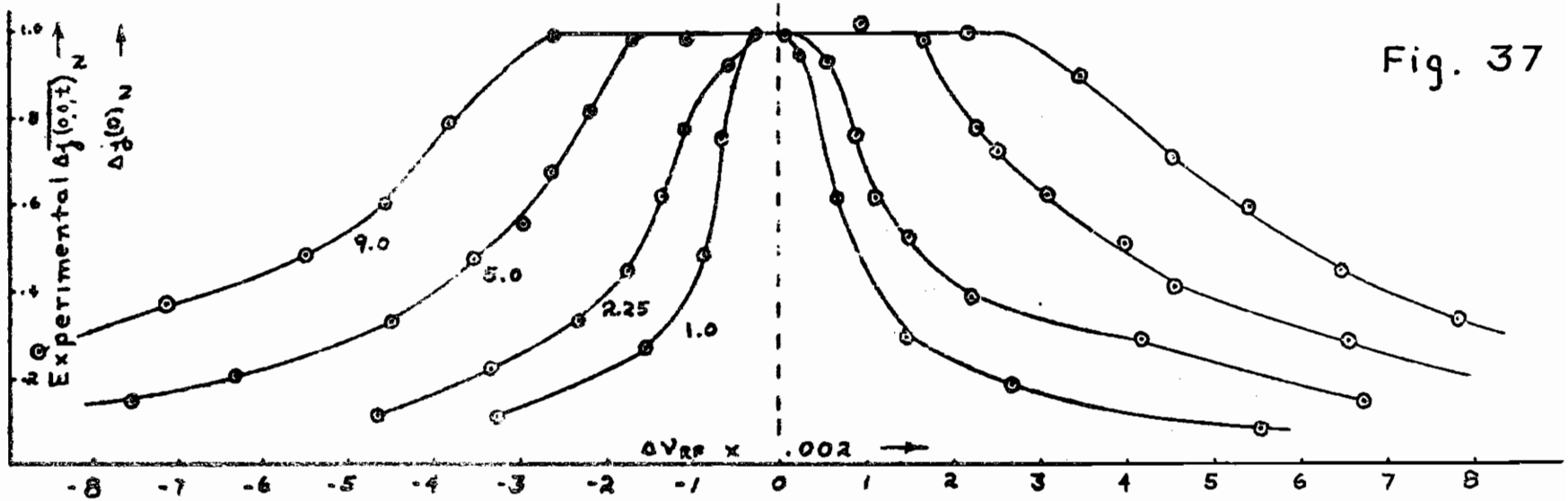
Experimental $\Delta\overline{j(0,t)}_N$
$\Delta j(0)_N$
9.0
5.0
2.25
1.0
$\Delta V_{RF} \times .002$
-8 -7 -6 -5 -4 -3 -2 -1 0 1 2 3 4 5 6 7 8

Fig. 38

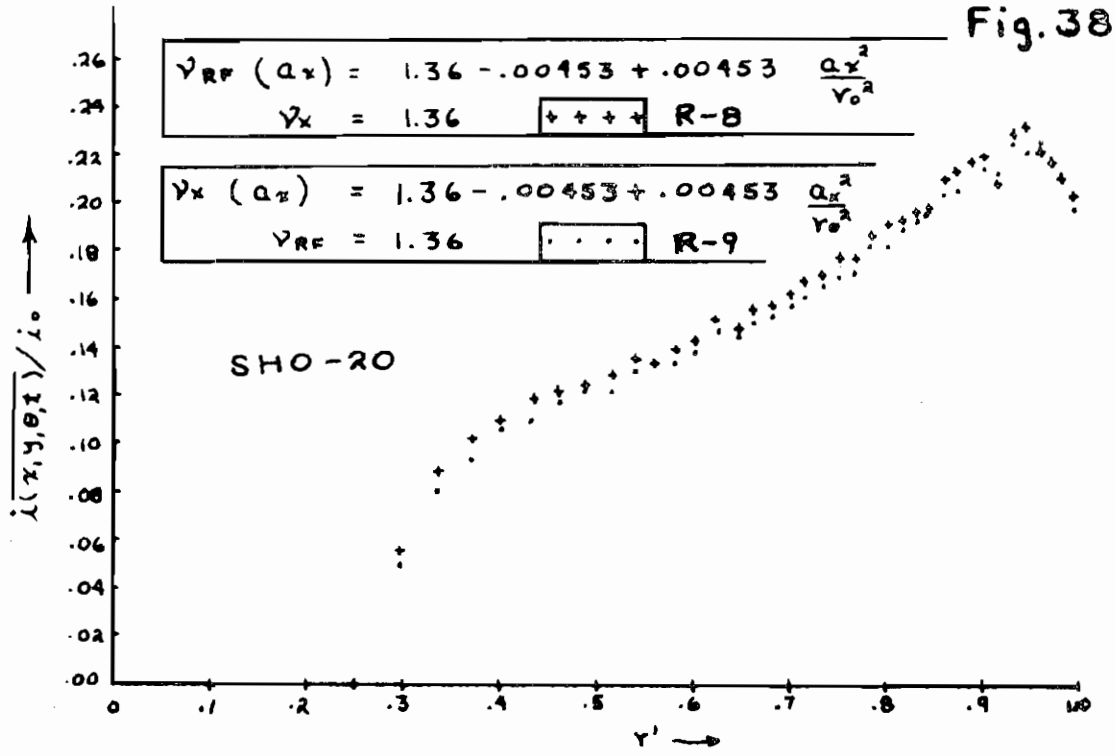

18

Fig. 39

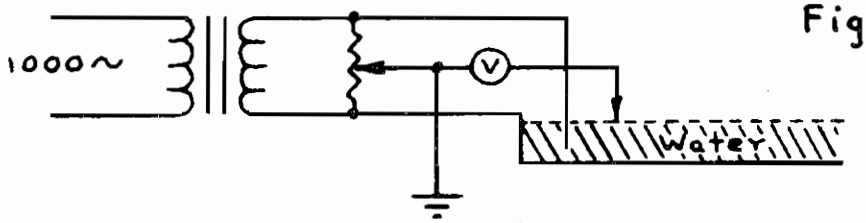

Fig. 40

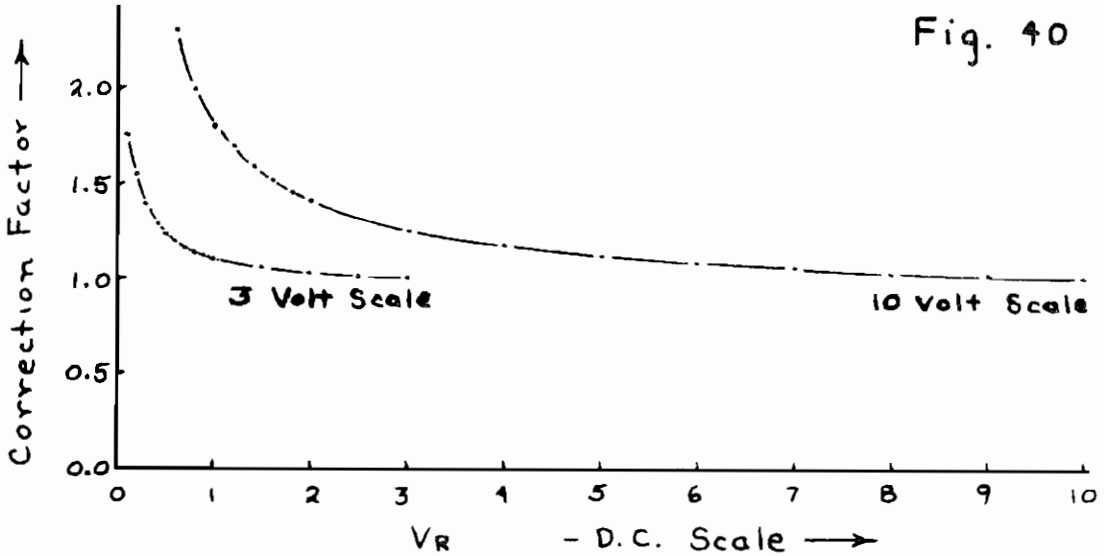

Fig. 41

SHO-20

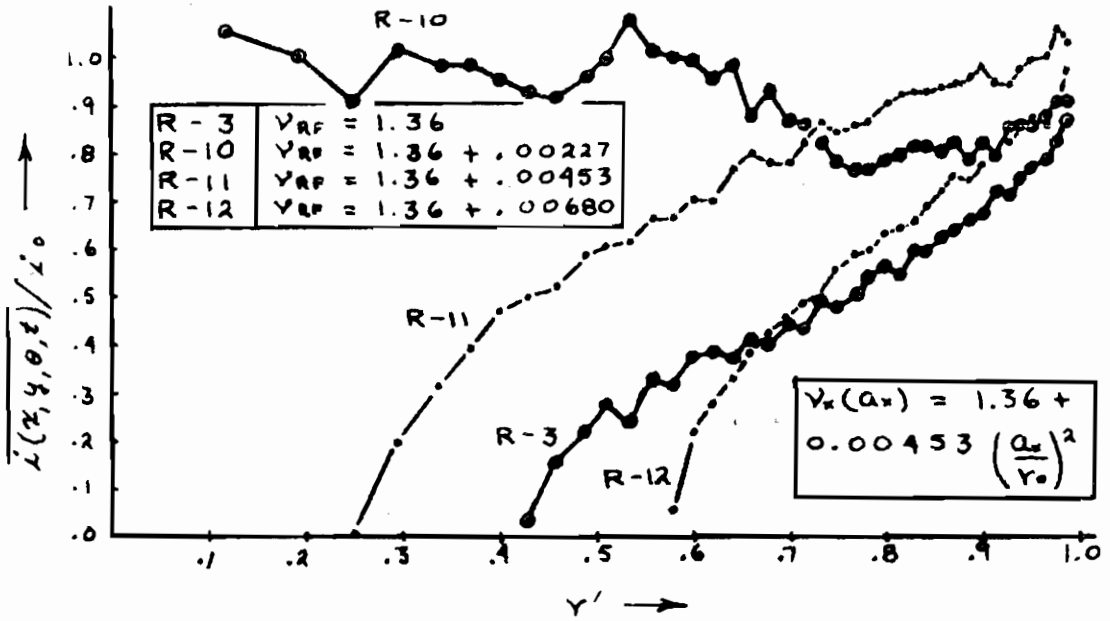

Fig. 42

SHO-20

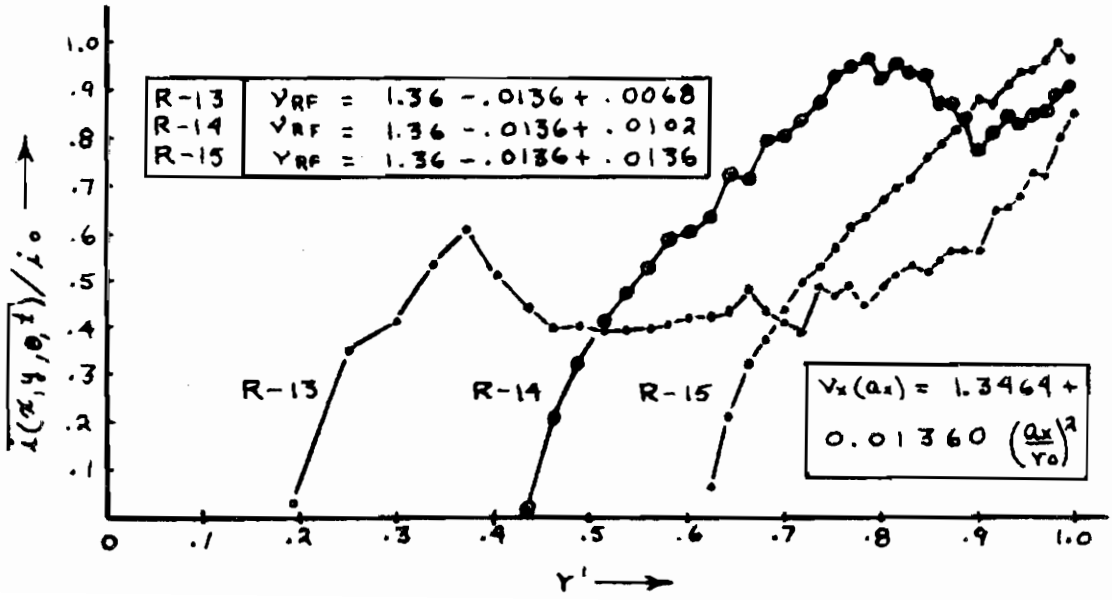

Fig. 43

Data grid for $i(x,y)_o$

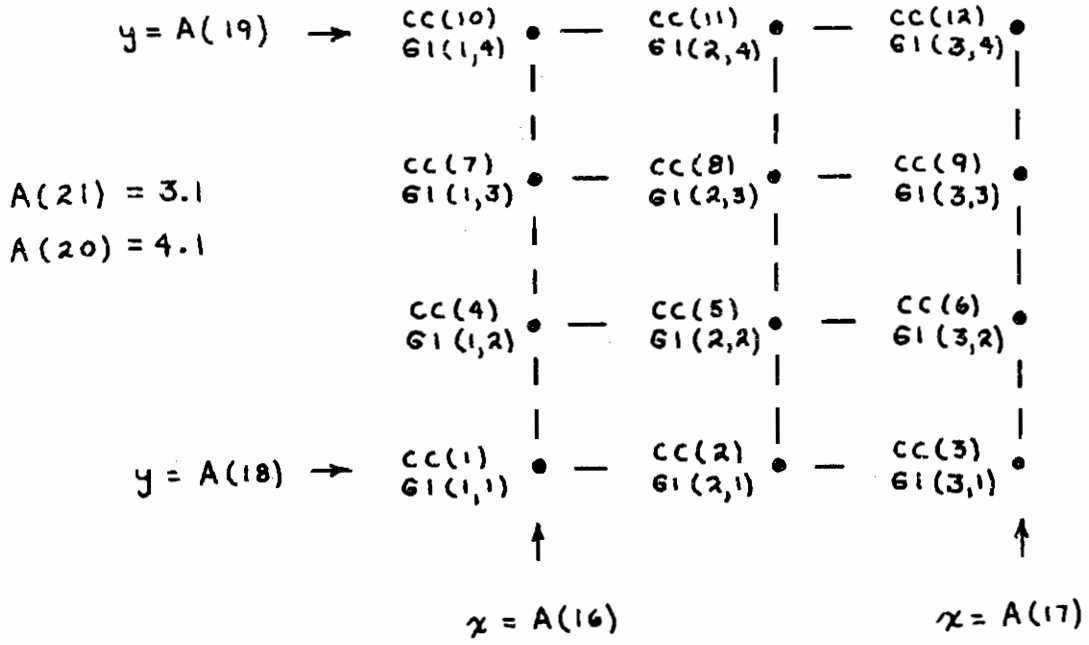

Fig. 44

Portion of $i(x,y)_o$ used

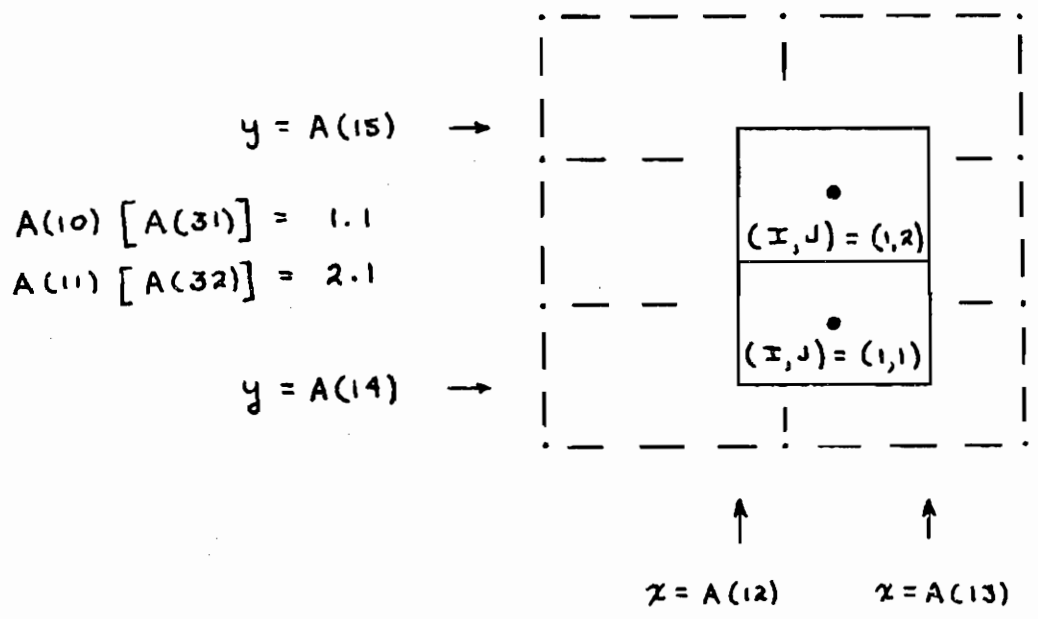

Fig. 45

Collision test

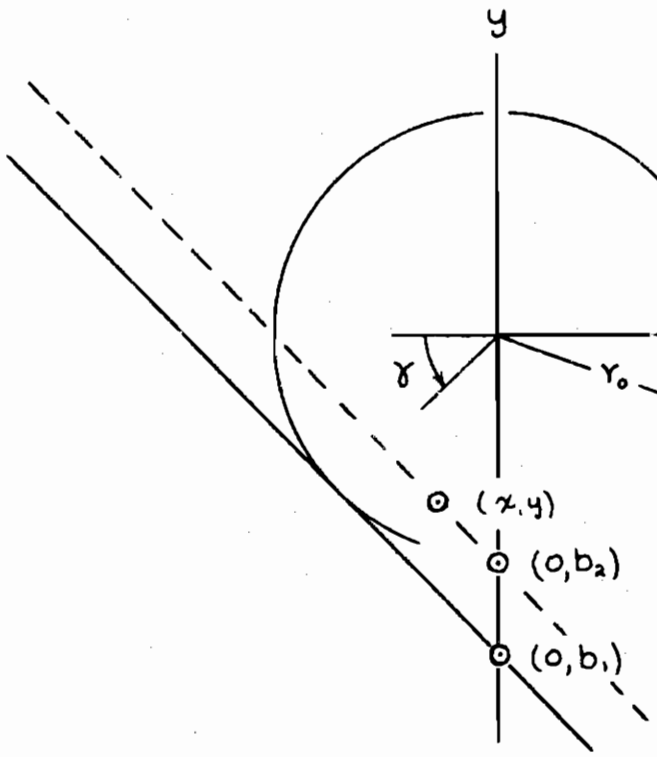

A(24) = r_o

$\gamma = 2\pi V_x$ A(25)